Trace gases in glaciated environments

Moya L. Macdonald

Bristol Glaciology Centre

University of Bristol

A dissertation submitted to the University of Bristol in accordance with the requirements for award of the degree of Doctor of Philosophy in the Faculty of Science.

School of Geographical Sciences

November 2018

Word Count: 42,655

Abstract

Trace gases play a variety of pivotal roles in atmospheric and earth surface processes despite being low in relative atmospheric abundance. Halogenated gases such as halocarbons contribute to the destruction of ozone; carbon dioxide (CO_2), hydrogen (H_2) and methane (CH_4) can act as electron donors or acceptors to provide microbial energy; and CO_2 links the chemical weathering of rocks to the global carbon cycle. However, there has been less research into the cycling of trace gases in glaciated environments. The subglacial environment can be isolated from the atmosphere and surface processes which would otherwise supply energy for microbial life and acidity for chemical weathering. It is unknown how such processes are driven when reactants become limited during long glaciations. The proglacial environment can be remote, particularly in regions such as the High Arctic, meaning fluxes of trace gases such as halocarbons can be particularly important due to distance from the major halocarbon source regions. Little research has been conducted on trace gas fluxes from the proglacial environment despite the ongoing expansion of these land surfaces as glaciers undergo widespread retreat in response to Arctic warming.

This thesis explores novel sources, sinks and the roles of trace gases in both sub- and pro-glacial environments using a combination of laboratory experiments, field experiments and analysis of long-term atmospheric datasets. Laboratory rock grinding experiments were used as an analogue to glacial bedrock erosion and demonstrated abiotic production of several trace gases at rates significant to subglacial microbial metabolism and chemical weathering. Field flux chamber measurements on the proglacial forefield of a High Arctic glacier demonstrated that halocarbon fluxes were significant despite the immaturity of the recently exposed soils. Analysis of long-term, frequent halocarbon measurements in the ambient Arctic atmosphere indicated the influence of local halocarbon production, with evidence of marine processes in particular. In conclusion, trace gases are important for a variety of processes related to the marginal and rapidly changing glaciated environment. Understanding the role of trace gases, and their sources and sinks in these environments can help further our understanding of extreme life, the influence of chemical weathering on the carbon cycle and the influence of marginal soils on the halogen budget of the atmosphere.

Acknowledgements

I would firstly like to thank my supervisor, Prof. Jemma Wadham, whose support and advice has been hugely invaluable to me and to the development of this project from its initial stages. In particular, her guidance and example have greatly developed my own abilities as a researcher at the start of my academic journey. I would also like to thank my second supervisor, Prof. Simon O'Doherty, whose patient teaching and support regarding the technical and analytical aspects of this project, in particular, were hugely instrumental to this project.

I would like to acknowledge Jon Telling, whose enthusiasm was influential in the early stages of this project and whose advice on techniques, analysis and paper writing was much appreciated. Thanks must be extended to Dickon Young, without his expertise in fixing instruments and data analysis, or polar bear guarding, the 2017 field season would not have been a success. Also, to Chris Lunder and Ove Hermansen from NILU who helped secure funding and equipment for Svalbard and who allowed me to use their data in this thesis. To Nick Cox and Malcolm Airey for a wealth of experience, logistical support, and entertaining stories whilst at the UK station in Ny-Ålesund.

James Williams and Fotis Sgouridis are thanked for all their assistance over several years in the lab. My two gas lab partners in crime: Guillaume Lamarche-Gagnon and Beatriz Gill, are thanked for all the maths and other discussions and for making lab work that bit more fun. Further thanks to Guillaume for much field assistance, help with all things heavy lifting and many late night discussions about science and everything.

To the people of Browns, for being the best part of office work, particularly Gaz, Jenny, Diksha, Miranda, Amy, Nathan, the cyclists and many others. To the DTP crew for 4 fantastic years and to old friends for support throughout. To Tim Morris for thesis advice and support in the last few months. To Michael Cooper, an excellent flatmate for 4 whole years. And to the wonderful Emily 'Plant' Johnson, for brightening up the weekends.

Lastly, to Dad, Pamela, Fiona and Josh for all your support and love over the years, for providing me with so many opportunities, for putting up with my free-loading during the final months, and to Louis, for always giving the best morning greetings.

To Catriona, Ruth and John, I wish I could have shared this with you too.

Author’s declaration

I declare that the work in this dissertation was carried out in accordance with the requirements of the University’s *Regulations and Code of Practice for Research Degree Programmes* and that it has not been submitted for any other academic award. Except where indicated by specific reference in the text, the work is the candidate’s own work. Work done in collaboration with, or with the assistance of, others, is indicated as such. Any views expressed in the dissertation are those of the author.

Signed Date

Table of Contents

Abstract i

Acknowledgements iii

Author's declaration v

Table of Contents vii

Table of Figures xiii

Table of Tables xvii

1 Introduction and scientific background 1

1.1 Introduction 1

1.2 Aims and objectives 3

1.2.1 Research objective 1 3

1.2.2 Research objective 2 3

1.2.3 Research objective 3 4

1.3 Scientific background 5

1.3.1 Trace gases and the subglacial environment 5

1.3.1.1 Glacial erosion and subglacial chemical weathering 5

1.3.1.2 Subglacial microbial life 7

1.3.1.3 Trace gases in rocks and minerals 9

1.3.2 Trace gases and the proglacial environment 12

1.3.2.1 Halocarbons and atmospheric chemistry 12

1.3.2.2 Natural sources and sinks of halocarbons 13

1.3.2.3 The main halocarbons of interest – a summary of sources and sinks 17

1.3.2.4 Halocarbons in the Arctic 20

1.3.2.5 The proglacial environment 21

1.3.3 Summary 23

2 Methodological and data overview 24

2.1 Rock grinding experiments 24

2.1.1 Rock grinding equipment 24

2.1.2 Analysis of gas samples by gas chromatograph (GC) 25

2.1.2.1 The Gas Chromatograph 25
2.1.2.2 Identification and quantification 26
2.2 Fieldwork 28
2.2.1 Overview of field site and experiments 28
2.2.2 Collection of rock samples 29
2.2.3 Proglacial gas flux experimental design and modification 30
2.3 Analysis of halocarbon trace gases 32
2.3.1 Introduction to trace gas analysis 32
2.3.2 The Adsorption Desorption System – Gas Chromatograph Mass Spectrometer 32
2.3.2.1 Description of the Adsorption Desorption System 32
2.3.2.2 Description of the Gas Chromatograph Mass Spectrometer 33
2.3.3 Optimization of the ADS-GCMS 35
2.3.3.1 Addition of automated multi-sampler 35
2.3.3.2 Optimisation of the mass spectrometer 36
2.3.4 Operation and maintenance of the ADS-GCMS 39
2.3.4.1 Operation of the ADS-GCMS 39
2.3.4.2 Checking and tuning the MS 39
2.3.5 Processing ADS-GCMS analyses 40
2.3.5.1 Peak integration 40
2.3.5.2 Monitoring of standards 41
2.3.6 Blank-testing equipment 41
2.4 Long-term halocarbon data 43
2.4.1 Overview of the datasets 43
2.4.2 Collection of long-term halogenated gas data 43
3 Glacial erosion liberates lithologic energy sources for microbes and acidity for chemical weathering beneath glaciers and ice sheets 45
3.1 Abstract 46
3.2 Introduction 47
3.3 Materials and methods 49
3.3.1 Rock and sediment sample selection 49

3.3.2 Experiments to simulate gas release via glacial erosion 50
3.3.3 Analysis of gases released during grinding 50
3.3.4 Grain size and total carbon analysis 51
3.3.5 Suspended sediment flux and discharge analysis for ML (2016) and RG 52
3.3.6 Calculation of catchment-scale gas generation from grinding experiments 54
3.3.7 Calculation of supported rates of hydrogenotrophic methanogenesis 55
3.3.8 Calculation of theoretical total flux of CO_2 and CH_4 in subglacial discharge 56
3.4 Results 57
3.5 Discussion 61
3.5.1 Sources and generation mechanisms for gases during glacial grinding 61
3.5.1.1 Hydrogen 61
3.5.1.2 Carbon dioxide and carbon monoxide 63
3.5.1.3 Hydrocarbons 65
3.5.2 Glacial erosion liberates potential energy sources for subglacial microbes 66
3.5.3 Glacial erosion liberates a source of acidity for chemical weathering 69
3.5.4 Glacial erosion as an abiogenic source of methane 71
3.6 Conclusion 73
4 Consumption and emission of halogenated trace gases from a retreating Arctic glacier's forefield 74
4.1 Abstract 75
4.2 Introduction 75
4.3 Study site 79
4.3.1 General description of the location 79
4.3.2 Specific descriptions of the sites 80
4.4 Methods 82
4.4.1 Flux experiments 82
4.4.2 CO_2 and CH_4 sampling and analysis 83
4.4.3 Halocarbon sampling and analysis 84
4.4.4 Physical, chemical and biological sampling and analysis 87
4.4.4.1 In-field measurements and sampling 87
4.4.4.2 Organic matter, total nitrogen, total carbon and soil texture 87

4.4.4.3 Heterotrophic bacterial abundance 88
4.4.5 Statistical analysis 89
4.4.6 Calculation of regional fluxes 89
4.4.6.1 Calculation of total proglacial fluxes in the Arctic 89
4.4.6.2 Calculation of Arctic tundra fluxes 90
4.5 Results 91
4.5.1 Physical, chemical and biological differences between sites 91
4.5.2 Halocarbon fluxes 91
4.5.2.1 Relationships between halocarbon fluxes and physical, chemical and biological variables 93
4.5.2.2 Halocarbon intercorrelations 94
4.5.2.3 Correlations of methyl halides and chemical, physical and biological variables 95
4.5.2.4 Correlations of polyhalomethanes and chemical, physical and biological variables 96
4.6 Discussion 97
4.6.1 Influence of exposure age on halocarbon fluxes from the proglacial environment 97
4.6.2 Terrestrial emission of typically marine-origin brominated compounds 98
4.6.3 Controls on halocarbon fluxes in the proglacial environment 99
4.6.3.1 Biological consumption of methyl halides and abiogenic production of CH_3I 99
4.6.3.2 Inconclusive influence of hydrology on methyl halide fluxes 99
4.6.3.3 Biogenic and abiogenic production of polyhalogenated species 100
4.6.4 Glacial forefields as a source and sink of halocarbons? 101
4.7 Conclusions 102
5 Influence of local sources and sinks on ambient tropospheric halocarbon observations in the High Arctic ... 104
5.1 Abstract 105
5.2 Introduction 105
5.3 Methods 109
5.3.1 Description of site 109

5.3.2 Measurement of halogenated gases 109
5.3.3 Measurement of non-halogenated gases and meteorological variables 112
5.3.4 Data processing 112
5.3.4.1 Removal of pollution events 113
5.3.4.2 Analysis of the influence of wind direction and speed 113
5.3.5 Comparison of ground-level to Zeppelin measurements 115
5.3.6 Calculation of macroalgal halocarbon fluxes 115
5.3.7 Estimated areal coverage of known marine and soil fluxes 116
5.4 Results 118
5.4.1 Five year trends 118
5.4.2 Seasonal variation 118
5.4.3 Variability in August 118
5.4.3.1 Gas variability and the relationship with wind speed and direction 121
5.4.3.2 Comparison between Zeppelin measurements and ground-level measurements 123
5.5 Discussion 125
5.5.1 Long-term and seasonal variation 125
5.5.2 Do the Zeppelin observations show the influence of local fluxes? 125
5.5.2.1 Limited evidence for a soil sink of CH_3Cl and CH_3Br 126
5.5.2.2 Evidence of a local source of CH_3I, CH_2Br_2, $CHCl_3$ and $CHBr_3$ 127
5.6 Conclusion 129
6 Conclusions 130
6.1 Summary of main findings 130
6.1.1 The liberation of trace gases by glacial erosion into the subglacial environment 130
6.1.2 Halogenated trace gas fluxes from proglacial land surfaces 131
6.1.3 The influence of proglacial halocarbon fluxes on atmospheric concentrations 132
6.2 Limitations of this work and future research 133
6.2.1 Limitations and future work surrounding trace gas production by glacial erosion 133
6.2.2 Limitations and future work relating to proglacial trace gas fluxes 134
6.2.3 Limitations and future work relating to the influence of soil fluxes on ambient records 134

6.3 Concluding remarks.....135

7 Reference List 136

Table of Figures

Figure 1.1 Historical and future abundances of halogen source gases in the atmosphere. 14

Figure 1.2 The biogenic production of methyl halides by methyl transferase. 14

Figure 1.3 Production of $CHBr_3$ and CH_2Br_2 by decarboxylation of 3-ketooctanic acid 15

Figure 1.4 Schematic diagram of the abiogenic production of methyl halides in soil. .. 16

Figure 1.5 Abiotic production of chloroform ($CHCl_3$) or bromoform ($CHBr_3$) 17

Figure 1.6 Schematic diagram of nutrient inputs to a glacial forefield 22

Figure 2.1 Ball-mill used in grinding experiments 24

Figure 2.2 Peak area versus calculated concentrations (ppm) of each gas present in the manual dilutions of the mixed standard as analysed on the GC 27

Figure 2.3 Map of the Broggerhalvøya peninsula 28

Figure 2.4 Schematic diagram of the chamber set-up used in preliminary proglacial gas flux experiments in 2016 (a) and the modified chamber set-up used in 2017 (b). 31

Figure 2.5 The fragmentation spectra of the 6 main halocarbons of interest CH_3Cl (a), CH_3Br (b), CH_3I (c), CH_2Br_2 (d), $CHCl_3$ (e) and $CHBr_3$ (f)..... 34

Figure 2.6 The chromatogram of a standard run in TIC (a) and SIM (b) mode 35

Figure 2.7 An example of adjustments made to SIM windows..... 38

Figure 3.1 H_2 (A), CO (C), CH_4 (D), C_2H_6 (E), C_2H_4 (F) produced in nmol g^{-1}, and CO_2 (B) produced in μmol g^{-1} when grinding the rock and sediment samples to different average grain sizes. 58

Figure 3.2 Amounts of CO_2 (μmol g^{-1}) against (A) CH_4 (nmol g^{-1}) released during grinding of RG and ML rocks and against (B) CO (nmol g^{-1}) released during grinding of RG rocks 60

Figure 3.3 The relationship between the amount of C_2H_6 and CH_4 (A) and between CO_2 and H_2 (B) produced per gram of sample during grinding 60

Figure 3.4 The amount of CO_2, CH_4 and C_2H_6 produced (nmol g^{-1}) compared to the percentage weight of total carbon present in the sample. 65

Figure 4.1 Schematic diagram summarising natural sources and sinks for the 6 halocarbons of interest in temperate and tropical regions 77

Figure 4.2 Locations of sites *snout* (A), *pond mat* (B), *disturbed mat* (C), *established mat* (D) and *tundra* (E) on the proglacial forefield of Midtre Lovenbreen glacier 79

Figure 4.3 The visible differences in land-surface type and colonising species at site *snout* (a), *pond-mat* (b), *disturbed mat* (c), *mat* (d) and *tundra* (e), and a schematic diagram of the flux chamber's design (f) 80

Figure 4.4 Comparison of the flux in nmol m^{-2} d^{-1} of gas in un-darkened (light) and darkened (dark) chambers for CH3Cl (a), CH3Br (b), CH3I (c) from preliminary experiments in 2016. 82

Figure 4.5 Variation at each site of soil water content (a), water table depth (b), weight % of grains < 2 mm diameter (c), organic matter content (d), total carbon content (e), total nitrogen content (f), heterotrophic cell numbers (g), CO_2 flux (h) and CH_4 flux (i) 92

Figure 4.6 Daily fluxes (nmol m^{-2} d^{-1}) at each site of CH_3Cl (a), CH_3Br (b), CH_3I (c), $CHCl_3$ (d), $CHBr_3$ (e), CH_2Br_2 (f). 93

Figure 4.7 Correlations between halocarbon fluxes and the chemical, physical and biological variables across all sites (a), site *disturbed mat* (b), site *established mat* (c) and site *tundra* (d) 95

Figure 4.8 Schematic diagram summarising natural sources and sinks for the 6 halocarbons of interest in polar regions 101

Figure 5.1 The study area in northwest Svalbard 110

Figure 5.2 Halocarbon observations for August 2016 and 2017 114

Figure 5.3 Measurements of CH_3Cl, CH_3Br, CH_3I, CH_2Br_2, $CHCl_3$ and $CHBr_3$ made at the Zeppelin observatory between 2013-2017 119

Figure 5.4 Comparison of the relationship between halocarbon measurements across the whole year and across the month of August for CH_3Cl and CH_3Br in 2016 (a) and 2017 (b), CH_2Br_2 and $CHBr_3$ in 2016 (c) and 2017 (d) and for CH_3Cl and $CHCl_3$ in 2016 (e) and 2017 (f). 120

Figure 5.5 Pollution roses of CH_2Br_2 (a), $CHBr_3$ (b) and CH_3I (c) for all wind speeds in 2016 and 2017 121

Figure 5.6 Pollution roses of $CHCl_3$ comparing all wind speeds to low wind speeds in 2016 (a) and 2017 (b) 122

Figure 5.7 Pollution roses of CH_3Cl (a) and CH_3Br (b) for all wind speeds in 2016 and 2017 123

Table of Tables

Table 1.1 Known natural sources and sinks (non-atmospheric) for the compounds of interest..... 19

Table 2.1 Compound name, formulas, molecular weights (MW), retention time (RT), target and qualifier ion(s), SIM window and whether the compound's concentration was determined using peak area or height is shown for each compound analysed 37

Table 2.2 The finalised SIM window start times, the number of ions in each window, the dwell time per ion, the cycles per second and the m/z of the ions..... 38

Table 2.3 Results of equipment testing for the halocarbons of interest..... 42

Table 3.1 Characteristics of the rock and sediment samples and their source glacial catchments, with estimates for the crystalline rock samples of the areal percentage of major rock forming minerals 49

Table 3.2 The limit of quantification (variance) and detection (LOD) for each gas analysed 52

Table 3.3 Suspended sediment (SS) flux, average concentration and average grain size in meltwater for each glacier catchment. 53

Table 3.4 The hydrocarbons detected during crushing. 59

Table 3.5 Comparison of estimated long-term catchment production rates of H_2, CO_2 and CH_4 (nmol gas m^{-2} day^{-1}) by subglacial grinding 67

Table 4.1 The standard concentration, limit of quantification (variance) and limit of detection (LOD) for each gas analysed, with the target ion and qualifier ion(s) shown for gases analysed by GCMS. 84

Table 5.1 Details of each compound analysed here, with length of total atmospheric lifetime in years (yr) or days (d), indication of whether the 'source type' of the compound is anthropogenic (A) and/or natural (N) 106

Table 5.2 The precisions and the calibration scales used for the 6 halocarbons of interest plus the two HFC compounds analysed here..... 111

1 Introduction and scientific background

1.1 Introduction

Trace gases are present in relatively small volumes (<1 %) in the Earth's atmosphere. Despite their relatively low abundance, many play hugely important roles in the atmosphere. For example, carbon dioxide (CO_2) and methane (CH_4) are major contributors to climate forcing despite having average global concentrations in 2017 of 405.0 ± 0.1 parts per million (ppm) and 1849.7 ± 0.8 parts per billion (ppb), respectively (Blunden et al., 2018). Even gases present in the atmosphere at an order of magnitude lower (parts per trillion, ppt) can play a critical role in atmospheric chemistry. For example, halocarbons, which are hydrocarbons with at least one carbon-halogen bond (typically chlorine, bromine and/or iodine), are a major source of halogens to the atmosphere and thus major drivers of ozone (O_3) destruction (Montzka et al., 2011). The halocarbons include anthropogenic compounds such as chlorofluorocarbons (CFCs) as well as a large variety of naturally occurring halocarbons such as simple halomethanes (i.e. based upon methane, CH_4, where one or more H atoms has been replaced with a halogen; CH_yX_{4-y}). Shorter-lived halocarbons (e.g. methyl iodide and dibromomethane) primarily contribute to O_3 destruction in the troposphere whilst the longer-lived halocarbons (e.g. methyl chloride and methyl bromide) contribute to O_3 destruction in the stratosphere where it forms an essential protective barrier against ultraviolet light (e.g. Carpenter et al., 2014).

Trace gases also play important roles in a wide variety of Earth surface processes. CO_2, CH_4 and H_2 are used as energy and/or carbon sources by a variety of microbial life (Conrad, 1996). The dissolution and dissociation of CO_2 in water to form carbonic acid drives chemical weathering of rocks, influencing the global carbon cycle (Raymo and Ruddiman, 1992). Halocarbons are produced by a huge variety of algae, plants and fungi, from the tropics to the poles, and are additionally consumed by a wide variety of bacteria (see Montzka et al., 2011 for review).

One of the lesser explored environments with respect to trace gases are glaciated environments. Glaciers and ice sheets are currently experiencing rapid change, particularly in the Arctic, where recent and predicted global warming is amplified (ACIA, 2005). It is of great importance to understand these environments now so that how they

will change in the future and the impacts this will have on the wider environment can be predicted. Interest in the subglacial environment has grown greatly in recent decades following the discovery of active microbial communities in the basal ice and subglacial meltwaters of glaciers (Sharp et al., 1999; Skidmore et al., 2000). Subsequent studies have revealed diverse microbial communities involved in chemical weathering and nutrient cycling with implications for our understanding of life in extreme environments and the long-term global carbon cycle (e.g. Bhatia et al., 2010; Hawkings et al., 2016; Sharp et al., 1999). Understanding sources of trace gases which are utilised for microbial energy and carbon in these environments could help explain how life survives long periods of glaciation, including 'snowball' earth scenarios, and how life could survive on other planets. Understanding the delivery of CO_2 to the subglacial environment for chemical weathering will improve our ability to link glacial weathering to carbon cycling and the drawdown of atmospheric CO_2.

Decreasing anthropogenic emissions of halocarbons, particularly CFCs, and the predicted future decrease of some of their more harmful replacement compounds (e.g. HCFCs), means the proportion of naturally-emitted halocarbons in the atmosphere will increase (Carpenter et al., 2014; Montzka et al., 2011). However, some uncertainties remain in the natural cycles of many of these compounds, not least, in the spatial variability of their sources and sinks. In the Arctic, research of natural sources and sinks has been dominated by marine micro-algal (e.g. sea-ice diatoms) and macro-algal (seaweed) production and studies of tundra soil sinks (Laturnus, 2001; Rhew et al., 2007; Sturges et al., 1992; Teh et al., 2009). Little research has been conducted into how young soils with different levels of development could influence halocarbon fluxes. Retreating glaciers expose new soils for microbial colonisation and ecological succession (Hodkinson et al., 2003). With the ongoing retreat of glaciers predicted across the Arctic, understanding halocarbon fluxes in this marginal environment, and their influence upon ambient atmospheric concentrations is of importance.

1.2 Aims and objectives

The primary aims of this thesis are to identify fluxes of various trace gases in the subglacial and proglacial environment and to develop a better understanding of the interaction between biotic and abiotic processes which involve trace gases in these marginal environments.

1.2.1 Research objective 1

(i) To identify and quantify gases generated by the mechanical breakdown of rocks and minerals during glacial grinding.

(ii) To assess the potential impact of gases released by this process on *in situ* subglacial microbial communities and subglacial chemical weathering processes.

Laboratory rock grinding experiments were used to simulate glacial abrasion with direct measurement of gases generated by the mechanical breakdown of rocks and sediments which have been collected from a variety of glaciated catchments. As a proxy for glacial abrasion rates, suspended sediment export rates from the catchments were obtained, using data collected in the field or published values. These rates were used to calculate theoretical rates of catchment-wide gas generation by glacial abrasion which were directly comparable with published rates of subglacial microbial gas consumption and chemical weathering. The results and discussion of this objective are presented in Chapter 3.

1.2.2 Research objective 2

(i) To identify and quantify fluxes of trace halocarbon gases from the glacial forefield of a retreating glacier as a previously unexplored environment.

(ii) To identify the influence of soil age and development upon halocarbon fluxes in Arctic soils.

Flux chambers were designed and employed on the glacial forefield of Midtre Lovenbreen, Svalbard to measure net fluxes of halocarbons. A variety of surfaces with different exposure ages and degrees of microbial and plant colonisation were investigated. These differences were used in combination with geochemical variability in the soil to interpret the influence that exposure age and the degree of soil development

have on halocarbon fluxes. The results and discussion of this objective are presented in Chapter 4.

1.2.3 Research objective 3

(i) To examine the long-term and seasonal variability in concentrations of halocarbon gases in the High Arctic as measured at an observatory in Kongsfjorden, Svalbard.

(ii) To determine if proglacial fluxes or other local fluxes (i.e. from the fjord) are observable in trace gas data measured at an observatory in Kongsfjorden, Svalbard.

A 5-year (2013-2017) dataset of baseline halocarbon measurements, and a 2-year (2016-2017) dataset of all halocarbon measurements, non-halogenated gas data (including carbon monoxide and methane) and meteorological data (wind speed, direction, temperature) were obtained from the Norwegian Air Institute (NILU) who perform hourly to daily measurements at the Zeppelin observatory in Kongsfjorden, Svalbard. The 5-year dataset was analysed for year-on-year trends and seasonal variations of the halocarbons. To investigate the influence of local fluxes on the ambient measurements, detailed analysis of the halocarbons were conducted on data from August in 2016 and 2017 where 'pollution events' and periods of high wind speeds have been removed from the data. The results and discussion of this objective are presented in Chapter 5.

1.3 Scientific background

This section provides an overview of research relevant to the stated thesis aims and objectives and is divided into two main strands: (1) trace gases in the subglacial environment (Section 1.3.1) and (2) trace gases in the proglacial environment (Section 1.3.2). Strand (1) contains an overview of subglacial erosion, weathering and microbial processes, followed by evidence for the release or generation of trace gases during mechanical rock breakdown, particularly CO_2, H_2 and short chain hydrocarbons. Strand (2) is primarily concerned with halocarbon gas fluxes in the Arctic and from proglacial land surfaces and, thus, gives an overview of the importance of halocarbons in the atmosphere, the natural sources and sinks of these gases globally and in the Arctic, and an overview of the characteristics of the proglacial environment.

1.3.1 Trace gases and the subglacial environment

1.3.1.1 Glacial erosion and subglacial chemical weathering

Through the processes of plucking and abrasion, glaciers erode their underlying bedrock, producing large quantities of sediment, from the < 100 μm glacial flour to large clasts and erratics (e.g. Hallet et al., 1996; Lee and Rutter, 2004). The process of plucking is enhanced by stick-slip motion causing glacial microearthquakes which encourage hydrofracturing of the bedrock (Ekström et al., 2003; Zoet et al., 2013). Abrasion of plucked clasts frozen into the basal ice grinding against the bedrock is the primary generation mechanism of glacial flour (Lee and Rutter, 2004). The flour is flushed from beneath the glacier by seasonal melt water and the resultant suspended sediment flux and/or redeposited flour in the proglacial zone is commonly used to calculate glacial erosion rates (e.g. Cowton et al., 2012; Hallet et al., 1996; Hodson et al., 1998). Glacial erosion rates vary from thin glaciers on hard bedrock or at high latitudes which have low erosion rates (0.01 mm yr^{-1}) compared to large valley glaciers in temperate regions which have high erosion rates (10-100 mm yr^{-1}; Hallet et al., 1996). However, a more recent study has calculated erosion rates 1-2 orders of magnitude greater (4.8 +/- 2.6 mm yr^{-1} at Leverett Glacier, southwestern Greenland) than has previously been assumed for Greenlandic glaciers on hard crystalline bedrock (Cowton et al., 2012). It is thought this higher rate was due to surface meltwaters reaching the base of the glacier which reduces friction and results in an increase in speed and a behaviour more similar to small valley glaciers (Chandler et al., 2013).

The production of fine grained sediments requires the fracturing of minerals, exposing fresh surfaces which are readily reactive and thus enhancing subglacial chemical weathering (e.g. Anderson et al., 1997; Tranter et al., 1996; Wadham et al., 1998). Chemical weathering is broadly driven by two different processes: the carbonation of carbonates and silicates (Equation 1.1 and 1.2) and the coupling of sulphide oxidation with carbonate and/or silicate dissolution (Equation 1.3 and 1.4; Tranter et al., 2002).

Equation 1.1

$$\mathbf{CO_2}_{(aq)} + \mathbf{H_2O}_{(l)} + \mathbf{Ca_{(1-x)}Mg_{(x)}CO_3}_{(s)} \rightleftharpoons \mathbf{(1-x)Ca^{2+}}_{(aq)} + \mathbf{xMg^{2+}}_{(aq)} + \mathbf{2HCO_3^-}_{(aq)}$$

(Mg-)Calcite

Equation 1.2

$$\mathbf{2CO_2}_{(aq)} + \mathbf{3H_2O}_{(l)} + \mathbf{CaAl_2Si_2O_8}_{(s)} \rightleftharpoons \mathbf{Ca^{2+}}_{(aq)} + \mathbf{2HCO_3^-}_{(aq)} + \mathbf{Al_2Si_2O_5(OH)_4}_{(s)}$$

Anorthite (feldspar) *Kaolinite (clay)*

Equation 1.3

$$\mathbf{4FeS_2}_{(s)} + \mathbf{15O_2}_{(aq)} + \mathbf{16Ca_{(1-x)}Mg_{(x)}CO_3}_{(s)} + \mathbf{14H_2O}_{(l)} \rightleftharpoons \mathbf{16(1-x)Ca^{2+}}_{(aq)} + \mathbf{16xMg^{2+}}_{(aq)} + \mathbf{16HCO_3^-}_{(aq)} + \mathbf{8SO_4^{2-}}_{(aq)} + \mathbf{4Fe(OH)_3}_{(s)}$$

Pyrite *Ferric oxyhydroxides*

Equation 1.4

$$\mathbf{16Na_{(1-x)}K_{(x)}AlSi_3O_8}_{(s)} + \mathbf{4FeS_2}_{(s)} + \mathbf{15O_2}_{(aq)} + \mathbf{86H_2O}_{(l)} \rightleftharpoons \mathbf{16(1-x)Na^+}_{(aq)} + \mathbf{16xK^+}_{(aq)} + \mathbf{8SO_4^{2-}}_{(aq)} + \mathbf{8Al_2Si_2O_5(OH)_4}_{(s)} + \mathbf{32H_4SiO_4}_{(aq)} + \mathbf{4Fe(OH)_3}_{(s)}$$

Alkali feldspar *silicic acid*

For carbonation processes (Equations 1.1-1.2), protons are provided by dissociated carbonic acid which forms when CO_2 dissolves in solution. As a result, this weathering process dominates in large, aerated subglacial channels where there is an abundant supply of atmospheric CO_2 (Tranter et al., 2002). However, subglacial microbial respiration and the release of ice-trapped, palaeo-atmospheric bubbles during basal melt are additional sources of CO_2 in areas isolated from present-day atmospheric influxes (Montross et al., 2013; Tranter et al., 2002; Wadham et al., 2010a). The second subglacial chemical weathering process involves the coupling of sulphide oxidation with carbonate or silicate dissolution (Sharp et al., 1999; Tranter et al., 2002). It is microbially-driven and

dominates in distributed drainage systems. Carbonate dissolution and sulphide oxidation are usually the dominant reactions occurring in a catchment, even when they are minor components of the bedrock, because of their higher reactivity compared to silicate minerals (Tranter et al., 1996). However, beneath large ice sheets it is thought that silicate weathering is enhanced due to calcite saturation or exhaustion of trace calcite minerals in bedrock (Wadham et al., 2010b).

1.3.1.2 Subglacial microbial life

Initially thought to be inhospitable to life due to constant darkness, assumed limited nutrient input, low temperatures and high pressures, active microbial communities are now recognised to exist in the subglacial environment (e.g. Sharp et al., 1999; Skidmore et al., 2000, 2005). Despite the challenges of the subglacial environment, microbial habitats are possible wherever there is liquid water, nutrients, carbon and electron acceptors (Sharp et al., 1999). Liquid water occurs beneath large areas of glaciers and ice sheets, and can result in the formation of sub-glacial lakes where, even 800 metres beneath the ice surface, viable and diverse communities of bacteria and archaea have been discovered (Christner et al., 2014; Karl et al., 1999; Priscu et al., 2007). Additionally, nutrients and dissolved gases are carried by supraglacial meltwaters via moulins to the bed near the ice margins; palaeo-atmospheric trace gases are released from the ice by basal melting; organic matter in overridden soils is oxidised; and subglacial erosion liberates nutrients (e.g. phosphorous and iron) from bedrock minerals (e.g. Bakermans and Skidmore, 2011; Hodson et al., 2005; Sharp et al., 1999; Tranter et al., 2005). The latter two sources are likely microbially mediated with bacteria oxidising reduced organic matter from the overridden soils and a range of species involved in mediating chemical weathering reactions (e.g. Montross et al., 2013; Sharp et al., 1999; Stibal et al., 2012a).

A diverse range of bacteria and archaea beneath glaciers and ice sheets drive the cycling of several nutrients. For example, both sulphide oxidising bacteria (Sharp et al., 1999) and sulphate reducing bacteria have been identified (Wadham et al., 2004). Similarly, denitrifying and nitrogen mineralizing microorganisms (Christner et al., 2014; Hodson et al., 2005; Skidmore et al., 2000); bacteria that catalyse the oxidation of iron from iron sulphide and that reduce iron(III) (Mitchell et al., 2013); and archaea that generate methane (CH_4) and bacteria that metabolise it (Boyd et al., 2010; Dieser et al., 2014) have all been identified in the subglacial environment. In recent years it has been identified

that subglacial biogeochemical cycling results in the export of nutrients downstream (Hawkings et al., 2016, 2017; Lawson et al., 2014). Additionally, proposed CH_4 generation beneath ice sheets has been linked to the global carbon cycle, the global CH_4 budget and post-deglaciation climate warming (Wadham et al., 2008, 2012). Substantial CH_4 generation beneath ice sheets is supported by: modelling of methane clathrate formation beneath Antarctica (Wadham et al., 2012); evidence of elevated CH_4 and anoxic conditions in basal ice of the GRIP ice core in Greenland (Christner et al., 2012); and the widespread identification of methanogens, including obligate anaerobes, in subglacial sediments and basal ice (e.g. Boyd et al., 2010; Skidmore et al., 2000; Stibal et al., 2012). Recent evidence has suggested that methanotrophs in subglacial lakes and in aerated channels at the margin of the ice sheet may oxidise much of this CH_4, potentially reducing the influence of subglacial and sub-ice sheet methanogenesis on the wider CH_4 cycle (Dieser et al., 2014; Michaud et al., 2017).

Methanogenesis can occur via acetate fermentation (Equation 1.5) or via the hydrogenotrophic pathway (Equation 1.6). The latter oxidises hydrogen whilst reducing an electron acceptor such as nitrate, Mn(IV), Fe (III), sulphate or CO_2 (Lovley and Goodwin, 1990).

Equation 1.5

$$\mathbf{CH_3COOH \rightarrow CH_4 + CO_2}$$

Equation 1.6

$$\mathbf{4H_2 + CO_2 \rightarrow CH_4 + 2H_2O}$$

It has been suggested that over time, with older organic carbon and increased microbial degradation, methanogenesis would transition from acetate fermentation to H_2 oxidation by CO_2 reduction (Wadham et al., 2008). Hydrogenotrophic methanogens have been found as the sole methanogen in subglacial sediments beneath a Greenlandic glacier with isotopic evidence from the GRIP ice core further supporting the hydrogenotrophic pathway (Stibal et al., 2012b). Sources of CO_2 include palaeo-atmospheric release from ice-trapped bubbles by basal melt, microbial oxidation of organic matter, and microbial reduction of nitrate, sulphate and Fe(III) during anaerobic respiration (Wadham et al., 2008). Sources of hydrogen are more limited. Bacteria, including anaerobes, can produce hydrogen (e.g. Nandi and Sengupta, 1998) but have not been identified in the subglacial environment. However, a recent study has shown the potential for abiotic hydrogen generation at subglacially relevant temperatures (0 °C) where there is a supply of freshly

ground rock (Telling et al., 2015; discussed in more detail in Section 1.3.1.3.2). Abiotic supply of these gases would provide support for microbial ecosystems beneath ice sheets being a potential refugia for life during past ice ages and snowball earths and would provide possible pathways for the development of early life on Earth and life on other planets (Telling et al., 2015; Wadham et al., 2004).

1.3.1.3 Trace gases in rocks and minerals

Trace gas release by the mechanical breakdown of rocks and minerals is a previously unrecognised source of trace gases (with the exception of hydrogen) to the subglacial environment. Potential sources of trace gases during the mechanical breakdown of rocks and minerals are described below.

1.3.1.3.1 Trace gases trapped in fluid inclusions and pore spaces

Most natural minerals contain gases trapped within fluid inclusions or chemically within the mineral structure (Burke, 2001; Harnisch and Eisenhauer, 1998). The most common gaseous species of fluid inclusions include CO_2, CH_4, N_2 and H_2O, where CO_2 and H_2O can also be present in a liquid state depending on the vapour pressure of the inclusion (Roedder, 1990). Less common gaseous species include H_2S, C_2H_6 and C_3H_8 with SO_2, CO, COS, H_2, O_2, NH_3, higher hydrocarbons, He and Ar more rarely present (Roedder, 1990). In igneous rocks, the CH_4 (and other hydrocarbons) in fluid inclusions can be organic in origin if organic matter is engulfed by the magma during rock formation (Potter and Konnerup-Madsen, 2003). However, there are instances of hydrocarbons being formed abiogenically, likely during late or post-magmatic processes, within basic or SiO_2-poor alkaline igneous rocks (Potter and Konnerup-Madsen, 2003). There are large alkali igneous complexes, primarily composed of granites and quartz syenites, in southern Greenland which contain fluid inclusions of mostly CH_4 (80-90 vol%), with exponentially decreasing concentrations of higher hydrocarbons up to C5 as well as CO_2 and/or CO (Konnerup-Madsen, 2001; Konnerup-Madsen and Rose-Hansen, 1982). Metamorphic fluid inclusions have also been found to contain hydrocarbons, with CH_4 most abundant (Khomenko and Langer, 1999). H_2 has been found in fluid inclusions in some metamorphic rocks, although this is very rare (Peretti et al., 1992).

The mineral grains that are incorporated into a sedimentary rock may also contain trace gases trapped in fluid inclusions. However, pore spaces and gases absorbed onto mineral grains are likely much larger stores of trace gases for sedimentary rocks or lower-grade

metamorphic rocks with a sedimentary origin (Wang et al., 2015; Zhang et al., 2014). Depending on the rock type, pore sizes can be large (~ 200 μm) with the potential to store large quantities of gases, commonly formed during the breakdown of trapped organic matter. Gases commonly found in the pore spaces of a sedimentary rock include CO_2 and CH_4, with varying proportions of other short chain hydrocarbons, commonly ethane, propane and butane, depending upon the diagenetic history and source of the gas (Zhang et al., 2014). H_2 is found in increasing proportions with increasing temperatures that the sedimentary rock or metapelite has experienced during burial diagenesis and/or metamorphism (Suzuki et al., 2017).

1.3.1.3.2 Generation of trace gases by fracturing minerals

Fracturing minerals can generate trace gases by three primary mechanisms: dissociation from the crystal structure, surface radical reaction with external compounds, and internal crystal structure re-organisation in response to surface radical formation. Dissociation of CO_2 has been observed from crushing carbonate rocks and attributed to fracturing, compression and slippage of planes of calcium carbonate (Martinelli and Plescia, 2005). Some CH_4 release from shale has also been attributed to release from carbonate crystals (Wang et al., 2015).

Surface radicals form when bonds are broken by the fracturing of a mineral. This causes instability within the crystal structure meaning surface radicals rapidly react with other compounds or atoms to form stable bonds (Sugisaki et al., 1983). A common mechanism in fractured silicate rocks is the reaction of silica radicals with water to form H_2 (Equation 1.7).

Equation 1.7

$$\equiv \mathbf{Si}\bullet + \mathbf{H_2O} \rightarrow \equiv \mathbf{Si} - \mathbf{OH} + \mathbf{H}\bullet$$

$$\mathbf{2H}\bullet \rightarrow \mathbf{H_2}$$

Hydrogen generation in fault zones is commonly attributed to this mechanism (e.g. Ito et al., 1999; Sugisaki et al., 1983). The Telling et al. (2015) study was the first to show that this mechanism occurred at subglacially relevant temperatures (0°C) as opposed to the elevated temperatures caused by friction in fault zones. Crushing experiments of various rocks and minerals have shown linear relationships between the volume of H_2 produced

and the surface area of the sediment, particularly when molar silica content is taken into account (Kameda et al., 2003; Telling et al., 2015). However, experiments have shown that hydrogen is generated even when crushing under dry conditions and when crushing non-silicate rocks (e.g. marble), suggesting that hydrogen can form on any surface radical and can occur without water (Hirose et al., 2011).

Further evidence that water is not required to generate hydrogen in silicate rocks can be seen from a set of laboratory crushing experiments of biotite in D_2O which showed that only 10% of the total H_2 generated was composed of D_2 and more than 90% of the H_2 was a mixture of HD and H_2 (Kameda et al., 2004). The authors suggested the reaction between Si-radicals and hydroxyl groups (–OH) as the source of the hydrogen atoms as opposed to reduction of a proton by Fe^{2+} due to the similar amounts of H_2 generated when crushing minerals with different iron contents. The generation of hydrogen from reaction of Si-radicals and hydroxyls within the crystals surface may also explain why the micas (containing significantly more hydroxyls in their crystal structures) generate more hydrogen than other silicate minerals (e.g. quartz, alkali feldspar) (Kameda et al., 2003).

In an analogue to the isolated sub-glacial and sub-ice sheet microbial communities, the sub-lithosphere is completely isolated from photosynthetic primary production, yet microbial ecosystems also thrive here (Hirose et al., 2011; Lin et al., 2005). Sub-lithospheric hydrogen is generated from the radiolytic dissociation of water (driven by radioactive decay of elements within the rocks; Lin et al., 2005) and/or fault-driven rock-water reactions (i.e. Equation 1.7; Hirose et al., 2011). By acting as an electron donor and contributing to production of organic compounds via Fischer-Tropsch synthesis, abiotic hydrogen production could support isolated microbial ecosystems for millions to billions of years (Lin et al., 2005; Sleep and Zoback, 2007).

1.3.2 Trace gases and the proglacial environment

1.3.2.1 Halocarbons and atmospheric chemistry

In atmospheric chemistry, many of the most important naturally-occurring halocarbons are halomethanes. This includes methyl halides (CH_3X; where X = Cl, Br or I), di-halomethanes (CH_2X_2), haloforms (CHX_3) and mixed-halide compounds (e.g. CH_2BrCl). Halocarbons can be sub-divided into 'long-lived' substances (LLS) which have atmospheric lifetimes greater than the typical mixing time of the troposphere and 'very-short-lived substances' (VSLS) which generally have lifetimes shorter than 6 months and a non-uniform distribution in the troposphere (Law et al., 2006). LLS includes many anthropogenic compounds as well as natural and mixed-source compounds, such as CH_3Cl (atmospheric lifetime of 0.9 years) and CH_3Br (0.8 years; Carpenter et al., 2014). VSLS include CH_3I (atmospheric lifetime of 7 days), CH_2Br_2 (123 days), $CHCl_3$ (149 days) and $CHBr_3$ (24 days) (Montzka et al., 2011). The atmospheric lifetime is determined by the compound's rate of removal from the atmosphere. The main atmospheric removal processes of these halocarbons are by reaction with hydroxyl radicals (Equation 1.8) and UV photolysis (Carpenter et al., 2014). The former is the main atmospheric destruction process for chlorine-containing halocarbons and some bromine-containing halocarbons. The latter is the primary atmospheric sink for halocarbons containing iodine and some bromine containing compounds (Montzka et al., 2011).

Equation 1.8

$$\mathbf{OH\bullet + CH_3X \rightarrow H_2O + CH_2X\bullet}$$

Atmospheric degradation of natural halocarbons releases halogens into the atmosphere which catalyse ozone (O_3) destruction (Butler, 2000; Mellouki et al., 1992; Montzka et al., 2011). Equation 1.9 is an example reaction of O_3 destruction by a halide radical ($X\cdot$) and illustrates how one halogen atom can be involved in the destruction of many molecules of O_3 (Staehelin et al., 2001).

Equation 1.9

$$\mathbf{X\bullet + O_3 \rightarrow XO + O_2}$$

$$\mathbf{XO + O_3 \rightarrow X\bullet + 2O_2}$$

The LLS deliver halogens to the stratosphere and are thus important drivers of stratospheric O_3 loss. Many VSLS have primarily local atmospheric impacts (e.g. in the

boundary layer), however, several VSLS, such as $CHBr_3$ and CH_2Br_2, do deliver halogens to the stratosphere as well (e.g. Atkinson et al., 2012; Montzka et al., 2011; Wingenter et al., 2003).

1.3.2.2 Natural sources and sinks of halocarbons

Several halocarbons have anthropogenic sources of varying importance. For example, anthropogenic sources supply an estimated 25% of $CHCl_3$ to the atmosphere, including by release from HCFC-22 production, paper bleaching and water treatment industries (Montzka et al., 2011). A major source of CH_3Br is as a fumigant, particularly in shipping (Montzka et al., 2011). For other halocarbons, most sources are natural, such as CH_2Br_2 and $CHBr_3$ which are primarily emitted by biogenic marine sources (Law et al., 2006). The Montreal Protocol has resulted in the decrease of anthropogenic emissions of halogenated compounds including CFCs, HCFCs and CH_3Br, with this trend set to continue in the future (Figure 1.1; Montzka et al., 2011). The decreasing anthropogenic burden has raised the importance of understanding natural sources and sinks of halocarbons. The following sections give an overview of the most important biotic and abiotic processes involved in the terrestrial and marine sources and sinks for the main halocarbons of interest to this thesis: CH_3Cl, CH_3Br, CH_3I, CH_2Br_2, $CHCl_3$ and $CHBr_3$.

1.3.2.2.1 Processes of biogenic production

Many natural sources of halocarbons involve biological processes, with many varieties of macro-algae (e.g. seaweed), microalgae (e.g. phytoplankton), plants and fungi found to emit halocarbons (e.g. Forczek et al., 2015; Leedham et al., 2013; Redeker et al., 2004; Sturges et al., 1993). Methyl halides and polyhalide compounds are formed by different processes. Biogenic methyl halides are largely formed by methyltransferase enzyme activity involving a halide ion (Cl^-, Br^- or I^-) and the methyl donor, *S*-adenosyl-$_L$-methionine (Figure 1.2; Paul and Pohnert, 2011; Wuosmaa and Hager, 1990). Methyl halides are produced by the same methyl transferase activity in plants, algae and fungi. In plants and algae it is unclear what role methyl-halide production has. The two primary theories are that it regulates halide levels within an organism's tissues (Ni and Hager, 1999) or that it is a metabolic 'accident' where halides are not the intended methyl-acceptor in the process (Manley, 2002).

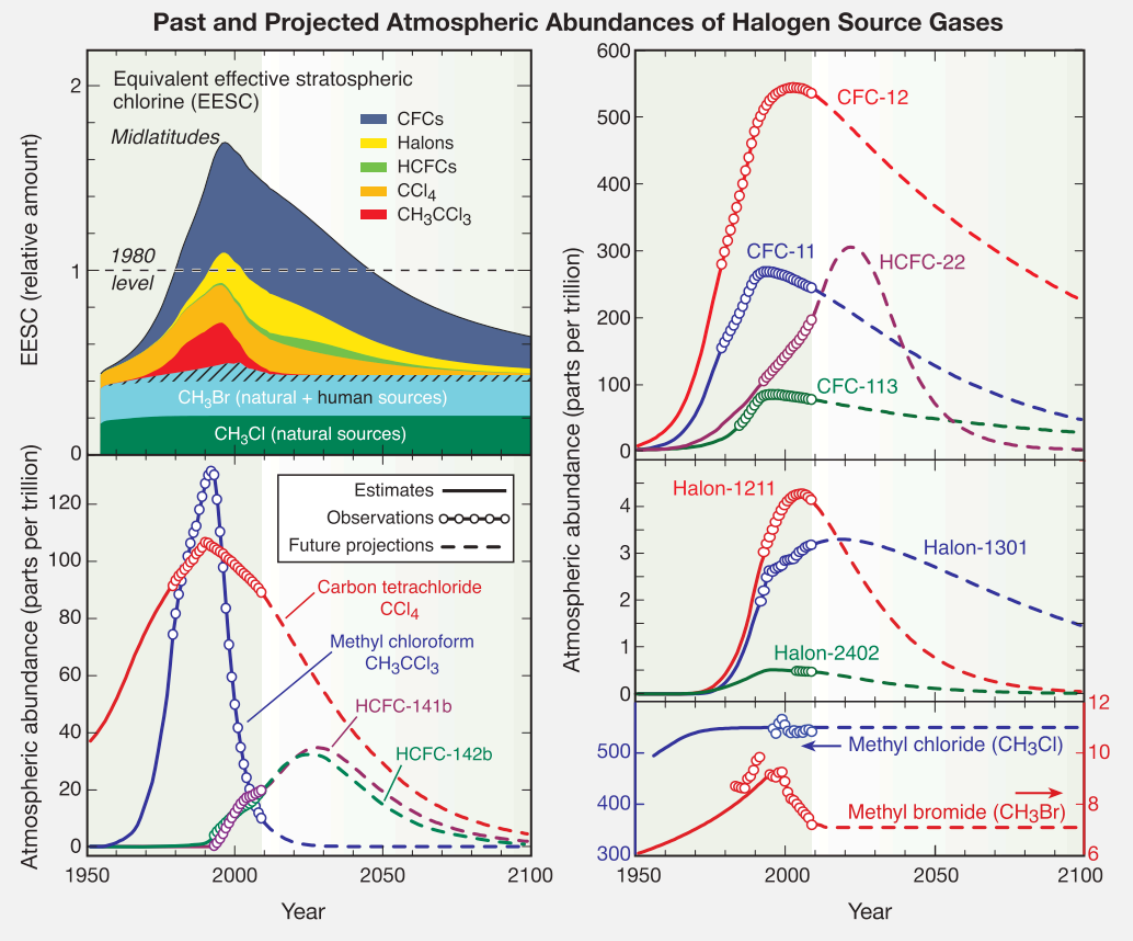

Figure 1.1 Historical and future abundances of halogen source gases in the atmosphere showing the rapid rise in anthropogenic compounds particularly up to the turn of the century, with measurements of declining concentrations of CFCs, CCl_4, CH_3CCl_3 and CH_3Br since the turn of the century due to the Montreal Protocol. The subsequent rise of HCFC and Halon-1301 CFC-replacements has also been observed with their use also predicted to be phased out over time. Natural sources of CH_3Br and CH_3Cl will remain relatively constant over time meaning these natural emissions will be considerably more important by the end of the century. Figure from Fahey and Hegglin (2011).

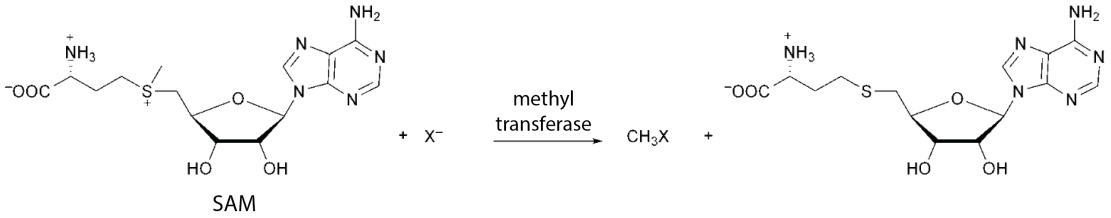

Figure 1.2 The biogenic production of methyl halides by methyl transferase using the methyl donor S-adenosyl-L-methionine (SAM). X = Cl, Br or I. Figure from Paul and Pohnert (2011).

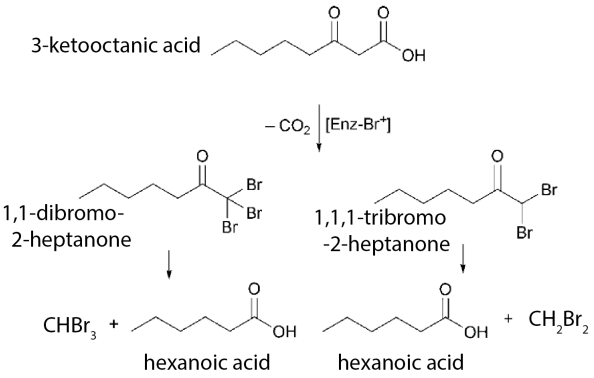

Figure 1.3 Production of $CHBr_3$ and CH_2Br_2 by decarboxylation of 3-ketooctanic acid which is then brominated to two intermediate compounds (1,1-dibromo-2-heptanone and 1,1,1-tribromo-2-heptanone). The intermediate compounds are then hydrolysed to hexanoic acid and $CHBr_3$ or CH_2Br_2. From Paul and Pohnert (2011).

Poly-halide compounds are produced indirectly by haloperoxidase enzymes (HPOs) within algae and fungi (Manley, 2002). HPOs catalyse the reaction between halide ions and hydrogen peroxide (H_2O_2) to create hypohalous acid (HOX) which readily reacts with organic compounds (RH) to produce halocarbons (RX; Wever and van der Horst, 2013). Equation 1.10 shows a simplified example of this process:

Equation 1.10

$$\mathbf{H_2O_2 + H^+ + X^- \rightarrow HOX + H_2O}$$

$$\mathbf{HOX + RH \rightarrow RX + H_2O}$$

Production of CH_2Br_2 and $CHBr_3$ can also occur directly through decarboxylation of 3-ketooctanoic acid, followed by bromination to create an intermediate compound, that is then hydrolysed to a hexanoic acid and CH_2Br_2 or $CHBr_3$ (Figure 1.3; Paul and Pohnert, 2011).

One of the key benefits to the organism of HPO activity and production of polyhalide compounds is that it removes the H_2O_2 generated by photosynthesis, respiration and other processes (Manley and Barbero, 2001). Additionally, it is thought that the production of brominated polyhalomethanes in particular can provide herbivory or microbial defence (Wever and van der Horst, 2013 and references therein).

1.3.2.2.2 Processes of biogenic consumption

Microbial degradation of a wide variety of halocarbons has been identified in environments ranging from deep ocean sediments to Arctic soils (e.g. Atashgahi et al., 2017). The degradation of methyl halides, and methyl chloride in particular, has been well studied with several *cmu* (chloromethane utilisation) genes identified and possible degradation pathways involving methyltransferases proposed. These pathways ultimately result in the methyl group being metabolised to CO_2 (McDonald et al., 2002).

Primarily aerobic bacteria have been identified as using the *cmu* pathway with several able to use CH_3Cl as their carbon and energy source (Doronina et al., 1996). However anaerobic bacterial genomes have also been found to contain *cmu* genes, and some bacteria have been found that can degrade CH_3Cl but which do not have *cmu* genes, suggesting different pathways exist (Jaeger et al., 2018; Nadalig et al., 2014). CH_3Br degradation has also been observed by soil bacteria, including by nitrifying bacteria (Rasche et al., 1990; Shorter et al., 1995), and $CHBr_3$ degradation, as well as cycling to CH_2Br_2, has been observed by marine bacteria (Ichikawa et al., 2015).

1.3.2.2.3 Processes of abiogenic production and consumption

Halomethanes can be abiogenically produced and destroyed. In soils, methyl halides can be produced by the oxidation of organic matter when halides are present, with Fe (III) an example electron acceptor (Figure 1.4; Keppler et al., 2000). Chloroform and bromoform can also be produced by Fe (III) oxidising organic matter, if H_2O_2 is also present (Figure 1.5; Huber et al., 2009). Additionally, abiotic methyl halide production from decaying plant material (e.g. leaf litter) occurs by reaction between methoxyl groups on plant pectin and halide ions present in the plant (Derendorp et al., 2012; Wishkerman et al., 2008).

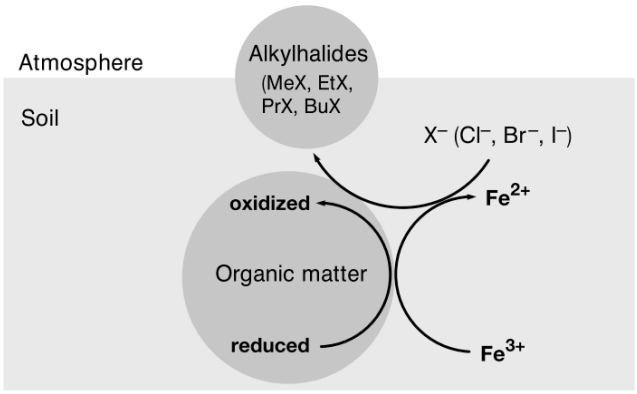

Figure 1.4 Schematic diagram of the abiogenic production of methyl halides (and ethyl, propyl and butyl halides) in soil by the oxidation of organic matter by Fe^{3+} (which is reduced to Fe^{2+}) in the presence of halides (X^-). From Keppler et al., 2000.

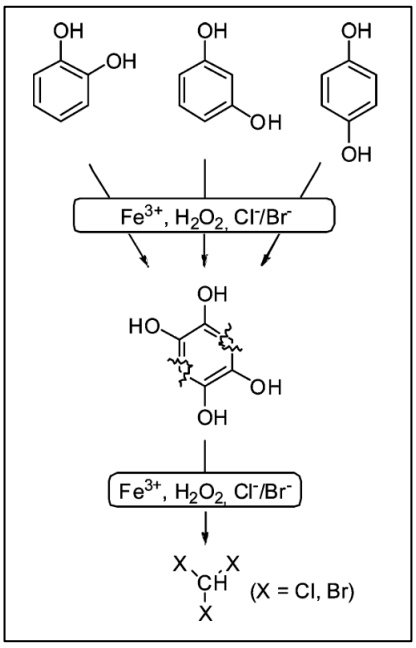

Figure 1.5 Hydrogen peroxide (H_2O_2) and Fe^{3+} produces hydroxyl radicals which hydrolyse the aromatic ring of reduced organic compounds (catechol, resorcin and hydroquinone) to form a hypothesized intermediate compound (1,2,4,5-tetrahydroxyl-benzene). This compound is then chlorinated or brominated with a ring cleavage to form chloroform ($CHCl_3$) or bromoform ($CHBr_3$). From Huber et al., 2009.

Consequently, methyl halide production is higher in plant litter and vegetation of halophytes (plants growing in brackish or saline waters, e.g. mangroves and saltmarshes) and is enhanced by elevated temperatures, particularly during biomass burning (Derendorp et al., 2012; Wishkerman et al., 2008).

In the oceans, abiogenic halomethane production can occur due to photochemically produced methyl radicals reacting with halide atoms or photochemically produced reactive halogen species (e.g. Br•, BrCl, HOI, etc) reacting with dissolved organic matter (Méndez-Díaz et al., 2014; Moore and Zafiriou, 1994). The two major abiogenic destruction processes for most halomethanes is hydroxyl radical reaction and photolysis in the atmosphere (see Section 1.3.2.1). However, halocarbons can also be photolytically destroyed in the oceans (Jones and Carpenter, 2005).

1.3.2.3 The main halocarbons of interest – a summary of sources and sinks

The main halocarbons of interest in this thesis are the methyl halides (CH_3Cl, CH_3Br and CH_3I), dibromomethane (CH_2Br_2) and the two haloforms ($CHCl_3$ and $CHBr_3$). A combination of the biotic and abiotic processes previously described are involved in the emission and consumption of each compound. Simultaneous production and destruction of halomethanes has been identified in many environments (e.g. Jaeger et al., 2018; Rhew et al., 2010). The balance between these processes determines the direction and magnitude of a compound's net flux from marine and terrestrial environments. There are

some general patterns of note in the sources and sinks of the primary compounds of interest (Table 1.1). The methyl halides, CH_2Br_2 and $CHBr_3$ all have multiple marine sources, with the polybromide compounds almost exclusively marine in origin (Law et al., 2006). The exception for $CHBr_3$ is the marginal marine habitat of salt marshes (Wang et al., 2016), organic matter oxidation in soil (Huber et al., 2009) and emission from rice paddies (Redeker et al., 2003). CH_2Br_2 is almost exclusively marine, with one recording of unquantified CH_2Br_2 emission by temperate peatlands (Dimmer et al., 2001). In contrast, CH_3Cl and CH_3Br have a wide variety of terrestrial sources. CH_3I shares half of these terrestrial sources, with rice paddy emission the most important terrestrial source, however, it is primarily produced in marine environments (Law et al., 2006; Lee-Taylor and Redeker, 2005). Marine algae do produce $CHCl_3$, but global sources are dominated by terrestrial environments (Nightingale et al., 1995). The open ocean is a general sink for most compounds, with soil bacteria a sink for the methyl halides (Doronina et al., 1996; McDonald et al., 2002).

Despite the considerable research of the past few decades into the natural sources and sinks of these gases, their atmospheric budgets remain unbalanced, for example, net sinks outweigh sources for CH_3Cl and CH_3Br (Carpenter et al., 2014). This is partly due to spatial and temporal variability of most natural sources and sinks. For example, biogenic production processes in temperate and polar regions are strongly seasonal and huge varieties in halocarbon production rates can exist between species of one type of organism, e.g. in macroalgae (Dimmer et al., 2001; Leedham et al., 2013; Yokouchi et al., 2008). As a result, the calculation of global sources or sinks are commonly reported with large ranges, e.g. the global CH_3Cl source from salt marshes is estimated at 85 Gg yr^{-1}, with a range of 1.1–170 Gg yr^{-1} (Carpenter et al., 2014). Additional studies understanding variability in natural fluxes would help to reduce these uncertainties.

Table 1.1 Known natural sources and sinks (non-atmospheric) for the compounds of interest are marked with (✓).

	CH_3Cl	CH_3Br	CH_3I	CH_2Br_2	$CHCl_3$	$CHBr_3$
Sources: Marine						
Macroalgae	✓ [1]	✓ [1]	✓ [1,2,3]	✓ [2,3,4]	✓ [3]	✓ [3,4,5]
Microalgae	✓ [6]	✓ [6, 7]	✓ [6,7]	✓ [8,9]	✓ [7]	✓ [8,10]
Bacteria	✓ [11]	✓ [11]	✓ [11,12]	✓ [12,13]		✓ [12]
Open ocean	✓ [14]	✓ [15]	✓ [16,17]	✓ [16]		✓ [16,17]
Seagrass meadows	✓ [18]	✓ [18]	✓ [19]			✓ [19]
Sources: Terrestrial						
Salt marsh/ coastal wetlands	✓ [20]	✓ [20]			✓ [21]	✓ [21]
Mangroves	✓ [22, 23]	✓ [23]	✓ [23]			
Peatlands, temperate	✓ [24, 25]	✓ [24]		✓ [24]	✓ [24, 25]	
Grasslands, polar (tundra)					✓ [26]	
Shrubland	✓ [27]	✓ [27]			✓ [28]	
Forest soils, temperate	✓ [29]	✓ [29]	✓ [29]			
Plants, tropical - temperate	✓ [30]				✓ [31]	
Rice paddies	✓ [32]	✓ [32]	✓ [32]			✓ [33]
Fungi	✓ [34]	✓ [34]	✓ [34]			
Organic matter oxidation	✓ [35]	✓ [35]	✓ [35,36]		✓ [37]	✓ [37]
Plant matter decay	✓ [38]	✓ [39]				
Sinks: Marine						
Open ocean	✓ [14]	✓ [15]	✓ [17]			✓ [13, 17]
Sinks: Terrestrial						
Soil: oak-savanna	✓ [40]	✓ [40]				
Soil: grassland, polar (tundra)	✓ [41]	✓ [41]	✓ [41]			
Soil: peatland, temperate		✓ [25]				
Phyllosphere (tropical, temperate)	✓ [42]					

[1] (Laturnus et al., 1998); [2] (Mithoo-Singh et al., 2017); [3] (Nightingale et al., 1995); [4] (Leedham et al., 2013); [5] (Keng et al., 2013); [6] (Scarratt and Moore, 1996); [7] (Scarratt and Moore, 1999); [8] (Atkinson et al., 2014); [9] (Tokarczyk and Moore, 1994); [10] (Sturges et al., 1992); [11] (Fujimori et al., 2012); [12] (Karlsson et al., 2008); [13] (Ichikawa et al., 2015); [14] (Hu et al., 2013); [15] (Hu et al., 2012); [16] (Ziska et al., 2013); [17] (Chuck et al., 2005); [18] (Weinberg et al., 2013); [19] (Weinberg et al., 2015); [20] (Rhew et al., 2014); [21] (Wang et al., 2016); [22] (Kolusu et al., 2018); [23] (Manley et al., 2007); [24] (Dimmer et al., 2001); [25] (Khan et al., 2012); [26] (Rhew et al., 2008b); [27] (Rhew et al., 2001); [28] (Rhew et al., 2008a); [29] (Redeker and Kalin, 2012); [30] (Jaeger et al., 2018); [31] (Forczek et al., 2015); [32] (Redeker and Cicerone, 2004); [33] (Redeker et al., 2003); [34] (Redeker et al., 2004); [35] (Keppler et al., 2000); [36] (Amachi et al., 2001); [37] (Huber et al., 2009); [38] (Derendorp et al., 2012); [39] (Wishkerman et al., 2008); [40] (Rhew et al., 2010); [41] (Rhew et al., 2007); [42] (Farhan Ul Haque et al., 2017).

1.3.2.4 Halocarbons in the Arctic

The geography of the Arctic means that the area of the ocean compared to the area of the land is relatively large and as such the halocarbon sources of importance shift primarily to the marine environment. Several brown, green and red macroalgal species have been measured emitting $CHBr_3$, CH_2Br_2 and other halocarbons in the Arctic, with brown macroalgal species having the highest emission rates and biomass (Laturnus, 1996). Emission of methyl halides has also been observed, with rates of CH_3Cl being the highest, but emissions are generally restricted to fewer species, compared to lower but more ubiquitous release of CH_3Br and CH_3I (Laturnus et al., 1998). Polar macroalgal species generally have rates of emission that are more than two times lower than temperate or tropical species, meaning Arctic emissions are not globally important as a source of halocarbons to the atmosphere (Laturnus, 2001). However, they can be locally important sources due to high rates of emission along coastlines where their biomass is concentrated (Laturnus, 2001).

Sea-ice microalgae are important halocarbon emitters in the Arctic, with evidence of significant CH_2Br_2, $CHBr_3$ and CH_3I emission, among other halocarbons (Atkinson et al., 2014; Sturges et al., 1992; Tokarczyk and Moore, 1994). Microalgae colonise the underside of sea-ice, meaning halocarbon emissions to the air occur via cracks in the ice and during seasonal ice melt (Atkinson et al., 2014; Sturges et al., 1992). This source will be reduced with continued sea-ice loss in the future. Photochemical reactions in snow, including that covering sea-ice, glaciers, ice-sheets and land, can also generate a range of halogenated compounds including the methyl halides (Swanson et al., 2007). Additionally, microbial production of CH_3I and CH_3Cl has been identified in the snowpacks of glaciers in the Arctic and Antarctica (Redeker et al., 2017).

Terrestrial Arctic sources of halocarbons are more limited, but studies have shown emission of $CHCl_3$ from Arctic tundra in Alaska, which, when scaled-up to the global tundra area, could account for 1-2 % of global atmospheric $CHCl_3$ (Rhew et al., 2008b). $CHCl_3$ emissions from tundra soils have also been recorded in western and southern Greenland and northern Norway (Albers et al., 2017). Further, the Arctic tundra sink of CH_3Cl and CH_3Br is thought to be regionally important based upon extrapolations of measurements made in the Alaskan Arctic (Rhew et al., 2007). Other non-atmospheric

sinks, include ice-free oceans during the winter, e.g. the North Atlantic, which acts as a sink for CH_3I (Stemmler et al., 2014).

In addition to *in situ* Arctic sources, the source of many gases in the Arctic troposphere and stratosphere is by long-range transport from lower latitudes. This includes pollutants (e.g. CFCs), particularly from Europe (but also Russia and, more rarely, North America), and longer lived natural compounds whose major sources are in the tropics and temperate regions, e.g. a major source for CH_3Cl is tropical plants (Beine et al., 1996; Stohl, 2006; Yokouchi et al., 2000).

The primary atmospheric sinks of the methyl halides, dihalomethanes and haloforms are oxidation by hydroxyl radicals and UV photolysis (Section 1.3.2.1). The main atmospheric formation mechanism of hydroxyl radicals (OH•) is O_3 photolysis by UV light (photons, *hv*, wavelengths < 330 nm) in the presence of water vapour (Equation 1.11):

Equation 1.11

$$\mathbf{O_3 + h\nu \rightarrow O(^1D) + O_2}$$

$$\mathbf{O(^1D) + H_2O \rightarrow 2OH\bullet}$$

OH• are highly reactive, with an average tropospheric lifetime of 1-2 seconds. They oxidize reduced or partially reduced gases, including volatile organic compounds (VOCs) such as CH_4 (Stone et al., 2012 and references therein). OH• can also be 'recycled', that is, it initiates reaction chains involving the oxidation of VOCs and nitrous oxide (NO; important in polluted regions) which ultimately result in the (re-)generation of OH• (Lelieveld et al., 2016). Because OH• generation is primarily driven by light, both of the major atmospheric sinks of the halocarbons of interest here are also driven by the presence of sunlight. Therefore, these sinks are strongly seasonal in the Arctic, due to the occurrence of complete darkness in the polar night (at high latitudes) and 24-hour daylight in the summer.

1.3.2.5 The proglacial environment

Identified halocarbon sources and sinks in the Arctic are primarily marine (Section 1.3.2.4), with tundra the only terrestrial source that has been investigated (Albers et al., 2017; Rhew et al., 2007, 2008b). In the High Arctic, north of the tree line, tundra plants are the climax community of the ecological succession which begins on the new soils

exposed by retreating glaciers. In glacierised areas, increased distance from the ice front is roughly analogous to increased soil exposure age (i.e. a 'chronosequence'), and thus the microbial colonisation and succession to higher plants can be studied across proglacial forefields (Vetaas, 1994). The newly exposed land surface is composed of glacial deposits which range from large clasts or erratics to fine-grained sediments composed of ground bedrock and minerals which lack organic matter (Moreau et al., 2008). As a result, colonisation and succession are influenced by the mineralogy of the exposed soils which can impact geochemical variables, such as soil pH (Gray et al., 2014). Nutrient inputs are from a range of sources, including supraglacial run-off and snow-melt, subglacial sediments, atmospheric deposition, input from birds and animals and production by colonising microbial communities (Figure 1.6; Bradley et al., 2014).

Bacteria and archaea are the early colonisers on new proglacial land surfaces, which produce nutrients autochthonously and stabilise the soil through the formation of soil crusts (Hodkinson et al., 2003; Kateřina et al., 2013). Cyanobacteria, including *Nostoc* spp., are particularly important for the formation of soil crusts, forming visible mats and playing a key role in nitrogen fixing (Bradley et al., 2016; Hodkinson et al., 2003; Kastovská et al., 2005). Following soil stabilisation and nutrient fixation, vascular plants appear, with increasing diversity on older and more developed soils (Moreau et al., 2008). In the High Arctic, cooler temperatures and a shorter growing season means the succession to vascular plants is slower than for lower Arctic and Alpine glaciers, resulting in the persistence of lichens and cyanobacteria even in soil exposed for more than 100 years (Hodkinson et al., 2003).

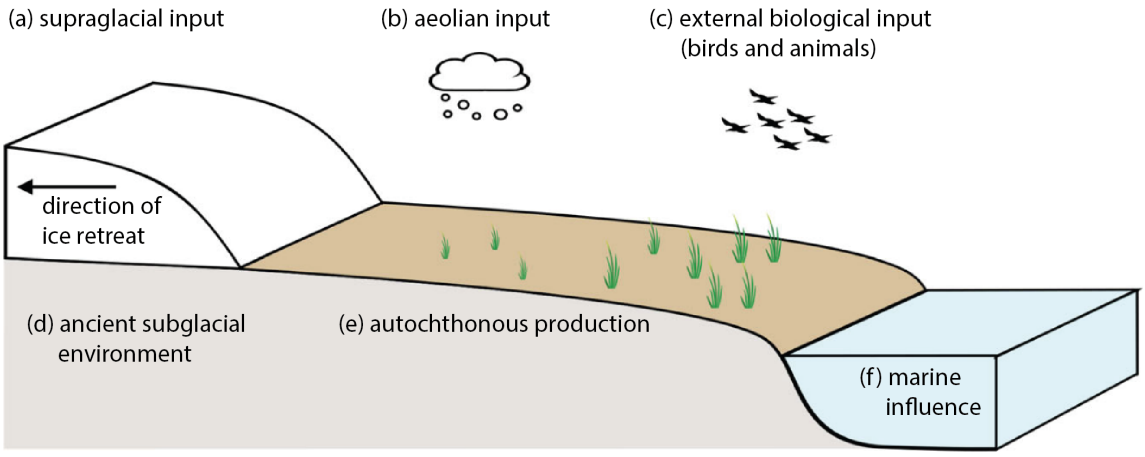

Figure 1.6 Schematic diagram of nutrient inputs to a glacial forefield. From Bradley et al., 2014.

1.3.3 Summary

In recent decades, interest in the subglacial microbial environment and subglacial chemical weathering has greatly increased. It is recognised that several trace gases play key roles in isolated microbial ecosystems and in chemical weathering processes. However, with the exception of a sole study which determined that rock-water reactions could generate hydrogen at subglacially relevant temperatures (Telling et al., 2015), the minerals in bedrock and sediments are an unquantified source of trace gases to the subglacial environment. This is despite the fact that several trace gases with roles in subglacial microbial ecosystems (e.g. CH_4, H_2, CO_2) and chemical weathering (CO_2) can be either released or generated by fracturing rocks and/or minerals (e.g. Deeds et al., 2015; Wang et al., 2015; Zhang et al., 2014). Glaciers are efficient at eroding rocks and sediment (Hallet et al., 1996) and thus the mechanical breakdown of rocks and minerals in the subglacial environment should be investigated as a potential source of trace gases.

Natural sources and sinks of halocarbons are contributing an increasing proportion of halogens to the atmosphere due to the continued phase-out of anthropogenic halogenated gases (Montzka et al., 2011). There is a need for greater spatial variability of natural flux measurements, particularly across data-poor regions of the globe, such as the Arctic. Transitional terrestrial environments have been little explored for their influence on trace gas fluxes, thus recently exposed proglacial land surfaces with their transition from development of soil and succession of communities of microbes and higher species, provides an opportunity to investigate this.

Interpretation of long-term datasets of natural halocarbons has generally focussed on low and mid-latitudes where the major sources are (e.g. O'Doherty et al., 2001; Simmonds et al., 2004). Analysis of long-term datasets at high latitudes primarily focuses on long-range transport of pollutants (Beine et al., 1996; O'Doherty et al., 2009) and/or gas species that influence major atmospheric phenomena, for example the spring ODEs (Barrie et al., 1988; Yang et al., 2010). Therefore, interrogating a long-term dataset of methyl halides, dihalomethanes and haloforms for evidence of natural Arctic sources and sinks will provide valuable context to the investigation of halocarbon sources from proglacial surfaces.

2 Methodological and data overview

The following sections provide an overview of the methods employed in this thesis and describe the development and testing of equipment and the optimisation of instruments conducted prior to results gathering. Detail of the methodologies used are provided in Chapters 3, 4 and 5 in sections 3.3, 4.3-4.4, and 5.3, respectively.

2.1 Rock grinding experiments

2.1.1 Rock grinding equipment

Experiments were conducted to simulate the grinding of rocks by glacial abrasion in Chapter 3. This was done using a ball mill (Fritsch Planetary Mono Mill Pulverisette 6) which rotates a zirconium-oxide mill containing 3 balls of the same material and approximately 10 g of pre-crushed sample at 500 rpm. The mill's lid had been modified with two valves to allow flushing of the headspace with an inert gas, here Argon (5.0 Grade, with in-line desiccator), and to allow direct sampling of the headspace through a septum (Figure 2.1). A PTFE o-ring formed an air-tight seal between the mill and the lid. Analysis of the mill's headspace determined that flushing the sealed mill for 1.5 minutes at 30 psi with Argon removed all traces of the gases of interest to this study, with the exception of the trace CO_2 (0.3 nmol g^{-1}, equivalent) present in the Argon gas. Removal of the gases of interest prior to grinding lowered the limit of detection of these compounds during the experiment. Additionally, conducting the experiments under an inert atmosphere removes possible reactants from the headspace, especially water vapour and oxygen.

Sampling of the headspace from the ball mill (during tests and during the experiments) was conducted using a 5 mL gas-tight syringe (Hamilton) with a Luer Lock fitting which was flushed 3 times prior with 5.0 grade Argon. The syringe was over-pressurised with Argon and fitted with a needle (21 gauge; BD). The plunger of the syringe was depressed to 5 mL and the over-pressurised Argon released whilst hovering over the septum before immediately plunging the needle through septum. This flushed the needle with Argon whilst also

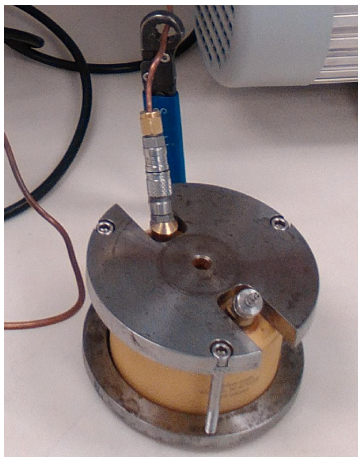

Figure 2.1 Ball-mill inside metal clamp connected to Argon gas line via a valve for headspace flushing. Mill diameter is 9 cm.

ensuring that the 5 mL of Argon injected into the mill was at ambient pressure. The 5 mL of Argon was then injected rapidly (to flush rock dust from the valve) into the ball mill and was then mixed thoroughly with the headspace using the syringe. 5 mL of mixed headspace gas was removed with the syringe and injected into the gas chromatograph for analysis. The dilution from the added 5 mL of Argon was corrected for in the experimental results. This sampling procedure was tested (n = 3) with the ball mill flushed and empty and showed no detectable ingress of lab air.

Cleaning of the ball mill between each grinding was conducted by twice grinding 10 g of sand ('extra pure, low iron', 20-30 mesh; Fischer Scientific) for 2 minutes at 500 rpm to remove any compacted ground material from the inside of the ball mill. The valves were then cleaned using pressurised gas and the ball mill was brushed with a soft clean brush to remove any final traces of rock dust.

Sample descriptions, sample preparation, the grinding experiments and the procedural blank are described in detail in Sections 3.3.1-3.3.2.

2.1.2 Analysis of gas samples by a gas chromatograph (GC)

Gas samples taken from the mill were analysed on a gas chromatograph (GC). The gases of interest in the rock-grinding experiments were primarily: methane (CH_4), carbon dioxide (CO_2), ethane (C_2H_6), ethylene (C_2H_4), propane (C_3H_8) and hydrogen (H_2). Oxygen (O_2) and nitrogen (N_2) were also measured in each analysis to ensure that the ball mill had not leaked during grinding or sampling. Gas samples from the proglacial experiments (Chapter 4) were also analysed for CO_2 and CH_4 using the same GC.

2.1.2.1 The Gas Chromatograph

The gas chromatograph (GC) used here was an Agilent 7890A with a methaniser and two detectors: a flame ionising detector (FID) and a temperature-controlled detector (TCD). Prior to analysis, the FID was lit and both detectors were raised to their operating temperatures of 300 ^{o}C for the FID and 250 ^{o}C for the TCD for at least 1 hour to allow the baseline to stabilise. The carrier gases required for operation of the GC were argon (for the TCD and associated column), helium (for the FID and associated column), hydrogen (for the methaniser) and air (to keep the FID's flame lit).

Samples and standards were injected into the GC via 2 sample loops: a 0.5 mL loop leading to the FID column and a 1 mL loop leading to the TCD column. The slightly

larger volume loop used for TCD column allowed for a lower limit of detection for H_2. 5 mL of sample or standard was used to adequately flush the loops 3 times. Immediately after injecting the sample/ standard onto the loops, the GC run was started, switching the valve to which the loops were attached and injecting the sample/ standard onto the columns.

The columns separate the compounds so that each elutes as a distinct peak and, thus, can be identified and quantified accurately. A molecular 5a, 60-80 mesh, 8ft x 1/8-inch column was used to separate the compounds detected by the FID, which elute in this order: CH_4, CO_2, C_2H_6, C_2H_4, C_3H_8. The methaniser (at 395 ºC) converts CO_2 to CH_4 by reaction with hydrogen to enable its detection by the FID. The CH_4 generated by the methaniser from CO_2 elutes after the CH_4 naturally present in the sample. A Haysep D 80-100 mesh, 2m x 1/8-inch SS column was used to separate compounds detected by the TCD which elute in this order: helium (He), H_2, O_2 and N_2.

2.1.2.2 Identification and quantification

Identification of compounds was by retention time and by comparing to a standard with known concentrations (± 5 %) of the following compounds: CH_4, CO_2, C_2H_6, C_3H_8, n-butane, iso-butane, He, H_2, O_2 and the balance with N_2. The standard was run at least twice daily, with one always at the start of the day (to ensure the GC was running optimally) and one at the end of the day to detect any changes in the GC's operation over the analysis period.

To calculate the concentration of the samples, a standard curve was created by analysing manual dilutions of the standard. This was conducted using a 118.5 mL clean, dry, borosilicate serum vial with a thick butyl rubber stopper which was flushed for 3 minutes with Argon, then injected with 25, 10, 5, 2, 1, 0.5 or 0.1 mL of the mixed standard. 5 mL of this mixture was then analysed on the GC (using an Argon flushed gas tight syringe) and the peak area measured. The manual dilutions were run in triplicate. The concentration of the gases in the vial were calculated and compared to the peak areas showing that peak area was linear to concentration with an $R^2 > 0.99$ for all gases (Figure 2.2). The limit of detection was also determined by this method as the last concentration detectable by mixing. CH_4 and CO_2 were still detectable when only 0.1 mL of standard was used, but both peaks were small. Therefore, the limit of detection of CH_4 and CO_2 was assumed to be less than the concentration of standard in the 0.1 mL mix (0.2 and 0.3

ppm, respectively). The detection limit for all gases of interest is shown in Chapter 3 (Table 3.2). Additionally, the detection limit for O_2 and N_2 was calculated as 0.08 and 0.06 %, respectively.

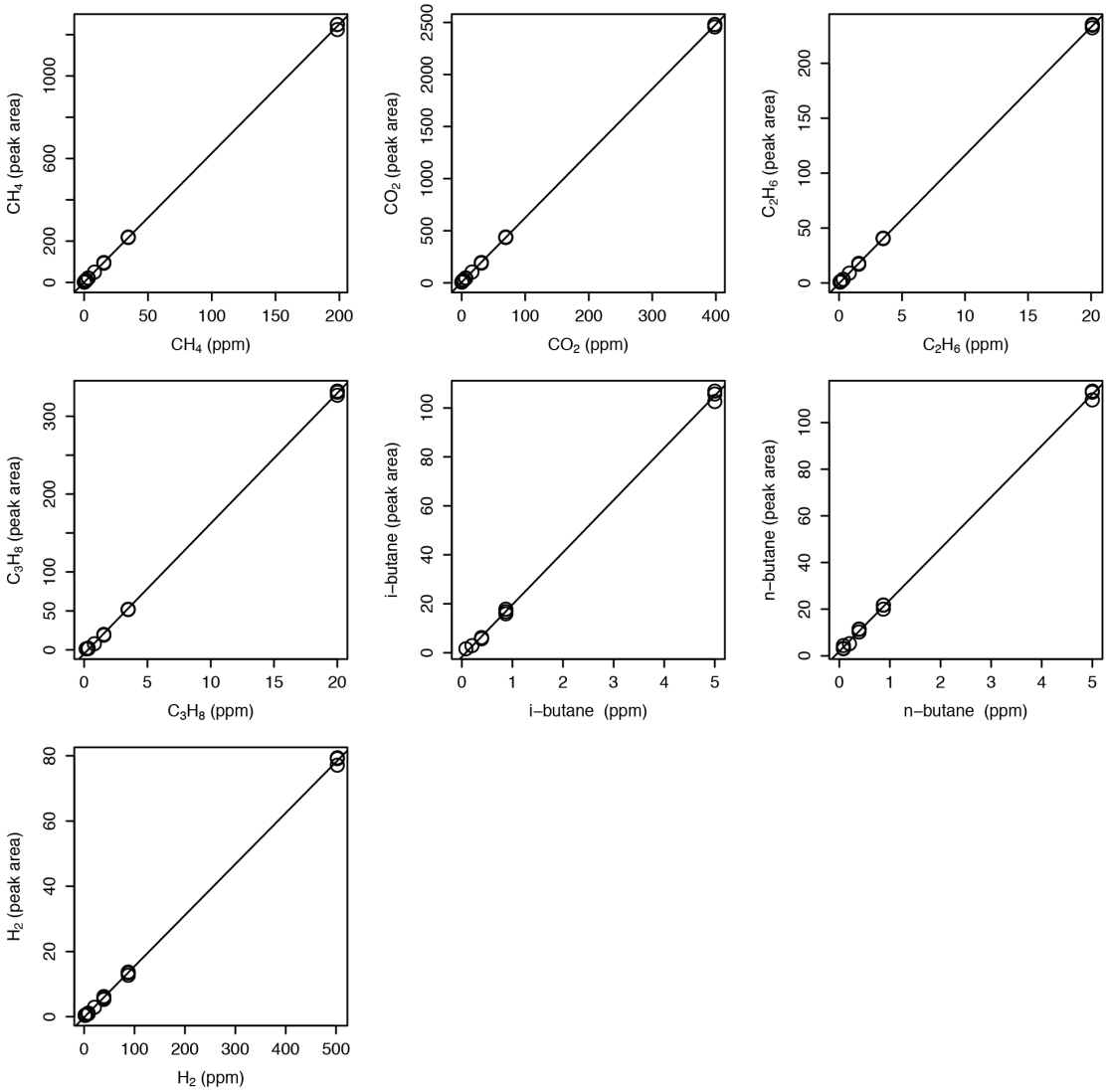

Figure 2.2 Peak area versus calculated concentrations (ppm) of each gas present in the manual dilutions of the mixed standard as analysed on the GC. Each dilution was run in triplicates (open circles). The solid line represents the linear regression line between peak area and gas concentration. All had an $R^2 > 0.99$.

2.2 Fieldwork

2.2.1 Overview of field site and experiments

Fieldwork was conducted at Midtre Lovenbreen (78º 53' N, 12º 04' E), a small (~ 5.4 km^2) polythermal glacier in Kongsfjorden, Svalbard (Figure 2.3). The glacier has been well studied, due to its proximity to the research town of Ny-Ålesund (~ 4.5 km). This has provided records of mass-balance since 1950 showing continual loss, with aerial photography and carbon dating records mapping the approximately 1.1 km of glacial retreat over the last ~100 years (Hodkinson et al., 2003; Kohler et al., 2007; Moreau et al., 2008). Additionally, studies have been conducted on ecological succession on the forefield (Hodkinson et al., 2003) and on various aspects of glacial hydrochemistry (e.g. Hodson et al., 2000; Irvine-Fynn and Hodson, 2010). Further detail on the field site is provided in Section 4.3.

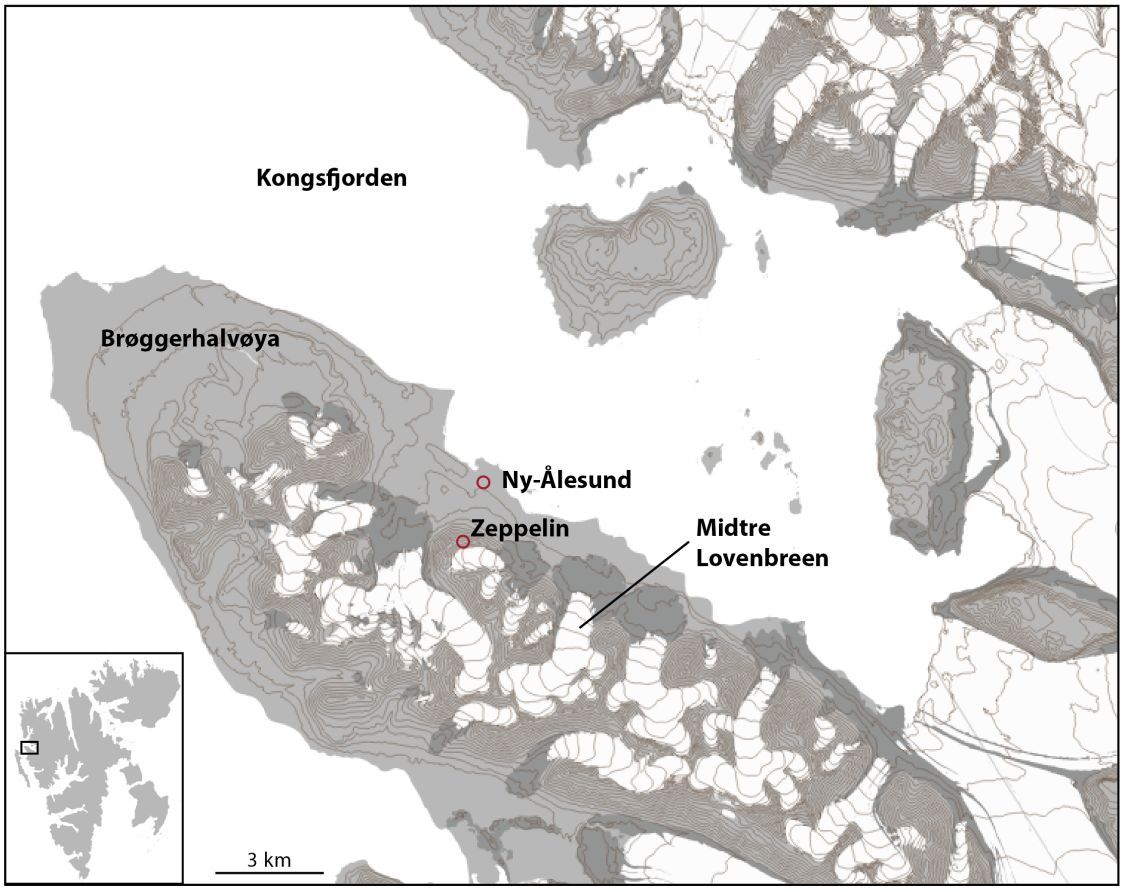

Figure 2.3 Map of the Broggerhalvøya peninsula showing the location of the research town Ny-Ålesund, the study glacier used in Chapter 3 and 4 (Midtre Lovenbreen) and the atmospheric Zeppelin observatory where data used in Chapter 5 was measured. Data used to create the base map from: Norwegian Polar Institute (2014).

Fieldwork at Midtre Lovenbreen was conducted in 2016 and 2017. The 2016 field season had two objectives: the collection of rock samples and discharge data which were required for Chapter 3, and to conduct initial trace gas measurements on the proglacial forefield for Chapter 4. The 2017 field season built upon the proglacial work conducted in 2016 and provides the dataset for Chapter 4. The field equipment and experimental design used for the proglacial measurements were modified between the 2016 and 2017 field seasons, as detailed in the following sections.

The Zeppelin atmospheric observatory (78° 54' 29" N, 11° 52' 53" E) is located on Zeppelinfjellet mountain (475 m a.s.l), 2 km south of Ny-Ålesund and 4 km northwest of the Midtre Lovenbreen proglacial field site (Chapter 4; Figure 2.3). The observatory, among other functions, provides a long-term, high-frequency record of halocarbon concentration in the troposphere as part of the Advanced Global Atmospheric Gases Experiment's (AGAGE) network of monitoring stations. It is operated by the Norwegian Institute for Air Research (Norsk Institutt for Luftforskning; NILU).

2.2.2 Collection of rock samples

For the rock-grinding experiments conducted in Chapter 3, rock samples needed to be obtained from glacial catchments with a wide range of geologies. Therefore, in addition to the rock samples already obtained from Greenland and Canada (by Jon Telling and Mark Skidmore), samples were collected from Midtre Lovenbreen catchment in 2016. Midtre Lovenbreen catchment has a mixed lithology with both metamorphic and sedimentary rock types present. The sedimentary rocks lie beyond the glacier's snout. The glacier is underlain with metamorphic rocks of the Neilsenfjellet formation which consists of pre-Devonian basement rocks from the lower amphibolite facies (Challinor, 1967). The dominant rock types of this formation are phyllite, mica-schist and quartzite (Saalmann and Thiedig, 2002). Schist and quartzite samples were obtained for the rock grinding experiments in Chapter 3. Phyllite samples were not obtained because whole pieces were difficult to collect due to the rock's vulnerability to shattering under freeze-thaw conditions. Discharge data and suspended sediment samples were also collected from the Midtre Lovenbreen catchment in 2016 to enable calculation of catchment-wide gas-generation rates for Chapter 3 and are described there in detail (Section 3.3.5).

2.2.3 Proglacial gas flux experimental design and modification

The proglacial field work centred around the measurement of halocarbon gas fluxes from different land surfaces exposed by the retreat of Midtre Lovenbreen. Dynamic flux chambers were designed to measure the gases. These were deployed in 2016 in preliminary experiments to test whether halocarbon fluxes were measurable at the site, and then modified for the 2017 experiments. The original chambers were composed of a single cylindrical piece of Perspex (height 30 cm; wall width 1 cm; internal diameter 39 cm) with a circular piece of Perspex glued to one end as a lid. Perspex was chosen for its robustness, lack of halogens in its chemical structure (unlike many plastics) and light transmitting properties (transmission of visible-spectrum and near ultraviolet light) as the chambers were originally designed so experiments could be conducted in the light. However, experiments were ultimately conducted solely in the dark by covering the chambers with an opaque reflective material to minimise heating of the chambers in direct sunlight.

To enable sampling from the chambers whilst embedded in the sediment/ soil surface, two sampling ports were created by drilling two ¼ inch holes (British Standard Pipe threading; BSP) in the top of the lid to accommodate ¼ inch polypropylene BSP to Luer lock adapters (Cole-Parmer). Attached to each adapter were Luer lock three-way stop-cocks (high-density polyethylene; HDPE, Cole-Parmer) which controlled air movement through these sampling ports into the chamber. From one port, 20 cm of polypropylene tubing was wedged into the BSP-Luer lock adapter using PTFE tape to make a seal. The addition of tubing to one port staggered the heights of the port and so encouraged circulation of the headspace air during sampling. These chambers were inserted directly into the sediment surface for the preliminary experiments (Figure 2.4a). During the original 2016 experiments, the chambers were left in the sediment for 5 hours, and sampling was conducted at 2 and 5 hours after chamber placement. These preliminary experiments demonstrated that measurable change in chamber headspace gas concentration occurred within 2 hours. Therefore, the experiments were shortened to a maximum of 2 hours for the 2017 experiments, with measurements conducted after 1 and 2 hours. The chambers were modified for the 2017 experiments by cutting a 7 cm section off the bottom of each chamber to create a separate collar that could be placed in the sediment or soil the day before the experiments were conducted (Figure 2.4b). This allowed any gases disturbed when breaking the sediment/ soil surface during chamber

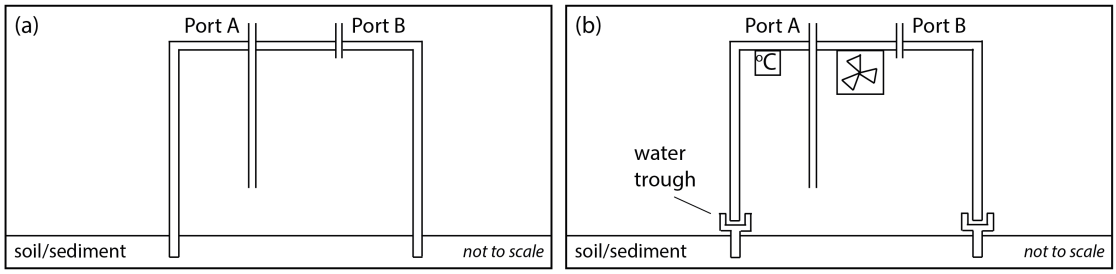

Figure 2.4 Schematic diagram of the chamber set-up used in preliminary proglacial gas flux experiments in 2016 (a) and the modified chamber set-up used in 2017 (b) which consisted of a chamber top and a collar which was embedded in the soil/sediment with a water trough to create a gas-tight seal between the top and the collar. The modified set-up also contained a temperature logger and a fan. Sampling was conducted through Port A, with a sample bag of 'blank' air attached to Port B to maintain ambient pressure.

placement to re-equilibrate with the ambient atmospheric concentration. To seal the chamber top to the collar, an 'H' shaped trough (Perspex) was attached to the top of the collar. The trough was filled with deionised water and the chamber-top was placed within it to create a completely inert seal. Additional modifications for the 2017 experiments included the addition of a Tinytag temperature logger and a small fan (24 m^3 h^{-1}) to enable monitoring of the headspace temperature and prevent stratification of the headspace air, respectively (Figure 2.4b). The experiments that were conducted for Chapter 4, are described in detail in Section 4.4.1.

2.3 Analysis of halocarbon trace gases

2.3.1 Introduction to trace gas analysis

The halocarbons are halogenated volatile organic compounds which are present in the atmosphere at parts per trillion by volume (pptv). Their low concentration makes halocarbons harder to analyse than the more abundant trace gases such as CH_4 and CO_2 which, as discussed above (Section 2.1.2) can be analysed quickly (< 25 minutes) by GC with comparatively simple detectors (FID and TCD). To analyse these lower concentration gases, the more sensitive Gas Chromatograph Mass Spectrometer (GCMS) can be used. However, pre-concentration is still required for compounds with very low concentrations (sub-pptv to pptv). Pre-concentration was originally done by cryo-trapping air with liquid nitrogen but this system was challenging to maintain and operate. Thus, the ADS-GCMS (Adsorption Desorption System – Gas Chromatograph Mass Spectrometer) was developed at the University of Bristol as a system that did not require liquid nitrogen and which allowed automated, routine analysis of low concentration compounds (Simmonds et al., 1995). The ADS-GCMS which was used for trace gas analysis in this thesis is described in detail in the following section.

2.3.2 The Adsorption Desorption System – Gas Chromatograph Mass Spectrometer

2.3.2.1 Description of the Adsorption Desorption System

The Adsorption Desorption System (ADS) pre-concentrates a 1-2 litre whole-air sample for analysis of low concentration compounds by GCMS. Standards, blanks and samples are connected to the ADS by a series of Swagelok ports and are selected by a 6-port 6-position valve (Valco). The standard used in Chapter 4 was a calibrated working-air standard of 'clean' air from the Zeppelin observatory in Ny-Ålesund (details in Chapter 4, Table 4.1). The blank was a cylinder of synthetic air (grade 5.0, ultra). The samples were collected in 3 L Tedlar gas-tight sample bags (see Chapter 4, Section 4.4.3 for detailed sampling methodology). Because the samples were in unpressurised sample bags, a small bellows pump inside the ADS was used to draw samples in through the 6-position valve. The pump was not required for the standard and the blank which were both in pressurised cylinders. The flow of the samples, standards and blanks (hereafter, the analyte) was maintained at a rate of 50 mL min^{-1} by a mass flow controller (MFC, Tylan). Water is removed from the analyte by flowing through a Nafion permeation drier

with a continuous counter-purge of dry 5.0 ultra grade synthetic air at 170 mL min^{-1}. The Nafion membrane is impermeable to most compounds except strongly polar compounds (e.g. water and nitrous oxide) resulting in their removal. The analyte is then directed onto the microtrap by a second valve (6-port, 2-position) which controls the flow of gas through the microtrap (normally helium carrier gas, 5.0 grade with Universal Trap, when not trapping analyte). The analyte is condensed onto the microtrap which is an absorbent-filled (5 mg Carbotrap, 5 mg Carboren 1003 and 4 mg Carboxen 1000), thin-walled (0.068 cm id, 0.109 cm o.d.), stainless steel (type 304) tube held at -50 ^{o}C during trapping. Compounds such as the halocarbons, CFCs and HFCs are trapped, whereas more volatile compounds, such as CH_4, CO_2 and formaldehyde (CH_2O), are lost. The temperature of the microtrap is controlled by a pair of thermo-electric Peltier devices which can achieve minimum temperatures of -50 ^{o}C by transferring electric current across the device to cool one side. The volume of analyte trapped on the microtrap is controlled by the constant flow rate of 50 mL min^{-1} and the length of trapping time. After trapping is complete, a third valve (6-port, 2-position) switches to reverse the flow of the helium carrier through the microtrap and inject the condensed analyte onto the GC column. Using electrical resistance, the microtrap was heated to 240 ^{o}C for 30 seconds to desorb the concentrated analyte which passes into the GC via a transfer line held at 100^{o}C.

2.3.2.2 Description of the Gas Chromatograph Mass Spectrometer

The gas chromatograph mass spectrometer (GCMS) used with the ADS was a HP 6890 series (version A.03.08) GC and an HP 5973 MS. The method by which the GCMS detects and quantifies compounds concentrated by the ADS is briefly described here. The concentrated compounds were injected onto the GC column for separation. The GC column was a 25 metre PoraBOND Q capillary column (Varian) with an internal diameter of 320 μm, which restricts the column flow rate to 2.7 mL min^{-1}. The starting temperature of 40 ^{o}C was held for 3 minutes, then ramped at 22 ^{o}C min^{-1} to 84 ^{o}C and held for 1 minute, then ramped at 22 ^{o}C min^{-1} to 250 ^{o}C where it is held for 37.73 minutes (total time: 49 minutes). The compounds elute from the column individually because they absorb and desorb from the column at different rates. Temperature ramping of the column speeds up desorption of the compounds which occurs roughly in the order of increasing boiling points.

The separated compounds then travel into the mass spectrometer (MS) which is under vacuum (generated by a vacuum pump; E2M1.5, Edwards). Electrons are generated by the ion source (230 °C) and accelerated to bombard the compounds. The compounds are fragmented by the electron bombardment into ions of a characteristic pattern which, in combination with the retention time (time at which the compounds elutes from the column), allows the compound to be identified (Figure 2.5). The fragments are repelled through a lens to focus them, where they travel through the quadrupole mass filter (150 °C) to the detector. Fragments are identified by their mass/charge ratio (m/z). The MS has two operating modes: total ion current (TIC) and selected ion monitoring (SIM). When

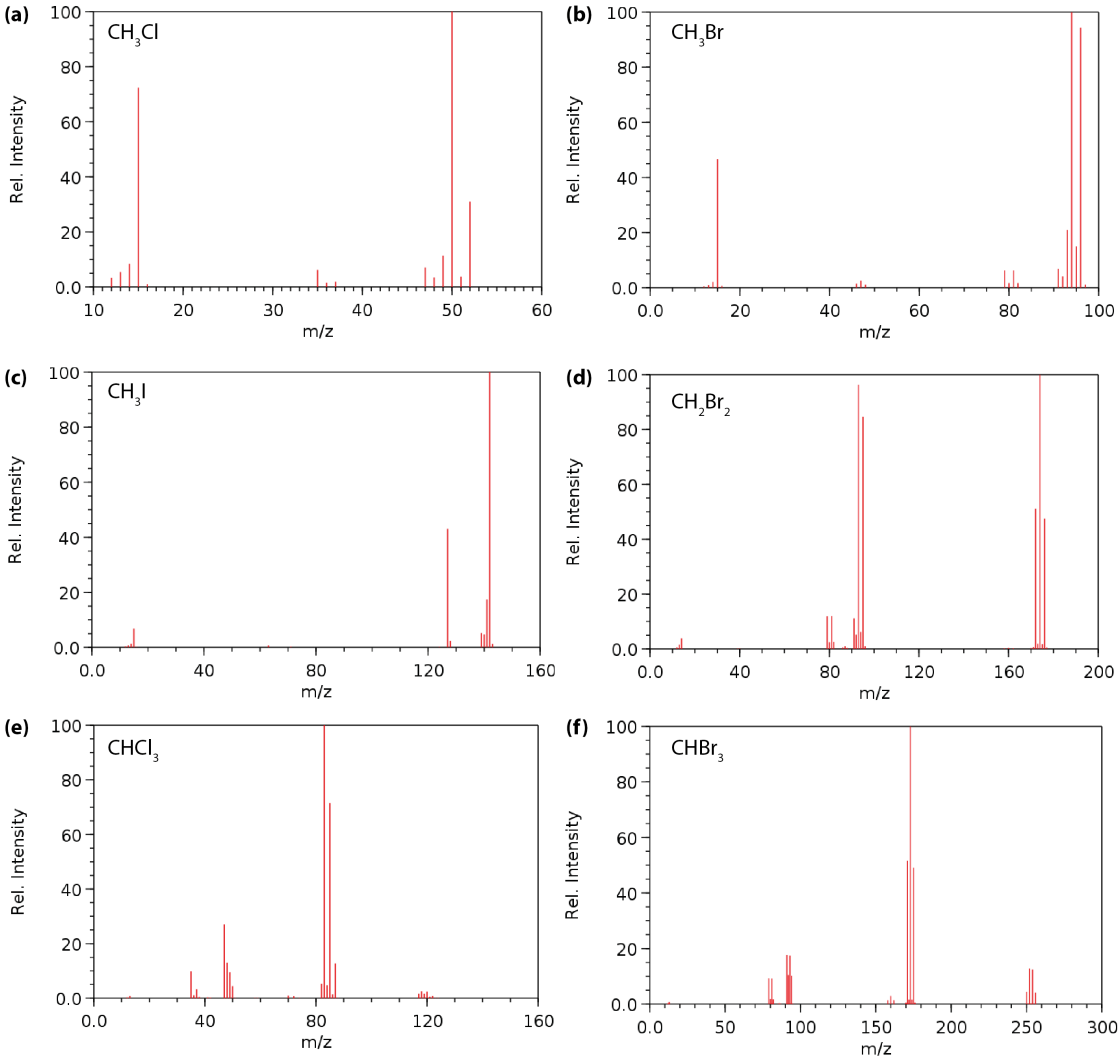

Figure 2.5 The fragmentation spectra of the 6 main halocarbons of interest CH_3Cl (a), CH_3Br (b), CH_3I (c), CH_2Br_2 (d), $CHCl_3$ (e) and $CHBr_3$ (f). In general, the most abundant ion(s) that have a mass greater than 40 m/z are chosen as the target and qualifier ion. For example, the target ion for CH_3Cl is 50, and the qualifier 52 which are the most abundant ions with >40 m/z. Spectra are adapted from NIST (2014).

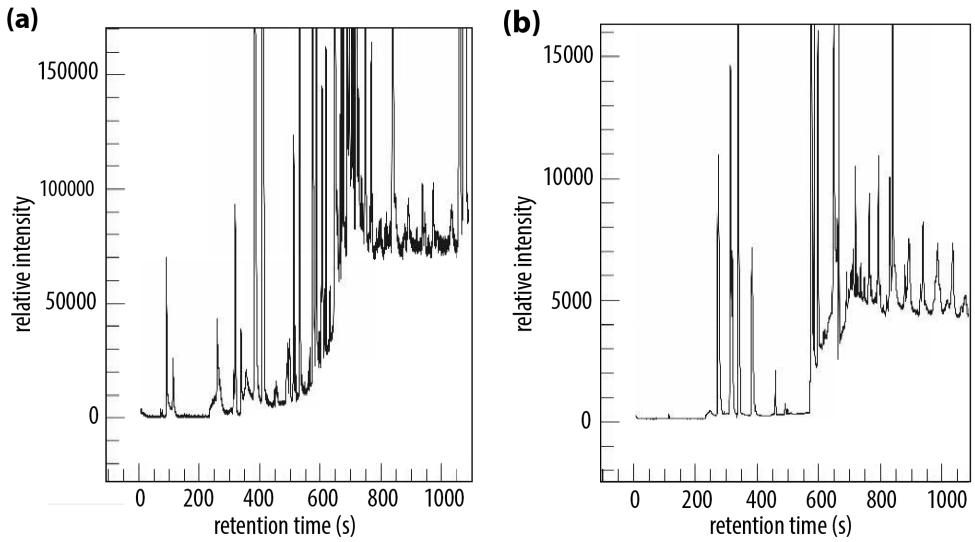

Figure 2.6 The chromatogram of a standard run in TIC (a) and SIM (b) mode showing the lower background and reduced baseline noise when run in SIM mode.

the MS is scanning in TIC mode it analyses every m/z from 40-250 m/z across the entire run time meaning that compounds that coelute can become obscured. Fragments with < 40 m/z are not scanned for due to high levels of noise below this threshold. When the MS is operating in SIM mode, only specified m/z are scanned for over specified time periods (or windows). Electrical fields generated by the quadrupole filter out fragments that are out with the specified m/z range. Focussing on only the compounds of interest results in much higher sensitivity, i.e. the background is reduced relative to the peaks of interest (Figure 2.6).

2.3.3 Optimization of the ADS-GCMS

The ADS-GCMS unit that was used for this research had previously been used for the routine monitoring of CFCs and HFCs in the atmosphere. Thus, the ADS-GCMS required modification to optimise it for the purposes required in this thesis. This involved the addition of an automated multi-sampler to the ADS and optimisation of the MS for the specific compounds of interest here. The changes made are described in the following sections.

2.3.3.1 Addition of automated multi-sampler

The ADS has a built-in bellows pump that can draw in sample through one port (P1). However, the limited time available to conduct the proglacial halocarbon flux experiments (Chapter 4) meant that samples needed to be analysed overnight. Therefore, a 6-position 6-port valve (Valco) was externally attached to P1 to allow automated

analysis of 6 samples. The 6-ports were connected via Valco fittings to 7 cm lengths of stainless steel 1/16th inch tubing with ¼ inch Swagelok adapters on the opposite end. A ¼ inch PTFE ferrule combined with a ¼ inch nut (Swagelok) was used to create a seal between the port and the polypropylene valves of the sample bags. The stainless steel tubing and fittings were cleaned prior to use by injecting through the tubing two 5 mL syringes of ethanol, and one 5 mL syringe of acetone, followed by being heated in an oven at 100 ^{o}C for 30 minutes. The cleaned fittings and tubing were then attached to the valve. The position of the valve was controlled by the GC. The GC was programmed to select the valve position for the next sample at the end of the previous sample run. This set-up removed the need to manually change the sample bag every 1 hour 10 minutes, allowing 6 samples to be run automatically.

2.3.3.2 Optimisation of the mass spectrometer

Because the ADS GCMS had primarily been used for analysing anthropogenic compounds, the windows and fragments scanned for in the SIM mode were optimised for the compounds of interest in this thesis. The compounds of interest to this thesis were the halocarbons most commonly produced in natural systems which contained chlorine, bromine and iodine. These were: methyl chloride (CH_3Cl), methyl bromide (CH_3Br), methyl iodide (CH_3I), dichloromethane (CH_2Cl_2), dibromomethane (CH_2Br_2), diiodomethane (CH_2I_2), chloroform ($CHCl_3$), bromoform ($CHBr_3$), bromochloromethane (CH_2BrCl) and carbon tetra-chloride (CCl_4). Additionally, the following anthropogenic compounds were used as marker compounds to aide location of the compounds of interest: HFC-125, HFC-134a, HCFC-22, HCFC-141b and benzene. To identify the compounds of interest, the fragmentation spectrum of each compound was obtained from the National Institute of Standards and Technology (NIST)'s online archive (NIST, 2014), examples of which are shown in Figure 2.5. The MS in SIM mode scans for one target ion and one or two qualifier ions per compound. The ions chosen for scanning are the most abundant fragments with > 40 m/z (due to noise below this size) as these are the most representative of the compound (Table 2.1).

To identify the retention time of each compound, a TIC analysis was conducted to locate the peaks with fragmentation spectra which matched the compounds of interest. To ensure that the chosen peaks were adequate for quantification, a GCMS analysis in SIM mode

Table 2.1 Compound name, formulas, molecular weights (MW), retention time (RT), target and qualifier ion(s), SIM window and whether the compound's concentration was determined using peak area or height is shown for each compound analysed. (*) denotes anthropogenic marker compounds. (^{H}) concentration of these compounds was calculated from the peak height (rather than area) due to co-elution. Some compounds were ultimately not used in chapter 4 due to coelution ($^{+}$) or high blanks ($^{++}$).

Compound	Formula	MW (g mol^{-1})	RT (secs)	Target ion (m/z)	Qualifier ion (m/z)	SIM window
HFC-125 *	CF_2HCF_3	120.02	274	101	51	1
HFC-134a *	CH_2FCF_3	102.03	312	83	50	1
HCFC-22 *	$CHClF_2$	86.47	318	67	50, 52	1
Methyl chloride	CH_3Cl	50.49	337	52	50	1
Methyl bromide	CH_3Br	94.94	458	94	96	2
Methyl iodide	CH_3I	141.94	576	142	127	2
Dichloromethane^{++}	CH_2Cl_2	84.93	577	88	0	2
HCFC-141b *	CH_3CCl_2F	116.94	598	81	83, 61	3
Bromochloromethane	CH_2BrCl	129.38	646	128	130	3
Chloroform	$CHCl_3$	119.37	664	83	85	3
Benzene *	C_6H_6	78.11	706	78	0	4
Carbon tetrachloride^{H+}	CCl_4	153.81	708	82	84	4
Methyl chloroform *$^{H+}$	CH_3CCl_3	133.40	708	99	97	4
Dibromomethane	CH_2Br_2	173.84	709	174	93, 95	4
Bromoform	$CHBr_3$	252.73	846	171	173, 175	5
Diiodomethane	CH_2I_2	267.84	1135	268	141	5

with one window containing only the fragmentation ions of the compounds of interest was run. Peaks qualified as being adequate for quantification if the peak size in the SIM run was comparable to the same peak in the TIC run. If the SIM peak was much smaller than the TIC, this suggested co-elution with another compound. In this case, a peak with a different retention time but with ion masses representative of the compound of interest was chosen.

SIM windows were created where specific ions were scanned for over specific periods of time. The more ion masses in a window, the shorter the 'dwell' time per ion, i.e. the shorter the time spent scanning for that specific mass. Taking into account the number of ions per window and the fact that each cycle is 100 seconds, the 'dwell' time of each ion

Table 2.2 The finalised SIM window start times, the number of ions in each window, the dwell time per ion, the cycles per second and the m/z of the ions as used for GCMS runs in Chapter 4.

SIM window	Start time (mins)	Number of ions	Dwell time (msec)	Cycles/ sec	Ions (m/z)
1	0.00	6	30	4.89	50, 51, 52, 67, 83, 101
2	6.33	5	35	5.03	88, 94, 96, 127, 142
3	9.80	6	30	489	61, 81, 83, 85, 128, 130
4	11.55	8	25	4.42	78, 82, 84, 93, 95, 97, 99, 174
5	12.51	5	35	5.02	141, 171, 173, 175, 268

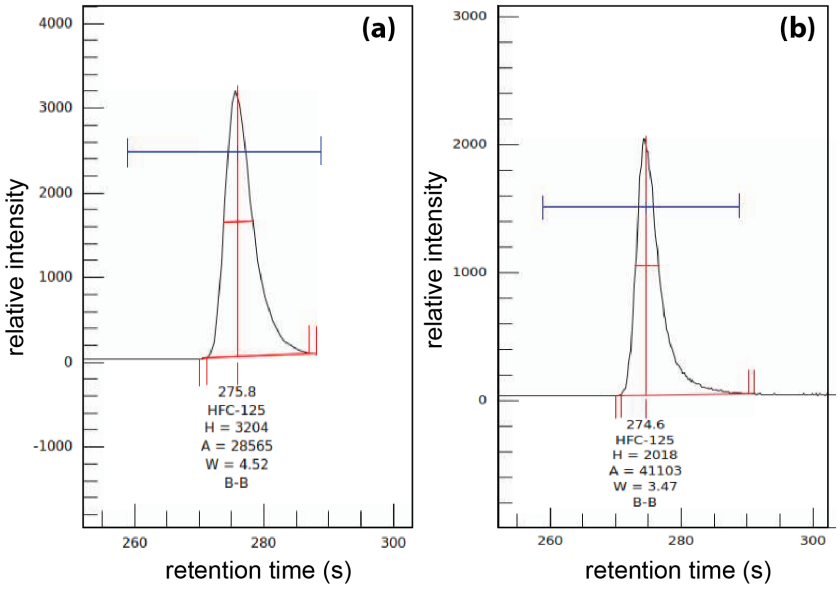

Figure 2.7 An example of adjustments made to SIM windows: originally the tail of the peak for HFC-125 was cut-off by the start of a new SIM window (a) so the new window start time was moved to later than 300 s to ensure the whole peak was captured (b).

was adjusted so that the cycles per second is 5-6, and at least 4.5. This ensures that enough data points are collected to define the shape of each peak on the chromatogram. Therefore, to optimise the SIM windows, the window lengths, window start times, ions analysed, and number of ions per window was modified (Table 2.2). These modifications also ensured that the SIM windows were long enough to prevent the tails on either side of each peak of interest from being cut off (Figure 2.7).

2.3.4 Operation and maintenance of the ADS-GCMS

2.3.4.1 Operation of the ADS-GCMS

For optimum performance, the ADS-GCMS was kept powered on at all times with a constant flow of carrier gas and with semi-frequent analyses of standards, blanks or simply lab air. This keeps the MS under vacuum and the microtrap and column clean which helps to lower the background, raising the sensitivity of the analysis. If the ADS-GCMS was idle for more than a day, the first 1-2 standard runs would be discarded until the background was reduced. If the instrument had been idle for a more extended period of time (i.e. more than 2 weeks), a ramping cycle was run on the microtrap consisting of three repetitions of heating to 50, 150 and 245 ^{o}C for 30 seconds and allowing the trap to return to ambient temperature before heating again. Additionally, the GC oven could be ramped with only Helium (i.e. with no air sample trapped by the ADS) to ensure the column was clean.

Blank air was also analysed to test that the ADS-GCMS was running optimally. The blank was a cylinder of purified air created in the laboratory using a pressure differential over a -70 ^{o}C universal trap to remove, primarily, halocarbons, CFCs, HFCs, HCFCs and hydrocarbons. The resultant gas was similar in bulk composition to atmospheric air which ensured it was analogous to the standard's and the sample's composition. The blank cylinder was connected to the back of the ADS using 1/18th inch cut-to-length stainless steel tubing with appropriate Swagelok fittings, cleaned by injecting ethanol (2 x 5 mL) and acetone (1 x 5 mL) and heating to 100 ^{o}C for 30 minutes. Once attached the cylinder was static leak checked under pressure (at 1.8 bar).

2.3.4.2 Checking and tuning the MS

The MS was leak-checked at least monthly by checking levels of air and water inside the MS. An air-water scan was run which analyses for water (m/z 18), nitrogen (m/z 28) and oxygen (m/z 32) inside the MS by comparing their abundances in the MS to the fragmentation ions of perfluorotributylamine (PFTBA) as a calibrant. The PFTBA is held in a small vial connected to the MS. The relative abundances of air, water and oxygen are compared to the abundances of three major PFTBA ions (69, 219 and 502 m/z). Oxygen and water were kept below 5 % and nitrogen was kept below 10 %.

The MS was tuned every few months using the automated tune programme (auto-tune) in the GCMS operating software (MSD-1). The auto-tune calibrates and adjusts the MS using the PFTBA calibration gas. It adjusts the x-axis of the MS spectrum so that the correct mass fragments are analysed at the correct point in the scan and adjusts the analyser so the same relative height or abundance of PFTBA ion fragments is seen each time.

2.3.5 Processing ADS-GCMS analyses

Chromatograms produced by the GCMS were uploaded for analysis to the Linux-based software GCWerks which was developed by the Scripps Oceanography Institute for the Medusa system, which is similar to the ADS. In this software, peak integration was optimised, standard analyses were checked for consistency, machine drift was monitored and results were exported for data visualisation, statistical analysis and scaling calculations. The former two were conducted in R version 3.5.0 (2018).

2.3.5.1 Peak integration

The expected retention time (RT) and the m/z of the qualifier and target ions for each compound was inputted into the GCWerks programme to guide the software during identification. GCWerks measures the area of each peak (and therefore calculates the concentration of the compound) by determining where a peak begins and ends. However, problems with this peak integration can occur due to non-horizontal baselines, co-elution and elevated background. Therefore, peak integration was optimised for each compound using various integration parameters within the software. Peak width and peak threshold were adjusted to ensure only peaks that were larger than the background were integrated, whilst also preventing the software from integrating adjacent peaks or background noise. The parameter ‘valley-to-valley’ was used to prevent the software integrating both the peak of interest and a peak or hump immediately adjacent to the peak of interest. The ‘regain baseline’ parameter was used to standardise the length of a peak’s tail where the software was otherwise integrating the tail length inconsistently. Once the integration parameters were optimised, the same parameters were used for standards and analyses throughout a sample block (i.e. all analyses in Chapter 4 were conducted with the same parameters).

2.3.5.2 Monitoring of standards

Analyses of standards were checked using the GCWerks software throughout operation of the ADS-GCMS. The peak area of the compounds in the standard was monitored over time to check for machine drift and column decay (i.e. gradual changes in peak area or retention time over time). Compounds can be plotted in a variety of ways using the GCWerks software, including by peak area, concentration and relative counts. The latter plots each data point relative to the size of the peak area of the analysis before and after it. The relative counts were used to indicate outliers in the standard analyses, i.e. analyses that were out with the 'normal' spread for that compound. Outliers were 'flagged' so that these standard analyses were not used to calculate the concentration of any sample runs. This also meant that any contamination in the column, microtrap or in the lines could be identified. Standard concentrations, precisions and limits of detection of the compounds are detailed in Chapter 4, Table 4.1.

2.3.6 Blank-testing equipment

The gas sampling bags and chambers used for halocarbon flux experiments were tested prior to use in the proglacial experiments both in the laboratory and in the field. The gas sample bags (Tedlar® with polypropylene valves; SKC Inc.) were tested for background levels of halocarbons by flushing with blank air 3 times and analysing on the ADS-GCMS. CH_2Cl_2 had a high background in the flushed bags and was therefore discounted from the experiment. All other halocarbons of interest were detected only in small amounts (Table 2.3). The bags were also flushed 3 times with standard air and analysed on the ADS-GCMS after 0 and 12 hours to determine if the concentration of compounds within the bags changed over time. Changes were small and were either similar to or smaller than the limit of quantification for each compound (Table 2.3).

The chambers used in the proglacial experiments were tested for background emission of the compounds of interest in the laboratory and in the field by placing the chamber onto a double sheet of aluminium foil which was folded up at the edges to form a tray. Deionised water (14-18 MΩ-cm) was then poured into the base of the chamber to create a seal between the chamber and the foil. The chamber top was placed into the collar's trough (filled with deionised water) as when sampling. The chamber was sampled after 0, 1 and 2 hours to check for changes in background concentration of the halocarbons of

interest. The changes measured in the field blank were corrected for in the proglacial chamber experiments (Table 2.3).

Table 2.3 Results of equipment testing for the halocarbons of interest with the limit of detection (three times the baseline noise; LOD) and limit of quantification (variance, of measurement precision). Sample bags were flushed 3 times with blank air to test for background levels (ppt and nmol m^{-2} equivalent). Sample bags were flushed 3 times with standard and analysed after 0 and 12 hours to test changes in concentration over 12 hours (ppt $[12\ hr]^{-1}$, nmol m^{-2}equivalent). The laboratory and field chamber blanks were measured 0 and 1 hours after testing, and are presented as the change in headspace concentration in one hour (ppt) and the change in nmol m^{-2} in one hour. The latter was corrected for the dilution of the sample bag and normalised to the chamber surface area (nmol m^{-2}). All values are the mean of 3 repeats, except the field chamber blanks which are the mean of 4. St. dev. = standard deviation.

	unit	CH_3Cl	CH_3Br	CH_3I	$CHCl_3$	$CHBr_3$	CH_2Br_2
Sample bag							
Background	ppt	19.9	0.33	0.57	2.16	0.46	0.09
- equivalent	nmol m^{-2}	0.02	0.0003	0.0005	0.002	0.0004	0.0001
- st. dev.	nmol m^{-2}	0.003	0.0001	0.0001	0.0008	0.0001	0.00004
Change, 12 hrs	ppt $[12\ hr]^{-1}$	-5	-0.001	-0.08	1.31	0.21	0.02
- equivalent	nmol m^{-2}	-0.02	-0.0003	-0.0006	-0.0007	-0.0002	-0.0001
- st. dev.	nmol m^{-2}	0.0001	0.0001	0.00004	0.0002	0.00002	0.00002
Chamber							
Laboratory blank	ppt	11.35	0.39	-0.10	-13.65	0.07	-0.01
- equivalent	nmol m^{-2}	0.13	0.01	-0.002	-0.16	0.001	-0.0001
- st. dev.	nmol m^{-2}	0.2	0.004	0.002	0.1	0.007	0.0002
Field blank	ppt	24.08	1.11	0.25	-1.73	-0.74	-0.65
- equivalent	nmol m^{-2}	0.15	0.01	0.003	0.03	-0.009	-0.002
- st. dev.	nmol m^{-2}	0.27	0.005	0.003	0.02	0.002	0.001
LOD, equivalent	nmol m^{-2}	0.01	0.003	0.0001	0.002	0.004	0.0009
Variance, equivalent	nmol m^{-2}	0.1	0.0007	0.0001	0.002	0.0009	0.0002

2.4 Long-term halocarbon data

2.4.1 Overview of the datasets

Trends and patterns in long-term halocarbon data were investigated using data collected by the Norsk Institutt for Luftforskning (NILU; Norwegian Institute for Air Research) at the Zeppelin observatory (described in Section 2.2.1). The halogenated gas datasets (2013-2017), the meteorological datasets (2016-2017) and the non-halogenated gas datasets (CO and CH_4; 2016-2017) were obtained from NILU's publicly available database, EBAS (ebas.nilu.no). The collection of the halogenated gas data is described briefly below (Section 2.4.2). The collection of the non-halogenated gases and meteorological datasets are described in Section 5.3.3. Processing and plotting of all data was conducted in R (Version 3.5.0; R Development Core Team, 2018) and is further described in Chapter 5 (Section 5.3.5 and 5.4).

2.4.2 Collection of long-term halogenated gas data

The ambient air at Zeppelin was measured using a 'Medusa' system, which is a custom preconcentration system coupled with a gas chromatograph mass spectrometer. This system was designed to enable analysis of very volatile gases which the ADS-GCMS system could not analyse, including the perfluorocarbons (PFCs; e.g. CF_4 and CF_3CF_3) owing to the much colder temperatures achieved on the microtraps (-165 ^oC, compared to -50 ^oC in the ADS) and the use of a secondary trap to further cryo-focus the most volatile compound, CF_4 (Miller et al., 2008). Otherwise, the principle is broadly the same as the ADS, and is described in detail elsewhere (Miller et al., 2008). Briefly, water is removed from the sample by counter-purge of dry zero air over a Nafion membrane (which is permeable to water, but not the analytes of interest). The sample is then preconcentrated onto the first microtrap (T1; 1.6 mm i.d, 76.8 cm length) at -165 ^oC which contains 200 mg of divinylbenzene absorbent (100/120 mesh HayeSep D). The remaining abundant atmospheric gases (N_2, O_2, Ar and Kr) and CF_4 (which is the most volatile compound) are refocussed onto a second microtrap (T2) by raising the temperature of T1 to -65 ^oC. T2 contains 5.5 mg of HayeSep D absorbant and is held at -165 ^oC. T2 is heated to 100 ^oC to desorb the compounds which are flushed onto a custom micropacked precolumn (containing 40 mg of 100/120 mesh molecular sieve 4 Å and 160 mg of 100/120 mesh HiSiv-3000) at 40 ^oC for separation. The separated T2 gases are injected onto the main column (CP-PoraBOND Q fused silica PLOT; 25 m, 0.32 mm i.d.; Varian

Inc.) of the Gas Chromatograph (6890N Agilent). The compounds trapped on T1 are desorbed by heating to +100 ºC and also injected onto the main column. The column is held at 40 ºC for 1 minute before being ramped at 22.9 ºC/minute to 200 ºC where it is held for the remainder of the run. The separated compounds are identified and quantified by the quadrupole mass spectrometer (5975B Agilent). Calibration information is provided in Section 5.3.2.

3 Glacial erosion liberates lithologic energy sources for microbes and acidity for chemical weathering beneath glaciers and ice sheets

This chapter identifies and quantifies the mechanical breakdown of rocks and minerals by glacial erosion as a previously un-recognised source of trace gases, including CO_2, CO and CH_4, and as a less well known source of H_2, to the subglacial environment. Rock grinding experiments in the laboratory were used to emulate glacial abrasion with gas production quantified and scaled to catchment-wide production rates that are comparable to microbial and weathering processes. In this manner, we identified how trace gas production by the mechanical breakdown of minerals can influence both chemical weathering reactions and biological processes involving microbiota, particularly methanogens, in the subglacial environment.

This chapter was published in November 2018 in its entirety by *Frontiers in Earth Science: Geochemistry*, with the following citation:

> Macdonald, M.L., Wadham, J.L., Telling, J.T., Skidmore, M.L. (2018). Glacial erosion liberates lithologic energy sources for microbes and acidity for chemical weathering beneath glaciers and ice sheets, *Frontiers in Earth Science: Geochemistry*, 6 (212), doi: 10.3389/feart.2018.00212.

The study was conceived by Jon Telling with rock, sediment and suspended sediment samples collected by him (from Leverett, Mittivakkat and Engabreen glaciers), Mark Skidmore (Robertson) and myself (Midtre Lovenbreen). Discharge data from Robertson was supplied by Mark Skidmore. Discharge data and suspended sediment samples from Midtre Lovenbreen were collected and processed by myself. The experiments, analysis and writing were conducted wholly by myself, with review provided by all authors.

3.1 Abstract

Wet-based regions of glaciers and ice sheets are now recognised to host unique and diverse microbial communities capable of influencing global biogeochemical cycles. However, the isolated nature of subglacial environments poses limitations upon the supply of protons for chemical weathering and energy sources (electron donors/acceptors) to support *in situ* microbial communities. A less well recognised source of these substrates is the release of gases from mineral structures, pore spaces or fluid inclusions and the generation of gases from the breakage of mineral bonds during the mechanical breakdown of rocks by moving ice. Here, we investigate the potential release of H_2, CO_2, CO and short chain hydrocarbons, particularly CH_4, by glacial erosion at rates relevant to chemical weathering and microbial activity beneath glaciers. A wide range of magmatic, metamorphic and sedimentary rocks and subglacial sediments from glaciated catchments in Greenland, Norway and Canada were ground in the laboratory to varying grain sizes and the release of gases was measured. The volume of gas released increased as the grain size of the ground sediments decreased. The results of these laboratory experiments were used to estimate rates of catchment-scale gas release based upon estimates of long term abrasion rates at each glacier. H_2 generation was calculated to be sufficient to potentially support previously estimated rates of methanogenesis in the upper centimetres of subglacial sediment at a gneissic catchment in Greenland and a sedimentary catchment in Canada. Sufficient CO_2 could be released by grinding to drive as much as 20% of subglacial chemical weathering at a metamorphic catchment in Svalbard, with potential implications for the inferred quantity of CO_2 drawn-down from the atmosphere by glacial weathering. Rates of CH_4 generation from grinding bedrock has the potential to be greater than subglacial microbial generation in a sedimentary catchment in Canada with carbon rich bedrock, suggesting a potentially important source of CH_4 for methanotrophic microorganisms. We conclude that mechanical erosion beneath a range of glaciers generates significant quantities of gases which have the potential to enhance chemical weathering and/or support subglacial microbial communities in the deep icy biosphere.

3.2 Introduction

Subglacial environments have become of increasing interest for understanding how microbial life survives in cold, dark, environments and for investigating the impact of glaciation upon global biogeochemical cycles (e.g. Skidmore et al., 2000; Christner et al., 2012; Wadham et al., 2013). Despite darkness, high pressures, low temperatures and assumed low nutrient input, the subglacial environment hosts active microbial ecosystems (e.g. Sharp et al., 1999; Christner et al., 2014; Dieser et al., 2014). The ubiquitous presence of geochemically reactive rock flour, coupled with isolation from surface inputs of organic matter and complete darkness, suggests that chemolithotrophic communities are important primary producers in subglacial systems (Boyd et al., 2014; Christner et al., 2014; Sharp et al., 1999; Tranter et al., 2002). Chemolithotrophic microbes exploit chemical disequilibria to derive their energy, often utilising dissolved gases as electron acceptors or donors (Lovley and Goodwin, 1990; Sharp et al., 1999). For example, hydrogenotrophic methanogens can subsist upon dissolved gases (i.e. H_2/CO_2) as their sole energy source (Lovley and Goodwin, 1990). However, due to the isolation of areas of the subglacial environment from surface processes and the atmosphere, there is a limited supply of energy sources resulting in their depletion over time, particularly during long periods of glaciation (Wadham et al., 2004).

Similarly, the proton pool available to fuel chemical weathering reactions can become limited during long periods of isolation from the atmosphere and surface processes (Hallet et al., 1996). Important proton sources in subglacial environments include carbonic acid generated from the dissolution of atmospheric and microbially-respired CO_2 and the oxidation of sulphide minerals under both oxic and anoxic conditions (Montross et al., 2013; Sharp et al., 1999; Tranter et al., 1996, 2002). However, vast areas beneath ice sheets are isolated from the influx of surface waters carrying atmospheric CO_2. Varying rates of basal melt across the bed impacts the volume of palaeo-atmospheric CO_2 released from bubbles trapped in the ice, limiting this source in low melt areas. Proton supply via sulphide oxidation is only significant where there are sulphide-bearing rocks being physically eroded to comminuted rock flour. This source may become, at least locally, limited. Microbially-respired CO_2 has been shown to enhance chemical weathering rates (Montross et al., 2013), but would be limited in areas where there are limited growth substrates (e.g. low organic carbon) and subsequently lower rates of respiration.

We postulate that a previously unrecognised abiogenic source of protons (through the generation of carbonic acid) and microbial energy is the bedrock, which is eroded at rates of 0.01 to 100 mm yr^{-1} by moving ice in wet-based areas via fracturing, plucking and abrasion (Hallet et al., 1996; Lee and Rutter, 2004; Cowton et al., 2012). Tentative evidence from the literature supports this notion. Gases trapped within rocks can be released by mechanical grinding (Deeds et al., 2015; Wang et al., 2015; Zhang et al., 2014). For example, crystalline rocks, such as granitoids, which constitute the major basement rocks beneath the Greenland Ice Sheet, contain gases (e.g. hydrocarbons) trapped within their minerals' crystal structure or within fluid inclusions (Potter and Konnerup-Madsen, 2003). Sedimentary rocks can retain even larger volumes of hydrocarbons and CO_2 within their pore spaces and mineral structures (e.g. Martinelli and Plescia, 2005; Osborn and McIntosh, 2010; Wang et al., 2015). In addition, gases such as H_2 can be generated from mechanical grinding of rocks and minerals through fault action (e.g. Ito et al., 1999; Kameda et al., 2004). Despite the potential for glacial erosion to generate these gases, there has been only one experimental investigation, focussing solely on H_2 generation, using field-collected samples from glacial catchments to date (Telling et al., 2015).

This study aims to investigate the potential of subglacial mechanical erosion as an abiotic source of gases, at generation rates that are relevant to chemical weathering and microbial activity. Rock and sediment samples from a range of lithologically contrasting (igneous, metamorphic and sedimentary rock types) glaciated catchments across the Northern hemisphere were ground in a ball-mill to simulate the process of glacial abrasion. The release of H_2, CO_2, CO and several short-chained hydrocarbons was quantified to determine their significance for providing protons for chemical weathering via carbonic acid generation and as electron acceptors and donors for microbial energy.

3.3 Materials and methods

3.3.1 Rock and sediment sample selection

Rock samples were collected from a diverse range of glaciated catchments in the Northern hemisphere. These glaciers were Mittivakkat (MG) and Leverett (LG) in Greenland, Engabreen (EG) and Midtre Lovenbreen (ML) in Norway, and Robertson (RG) in Canada. The details of the catchment location, general lithology and rock sample type(s) are shown in Table 3.1. Glacial sediment samples were also obtained at two catchments (LG and ML). The LG sediment was melted out of a basal ice sample. The ML sediment was collected immediately in front of the glacier terminus and had thus been recently exposed. Approximate percentage areal composition of five major minerals (quartz, feldspar, biotite, muscovite and pyroxene) was determined for the crystalline rock samples (Table 3.1). Identification was conducted using established physical properties of minerals that were visible with the naked-eye or with a hand-lens (x10 magnification). Mineral quantification was not conducted for the sediment samples or the RG rock samples because they were too fine-grained to identify by this method.

Table 3.1 Characteristics of the rock and sediment samples and their source glacial catchments, with estimates for the crystalline rock samples of the areal percentage of major rock forming minerals, quartz (Q), feldspar (F), muscovite mica (Mu), biotite mica (Bt) and pyroxene (Py) (NB totals may not be 100 % where other minerals were present). (-) sediment samples and the rock samples of RG were too fine grained for the method of identification. (n.d.) mineral not detected. (*) 'hard' and 'soft' describes the relative 'hardness' of the two samples based on how quickly they powdered during grinding, 'muddy carb.' is short for muddy carbonate.

Glacial catchment	Location	Catchment lithology	Sample type(s)	Mineral composition (areal %)				
				Q	F	Mu	Bt	Py
MG	Southeast Greenland	igneous & metamorphic	porphyritic granite	60	15	2	15	n.d.
LG	West Greenland	basement rock (metamorphic)	orthogneiss	35	30	n.d.	5	30
			sediment	-	-	-	-	-
EG	Norway	metamorphic	mica-schist	10	5	55	15	n.d.
ML	Northwest Svalbard	metamorphic	schist	30	10	50	10	n.d.
			quartzite	95	n.d.	n.d.	n.d.	n.d.
			sediment	-	-	-	-	-
RG	Alberta, Canada	sedimentary	hard* muddy carb.	-	-	-	-	-
			soft* muddy carb.	-	-	-	-	-
			shale	-	-	-	-	-

3.3.2 Experiments to simulate gas release via glacial erosion

A sledgehammer on a metal plate was used to reduce the rock samples in size. To minimize contamination, samples were wrapped in durable polyethylene bags and the plate and hammer were cleaned between samples with ethanol (100%). The 250 μm – 2 mm fraction was collected and dried at 105 °C for 48 hours to remove moisture prior to milling. The rock and sediment samples were ground to finer powders in a zirconium oxide ball-mill sealed with a PTFE O-ring. We advocate that this process is analogous to glacial abrasion where clasts frozen into the glacier's base grind the bedrock beneath, producing large quantities of fine-grained sediment (e.g. Hallet *et al.*, 1996). The ball-mill was modified with two valves so it could be flushed with 5.0 grade Argon, which was dried with an in-line moisture trap (Agilent), prior to grinding. Approximately 10 g of sample was ground in triplicate for 1, 3, 5, 10 and 30 minutes using a ball mill (Fritsch Planetary Mono Mill Pulverisette 6) at 500 rpm. The same length of grinding produced different mean grain sizes, depending upon the rock type, and thus comparison between the samples was standardized to mean grain size measured by Mastersizer (Section 3.3.4). Grinding beyond 30 minutes did not produce smaller grain sizes. Immediately after grinding, 5 mL of 5.0 grade argon was injected into the ball-mill (to maintain ambient pressure) using a gas-tight syringe and mixed with the headspace before removing 5 mL of sample for analysis. Quartz mineral specimens (purchased from thegeologysuperstore.com) were used as a procedural blank to ensure that no gases were generated by the ball-mill during grinding. The quartz minerals were pre-crushed and sieved, by the same method as the samples, before being furnaced at 1000 °C for 2 hours, in order to dissociate gases from the mineral surface and release gases trapped within fluid inclusions. Grinding of the prepared quartz was conducted in duplicate for 1, 10 and 30 minutes. Methane was the only gas detected in the blank runs and averaged at 0.01 nmol CH_4 g^{-1} (standard deviation of 0.002 nmol g^{-1}) across all the blank runs. Minor (0.3 nmol g^{-1}) carbon dioxide was present in the Argon gas used to flush the headspace. No other gases were detected in the procedural blank.

3.3.3 Analysis of gases released during grinding

Gas samples were injected into an Agilent 7890A gas chromatograph (GC) fitted with a methaniser (at 395 °C) and two detectors: an FID (flame ionising detector, at 300 °C) and a TCD (thermal conductivity detector, at 250 °C). Separation of methane (CH_4), carbon dioxide (CO_2), ethane (C_2H_6), ethylene (C_2H_4) and propane (C_3H_8) was achieved using a

molecular sieve 5a, 60-80 mesh, 8ft × 1/8-inch column. Separation of hydrogen (H_2) was achieved using a Haysep D 80-100 mesh, 2m × 1/8-inch SS column. The columns were held at 25 °C for 4 minutes, before being ramped at 50 °C per minute to 200 °C.

Gas samples obtained from grinding rock samples from two catchments with contrasting geologies (sedimentary RG and granitic MG) were also analysed for carbon monoxide (CO) on an SRI 8610C GC fitted with a molecular sieve 5A column at 30 °C and a reduction gas detector (mercuric oxide with UV lamp) held at 295 °C.

Calibration standards were run twice daily on both GCs, apart from ethylene, which was calibrated with a standard obtained later in the experimental period as the peak was initially unidentified. The percentage variance, limit of quantification and detection for the standards are displayed in Table 3.2. Concentrations of the samples were calculated from a linear regression line of manual dilutions of certified (+/- 5 %) standards with 5.0 grade Argon. Gas concentrations were converted to moles using the Ideal Gas Law, corrected for dilution, and normalised to the mass of dry sediment.

3.3.4 Grain size and total carbon analysis

The grain size after grinding was measured to standardize comparison of the samples. Mean grain size was measured using a Malvern Mastersizer 3000 which utilises laser diffraction to estimate a mean grain size from 5 replicates per sample. The mean percentage variation for the 5 replicates was 3.5 % (n=200). An Elemental Analyser (EA) 1110 was used to measure percentage weight of total carbon in an 8 to 19 mg, < 250 μm, well-mixed aliquot of each sample which was flash heated to 1000 °C. The EA was calibrated with a certified Aspartic acid standard containing 36.14 % total carbon (n=3, per 20 samples). Reproducibility of the total carbon content analyses was determined using a soil reference standard containing 2.36 % total carbon with the precision at 0.07 wt % total carbon (n=4). The limit of detection was 0.01 wt % total carbon.

Table 3.2 The limit of quantification (variance) and detection (LOD) for each gas analysed. Serial dilution was not conducted for CO. ^ for ethylene, n =7. ^^ for CO, n = 24.

	H_2	CO_2	CH_4	C_2H_6	C_3H_8	C_2H_4	CO
Standard concentration, ppm (+/- 5 %)	493	406	195	19	21	104	0.7
% variance (n=48)	1.8	1.7	1.1	1.4	1.8	2.2^	12^^
Variance nmol g^{-1} equivalent	2.0	1.5	0.6	0.1	0.1	0.5	0.02
LOD, ppm	2.0	0.3	0.2	0.1	0.3	0.1	-
LOD, nmol g^{-1} equivalent	0.5	<0.1	<0.04	0.02	0.1	0.02	-
R^2 relationship of serial dilution (n=5)	>0.99	>0.99	>0.99	>0.99	>0.99	>0.99	-

3.3.5 Suspended sediment flux and discharge analysis for ML (2016) and RG

To compare the potential gas generation by glacial erosion between catchments the rate of gas production was scaled up to a 'catchment-rate' (Section 3.3.6). To conduct this calculation, the flux of suspended sediment (SS) was used. We assumed that this is approximately equivalent to the rate of mechanical erosion; a common method used to calculate erosion rates (e.g. Hallet et al., 1996) and that which is likely to be representative of the average erosion rate over longer timescales despite the potential for errors on an annual basis. For the 2016 ML melt season and the 2014 RG melt season, this was calculated here using the product of the SS concentration and discharge measurements. The SS flux at ML was measured at the eastern subglacial upwelling (78.8956°N, 12.0730°E). There was no evidence of a western subglacial upwelling forming that year, as has occasionally been described previously (e.g. Wynn et al., 2006). SS concentration was measured (n=16) every 3-4 days from the 24th June to the 21st July 2016. Water was collected in a rinsed 1 L Nalgene bottle and 100-500 mL (depending on the perceived turbidity) was filtered using a hand-pump with a Nalgene filtration tower onto a 0.45 µm cellulose nitrate filter paper. The paper was dried at 50 °C for approximately 24 hours and the dry weight of sediment per litre of water calculated and averaged (Table 3.3). The average grain size of the SS samples was 18.4 µm (standard deviation of 1.4, n=7; Section 3.3.4). The discharge ($m^3\ s^{-1}$) was calculated for 9 days over the melt season from water velocity ($m\ s^{-1}$) and water depth (m) measured at 5-7 points across the width (m) of the river (number of measurements varied with river width). This was extrapolated across the estimated number of days the subglacial upwelling was flowing (47 days) to give a total

melt season discharge of approximately 6.1×10^6 m^3. The product of the SS concentration and discharge provided an estimated SS flux of 95×10^8 g during the summer melt season, the same order of magnitude as that reported by Hodson et al.'s (2000) study.

Here, we present the first data for SS flux and bulk meltwater discharge for RG. An average SS concentration for RG of 0.19 g L^{-1} was obtained by the same method as described for ML from measurements taken on three days (n=5/ day), spread over the 2014 melt season. The average SS grain size was measured as 4.0 μm (n=7; Section 3.3.4; Table 3.3). The SS concentration was multiplied by an estimated average discharge of 0.3 m^3 s^{-1} over a 62-day melt season. This discharge is the average for July during the 2010 RG melt season, and the assumed average for August as both had similar numbers of positive degree days (PDD; 310 cf. 320) (Doxsey-Whitfield, 2012; Scanlon, 2017). We assumed that the average discharges in 2010 and 2014 were comparable, as the July and August 2010 PDD values were close to the 2006-2012 average for July (350) and August (340), and thus appear to be broadly representative (Scanlon, 2017).

Table 3.3 Suspended sediment (SS) flux, average concentration and average grain size in meltwater for each glacier catchment. Where data for multiple melt seasons is available, SS flux is an average. SS grain size is the average measured in that catchment with the range in brackets. (*) denotes data not available, therefore, the average of the non-sedimentary catchments (LG and ML) was used. Year of the season used to calculate SS flux is shown and this, SS concentration and SS grain size are from published values or obtained here as follows: [1](Hasholt and Mernild, 2006); [2](Hawkings et al., 2015); [3](Hawkings et al., 2016), [4] (Bone, 2014), [5](Bogen, 1996); [6](Bogen, 1996; Engelhardt et al., 2015); [7](Hodson et al., 2004); [8]this study (section 3.3.5).

Glacier	SS flux (10^8 g a^{-1})	SS flux year(s)	SS conc. (g L^{-1})	SS grain size (μm)
MG	176	2005 [1]	0.5 [1]	23.2 *
LG	29,000	2009-2012 [2]	1.1 [3]	20.7 [4]
EG	165	1987, 1989-1993 [5]	0.1 [6]	23.2 *
ML	95	2000 [7], 2016 [8]	1.2 [8]	25.7 [7,8]
RG	3	2010, 2014 [8]	0.2 [8]	4.0 [8]

3.3.6 Calculation of catchment-scale gas generation from grinding experiments

To compare potential gas generation by glacial erosion for catchments of contrasting size and erosion rates, the rate of gas production per m^2 of the catchment per day was calculated using Equation 3.1, after Telling et al. (2015):

$$\mathbf{G_{(catchment)}} = \frac{\mathbf{G \times E}}{\mathbf{A \times 365}} \quad \textbf{(3.1)}$$

where, $G_{(catchment)}$ is the catchment-wide rate of gas production (H_2, CH_4, or CO_2) generated by mechanical grinding (nmol m^{-2} d^{-1}); G is the amount of gas generated per gram of sample (nmol g^{-1}); E is the flux of suspended sediment (SS) exported from the catchment per year (g a^{-1}); A is the area of the catchment (m^2) and 365 converts the rate from yearly to daily. Note that G is the amount of gas generated per gram of sample when ground to the average grain size of SS measured in glacial runoff from the catchment (Table 3.3). G is calculated using the regression line equation of gas production against grain size (Figure 3.1). Values used for E and the average grain size of SS in each catchment are shown in Table 3.3. Where $G_{(catchment)}$ was calculated for H_2 generation by silica-water reactions at LG (Section 3.5.1.1), the value for G was 11.4 nmol H_2 g^{-1} as calculated by Telling et al. (2015).

These calculations assume that the measured suspended sediment flux in runoff from each catchment is in equilibrium with the rate of mechanical erosion. This is likely to be true over decadal and longer timescales, as otherwise sediment beneath glaciers would either run out or would accumulate. However, there is the potential for the erosion rate to be out of equilibrium with the suspended sediment flux in individual years, particularly at small, slowly eroding glaciers which are underlain by subglacial till (e.g. RG and ML). Here, in the absence of other data we have made the assumption that the present day rate is equivalent to a longer term abrasion rate measured over a number of years. These calculations also assume that the average suspended sediment grain size has been achieved from grinding an original grain size of between 250 μm and 2 mm. This is unlikely to be true, therefore, $G_{(catchment)}$ is likely a lower estimate as the reduction of bedrock to 2 mm sized particles will likely generate additional gas. Where multiple rock types were present in the catchment, we selected the dominant rock type to calculate values of G. The only exception to this was for CO_2 at LG which was calculated from experiments in which basal sediment was ground, rather than the bedrock (gneiss) which

did not produce quantifiable CO_2. Previous studies have shown that basal ice sediment at LG has an organic carbon content of 0.44 % (dry weight) (Lawson et al., 2014) which was presumably the origin of the CO_2 released during grinding of the basal sediment.

3.3.7 Calculation of supported rates of hydrogenotrophic methanogenesis

To determine the significance of the H_2 generated by glacial erosion to subglacial microbial processes, the degree of hydrogenotrophic methanogenesis that could be sustained by grinding-generated H_2 and CO_2 was determined for two catchments with contrasting geologies; gneissic LG and sedimentary RG. To calculate the depth of sediment throughout which hydrogenotrophic methanogenesis could be sustained by H_2 generated from grinding, we used Equation 3.2:

$$\mathbf{D} = \frac{\mathbf{H_{2\,(catchment)}}}{\mathbf{CH_{4\,(methanogenesis)}} \times \mathbf{4} \times \mathbf{S}} \quad \textbf{(3.2)}$$

Where, D is the depth of sediment (m) throughout which methanogenesis could be supported by grinding-generated H_2, $H_{2\,(catchment)}$ is the H_2 generated by mechanical grinding from Equation 3.1 (nmol m^{-2} d^{-1}), $CH_{4\,(methanogenesis)}$ is the measured rate of CH_4 production by methanogenesis at the catchment derived from incubation studies (nmol g^{-1} d^{-1}), 4 is the stoichiometric relationship between H_2 and CH_4 during methanogenesis (Equation 3.3), S is the grams of sediment per metre cubed where the wet sediment has a density of 2×10^6 g m^{-3} (as measured by Stibal et al., 2012) and therefore converts the rate of methanogenesis from nmol CH_4 g^{-1} d^{-1} to nmol CH_4 m^{-2} d^{-1}. For RG, values used for $CH_{4\,(methanogenesis)}$ were 0.0002-0.0012 nmol CH_4 g^{-1} d^{-1}, as measured during incubations at 4 °C of basal sediment from RG (Boyd et al., 2010). For LG, 0.00018 nmol CH_4 g^{-1} d^{-1} was used for $CH_{4\,(methanogenesis)}$ (Stibal et al., 2012b). This rate was measured during incubation at 1°C of sediment from Russell Glacier, which is adjacent to, and has the same bedrock geology as LG (Stibal et al., 2012b).

Since the H_2/CO_2 pathway for methanogenesis requires a source of CO_2 in addition to H_2, we also calculated whether sufficient CO_2 is generated by grinding to allow microbes to utilise mechanically generated H_2. This was calculated from the stoichiometric relationship of H_2 and CO_2 in the hydrogenotrophic methanogenesis pathway:

$$\mathbf{4H_2 + CO_2 \rightarrow CH_4 + 2H_2O} \quad \textbf{(3.3)}$$

3.3.8 Calculation of theoretical total flux of CO_2 and CH_4 in subglacial discharge

For ML and LG, it was necessary to calculate an estimated flux of gas from grinding per year to allow direct comparison with fluxes in the literature. At ML, CO_2 fluxes can be compared with estimates of CO_2 'used' in a chemical weathering study at the catchment (Hodson et al., 2000). CH_4 fluxes can be compared with measured CH_4 export at LG. The latter has been inferred to be microbial in origin (Lamarche-Gagnon et al., 2019), thus providing a comparison between grinding-generated abiogenic CH_4 and suspected subglacial microbial generation rates. The theoretical flux of CH_4 and CO_2 was calculated as shown:

$$\mathbf{G_{(flux)} = G_{(generated)} \times E} \quad \textbf{(3.4)}$$

where, $G_{(flux)}$ is the grinding-generated CH_4 exported from the catchment per year (t); $G_{(generated)}$ is the gas generated per gram of sample (t [g sample]$^{-1}$); E is the flux of suspended sediment exported from the catchment per year (g a^{-1}). Values used for E are shown in Table 3.3 for LG. For ML, we used only data for the year closest (2000) to when the comparison study was conducted, where E was 113 x 10^8 g a^{-1} and the mean SS grain size used to determine $G_{(generated)}$ was 33.1 μm (Hodson et al., 2004). $G_{(generated)}$ is calculated the same way as $G_{(catchment)}$ in Section 3.3.6 but converted to tonnes of gas per gram of sediment using the molecular weight of the gas.

3.4 Results

Variations in rock hardness of the samples analysed resulted in widely differing grain sizes when ground for the same time. Therefore, we used the average grain size of the ground sample rather than the grinding time to compare the amount of gas produced by grinding different samples. Decreasing average grain size equated to an increase in the amount of H_2, CO_2, CO, CH_4, C_2H_6, C_3H_8 and C_2H_4 emitted during grinding (Figure 3.1). The only exception to this pattern was a decrease in the CO_2 emitted with decreasing average grain size for LG basal sediment. It is likely that the amount of gas emitted would continue to increase with further reduction in grain size, however, using this method we were not able to further decrease the grain size by grinding for longer than 30 minutes.

The amount of H_2 measured during the grinding of rock and sediment samples varied by two orders of magnitude depending on the rock type investigated (Figure 3.1a). Mica-rich samples, EG schist, ML schist and ML sediment, produced up to one order of magnitude more H_2 than the non-mica-rich samples when ground to 17 μm (the average grain size of suspended sediment exported from LG, RG and ML, for which this data was available; Table 3.3).

CO_2 was detected during the grinding of all rock and sediment samples but was below the limit of quantification (<1.5 nmol g^{-1}) for the MG granite, LG gneiss and EG schist. However, large amounts of CO_2 (μmol g^{-1}) were produced during grinding of RG and ML rock samples (Figure 3.1b). Correlations between the amounts of gases measured were investigated in order to identify potential release mechanisms. For example, the correlation between CO_2 and CH_4 was highly linear within individual rock samples (R^2 > 0.8), but not within the entire population of rock samples (R^2 0.32) due to the higher CO_2: CH_4 ratios of the ML samples than of the RG rocks (Figure 3.2a).

CO was analysed during grinding of rocks from catchments with contrasting geologies; RG sedimentary rocks and MG granite. Small amounts of CO (1-4 nmol g^{-1}) were measured during grinding of MG granite. The three RG rocks produced similar amounts of CO (2-20 nmol g^{-1}) as each other when ground to the same average grain size (Figure 3.1c). There was a significant linear correlation between CO_2 and CO produced during grinding of the RG rocks (R^2 of 0.93). The strength of these correlations increased when considering only single rock types (R^2 of 0.96 to 0.99) (Figure 3.2b).

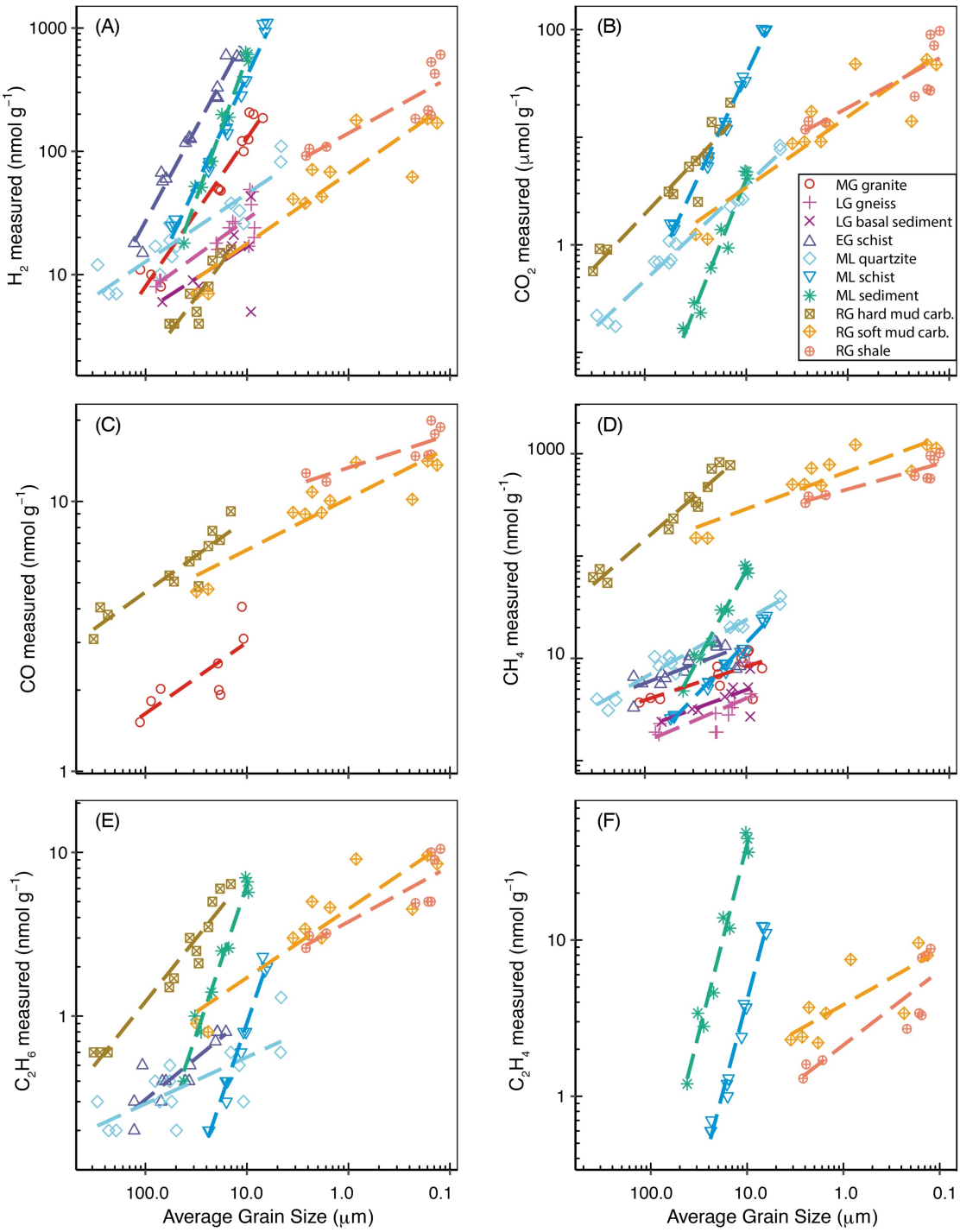

Figure 3.1 H_2 (A), CO (C), CH_4 (D), C_2H_6 (E), C_2H_4 (F) produced in nmol g^{-1}, and CO_2 (B) produced in μmol g^{-1} when grinding the rock and sediment samples to different average grain sizes. Grain size decreases and grinding time increases from left to right. Dashed lines are the power relationship between grain size and the respective gas for each sample (which is linear in log-log space).

Table 3.4 The hydrocarbons detected during crushing. Where quantifiable, the amount (nmol g^{-1}) released when crushed to an average grain size of 20µm is shown (calculated from linear regression equation). (<) detected but below limit of quantification, (-) detected but not quantified as no standard available for acetylene (C_2H_2). MC is muddy carbonate with 'hard' and 'soft' describing the relative 'hardness' of the samples to each other based on how quickly the entire starting sample was powdered during grinding.

glacier	sample	CH_4	C_2H_6	C_2H_4	C_2H_2	C_3H_8
MG	granite	6.6	<	<	n.d.	n.d.
LG	gneiss	3.0	<	<	n.d.	n.d.
	sediment	3.8	<	<	-	<
EG	schist	10.4	0.7	<	n.d.	n.d.
ML	schist	6.9	0.3	1.1	-	<
	quartzite	16.0	0.5	<	-	<
	sediment	20.2	1.8	7.6	-	0.3
RG	hard MC	575	4.2	<	-	<
	soft MC	222	1.3	0.7	-	<
	shale	195	1.4	0.5	-	<

A wide range of hydrocarbon species were produced during grinding, including CH_4, C_2H_6, C_2H_4, C_2H_2 and C_3H_8 (Table 3.4). CH_4 and C_2H_6 were produced during grinding of all rock and sediment samples, except for LG granite, where C_2H_6 was not detected. CH_4 production was notably higher for the sedimentary RG samples than for the crystalline samples of EG, MG and LG (Figure 3.1d). LG sediment samples produced similar amounts of CH_4 at all grain sizes as LG gneiss, whereas ML sediment produced three times more CH_4 than the crushed ML schist, one of the dominant rock types in the catchment. This suggests that ML schist is not the dominant composition of the basal till. ML sediment behaved as an outlier in several correlations with elevated C_2H_6:CH_4 (Figure 3.3a) and H_2:CO_2 (Figure 3.3b) ratios compared with the wider population of rocks. The H_2/CO_2 and C_2H_6/CH_4 relationships were highly linearly correlated for all other rocks (R^2 of 0.86 and 0.93, respectively) when ML sediment was not included.

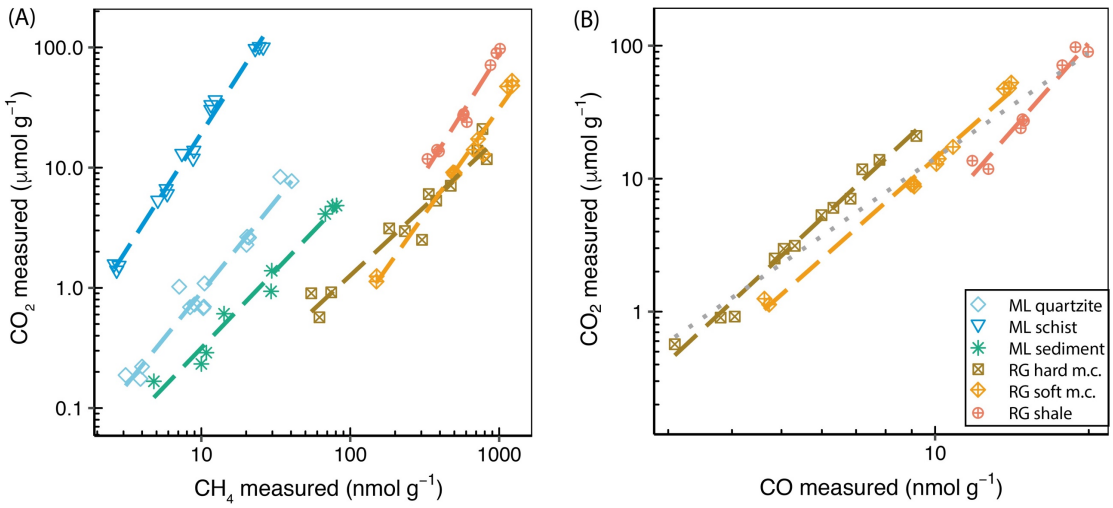

Figure 3.2 Amounts of CO_2 (µmol g^{-1}) against (A) CH_4 (nmol g^{-1}) released during grinding of RG and ML rocks and against (B) CO (nmol g^{-1}) released during grinding of RG rocks. Coloured dashed lines show the linear correlations between the respective gases. The grey dotted line is the linear regression of all samples in (B).

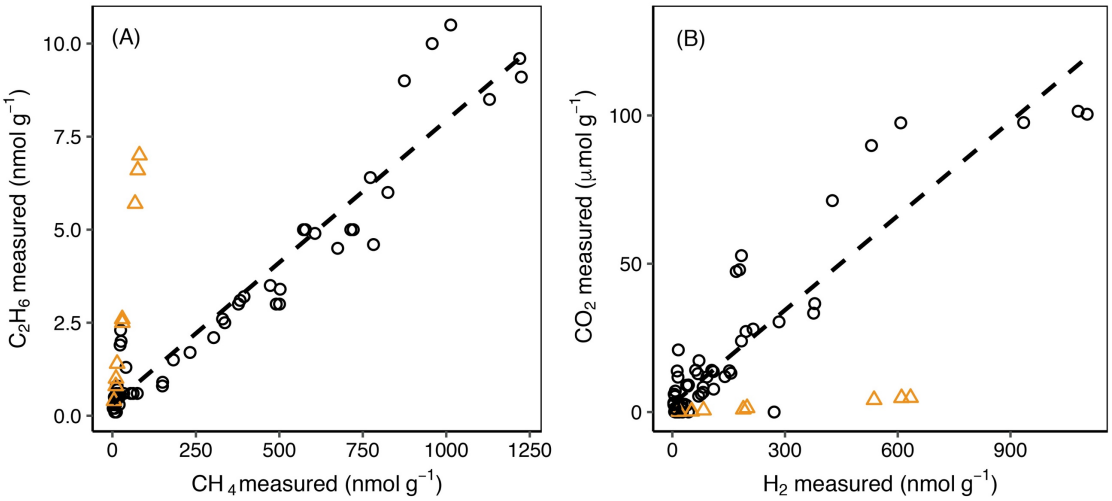

Figure 3.3 The relationship between the amount of C_2H_6 and CH_4 (A) and between CO_2 and H_2 (B) produced per gram of sample during grinding. Orange triangles represent analyses of ML sediment. The dashed line shows the correlation between the respective gas concentrations for all samples except ML sediment. When ML sediment is included in the highly linear relationship between C_2H_6 and CH_4, the R^2 drops from 0.93 to 0.79. When ML sediment is included in the linear relationship between CO_2 and H_2, the R^2 drops from 0.86 to 0.66.

3.5 Discussion

3.5.1 Sources and generation mechanisms for gases during glacial grinding

The potential sources of the different gases measured during grinding of rock and glacial sediment samples in this study likely reflect release from two primary mechanisms. First, gases may be released from pore spaces, fluid inclusions or crystal structures. Second, they may be formed as a consequence of bond breakages during grinding of the rock. The dominant source for each sample will be dependent upon the gas species and the rock type (i.e. sedimentary versus crystalline). We use our experimental data to infer the most likely source of each gas for the different rock types in the following sections.

3.5.1.1 Hydrogen

H_2 was measured during grinding of all of the samples. There is some evidence that H_2, generated by thermal degradation of organic matter during a rock's formation, can be trapped within the pore spaces of sedimentary rocks (Suzuki et al., 2017). The breaking open of pore spaces during grinding may be an important source of H_2 for the sedimentary RG rocks. For the crystalline samples (LG, MG, EG and ML) release of free H_2 trapped within the rock is a less likely source because, although H_2 can be contained within fluid inclusions, this is rare (Burke, 2001). We therefore propose that the majority of H_2 emitted by the grinding of the crystalline samples and at least some of the H_2 emitted by the sedimentary samples is likely formed during the grinding process, rather than released. There are two likely formation mechanisms for H_2, both of which involve reactions with surface radicals which form on the fractured surfaces of minerals where bonds have broken. The first generation mechanism results from the reaction of water with silica radicals (Si·) and is the most commonly attributed source of H_2 released from the grinding of rocks, e.g. in fault zones (e.g. Sugisaki et al., 1983; Ito et al., 1999):

$$\equiv \mathrm{Si}\bullet + \mathrm{H_2O} \rightarrow \equiv \mathrm{Si-OH} + \mathrm{H}\bullet \quad (3.5)$$

$$2\mathrm{H}\bullet \rightarrow \mathrm{H_2}$$

The second potential H_2 generation mechanism involves the reaction of hydroxyl functional groups (–OH) from within the crystal structure with Si· radicals which form on the surface of a fracture plane (Hirose et al., 2011; Kameda et al., 2004):

$$\equiv \mathrm{Si}\bullet + \mathrm{AlOH} \rightarrow \equiv \mathrm{Si-O-Al} + \mathrm{H}\bullet \quad (3.6)$$

This mechanism has been used to explain why the grinding of –OH rich minerals, such as phyllosilicates (e.g. muscovite and biotite mica) and the clays, generate more H_2 than grinding other silicate minerals to similar surface areas, and therefore, producing similar amounts of silica radicals (Kameda et al., 2003).

It seems unlikely that the first mechanism (Equation 3.5) was the primary production mechanism in our experiments, given the significant quantities of H_2 released under dry conditions (Section 3.3.2). Although it is possible that some H_2O, either as liquid or vapour, was released from fluid inclusions in our samples during grinding, we propose that an additional mechanism was required for the high amounts of H_2 emitted during grinding of, in particular, EG schist, ML schist, ML sediment and MG granite (Figure 3.1a). Therefore, to further investigate if the reaction of –OH groups with Si· (Equation 3.6) better explains the high production of H_2 measured, we compared the estimated content of the micas, biotite and muscovite, in hand specimen (Section 3.3.1) with the H_2 generated when the sample was ground to 17 μm (the average grain size of suspended sediment exported from LG, RG and ML, for which this data was available; Table 3.3). Of the samples here, excluding the RG rocks which were too fine-grained for hand-specimen mineral quantification, ML and EG schist had the most muscovite and biotite at an estimated 60 and 70 % area, respectively (Table 3.1) and generated the most H_2 when ground to 17 μm at 164 and 407 nmol g^{-1}, respectively. Comparatively, ML quartzite, which had no detectable mica by this method, and LG granite, which had approximately 5 % mica, produced the lowest amounts of H_2 when ground to 17 μm at 31 and 21 nmol g^{-1}, respectively. The three sedimentary rocks from RG were too fine-grained for mica identification in hand-specimen. However, based upon known characteristics of the rock types (shale and muddy-carbonates), we can broadly infer that they contained high quantities of "mud", i.e. clay minerals (hydrous aluminium phyllosilicates). Reaction of Si· with –OH groups present in clays could supply H_2 in addition to that released from pore spaces, thus helping to explain the high amounts of H_2 released when grinding the RG rocks (Figure 3.1a). Our results broadly support that increased mica or clay content and, therefore, increased presence of –OH groups stimulates greater H_2 generation during grinding. However, more detailed analysis of mineralogical composition would be required to definitively test this hypothesis.

Several experiments have shown that the loss of –OH groups from a phyllosilicate mineral (e.g. by Equation 3.6) leads to an amorphous structure (e.g. Takahashi, 1959; Kristof *et al.*, 1993; Martinelli and Plescia, 2005). Interestingly, a recent study by Hawkings *et al.* (2017) described significant quantities of amorphous material, particularly silica, on suspended sediments in LG's subglacial meltwaters. The authors hypothesised one potential source of this amorphous material as the mechanical grinding of bedrock beneath the ice sheet. The amorphous material on the suspended sediment grains was largely found on the edges of platy minerals (e.g. micas or clays) and contained varying amounts of auxiliary elements, including, aluminium (Hawkings et al., 2017). This tentatively supports the reaction of Si· with –OH groups in phyllosilicates (Equation 3.6) being an important driver of H_2 generation by mechanical erosion.

We propose that the main mechanism for generation of H_2 by grinding of crystalline rocks was by reaction of Si· with –OH due to the presence of phyllosilicate minerals in all rocks, the occurrence of higher estimated mica contents with higher H_2 generation, and the presence of amorphous material containing Al on platy minerals. Even for rocks containing minor quantities of –OH-rich minerals (e.g. LG gneiss and ML quartzite), studies have shown that more than half the H_2 generated from grinding can arise from the fracturing of minor minerals (Kameda *et al.*, 2003). This, in combination with the possible release of H_2O from fluid inclusions allowing some formation by Equation 3.5, explains the production of H_2 from samples that are poor in phyllosilicates.

A recent study by Telling et al. (2015) measured H_2 generated by rock-water reactions (Equation 3.5) during incubation of crushed rocks from glaciated catchments with water at subglacially-relevant temperatures (0 °C). At LG, data was available to directly compare estimated long-term catchment-scaled rates of H_2 generation by rock-water reactions from Telling et al.'s (2015) study with H_2 generation by dry grinding from this study (Section 3.3.6). Generation of H_2 by dry grinding at LG (244 nmol m^{-2} d^{-1}; Table 3.5) was the same order of magnitude as the generation previously inferred by rock-water reactions (151 nmol m^{-2} d^{-1}).

3.5.1.2 Carbon dioxide and carbon monoxide

Significant generation of CO_2 was measured during grinding of sedimentary rocks from RG and metamorphic rock and sediment from ML. Possible sources include release from fluid inclusions, release from pore spaces, dissociation from calcite/dolomite minerals

and oxidation of the released CH_4. The latter process seems unlikely to be occurring in these experiments because grinding occurred in an oxygen free atmosphere, temperatures were unlikely to be high enough for CH_4 combustion (the mill was never hot to the touch), and 1-4 orders of magnitude more CO_2 was measured than CH_4. Therefore, the remaining possible sources of CO_2 (fluid inclusions, pore spaces, and crystal dissociation) are more likely and vary by rock type. For ML samples, CO_2 was probably released from CO_2-rich fluid inclusions which are common in many minerals and can form during or post-metamorphism (Burke, 2001; Diamond, 2001). For RG shale, the majority of CO_2 (as with the hydrocarbons, Section 3.5.1.3) was likely released from pore spaces between the particles of clays and other minerals which were broken open upon grinding (Wang et al., 2015). For the RG muddy carbonates, we speculate that CO_2 was both released from pore spaces and released from the breakdown of calcite ($CaCO_3$) and/or dolomite ($CaMg(CO_3)_2$) crystals that make up the carbonate component of the rock. The latter process has been suggested to occur during the mechanical breakdown of marly carbonates, a similar rock type to the RG muddy carbonates, by the following mechanisms (Martinelli and Plescia, 2005):

$$\mathbf{CaCO_3 \rightarrow Ca - O + CO_2} \quad \textbf{(3.7)}$$

$$\mathbf{CaMg(CO_3)_2 \rightarrow CaMgO_2 + 2CO_2} \quad \textbf{(3.8)}$$

Emission of CO during grinding was analysed for rocks from two catchments with contrasting geologies; high total carbon sedimentary RG and low total carbon igneous MG (Figure 3.1c). There is little in the literature about the release or production of CO during the mechanical breakdown of rocks/minerals. CO can be found in fluid inclusions in crystalline rocks (Burke, 2001) making this the likely source of CO from grinding MG granite. The Martinelli and Plescia (2005) study on the mechanical breakdown of marly-carbonaceous rocks (broadly similar in composition to the RG muddy carbonates) notes that CO is produced in 'measurable quantities'. However, this was not quantified and no mechanism for release was described. The amount of CO and CO_2 released was highly linearly correlated for the RG rocks ($R^2 > 0.92$) (Figure 3.2b). We therefore tentatively suggest that the source of CO was similar to CO_2 for RG rocks, i.e. primarily pore spaces for the shale and both pore spaces and release from the breakdown of calcite and dolomite crystals for the muddy carbonates.

3.5.1.3 Hydrocarbons

A range of short chain hydrocarbon species were detected during grinding: CH_4 (methane), C_2H_6 (ethane), C_2H_4 (ethylene), C_2H_2 (acetylene) and C_3H_8 (propane). Most significantly, CH_4 was produced during grinding of all samples, with significantly higher amounts produced by grinding sedimentary rocks from RG than the other samples (Figure 3.1d). Three possible sources of hydrocarbons are fluid inclusions in the crystalline samples, pore spaces in the sedimentary samples and breakdown of carbon compounds in all samples. Fluid inclusions in igneous and metamorphic rocks commonly contain CH_4 with C_2H_6 as a more minor component and the higher hydrocarbons comparatively rare (Burke, 2001). This follows with the results found here: CH_4 was the most abundant hydrocarbon measured; C_2H_6, where quantifiable, was roughly 1-2 orders of magnitude lower; and lower or trace quantities of C_2H_4, C_2H_2 and C_3H_8 were found, if detected at all (Table 3.4). The higher CH_4 (1-2 orders of magnitude greater) and C_2H_6 (up to 1 order of magnitude greater) released when grinding the sedimentary RG rocks compared to all others (Figure 3.1d, 1e) is likely related to the presence of pore spaces which can trap gaseous hydrocarbons. These hydrocarbons were likely generated from the breakdown of organic matter during the rock's formation (Wang et al., 2015; Zhang et al., 2014).

The generation of hydrocarbons from the mechanical breakdown of carbon compounds within the rock samples during grinding is a possible source for all samples. To investigate this, the total carbon content (weight percent) of the rock was measured and compared to the amount of hydrocarbons, and other carbon-based gases, measured during grinding (Figure 3.4). Increasing total carbon content broadly correlated with higher emission of CH_4 (R^2 of 0.72, $p < 0.001$). There was a weaker correlation with C_2H_6 (R^2 of 0.46, $p < 0.001$) perhaps because C_2H_6 was a comparatively minor component of gas released.

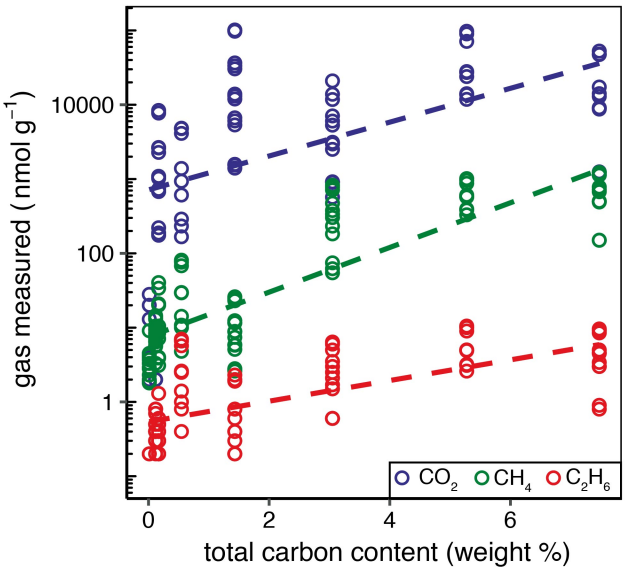

Figure 3.4 The amount of CO_2, CH_4 and C_2H_6 produced (nmol g^{-1}) compared to the percentage weight of total carbon present in the sample.

CO_2 was poorly correlated (R^2 of 0.28, $p < 0.001$), possibly because of the different suggested primary generation mechanism (dissociation from the crystal structure of calcite and dolomite; Section 3.5.1.2). CH_4 and C_2H_6 were correlated across all samples (Figure 3.3a) which could indicate that the hydrocarbons trapped within the rocks (in fluid inclusions or pore spaces) originally formed in similar proportions. However, the formation mechanisms are vastly different, i.e. post-magmatic processes influencing fluid inclusion composition in igneous rocks (Potter and Konnerup-Madsen, 2003), such as those from LG and MG, or biogenic and/or thermogenic processes influencing pore space composition during the formation of shale (Wang et al., 2015). It is therefore possible that the linear relationship between CH_4 and C_2H_6 could be explained by a common generation mechanism during grinding, i.e. from the mechanical breakdown of carbon compounds. Accurately distinguishing between the discussed sources of the measured hydrocarbons (fluid inclusions, pore spaces and generation by breakdown of carbon compounds) would require *in situ* detection of gases in fluid inclusions, e.g. by raman microscopy. Interestingly, ML sediment was an outlier to the high collinearity of CH_4 and C_2H_6 between all samples. If ML sediment was included within the analysis the R^2 of the correlation was reduced from 0.93 to 0.79. A similar pattern was seen for H_2/CO_2 ratios (Figure 3.3b) which were elevated for ML sediment. This sample was collected from in front of the glacier terminus and consequently was exposed to the atmosphere. We therefore suggest that the elevated ratios for ML sediment reflected post-depositional processes, such as oxidation of CH_4 and dissolution, causing loss of CO_2 trapped within the minerals.

3.5.2 Glacial erosion liberates potential energy sources for subglacial microbes

The generation of gases by mechanical grinding beneath glaciers and ice sheets could be significant for various microbiological processes in subglacial environments. A wide variety of microbes use different gases as their energy and/or carbon source (Conrad, 1996). Of the gases measured after grinding in these experiments, H_2, CO_2, CH_4 and CO are the most relevant to microbial processes. In the subglacial environment, an abiogenic source of these gases from bedrock grinding has the potential to sustain microbial populations during long periods of isolation from the atmosphere and surface processes or where other sources are scarce, e.g. where subglacial sediments are carbon-poor. Notably, H_2 is utilised by many methanogens as a growth substrate, with CO_2 as the preferred electron acceptor (Equation 3.3). These hydrogenotrophic methanogens are an

important species in isolated environments due to their ability to subsist upon abiogenic H_2 and CO_2 as their sole energy source (Sleep and Zoback, 2007; Hirose *et al*., 2011). Several studies have identified the presence of methanogens, including hydrogenotrophic methanogens, in subglacial sediments and waters, and long-term incubations of subglacial sediments have shown active CH_4 generation (Boyd et al., 2010; Stibal et al., 2012b).

In order for grinding-generated H_2 to be a source of energy for subglacial microbes, generation rates would need to be comparable with microbial rates of consumption. Therefore, catchment-scaled rates of H_2 generation by subglacial rock grinding were calculated (Section 3.3.6). These rates were calculated using suspended sediment (SS) export as a proxy for decadal and longer term abrasion rates. Varying rates were obtained depending upon bedrock type and erosion rate. For example, rates of H_2 generation at ML and EG were the same order of magnitude as for LG (Table 3.5) despite the order of magnitude more H_2 released per gram of the former samples (Figure 3.1a). This is because LG has a considerably higher sediment export and erosion rate. Similarly, grinding of porphyritic granite from MG produced more H_2 per gram of sample than LG gneiss (Figure 3.1a), but MG had a lower production rate due to the slower erosion rate at this much smaller glacier (Table 3.5). Therefore, although the magnitude of H_2 generation per gram is dependent on the bedrock type, the erosion rate is an important influence upon the significance of H_2 generation in a catchment.

Table 3.5 Comparison of estimated long-term catchment production rates of H_2, CO_2 and CH_4 (nmol gas m^{-2} day^{-1}) by subglacial grinding. Rates were calculated here (Section 3.3.6). Sediment export rates were adapted from Table 3.3. (<) concentrations too low to calculate catchment rates.

Glacier	Catchment area (km^2)	Sediment export (t km^{-2} a^{-1})	H_2 production (nmol m^{-2} d^{-1})	CO_2 production (nmol m^{-2} d^{-1})	CH_4 production (nmol m^{-2} d^{-1})
MG	14.4	1219	155	<	21
LG	600	4833	244	479	39
EG	36.2	456	311	<	12
ML	5.4	1751	369	26965	25
RG	1.4	237	37	13519	650

To determine if rates of grinding-generated H_2 are sufficient to act as an energy source for subglacial methanogens, we calculated the depth of sediment throughout which measured rates of methanogenesis could be supported, assuming the sediments are anoxic. Rates of methanogenesis were available for two lithologically contrasting catchments: gneissic LG and sedimentary RG (Section 3.3.7). At LG, we calculate that hydrogenotrophic methanogenesis could be supported throughout 17 cm of sediment depth beneath the entire LG catchment. It is important to note that the grinding of basal sediment at LG produces similar quantities of H_2 per gram as grinding bedrock (Figure 3.1a), indicating that reworking of basal sediment would sustain similar rates of methanogenesis as erosion of bedrock itself. The sediment depth throughout which methanogenesis could be supported by grinding-generated H_2 at RG was much lower (2 cm) due to the significantly lower rate of erosion at RG (~0.1 mm yr^{-1}) than at LG (4.8 mm yr^{-1}; Cowton et al., 2012). The sediment depths calculated here are within estimated sediment depths present at each catchment. At RG estimated depths are on the decimetre or sub-decimetre scale based upon observations that RG sits partly upon till and partly upon bare bedrock (Boyd et al., 2010). At LG, subglacial sediments could be present on the decimetre scale up to the multi-metre scale as indicated by 0 to decimetre thick sediments found at nearby Isunnguata Sermia and spatially-limited seismic evidence of sedimentary basins 10s of metres deep at LG (Dow et al., 2013; Harper et al., 2017; Kulessa et al., 2017).

Telling et al. (2015) calculated that water-Si• reactions (Equation 3.5) generated enough H_2 to support methanogenesis in the top 1 cm of sediment throughout the LG catchment (study described Section 3.5.1.1). However, the authors calculated that the rate of CO_2 released from bubbles trapped in the ice (10% of ice volume, CO_2 pre-industrial fraction of 0.0003) by basal melting (assumed rate of 6 mm/yr) was insufficient to act as the sole acceptor for their calculated rates of rock-water H_2 generation. Here, we show that grinding basal sediment at LG generates 8 times the CO_2 required as an electron donor for utilising grinding-generated-H_2 as an abiogenic energy source in hydrogenotrophic methanogenesis (Table 3.5; Section 3.3.6-3.3.7). At RG, grinding CO_2-rich carbonates and shale generates more than 90 times the CO_2 required for methanogens utilising grinding-generated-H_2 for the same process. Therefore, hydrogenotrophic methanogenesis could be sustained entirely by the process of glacial grinding throughout LG and RG catchments at sediment depths of 17cm and 2cm, respectively. RG is a small

glacier with a low erosion rate (~0.1 mm a^{-1}). Glaciers with faster erosion rates and similar bedrock to RG would generate more gases per m^{-2} d^{-1} by grinding and, therefore, could sustain hydrogenotrophic methanogenesis throughout greater depths of sediment, assuming a constant microbial metabolic rate. Further, the orthogneiss sample from LG is broadly representative of much of the basement rock that underlies the Greenland Ice Sheet. We therefore suggest that mechanical glacial erosion could provide an abiogenic source of energy, in the form of H_2 and CO_2, for subglacial microbial metabolism beneath the Greenland Ice Sheet and especially in marginal areas with higher ice flow and bedrock erosion rates.

Like H_2 and CO_2, CO was another gas emitted in our grinding experiments that may have similar potential to provide carbon and energy to subglacial microbes where other sources are limited. Several groups of bacteria and archaea can utilise CO as a source of carbon and/or energy. However, CO-utilising microbes have been little explored in the subglacial or sub-ice-sheet literature to date. Groups of microbes that can utilise CO include anaerobic sulphate reducers, hydrogenogens, methanogens and acetogens (Oelgeschläger and Rother, 2008). Given the wide range of anaerobic metabolisms that have been reported in subglacial systems (e.g. see Skidmore (2011) for review) it is plausible that CO-metabolizing species are present in subglacial environments. CO was measured after grinding rocks from two glaciated catchments with contrasting geologies: sedimentary RG, and igneous MG. The estimated long-term catchment-scaled rates of CO production at RG and MG were similar at 6 and 8 nmol m^{-2} d^{-1}, respectively (Section 3.3.6). At both catchments, CO generation rates are an order of magnitude lower than H_2 generation rates (Table 3.5). However, it is still plausible that grinding-generated CO could be metabolised beneath glaciers. Further work would be needed to establish the production of CO by subglacial erosion at additional catchments and to establish the existence and utilisation of CO by subglacial microbes to determine if this finding is significant.

3.5.3 Glacial erosion liberates a source of acidity for chemical weathering

The generation of CO_2 by subglacial erosion has the potential to influence glacial chemical weathering rates because CO_2 dissolves in water to form carbonic acid which dissociates to generate protons. This drives the chemical dissolution of carbonate (3.9) and silicate (3.10) minerals.

(3.9) $$CO_{2\,(aq)} + H_2O_{\,(l)} + CaCO_{3\,(s)} \rightleftharpoons Ca^{2+}{}_{(aq)} + 2HCO_3^-{}_{\,(aq)}$$

Calcite

(3.10)

$$2CO_{2\,(aq)} + 3H_2O_{\,(l)} + CaAl_2Si_2O_{8\,(s)} \rightleftharpoons Ca^{2+}{}_{(aq)} + 2HCO_3^-{}_{\,(aq)} + Al_2Si_2O_5(OH)_{4\,(s)}$$

Anorthite (Ca-feldspar) **Kaolinite (clay)**

Proton sources in the subglacial environment can become depleted due to isolation during glaciation, and the supply of protons can limit chemical weathering rates (Tranter et al., 1996). CO_2 is supplied to the subglacial environment by: periodic inputs of supraglacial meltwaters carrying atmospheric gases (isolated to small areas of the ice base where surface waters reach these depths); the release of palaeo-CO_2 from gas bubbles in the ice during basal melting (which occurs at a rate determined by basal melt rates which varies across the bed); and from microbial respiration (Montross et al., 2013; Sharp et al., 1999). The production of CO_2 from glacial crushing is therefore an additional source that can provide acidity to drive chemical weathering.

At ML, we calculated gas generation rates using suspended sediment fluxes as an estimate for the long term abrasion rate. Assuming that the present day rates match the longer term abrasion rate, we calculate that 18-21% of CO_2 required to sustain chemical weathering rates measured by Hodson et al., (2000) could be generated by grinding of the bedrock and sediment (Section 3.3.8). Although this may be an overestimate if there are significant rates of sediment redistribution relative to abrasion beneath the glacier, the calculation shows the clear potential for CO_2 released by grinding to have a significant impact upon CO_2 weathering budgets beneath glaciers. The data was not available to calculate weathering rates at RG but given the similarly high magnitudes of CO_2 production rates to ML, it is likely that grinding-generated CO_2 would be a potential influence on weathering rates at that catchment as well. The trace CO_2 generated by grinding igneous and some metamorphic rocks at LG, MG and EG is unlikely to significantly influence dissolution rates in comparison to other sources. However, for glaciers located on sedimentary and some metamorphic bedrock types, which can be found in the Rockies, the Alps, the Himalayas and Antarctica, grinding-generated CO_2 has the potential to decrease the amount of CO_2 that has previously been interpreted to have been drawn down from the atmosphere by glacial weathering (Hodson et al., 2000).

3.5.4 Glacial erosion as an abiogenic source of methane

It has been theorized that microbial breakdown of organic matter in overridden sediments has the potential to generate CH_4 clathrate beneath ice sheets (Wadham et al., 2008, 2012). Evidence of subglacial CH_4 oxidation has also been demonstrated indicating that methanotrophy can potentially remove large quantities of CH_4 in areas of the subglacial environment that are oxic, such as subglacial lakes and upper sediment layers (Dieser et al., 2014; Michaud et al., 2017). CH_4 has recently been reported in waters emerging from the Greenland Ice Sheet with some indication that net production is occurring in large areas beneath ice sheets (Dieser et al., 2014; Lamarche-Gagnon et al., 2019). These studies have inferred the source of this CH_4 to be microbial. CH_4 released by the mechanical subglacial erosion of bedrock has not previously been considered as a potential source. This abiogenic source could be significant in some catchments depending upon the catchment's bedrock type and erosion rate.

To investigate the significance of grinding as a source of CH_4, we compared estimated generation rates at two geologically contrasting catchments; sedimentary RG and gneissic LG (Section 3.3.6). Grinding at RG generated an order of magnitude more CH_4 than at LG despite the considerably lower erosion rate (Table 3.5), likely due to the order of magnitude higher CH_4 production per gram of sample (Figure 3.1d) from RG's comparatively carbon-rich bedrock. At LG, subglacial CH_4 production has recently been estimated to be at least 6 tonnes per year, for the 600 km^2 catchment (Lamarche-Gagnon et al., 2019). This flux was inferred to be from net microbial production of CH_4 based on stable isotope analyses of the CH_4 exported in subglacial meltwaters. We used catchment rates of CH_4 generation by grinding to estimate abiogenic CH_4 exported from the LG catchment (Section 3.3.8). Our estimated theoretical CH_4 flux from subglacial grinding amounted to 0.14 t y^{-1}, an order of magnitude lower than the measured flux of 6 t y^{-1} at LG (Lamarche-Gagnon et al., 2019). Thus, rock grinding is less significant than microbial generation as a source of CH_4 in catchments with carbon-poor bedrock.

There are no direct measurements of CH_4 in subglacial meltwaters at RG. The estimated grinding-generated abiogenic CH_4 export at RG was calculated to be 0.005 t y^{-1}, an order of magnitude lower than at LG. However, if the size of the glaciers is taken into account, the export of grinding-generated CH_4 per km^2 per year is an order of magnitude higher at RG (0.004 t km^{-2} y^{-1}) than at LG (0.0002 t km^{-2} y^{-1}). Methanogenesis rates measured in

incubated subglacial sediment from both catchments are similar at 0.0002-0.0012 nmol CH_4 g^{-1} d^{-1} at RG (Boyd et al., 2010) and 0.00018 nmol CH_4 g^{-1} d^{-1} at LG (Stibal et al., 2012b). The similar methanogenesis rates combined with the order of magnitude more CH_4 generated by grinding at RG than LG, both per gram of rock and per km^2, could indicate that grinding would release more CH_4 than methanogenesis at RG. Therefore, abiogenic grinding-generated CH_4 release could be a more significant source of CH_4 than methanogenesis in catchments with carbon-rich bedrock.

Our results show that abiotic CH_4 formation from the subglacial grinding of bedrock likely represents a previously unaccounted CH_4 source in subglacial catchments. Grinding of bedrock could even constitute the bulk of CH_4 released from subglacial systems in regions with carbon-rich bedrock. As such, grinding-generated CH_4 should be considered when analysing CH_4 export from regions experiencing high erosion rates or with bedrock with a high carbon content.

3.6 Conclusion

We demonstrate that mechanical erosion of rocks and minerals beneath glaciers generates a previously unappreciated source of gases relevant to subglacial microbial processes and chemical weathering. We present the first experimental evidence that the grinding of rock and sediment samples from glaciated catchments with widely varying geologies have the potential to generate significant quantities of CO_2, CO, CH_4, other short chain hydrocarbons and, consistent with previous work, H_2 (Telling et al., 2015). The significance of grinding-generated gases for microbial and chemical dissolution processes depends on three primary factors. First, the amount of gas emitted during the mechanical breakdown of a rock will depend upon its mineral composition, the presence of pore spaces in the rock and the presence of fluid inclusions and their composition. Second, the erosion rate in the glaciated catchment will determine how rapidly rocks, sediment and minerals are mechanically broken down and thus, the rate at which gas is emitted. Third, the significance of gas generation via erosion will be determined in part by the comparative rates of supply from other sources in the catchment. Our experiments have shown that glacial erosion has the potential to release CO_2 in sedimentary and some metamorphic catchments at rates that can influence the magnitude of the atmospheric CO_2 budget required to drive weathering. Beneath glaciers of all bedrock types, we would expect to see generation of H_2 and CH_4 by glacial erosion. For catchments where CO_2 is generated in addition to H_2, such as catchments with sedimentary bedrock or basement bedrock as found in Greenland, some portion of hydrogenotrophic methanogenesis could be supported by grinding-generated gases beneath the ice. CH_4 generation from glacial erosion was common to all bedrock types and was shown to be particularly important in sedimentary catchments where rates of grinding-generation could be greater than *in situ* microbial production. Future studies should determine whether the gases produced in this study are directly utilised by microbial processes or weathering reactions through laboratory incubations with grinding-generated gases. Our findings show that mechanically-generated H_2, CO_2, CO and CH_4 should be considered in future studies which investigate microbial or geochemical subglacial processes, particularly energy sources for microbes, CH_4 cycling beneath ice, and chemical weathering processes.

4 Consumption and emission of halogenated trace gases from a retreating Arctic glacier's forefield

This chapter identifies and quantifies halogenated trace gas sources and sinks using field flux measurements from different land surfaces across a retreating glacial forefield. The influence of abiogenic and biogenic processes on trace gas fluxes is considered, with a particular focus on the impact of increasing soil development and changes in vegetation type and coverage with increasing distance from the retreating glacier's snout.

This chapter is in preparation for submission to *Atmospheric Chemistry and Physics* under the following reference:

> Macdonald, M.L., Wadham, J.L., Young, D., Lunder, C., Hermansen, O., Lamarche-Gagnon, G., O'Doherty, S., (*in preparation*). Consumption and emission of halogenated trace gases from a retreating Arctic glacier's forefield, *Atmospheric Chemistry and Physics*.

The study was conceived and conducted by myself with assistance for field sampling, analysis of halocarbon samples and optimisation of the ADS-GCMS from Dickon Young. Simon O'Doherty assisted and provided guidance for the initial preparation and optimisation of the ADS-GCMS for halocarbon analysis. Chris Lunder and Ove Hermansen permitted access to ambient halocarbon measurements made at the Zeppelin observatory (a few km from the field site), and provided access to gas cylinders (standard, blank and carrier gas) in the field. The analysis of the data and the writing of the manuscript was conducted by myself with review by J Wadham and D Young.

4.1 Abstract

The Arctic is one of the fastest warming regions of the Earth, with predicted temperature increases of 5 - 7 °C and the accompanying extensive retreat of Arctic glacial systems by 2100. This will reveal new proglacial land surfaces for microbial colonisation, ultimately succeeding to tundra over decades to centuries. An unexplored dimension to these changes is the impact upon the emission and consumption of halogenated organic compounds (halocarbons) from proglacial land surfaces. Halocarbons are involved in several important atmospheric processes, including ozone destruction, and despite considerable research, uncertainties remain in the natural cycles of some of these compounds. Using flux chambers, we measured halocarbon fluxes from proglacial land surfaces spanning recently-exposed sediments (<10 years), to approximately 1950 year old tundra in front of a High Arctic glacier. Proglacial land surfaces were found to consume methyl chloride (CH_3Cl) and methyl bromide (CH_3Br), with both consumption and emission of methyl iodide (CH_3I) observed. The largest consumption rates of these compounds occurred at the oldest, vegetated, tundra sites (-126 ±4, -1.76 ±0.04 and -0.124 ±0.025 nmol m^{-2} d^{-1}, respectively for CH_3Cl, CH_3Br and CH_3I). However, similar consumption rates were recorded at much younger sites with little soil development, but with the presence of extensive cyanobacterial mats (means of -106 ±7, -1.67 ±0.12, -0.097 ±0.029 nmol m^{-2} d^{-1} for CH_3Cl, CH_3Br and CH_3I). Emission of chloroform ($CHCl_3$), bromoform ($CHBr_3$) and dibromomethane (CH_2Br_2) was detected across the forefield, with the highest emission of $CHCl_3$ from cyanobacterial mats (105.36 ±41.52 nmol m^{-2} d^{-1}), $CHBr_3$ from bare sediment adjacent to the mats (0.67 ± 0.29 nmol $CHBr_3$ m^{-2} d^{-1}) and CH_2Br_2 from the vegetated tundra (mean 0.751 ±0.317 nmol m^{-2} d^{-1}). We have demonstrated that proglacial surfaces can consume and emit halocarbons despite their younger age and lower soil development than most traditionally studied surfaces. With future glacial retreat and the expansion of these surfaces, these fluxes may become more important in the future.

4.2 Introduction

Despite being present at only low concentrations in the atmosphere (part per trillion, ppt), halocarbons play an important role in the destruction of ozone by supplying halogens to the stratosphere and troposphere (Butler, 2000; Mellouki et al., 1992; Montzka et al.,

2011). Methyl chloride (CH_3Cl) and methyl bromide (CH_3Br) are the most important sources of chlorine (16%) and bromine (50%) to the troposphere and are important contributors to stratospheric ozone loss (Carpenter et al., 2014). After CH_3Cl, chloroform ($CHCl_3$) is the next largest natural source of chlorine to the atmosphere. Bromoform ($CHBr_3$) and dibromomethane (CH_2Br_2) are the most abundant short-lived brominated compounds and contribute ~ 4 – 35 % of bromine to the stratosphere (Montzka et al., 2011). Methyl iodide (CH_3I) is the most important very-short lived iodinated gas species in the atmosphere with a lifetime of ~ 7 days (Montzka et al., 2011). Most of the aforementioned gases have anthropogenic sources, many of which have reduced in magnitude under the Montreal Protocol. This has increased the relative importance of the natural sources of these halocarbons. The contribution of halocarbons to atmospheric processes makes it important to fully constrain present day sources, and their likely change under climate change scenarios in the future.

Most natural sources of halocarbons involve biological processes driven by plants, algae and fungi, with methyl halides (CH_3X; X = Cl, Br, I) generated as a by-product of methyltransferase activity and polyhalomethanes (e.g. $CHBr_3$, $CHCl_3$, CH_2Br_2) produced as a by-product of haloperoxidase activity (Manley, 2002). Marine biogenic sources are predominantly driven by macro- and micro-algae and are particularly important for $CHBr_3$ and CH_2Br_2 which are considered to be exclusively marine (Laturnus et al., 1998; Montzka et al., 2011; Sturges et al., 1993; Tokarczyk and Moore, 1994). The other halocarbons studied here (CH_3X, $CHCl_3$) also have a wide range of terrestrial biogenic sources, including tropical and temperate forests, temperate peatlands and Arctic tundra (Figure 4.1; Farhan Ul Haque et al., 2017; Forczek et al., 2015; Rhew et al., 2008b; Simmonds et al., 2010).

Although biological sources dominate, abiotic sources are also possible, including emissions from open oceans (Chuck et al., 2005; Stemmler et al., 2014), oxidation of soil organic matter and degradation of leaf litter and plants (Derendorp et al., 2012; Keppler et al., 2000; Wishkerman et al., 2008). Major, non-atmospheric, natural sinks of the halocarbons are the oceans (primarily abiotic) and bacterial degradation in soils (Nadalig et al., 2014; Shorter et al., 1995; Ziska et al., 2013). The bacterial soil sink has been identified in wide ranging habitats from temperate forests to the tundra (e.g. Khan et al., 2012; Teh et al., 2009). Despite this considerable research, the magnitudes of the natural

sources and sinks of halocarbons still have uncertainties due in part to large variation around mean fluxes caused by spatial and temporal variability (e.g. Dimmer et al., 2001; Leedham et al., 2013; Montzka and Reimann, 2011; Stemmler et al., 2014). Reduction of the uncertainties and increased understanding of the processes influencing natural halocarbon fluxes are important for predicting future change.

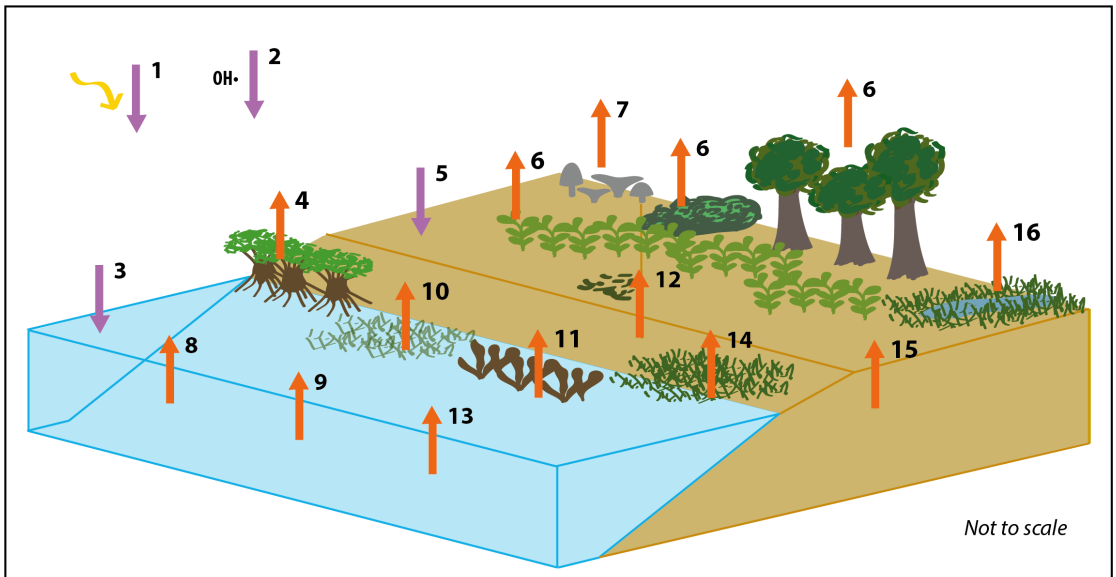

No.	Source/Sink	Compound
1	UV photolysis	All
2	Reaction with OH·	All
3	Open ocean	CH_3X, CH_2Br_2, $CHBr_3$
4	Mangroves (tropics)	CH_3X
5	Soil sink	CH_3X
6	Terrestrial plants (incl. shrubs, trees, grasses etc.)	CH_3Cl, $CHCl_3$, $CHBr_3$
7	Funghi	CH_3X
8	Open ocean	CH_3X, CH_2Br_2, $CHBr_3$
9	Phytoplankton	All
10	Seagrass meadows	CH_3X, $CHBr_3$
11	Macroalgae	All
12	Plant matter decay	CH_3Cl, CH_3Br
13	Marine bacteria	CH_3X, CH_2Br_2, $CHBr_3$
14	Salt marsh/coast. wetland	CH_3Cl, CH_3Br, $CHCl_3$,$CHBr_3$
15	Organic matter oxidation	CH_3X, $CHCl_3$, $CHBr_3$
16	Peatland (temperate)	CH_3Cl, CH_3Br, CH_2Br_2, $CHCl_3$

Figure 4.1 Schematic diagram summarising key natural sources and sinks for the 6 halocarbons of interest in temperate and tropical regions. (CH_3X = CH_3Cl, CH_3Br, CH_3I; coast. =coastal). References for presence of each flux are as follows: 1, 2 (see Montzka et al., 2011 for review), 3 (Hu et al., 2012, 2013; Ichikawa et al., 2015; Ziska et al., 2013), 4 (Kolusu et al., 2018; Manley et al., 2007), 5 (Khan et al., 2012; Rhew et al., 2010), 6 (Jaeger et al., 2018; Redeker and Kalin, 2012; Rhew et al., 2001), 7 (Redeker et al., 2004), 8 (Hu et al., 2012, 2013; Ziska et al., 2013), 9 (Scarratt and Moore, 1996, 1999; Tokarczyk and Moore, 1994), 10 (Weinberg et al., 2013, 2015), 11 (Leedham et al., 2013; Nightingale et al., 1995), 12 (Derendorp et al., 2012; Wishkerman et al., 2008), 13 (Fujimori et al., 2012; Karlsson et al., 2008), 14 (Rhew et al., 2014; Wang et al., 2016), 15 (Huber et al., 2009; Keppler et al., 2000), 16 (Dimmer et al., 2001; Khan et al., 2012).

A previously unstudied environment for halocarbon fluxes, is the young soil found on the forefields of retreating glaciers. As the Arctic warms, increasing areas of land are being exposed by ongoing glacial retreat, a process that is forecast to continue throughout the 21st century (ACIA, 2005; Graversen et al., 2008). The newly exposed sediment is colonised by microbes such as heterotrophic bacteria and fungi, CO_2- and nitrogen-fixing cyanobacteria and nitrogen-fixing diazotrophs who fix nutrients into the developing soil (Bradley et al., 2014; McCann et al., 2016). Soil stabilisation on newly exposed glacial forefields (i.e. prior to widespread plant colonisation) is primarily driven by cyanobacterial colonisation and the subsequent formation of soil crusts (Hodkinson et al., 2003). Through nutrient-fixing and soil stabilisation processes, the microbial community enables the succession of higher plants, eventually leading to a tundra-type ecosystem for High Arctic locations (e.g. Hodkinson et al., 2003; Moreau et al., 2008).

Despite the forecasting of enhanced glacial retreat, trace gas emissions from the proglacial environment have not been well-investigated with studies primarily focussing on CO_2 fluxes, particularly from higher plants on older surfaces, or CH_4 fluxes (Chiri et al., 2015; Muraoka et al., 2008). There have been no studies on halogenated trace gas fluxes from these environments and how they might be affected by the accelerated change occurring in the Arctic. With the expansion of proglacial soils through increasing glacial retreat in the coming decades, understanding the processes occurring in these soils is timely. To investigate the impact of soil development and the associated microbial to plant succession on halogenated trace gas fluxes, we conducted *in situ* flux measurements of CH_3Cl, CH_3Br, CH_3I, $CHCl_3$, $CHBr_3$ and CH_2Br_2 at five sites spanning newly exposed soils (exposed <10 years ago) to established tundra (exposed approximately 1950 years ago) in front of a high Arctic glacier.

4.3 Study site

4.3.1 General description of the location

Midtre Lovenbreen is a small (5.4 km^2) valley glacier situated on the northern side of the Brøggerhalvøya Peninsula, in northwestern Svalbard (78º 53' N, 12º 04' E; Figure 4.2). The glacier has been in near-constant negative mass balance since measurements began in 1968, and probably since at least the 1930s (Kohler et al., 2007). Warming mean annual temperatures since the 1920s have resulted in approximately 1.1 km of glacial retreat from a prominent moraine to its current position 1.8 km from the fjord edge (Figure 4.2). Between 1966 and 1990, this retreat resulted in the exposure of 2.3 km^2 of land, and is a process that continues today (Moreau et al., 2008). The exposed area is characterised by the dominance of large clasts (> 5 cm ⌀) and is influenced by glacial runoff with intermittent and shifting meltwater channels. The progression of the community assemblages along the proglacial chronosequence has occurred at slower rates than are typical, with cyanobacterial crust and lichens still prevalent beyond 150 years of exposure (Hodkinson et al., 2003). Vascular plants and byrophytes are present sporadically, and increasingly, with exposure age. The area experiences a maritime polar climate. The mean air temperature at the weather station in nearby Ny-Ålesund in July 2017, when this study was undertaken, was 6.1 ºC (Norway MET, 2017). Mean summer soil temperatures (~ 2mm below surface) on the proglacial foreland have been measured at 7-9 ºC (Hodkinson et al., 2003).

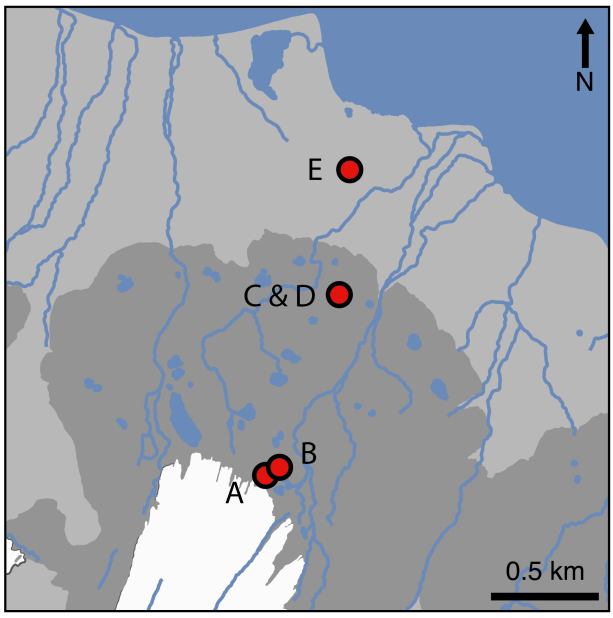

Figure 4.2 Locations of sites *snout* (A), *pond mat* (B), *disturbed mat* (C), *established mat* (D) and *tundra* (E) on the proglacial forefield of Midtre Lovenbreen glacier (white). The moraine field is denoted in dark grey, the furthest extent of which marks the furthest extent of the glacier during the Little Ice Age. Data used to create the base map from: Norwegian Polar Institute (2014).

4.3.2 Specific descriptions of the sites

Five different land surface types were studied in four different locations along a transect between the glacial snout and the fjord (Figure 4.2). The sites had different vegetation types and coverage (Figure 4.3). The exposure ages of the sites (in years before 2017) were estimated from dates obtained by ^{14}C dating and aerial photography in other studies (Hodkinson et al., 2003; Moreau et al., 2008). The site nearest the glacier's snout (site *snout*) had an exposure age of approximately 5 years and was characterised by bare sediment, with little to no visible signs of life (Figure 4.3a). Approximately 100 metres from the glacier snout, the second site (site *pond mat*) was located on the margins of a dried-up (by July) snow-melt pond in a small depression between the moraines. Around the margins of the pond, cyanobacterial mats had begun to form (Figure 4.3b). The surrounding moraines were still largely barren. The *pond mat* site is estimated to have been exposed for around 20 years. The third and fourth sites were located near the middle of the transect on an expanse of relatively flat land behind (~south) the prominent Little

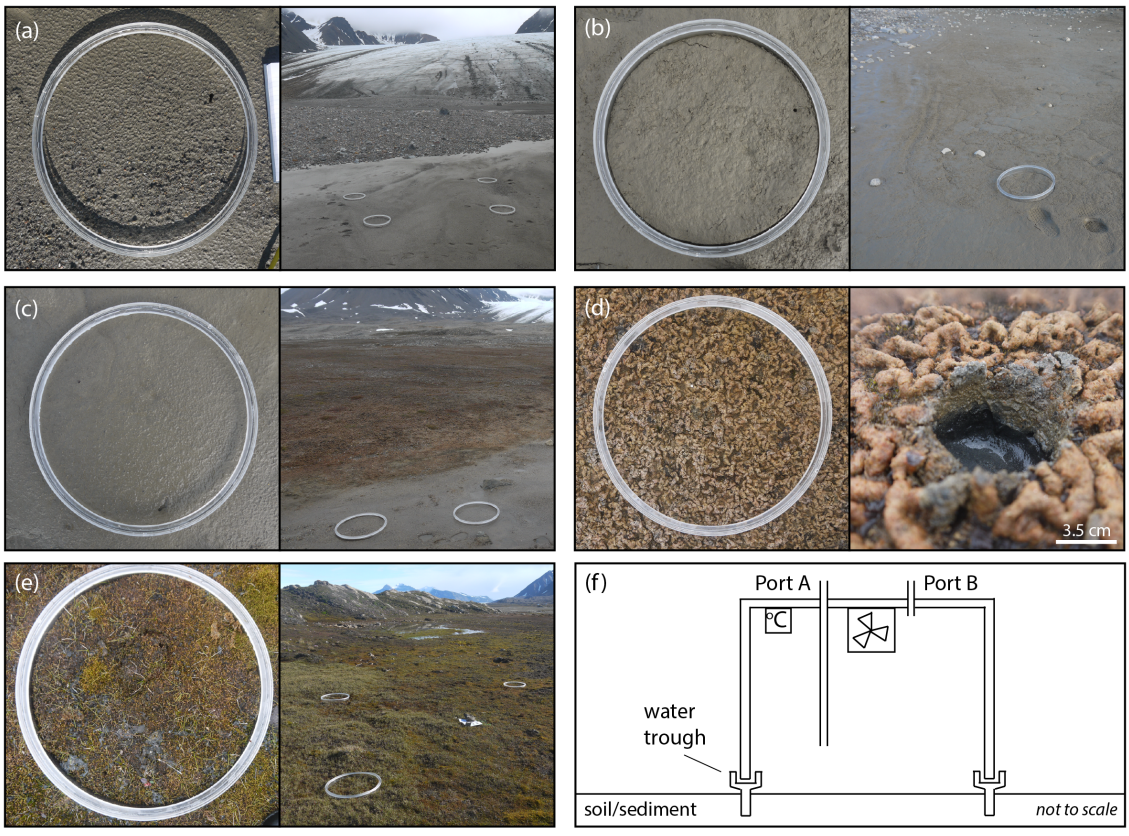

Figure 4.3 The visible differences in land-surface type and colonising species at site *snout* (a), *pond-mat* (b), *disturbed mat* (c), *mat* (d) and *tundra* (e), and a schematic diagram of the flux chamber's design showing sampling ports, fan and temperature logger (f). The width of the chamber collar in (a)-(e) is 0.39 m.

Ice Age moraine (Figure 4.2). Site *established mat* was located on the extensive cyanobacterial mats which cover large expanses of the flatter land (Figure 4.3d). A site immediately adjacent to the mats where the mats had been disturbed by snow melt flowing from ponds (site *disturbed mat*) was also studied as a direct comparison (Figure 4.3c). The exposure age of site *established mat* and *disturbed mat* was estimated at 100 years. The final site (site *tundra*) was located about 200 m from the coast (Figure 4.3e). At this site, small bluffs of limestone and siltstone provided some shelter from the shifting nature of the glacial runoff rivers which otherwise hamper colonisation of much of the flood plain between the moraines and the fjord. Site *tundra* had a soil depth of about 15 cm and 100 % vegetation coverage. Dominant species included *Bryophyta* spp. and *Carex rupestris*, *Salix polaris* and *Racomitrium lanuginosum*. Radiocarbon dating near site *tundra* (~70 m west) has provided a date of exposure of 1850-1926 BP (Hodkinson et al., 2003).

4.4 Methods

4.4.1 Flux experiments

Four custom-made, cylindrical, Perspex flux chambers (0.029 m^3) composed of a collar (0.07 m height) and top (0.22 m height, Figure 4.3f) were deployed for gas analysis between the 25th and 31st July 2017. Preliminary experiments were conducted near site *established mat* in 2016 to determine the impact on gas fluxes of covering the chambers with a reflective material and therefore conducting the experiments in the dark. The tests showed no statistical difference (2-sample t-test; Section 4.4.5) between covered and uncovered chambers (conducted in duplicates) for mean fluxes of CH_3Cl, CH_3Br and CH_3I (Figure 4.4; other halocarbons not analysed, experiment conducted over 5 hours). Despite there being no statistical difference in gas concentration change, the covered chambers were used for the main experiments in 2017 to prevent over-heating when in direct sunlight, therefore minimising the influence of heat on the soil processes involved in the fluxes. The collar was embedded in the sediment surface prior to sampling (at least 18 hrs) to allow gases released/ absorbed from breaking the surface to equilibrate with the background air concentrations. At site *tundra*, where plant roots were abundant, a small knife was used to cut through the roots as the collar alone could not break through the surface. An integrated "trough" on the collar was filled with deionised water (14-18 MΩ-cm) to provide a leak-tight seal with the upper section of the chamber (Figure 4.3f). A fan (24 m^3 h^{-1}; San Ace 60) was operated continuously during incubation to maintain continual mixing of the chamber air. Tinytag temperature loggers (Gemini Data Loggers) were fixed to the underside of the chamber lid.

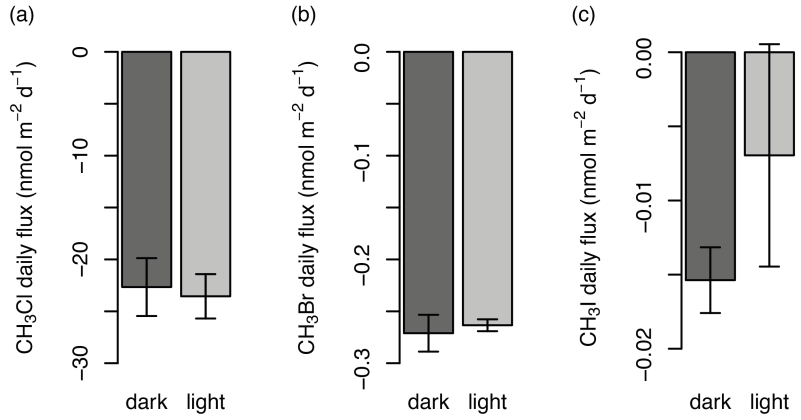

Figure 4.4 Comparison of the flux in nmol m^{-2} d^{-1} of gas in un-darkened (light) and darkened (dark) chambers for CH3Cl (a), CH3Br (b), CH3I (c) from preliminary experiments in 2016.

Two sampling ports, constructed from polypropylene BSP fittings, Luer-lock stop-cocks, and 20 cm polypropylene tubing (port A only, Figure 4.3f), enabled gas sampling to be conducted 1 and 2 hours after sealing the chamber. Two types of gas sampling were conducted; first, 3.7 mL samples were taken for CO_2 and CH_4 analysis in Bristol; second, 2.5 L samples were taken for halocarbon analysis by GCMS at the UK station in Svalbard. Sampling was conducted with four replicates (four chambers). Each site was analysed on a different day, with sites *snout* and *pond-mat* measured once (4 replicates), and sites *mat*, *disturbed mat* and *tundra* measured twice (two separate days of 4 replicates each, total 8 replicates). Chambers and collars were washed with deionised water and dried with paper towels between sites to minimise contamination.

Both a laboratory and a field blank test of the flux chamber equipment was conducted by placing the chambers onto aluminium-foil trays and filling the inside of the chamber collar with a 1 cm deep layer of de-ionised water to create a seal. For the field blank tests, the aluminium-foil trays were placed on wooden boards (to provide a flat surface) on the ground near to site *tundra*. The blank tests were conducted with four replicates and gases were measured as in Section 4.4.2 and 4.4.3.

4.4.2 CO_2 and CH_4 sampling and analysis

CO_2 and CH_4 were sampled in duplicate at each time point using a glass gas-tight syringe (Hamilton). Samples were taken from the ambient air (time 0) and from the chamber headspace via port B (Figure 4.3f, time 1 and 2). 5.5 mL of air was drawn through the tap and syringe and flushed to ambient prior to withdrawing a further 5.5 mL sample into the syringe. 1.5 mL of the sample was used to flush a syringe filter (0.2 μm) and needle. The remaining 4 mL sample was aseptically injected into a 3.7 mL evacuated vial (Exetainer®; Labco) via the flushed 0.2 μm syringe-filter. Exetainers were stored (within 4 hours of sampling) and transported at +4 °C until analysis in the UK which was conducted within 1 month of collection.

Exetainer samples were injected into an Agilent 7890A gas chromatograph (GC) fitted with a methaniser (at 395 °C) and an FID (flame ionising detector, at 300 °C). Separation of methane (CH_4) and carbon dioxide (CO_2) was achieved using a molecular sieve 5A, 60-80 mesh, 8 ft x 1/8-inch column, held at 30 °C for 4 minutes, before being ramped at 50 °C per minute to 180 °C. Calibration standards (mixed air; BOC) were run twice daily.

The percentage variance, limit of quantification and limit of detection for each gas is displayed in Table 4.1. Concentrations of the samples were calculated from a linear regression line (r >0.99, n=5) of manual dilutions of certified (± 5 %) standards with 5.0 grade Argon (BOC) fitted with an in-line gas desiccator. The Ideal Gas Law was used to convert gas concentrations to molar amounts which was then corrected for dilution.

4.4.3 Halocarbon sampling and analysis

2.5 L air samples for analysis of halocarbons were taken using a small pump (SKC, Twin Port Pocket Pump) at 250 mL min^{-1} into 3 L Tedlar gas tight bags (polypropylene fittings, SKC). All sample bags were flushed 3 times with synthetic air prior to use, with laboratory testing indicating this stopped any contamination of subsequent samples by prior ones. The length of sampling time (ten minutes) required the chambers to be sealed approximately twelve minutes apart to allow time for sampling. A sample of ambient air was taken between the sealing of the first and second and the third and fourth chambers. An average of the two ambient measurements was used as time 0 for the four chambers.

Table 4.1 The standard concentration, limit of quantification (variance) and limit of detection (LOD) for each gas analysed, with the target ion and qualifier ion(s) shown for gases analysed by GCMS. (*) ppt for the halocarbons, ppm for CO_2 and CH_4. (NA) not applicable to the method of measurement. 'equi.' is short for equivalent.

	Units	CH_3Cl	CH_3Br	CH_3I	$CHCl_3$	$CHBr_3$	CH_2Br_2	CO_2	CH_4
Target ion	m/z	52	94	142	83	171	174	NA	NA
Qualifier ion(s)	m/z	50	96	127	85	173, 175	93, 95	NA	NA
Standard conc.	ppt / ppm*	529	6.42	0.461	16.7	2.94	1.27	405.6 ±5%	194.7 ±5%
Variance (n=49)	%	2	1	3	1	3	2	1.7	1.1
Variance equi-valent	nmol m^{-2}	0.1	0.0007	0.0001	0.002	0.0009	0.0002	0.02	0.2
	nmol m^{-2} d^{-1}	3	0.02	0.003	0.06	0.02	0.005	0.5	4.7
LOD	ppt	1.4	0.3	0.01	0.18	0.38	0.08	0.32	0.16
LOD, equi.	nmol m^{-2}	0.01	0.003	0.0001	0.002	0.004	0.0009	0.003	0.002
LOD, equi-valent	nmol m^{-2} d^{-1}	0.3	0.07	0.003	0.04	0.09	0.02	0.07	0.05

Headspace analysis of each chamber was taken after 1 and 2 hours through the extended tubing of port A to further ensure mixing of the chamber air (Figure 4.3f). A 3 L sample bag flushed and filled with synthetic air was connected to port B during sampling to maintain ambient pressure within the chamber and prevent air being drawn through the soil. 50 mL of chamber air was flushed through the port A tubing and the pump prior to taking the 2.5 L sample. Sample bags were stored in the dark until analysis (which was within 20 hours or less) at the UK station in Ny-Ålesund.

Analysis of halocarbons with part per trillion (ppt) atmospheric concentration was conducted with a custom-built adsorption-desorption system (ADS; developed by the University of Bristol; Simmonds et al., 1995) connected to an automated gas chromatograph mass spectrometer (GCMS). 1.5 L of whole-air sample was drawn through a Nafion permeation drier (continuous counter-purge of dry 5.0 ultra grade synthetic air at 170 mL min^{-1}) before being condensed onto an absorbent filled microtrap at -50 ºC using electrical resistance (Peltier device). The concentrated sample was desorbed by heating the microtrap to 240 ºC using electrical resistance. The sample was carried through a fused silica transfer line (100 ºC) by 5.0 grade Helium, purified by a Universal Trap, into a Hewlett Packard 6890A Gas Chromatograph. Separation of methyl-chloride (CH_3Cl), methyl-bromide (CH_3Br), methyl-iodide (CH_3I), dibromomethane (CH_2Br_2), chloroform ($CHCl_3$) and bromoform ($CHBr_3$) was achieved using a 25 m capillary GC column (Varian, PoraBOND Q, 320 μm i.d., 5 μm film thickness) which was held at 40 ºC for 3 minutes, ramped at 22 ºC min^{-1} to 84 ºC and held for 1 minute, then ramped at 22 ºC min^{-1} to 250 ºC where it is held for 37.73 minutes (total time: 49 minutes). Samples were identified from their fragmentation spectra using a Hewlett Packard 5973 Mass Spectrometer Detector (quadrupole at 150 ºC, source at 230 ºC) scanning for selected ion masses (Table 4.1). Bromochloromethane (CH_2BrCl) and diiodomethane (CH_2I_2) were also scanned for (target ions of 128 and 268, respectively; qualifier ions of 130 and 141, respectively). CH_2BrCl was present in only trace amounts in the standard (below the limit of detection) and was thus not quantifiable. CH_2BrCl is discussed in this manuscript based on relative changes to the peak area. CH_2I_2 was not present in the standard, likely due to its exceptionally short atmospheric lifetime (0.003 days; Law et al., 2006) making it unlikely to persist in the ambient atmosphere. CH_2I_2 was not detected during the experiments, which follows with previous research that

has only identified its production in marine environments, particularly by macroalgae and sea-ice microalgae (Carpenter et al., 2000, 2007).

Quantification of compounds was determined using GCWerks software from the average peak area of the two closest standard analyses, which were run every second sample. The standard was cryo-filled from the ambient air on 11th January 2017 at the Norwegian Zeppelin Observatory (operated by the Norwegian Institute for Air Research, NILU), 2 km south of Ny-Ålesund at 475 m a.s.l. on Zeppelin Mountain. The standard was calibrated on the Zeppelin Medusa (part of the Advanced Global Atmospheric Gases Experiment (AGAGE); Prinn et al., 2018) using tertiary standards linked to the primary standards prepared at Scripps Institution of Oceanography (SIO) for CH_3Cl and CH_3Br (SIO-05 calibration scale), and for $CHCl_3$ (SIO-98 calibration scale). CH_3I, $CHBr_3$ and CH_2Br_2 are calibrated via AGAGE tank comparisons carried out in Boulder, Colorado against National Oceanic and Atmospheric Administration (NOAA) calibration scales (CH_3I, NOAA-2004; $CHBr_3$, NOAA-2003; CH_2Br_2, NOAA-2003) using SIO tanks T-005B, T-009B and T-102B. The detection limit (three times the baseline noise), limit of quantification (variance) and standard concentration for each halocarbon is displayed in Table 4.1. The Ideal Gas Law was used to convert gas concentrations to molar amounts. The dilution from the synthetic air bag used to maintain ambient pressure during sampling was corrected for. The results are presented as daily fluxes in nanomoles per metre squared of land surface per day (nmol m^{-2} d^{-1}). Daily fluxes were calculated from the change in the number of moles of gas present in the headspace over the first hour of the experiment, corrected for the mean change in moles during the first hour of the field blank tests. These mean blank changes were: 0.15 nmol CH_3Cl m^{-2}, 0.01 nmol CH_3Br m^{-2}, 0.003 nmol CH_3I m^{-2}, 0.03 nmol $CHCl_3$ m^{-2}, -0.009 nmol $CHBr_3$ m^{-2}, -0.002 nmol CH_2Br_2 m^{-2}. Mean daily fluxes are presented ± 1 standard deviation. The daily fluxes were calculated from the change in moles in 1 hour because the majority of the 2 hour total change occurred within the 1st hour. For example, 78 to 89 % of the initial moles of CH_3Cl and CH_3Br present in the chamber were consumed within the first hour at sites *established mat* and *tundra*, with only 0.01 to 4 % of additional consumption in the second hour. For the gases that were emitted, a similar pattern emerged where the proportion of gas emitted in the first hour of the total amount of gas emitted over the 2 hour experiment was 61 % of $CHCl_3$, 76 % of $CHBr_3$ and 86 % of CH_2Br_2 at sites *established mat* and *tundra*. Presumably the slow in rate of change after 1 hour was due to reactants being consumed

from the air trapped inside the chamber. Because of this, we advocate that our daily flux rates (nmol m^{-2} d^{-1}) are a minimum estimate.

4.4.4 Physical, chemical and biological sampling and analysis

4.4.4.1 In-field measurements and sampling

The internal chamber temperature was recorded at 5 minute intervals (Tinytag loggers; Gemini) and an average was calculated for the 2 hour duration of each experiment. At the end of the incubation, the chamber tops were carefully removed without disturbing the sediment surface. Aliquots of sediment (~1 g) from the centre of each collar were taken aseptically using 15 mL sterile falcon tubes. These samples were at -20 ºC within 4.5 hrs of sampling and were transported and stored at this temperature until analysis of cell numbers in Bristol within 55 days or less.

After the sterile samples were conducted, a soil moisture sensor (ML3 ThetaProbe, accuracy of ±1 %) was used to measure the volumetric water content of the sediment in each quarter (0.03 m^2) of the chamber. Small cores (~ 4 cm deep) of the sediment were taken from the centre of two opposite quarters of the chambers' footprint. The cored samples were broken up and dried for 20 hours at 60 ºC prior to transport to the UK for soil texture, total carbon (TC) content, total nitrogen (TN) content, and organic matter (OM) content analyses.

In the centre of each chamber, a corer was used to determine the depth of the water table. In some cases the water table could not be reached due to the presence of high numbers of large (> 5 cm diameter) rocks in the near sub-surface which were not practical to dig through. Where the water table was not reached, the depth at which rocks were hit was recorded.

4.4.4.2 Organic matter, total nitrogen, total carbon and soil texture

Prior to OM, TC and TN content and soil texture analyses, plant roots (present at site *tundra*) and pieces of cyanobacterial mat (present at site *established mat*) were removed with tweezers from the dried samples. Additionally, a sieve was used to remove small roots (> 2 mm) from the site *tundra* samples but it was not possible to remove roots smaller than this.

Samples for OM, TC and TN content analyses were re-dried at 105 ºC for 19 hours to ensure removal of water. Approximately 4 g of a known weight of the dried-sample from each quarter-chamber core was then furnaced at 450 ºC for 5 hours to determine the organic matter content (weight %) by mass loss on ignition. The larger weight of sample used here meant that some very small roots were likely present in these samples and may inflate the values. In comparison, TC and TN content was analysed on less than 20 mg of sample meaning no root matter was likely to be present.

An Elemental Analyser 1110 fitted with a TCD (temperature controlled detector) was used to measure percentage weight of TC and TN in an 8 to 19 mg, < 250 μm, well-mixed aliquot of the re-dried core sample by flash heating to 1000 ºC. TC and TN contents were quantified using a certified Aspartic acid standard containing 36.14 % C and 10.49 % N. This method has an LOD of 0.01 % for both TC and TN and a precision of 0.06 % for TC and 0.01 % for TN (n=6) as determined from a soil standard containing 2.29 % TC and 0.21 % TN.

To determine the heterogeneity and average size of grains at each site, the remaining approximately 10 g of re-dried core sample was sieved to determine the percentage weight of the sample with grain sizes greater and smaller than 2 mm.

4.4.4.3 Heterotrophic bacterial abundance

Counts of heterotrophic bacteria were conducted after methodology detailed by Bradley et al., (2016). Briefly, upon analysis the samples were defrosted and 100 mg sub-samples were placed in sterile microcentrifuge tubes (1.5 mL, Eppendorf). The sample was diluted with 932 μL of Milli-Q (MQ) water (0.2 μm filtered) and fixed in 68 μL of 0.2 μm filtered 37 % formaldehyde (final concentration of 2.5 %). Samples were vortexed for 10 seconds (s) and sonicated for 1 minute at 30 ºC to disaggregate soil particles and encourage cells to detach. The sample was vortexed for 3 s with 10 μL of fluorochrome DAPI (4' ,6-diamidino-2 phenylindole) prior to incubation for 10 minutes in the dark. The stained sample was vortexed for 10 s and 100 μL of this was filtered through a black Polycarbonate filter paper (25 mm diameter, 0.2 μm pore size) and then rinsed with 250 μL of MQ water (0.2 μm filtered). Bacterial cells were counted under UV light at 1000 X magnification with an Olympus BX41 microscope. MQ water (0.2 μm filtered) was used to wash the filtering apparatus between each sample. Blank controls, to which no

soil or sediment was added, were dispersed throughout the samples. Ten random grids (each 10^3 μm^2) were counted per sample. The number of cells per gram of wet weight sample was calculated. Cell numbers for the blank controls were below 50 cells mL^{-1}.

4.4.5 Statistical analysis

Differences between mean halocarbon fluxes from different sites were determined at the 95% confidence level (p-values < 0.05) using pair-wise Welch two sample t-tests conducted in R (version 3.02.1, 2015). Correlations between halocarbon fluxes and the physical, chemical and biological variables are estimated and presented using the 'corrplot' package in R (Wei and Simko, 2017). An average value per chamber was calculated for the physical and chemical variables where multiple analyses were conducted at each chamber (organic matter, total C and N and texture; n = 2). Matrices were produced from the data for all sites combined and from the data for three individual sites: *disturbed mat*, *established mat* and *tundra*. The individual site matrices were generated because of the disparity in land surface 'type' between sites which results in large variation in physical, chemical and biological variables. Heterotrophic cell numbers were excluded as a variable for the 'within site' correlation matrices because the 4 measurements conducted per site were deemed too few to be included in the analysis. Similarly, matrices were not produced for sites *snout* and *pond-mat* which only had 4 halocarbon flux data points each.

4.4.6 Calculation of regional fluxes

4.4.6.1 Calculation of total proglacial fluxes in the Arctic

To determine if halocarbon fluxes from glacial forefields were important regionally, we calculated an Arctic proglacial total flux. First, we assumed an averaged flux for each halocarbon across the Midtre Lovenbreen forefield by subdividing the land surface into thirds. The first third is represented by fluxes from sites *snout* and *pond-mat*, the middle by fluxes from sites *disturbed* and *established mat*, and the final third by fluxes from site *tundra*. This gave an average forefield flux of -62 nmol CH_3Cl m^{-2} d^{-1}, -0.94 nmol CH_3Br m^{-2} d^{-1}, -0.04 nmol CH_3I m^{-2} d^{-1}, 56 nmol $CHCl_3$ m^{-2} d^{-1}, 0.45 nmol $CHBr_3$ m^{-2} d^{-1}, 0.37 nmol CH_2Br_2 m^{-2} d^{-1}. The total area of proglacial land surface across the region has not been measured. Therefore, we assume that the size of Midtre Lovenbreen's forefield (2.7 x 10^6 m^2) is representative and combine this area with an estimated 9996 land terminating glaciers (minimum elevation > 50 m above sea level) located above 60°N (WGMS, 2012),

to calculated a total Arctic proglacial land surface area of 2.7 x 10^{10} m^2. The estimated Arctic proglacial land surface area was combined with the average proglacial halocarbon fluxes and an assumed growing season of 100 days (with negligible fluxes out with this time) to calculate the regional source and sink of each halocarbon in moles and tonnes per year. The growing season length of 100 days was determined as the approximate average number of days with no ground snow-cover (as done by others e.g. Bekku et al. (2003)) measured at Ny-Ålesund weather station from 2009-2017 (102 ± 26 days; Gjelten, 2018).

4.4.6.2 Calculation of Arctic tundra fluxes

For the halocarbons ($CHBr_3$ and CH_2Br_2) that have not been measured on tundra before, we calculate an Arctic tundra flux based on calculations by Rhew et al. (2007). We assume the growing season lasts 100 days (with negligible fluxes outside of this time) and the area of the Arctic tundra is 7.3 x 10^{12} m^2 (Matthews, 1983). By assuming our site *tundra* fluxes are broadly representative of tundra as a whole, the average fluxes of CH_2Br_2 and $CHBr_3$ measured at site *tundra* are combined with the Arctic tundra area and growing season length to calculate an annual Arctic flux in moles of gas per year, which was converted to Gigagrams of gas per year.

To calculate the importance of the Arctic tundra flux to the Arctic troposphere, the percentage of Arctic tropospheric $CHBr_3$ and CH_2Br_2 sourced from the tundra was calculated. We used our yearly tundra source of $CHBr_3$ (4.4 x 10^5 moles) and CH_2Br_2 (5.5 x 10^5 moles) with an assumed 1.0 x 10^{19} moles of air that constitute the Arctic troposphere (Rhew et al., 2007) to calculate the part per trillion concentration of each gas in the Arctic troposphere that is derived from a tundra source.

4.5 Results

4.5.1 Physical, chemical and biological differences between sites

The environmental context for the halocarbon fluxes measured here was provided by the inter- and intra-site variation of the following physical, chemical and biological parameters (Figure 4.5). Volumetric water content and water table depth both varied between and within sites with highest water content at site *tundra* (50 % v/v) but shallowest water tables at site *disturbed mat* (Figure 4.5 a-b). The texture of the sediment in the top 5 cm at the sites illustrated the heterogeneity of the moraine and fluvial outwash landscape, with near 100 % grains < 2 mm ∅ representing low-energy and sheltered environments at sites *tundra* and *pond-mat* compared to more variation at the other three sites (Figure 4.5c).

The chemical and biological parameters describe the increasing soil development with distance from the glacier's snout, and therefore with exposure age. For example, heterotrophic cell abundances increased with distance from the glacial snout, with highest mean abundances at sites *established mat* and *tundra* of 3.2 x 10^8 cells [g sediment]$^{-1}$, compared with 0.6 x 10^8 cells cells [g sediment]$^{-1}$ at site *snout* (Figure 4.5g). The highest soil contents of organic matter (OM), total carbon (TC) and total nitrogen (TN) were all measured at site *tundra* (Figure 4.5d-f). Net emission of CO_2 was seen at the *pond-mat*, *established mat* and *tundra* sites, with fluxes spanning zero at the *snout* and *disturbed-mat* sites. CH_4 emission was highest at site *pond-mat* with some consumption measured at site *tundra*.

4.5.2 Halocarbon fluxes

The behaviour of the halocarbons over each surface type is broadly dictated by the compound type: mono-halogenated compounds (CH_3Cl, CH_3Br, CH_3I) were either consumed or fluctuated around zero, whereas polyhalomethanes ($CHBr_3$, $CHCl_3$, CH_2Br_2) were emitted from all surfaces (Figure 4.6). The mono-halogenated compounds were strongly and consistently drawn down at sites *established mat* and *tundra* with mean fluxes of -106 ±7 and -126 ±4 nmol m^{-2} d^{-1}, respectively for CH_3Cl, -1.67 ±0.12 and -1.76 ±0.04 nmol m^{-2} d^{-1}, respectively for CH_3Br and -0.097 ±0.029 and -0.124 ±0.025 nmol m^{-2} d^{-1}, respectively for CH_3I. A minor drawdown of CH_3Cl (-11 ±5 nmol m^{-2} d^{-1}) and CH_3Br (-0.30 ±0.1 nmol m^{-2} d^{-1}) occurred at site *pond-mat*, with near zero fluxes at

site *snout*. Large variations in CH_3I were recorded at sites *snout*, *pond-mat* and *disturbed mat*.

The polyhalomethanes were emitted from all surfaces, although the emission was relatively small at site *snout*. For $CHCl_3$, the site with the highest mean flux of 105.36 ± 41.52 nmol m^{-2} d^{-1} was site *established mat*. However, due to the variation of $CHCl_3$

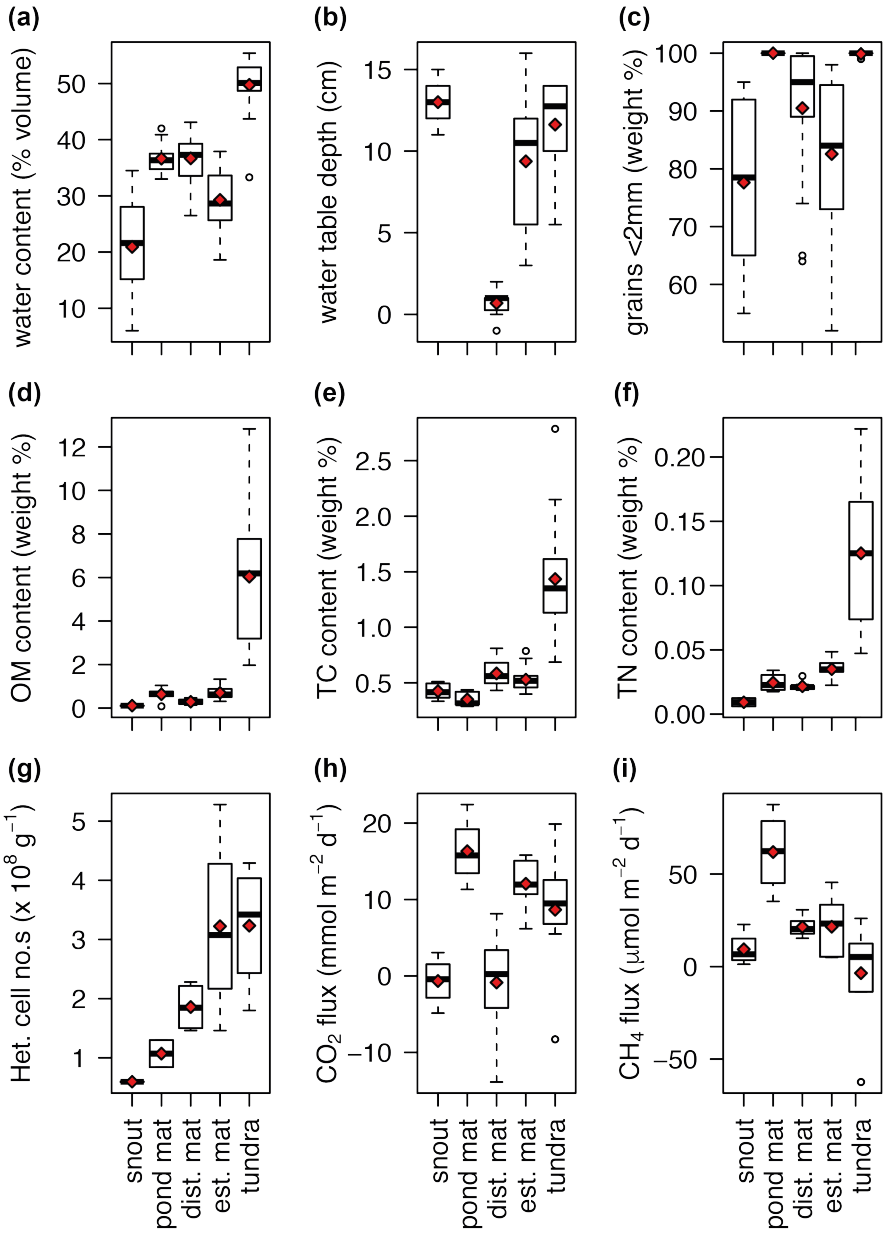

Figure 4.5 Variation at each site of soil water content (a), water table depth (b), weight % of grains < 2 mm diameter (c), organic matter content (d), total carbon content (e), total nitrogen content (f), heterotrophic cell numbers (g), CO_2 flux (h) and CH_4 flux (i). Horizontal black bar represents the median, red diamonds the mean for each site, open circles are outliers. 'dist. mat' is disturbed mat, 'est. mat' is established mat. Water table was not measurable for site *pond-mat* due to rocky ground.

fluxes, this was not statistically different from the mean *tundra* flux of 73.49 ± 32.71 nmol m^{-2} d^{-1} (p-value = 0.1). Fluxes of $CHBr_3$ were similarly varied, with the highest mean emission from site *disturbed-mat* of 0.67 ± 0.29 nmol m^{-2} d^{-1} being statistically similar to the flux at site *tundra* of 0.61 ± 0.11 nmol m^{-2} d^{-1} (p-value = 0.6). The highest mean flux of CH_2Br_2 was from site *tundra* (0.751 ± 0.317 nmol m^{-2} d^{-1}), with smaller and similar mean fluxes at sites *established mat*, *disturbed-mat* and *pond-mat* (0.223 to 0.224 nmol m^{-2} d^{-1}). CH_2BrCl was unquantified (Section 4.4.3) but was found to be emitted from all sites at similar relative magnitudes.

4.5.2.1 Relationships between halocarbon fluxes and physical, chemical and biological variables

To understand the different physical, chemical and biological factors associated with the halocarbon fluxes, correlations between them are presented in Figure 4.7. Some of the chemical, physical and biological variables were strongly related to site location because the five sites differed in key factors such as vegetation cover and type. For example, OM,

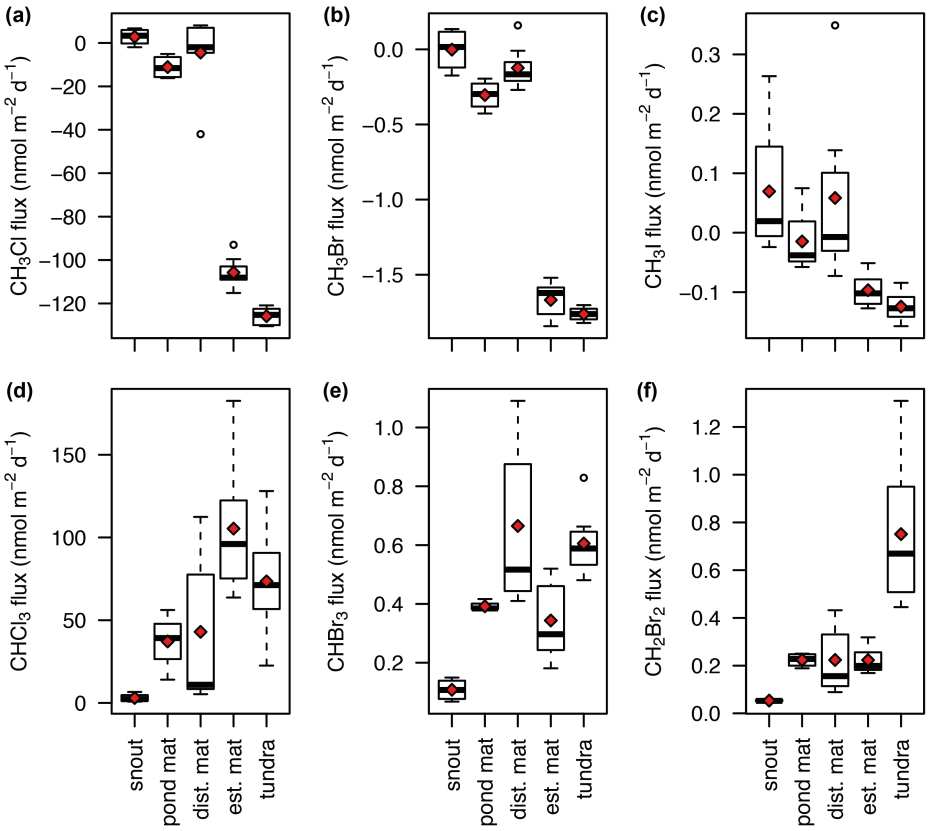

Figure 4.6 Daily fluxes (nmol m^{-2} d^{-1}) at each site of CH_3Cl (a), CH_3Br (b), CH_3I (c), $CHCl_3$ (d), $CHBr_3$ (e), CH_2Br_2 (f). Red diamonds represent the mean flux for each site. 'dist. mat' is disturbed mat, 'est. mat' = established mat.

TN and TC contents were considerably higher at site *tundra* than the other sites (Figure 4.5d-f). Some halocarbon fluxes also showed site-dependent variation such as the strong consumption of CH_3Cl and CH_3Br at site *established mat* and *tundra* compared to minor drawdown at the other sites. Because of the differences in physical variables and halocarbon fluxes at each site, we also calculated correlation matrices for sites *disturbed-mat*, *established mat* and *tundra* separately (Figure 4.7b-d). The difference in the correlations across all-sites (Figure 4.7a) compared with the correlations at individual sites (Figure 4.7b-d) showed that relationships between the different variables are not always consistent across sites.

4.5.2.2 Halocarbon intercorrelations

The two groups of halocarbons, the methyl halides (CH_3Cl, CH_3Br, CH_3I) and the polyhalomethanes ($CHBr_3$, $CHCl_3$, CH_2Br_2), show similar patterns of correlation (Figure 4.7a). The methyl halides were all positively correlated with each other ($r > 0.62$, $p < 0.05$), as were the polyhalomethanes, but more weakly ($r > 0.54$; correlations with $CHCl_3$ were not significant, $p > 0.05$). All correlations between the two groups were negative ($-0.18 < r < -0.62$; insignificant for $CHBr_3$ due to the weakness of the correlation; $0 > r > -0.2$, $p > 0.05$). The negative correlation between the two groups indicated that, broadly, increased consumption of mono-halogenated compounds (i.e. more negative fluxes) correlated with increased production of poly-halogenated compounds.

The relationships within and between these two groups (methyl halides and polyhalomethanes) did not always persist across the three individual site analyses. For example, at site *disturbed mat*, all the halocarbons except CH_3I were positively correlated (Figure 4.7b) suggesting higher emission of the polyhalomethanes occurred with lower consumption of CH_3Cl and CH_3Br, contrary to the all-site relationship. Furthermore, there were instances where correlations across all sites appeared to be driven by the large size of their relationship at one site. For example, the weak positive correlation across all sites between the haloforms (CHX_3; X = Cl, Br), $CHBr_3$ and $CHCl_3$ ($r = 0.29$), was inflated by their strong positive correlation at site *disturbed mat* ($r = 0.98$) which masked their negative correlation at sites *established mat* and *tundra* ($r = -0.29$ and -0.57, respectively). The results from the individual site analyses demonstrate the importance of investigating differences in halocarbon patterns by small scale geography.

4.5.2.3 Correlations of methyl halides and chemical, physical and biological variables

Across all sites, the mono-halogenated compounds were negatively correlated with OM, TC, TN and heterotrophic cell numbers with the strongest correlation for CH_3Cl (r < -0.60), and weakest for CH_3I (r < -0.39), indicating greater methyl halide consumption (i.e. more negative fluxes) occurred with higher concentrations of OM, TC, TN and cells in the sediment/ soil. This was largely driven by high methyl halide consumption at sites *established mat* and *tundra* where OM, TC, TN and cell contents were highest. The relationship broadly persisted at site *established mat* (Figure 4.7c), but not at sites *disturbed mat* and *tundra* (Figure 4.7b, d). Across all sites, the methyl halides were negatively correlated with water content and water table depth (r < -0.45; CH_3I and water

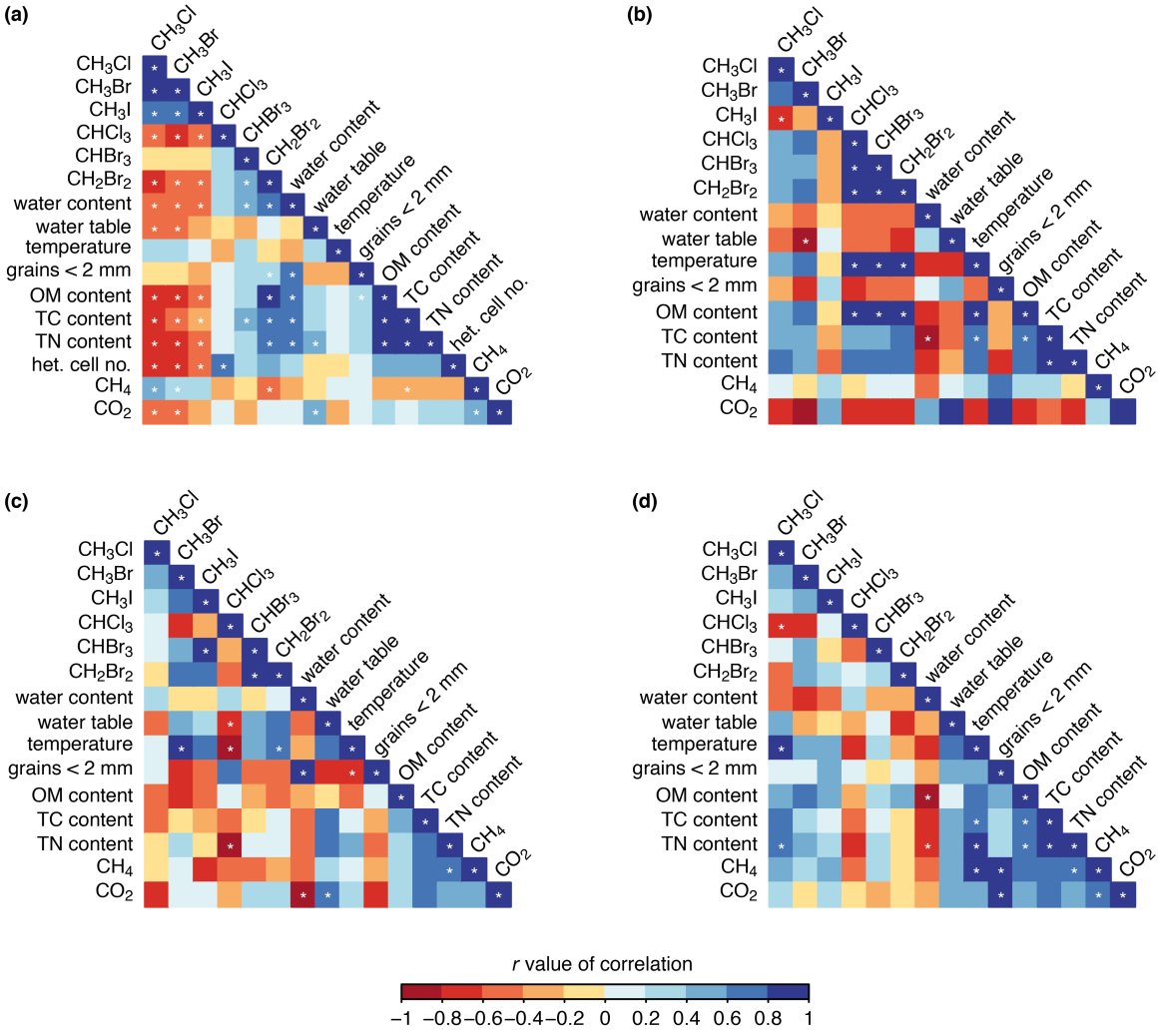

Figure 4.7 Correlations between halocarbon fluxes and the chemical, physical and biological variables across all sites (a), site *disturbed mat* (b), site *established mat* (c) and site *tundra* (d). White stars indicate correlations with 95 % confidence (p < 0.05).

table depth are insignificant) showing higher methyl halide consumption (i.e. lower fluxes) where water contents were higher, but the water table deeper. CH_3Cl and CH_3Br were negatively correlated with CO_2 (r = -0.41 and -0.45, respectively) indicating increased consumption correlated with CO_2 fluxes tending from consumption to production (i.e. becoming more positive). The opposite relationship was seen with CH_4 (r = 0.43 and 0.37), broadly indicating increased CH_3Cl and CH_3Br consumption occurred with smaller CH_4 fluxes, i.e. tending towards consumption.

4.5.2.4 Correlations of polyhalomethanes and chemical, physical and biological variables

Compared to the methyl halides, the polyhalomethanes ($CHCl_3$, $CHBr_3$ and CH_2Br_2) generally showed opposite and weaker correlations with positive correlations with OM, TC, TN contents, heterotrophic cell numbers and water content (Figure 4.7a). However, many of the correlations were not significant for the three gases. $CHCl_3$ and $CHBr_3$ were not strongly or significantly correlated with any variable ($-0.4 < r < 0.4$, $p > 0.05$) except heterotrophic cell numbers with $CHCl_3$ (r = 0.67) and TC content (r = 0.41) and water content (r = 0.56) with $CHBr_3$. However CH_2Br_2 was strongly positively correlated with water, OM, TC and TN contents ($r > 0.7$), showing that increased emission of CH_2Br_2 was correlated with increased OM, TC, TN and water contents. CH_2Br_2 was negatively correlated with CH_4 contents (r = -0.41) indicating greater CH_2Br_2 emission when CH_4 fluxes tended towards consumption (i.e. lower fluxes). Similarly to the methyl halides compounds, some of the all-site relationships for the polyhalomethanes were also present within an individual site and others were not (Figure 4.7 b-d). For example, an interesting intra-site trend at site *disturbed mat* is the very strong positive correlation between the three polyhalomethanes and temperature and OM content ($r > 0.9$).

4.6 Discussion

4.6.1 Influence of exposure age on halocarbon fluxes from the proglacial environment

Terrestrial halocarbon fluxes are predominantly driven by biological processes (e.g. Amachi et al., 2001; Dimmer et al., 2001; Redeker and Kalin, 2012), and a lower prevalence of abiogenic processes which often involve oxidation of organic matter (Huber et al., 2009; Keppler et al., 2000). Both these processes would suggest that increasing soil development would be an important driver of halocarbon fluxes. As such, immature soils, such as those exposed by retreating ice, may be assumed to have minor trace gas fluxes in comparison to more developed soils with established biota. Further, one might expect an increase in flux magnitude as the soil develops with increasing exposure age, i.e. with greater distance from the glacier terminus. Our study does indicate that some soil development is required for most halocarbon fluxes, with the lowest mean fluxes of all gases (except for CH_3I) measured at the youngest site (site *snout*; ~ 5 years), which has no vegetation and very little organic matter (0.1 % of soil). Whereas, site *tundra*, the oldest site (approximately 1950 years exposure), with full coverage of vegetation, high bacterial cell numbers (3.2 x 10^8 per gram soil), and more soil development (e.g. 6.0 % organic matter) had the highest mean consumption of CH_3Cl, CH_3Br and CH_3I and the highest mean emission of CH_2Br_2. However, there were exceptions to this trend which imply that soil development is not the only driver of halocarbon fluxes. For example, at *site established* mat similar consumption rates of CH_3Cl, CH_3Br and CH_3I were seen to site *tundra*, despite the large difference in soil development (total carbon (TC), total nitrogen (TN) and organic matter (OM) content; Figure 4.5). Further, fluxes at sites *established mat* and *tundra* of CH_3Cl (-106 ± 7 and -126 ± 4 nmol m^{-2} d^{-1}, respectively) and CH_3Br (-1.67 ± 0.12 and -1.76 ± 0.04 nmol m^{-2} d^{-1}, respectively) were within the range measured at a well-established coastal tundra site in Alaska where flooded and drained sites had respective mean fluxes of -14 to -620 nmol m^{-2} d^{-1} for CH_3Cl and +1.1 to -9.8 nmol m^{-2} d^{-1} for CH_3Br (Rhew et al., 2007). However, fluxes of CH_3I at site *tundra* and *established mat* (-0.124 ± 0.025 and -0.097 ± 0.029 nmol m^{-2} d^{-1}) were negative, contrasting a mean emission of 4.0 nmol m^{-2} d^{-1} measured from Alaskan tundra (Rhew et al., 2007).

This pattern whereby sites with younger, less-developed soils have similar fluxes to the older and developed-soil of site *tundra* also occurred for $CHCl_3$ and $CHBr_3$ where the highest mean fluxes were measured at site *established mat* and site *disturbed mat*, respectively, but were statistically similar to the flux measured at site *tundra* ($p = 0.1, 0.6$, respectively). This is even more surprising for site *disturbed mat* which is completely bare of vegetation and has comparatively low heterotrophic cell numbers (Figure 4.5g). Terrestrial fluxes of $CHBr_3$ have rarely been measured (see Section 4.6.2), whereas $CHCl_3$ emissions have been recorded, including from the Alaskan tundra where the average flux was 45 nmol m^{-2} d^{-1} (Rhew et al., 2008b). Mean emissions of $CHCl_3$ were larger at sites *tundra* and *established mat* and similar at site *disturbed mat* (73.49, 105.36 and 42.95 nmol m^{-2} d^{-1}, respectively). Considerable variability of $CHCl_3$ fluxes were measured, with the range for site *tundra* of 22 to 128 nmol m^{-2} d^{-1} and the range for site *established mat* of 63 to 183 nmol m^{-2} d^{-1}. This variability in $CHCl_3$ fluxes is less than, but comparable to, the variation measured at the Alaskan tundra of <1 to 260 nmol m^{-2} d^{-1} (Rhew et al., 2008b). We therefore postulate that younger surfaces are more important sources of $CHCl_3$ and $CHBr_3$ and more important sinks of CH_3Cl and CH_3Br than might otherwise be expected based on their lesser soil development and lower microbial and plant presence. In particular, it appears the presence of cyanobacterial mats negates the requirement for a more developed soil. To our knowledge, no studies have been conducted upon halogenated trace gas fluxes from cyanobacteria mats or freshwater cyanobacteria, although marine cyanobacteria have been suggested to be involved in production of CH_2Br_2, $CHBr_3$ and CH_3I (Karlsson et al., 2008; Roy et al., 2011). Determining if cyanobacteria themselves, or other microorganisms present in the mat are responsible for the elevated fluxes was beyond the scope of this study.

4.6.2 Terrestrial emission of typically marine-origin brominated compounds

A second novel finding of this study was the emission of $CHBr_3$ and CH_2Br_2 across the glacial forefield, with very small emissions at site *snout*, but more appreciable fluxes at all other sites (Figure 4.6e-f). $CHBr_3$ and CH_2Br_2 are typically attributed to marine sources (Law et al., 2006). However, there have been limited observations of emission of both compounds from terrestrial environments. $CHBr_3$ has been observed to be emitted from rice paddies, with algae in the water column the suggested source, however a rice-mediated production mechanism was not discounted (Redeker et al., 2003). CH_2Br_2 emissions have been observed from wet temperate peatlands, with no production

mechanism suggested (Dimmer et al., 2001). Emissions of $CHBr_3$ has been observed, but not quantified, from the transitional terrestrial-marine environment of a coastal wetland, where the emission was shown to be abiogenic in origin (Wang et al., 2016). Further, abiogenic production of $CHBr_3$ through the oxidation of organic matter by Fe(III) and H_2O_2 when halide ions are present has been documented in a laboratory based soil study (Huber et al., 2009). The largest flux of CH_2Br_2 is measured at site *tundra* which is analogous to an Arctic peatland ecosystem, and thus complements the emissions measured from temperate peatlands in Ireland (Dimmer et al., 2001). Our results provide further evidence of the emission of these two compounds in a terrestrial environment, and the first evidence of terrestrial emission of these compounds in the Arctic.

4.6.3 Controls on halocarbon fluxes in the proglacial environment

4.6.3.1 Biological consumption of methyl halides and abiogenic production of CH_3I

Methyl halides were primarily consumed on the glacier forefield, with all three compounds consistently consumed at sites *established mat* and *tundra* but with fluxes of CH_3I in both directions at sites *snout*, *pond-mat* and *disturbed mat*. The strong inter-correlations between different methyl halides suggest a similar consumption mechanism, particularly between CH_3Cl and CH_3Br. Strong correlations between CH_3Cl and CH_3Br have been found elsewhere, including in the Alaskan tundra, with similar suggestions of common consumption mechanisms or common limiting factors (Rhew et al., 2007). We suggest that the consumption of all three methyl halides observed across the forefield is driven by prokaryotic degradation, which is supported by methyl halide fluxes being correlated with heterotrophic bacterial cell concentrations ($r < -0.52$) and net microbial respiration (CO_2 emission; $r < -0.41$, not significant for CH_3I). Both biogenic and abiogenic (through organic matter oxidation) soil production mechanisms of CH_3I have previously been demonstrated (Amachi et al., 2001; Keppler et al., 2000). However, these mechanisms are not strongly supported here as CH_3I is emitted at the sites (*snout*, *pond-mat*, *disturbed mat*) with the lowest heterotrophic bacteria concentrations and lowest organic matter contents (0.1 – 0.6 %). Identifying the CH_3I production mechanism would require further study.

4.6.3.2 Inconclusive influence of water content on methyl halide fluxes

Several studies have identified the importance of soil water content for CH_3X fluxes, with very low water contents limiting biological activity and high water contents limiting the

mass transfer of reactants during CH_3X formation and degradation (Khan et al., 2012; Rhew et al., 2010; Teh et al., 2009). We find that increasing water content was correlated to greater consumption of CH_3X across all sites, despite high water contents (> 40 % v/v). This is driven largely by high water contents at site *tundra* where the highest consumption of CH_3X was found, presumably due to the more developed soils and biota at this site. Within site *tundra* the relationship with water content persists, in contrast to the Alaskan tundra studies which found that decreasing water content was the key factor causing increased consumption of CH_3Cl and CH_3Br (Teh et al., 2009). Our results are not consistent with this finding perhaps due to the noise caused by a small within-site sample size (n = 8) coupled with a smaller range of water volumes measured here (40-60 %, compared to < 30 to > 70 % in the Alaskan study). Further, the relationship between CH_3X and water content implied greater consumption in more anaerobic soils, however, higher consumption of CH_3X was found to occur where fluxes of CH_4 are tending towards the aerobic process of consumption, as found in the Alaskan tundra (Rhew et al., 2007). The contradiction between water content and aerobic CH_4 consumption shown here further indicates that more within-site data is required, as the disparity in the CH_3X fluxes of the different sites drives the all-site relationships.

4.6.3.3 Biogenic and abiogenic production of polyhalogenated species

Biogenic production mechanisms of $CHCl_3$, $CHBr_3$ and CH_2Br_2 are shared (haloperoxidase activity), as is the abiogenic production mechanism of the haloforms (CHX_3; . If either biogenic or abiogenic processes were the sole source of the polyhalogenated species, then we would expect that, at least, CHX_3 fluxes would be correlated. However, $CHCl_3$ and $CHBr_3$ are not well correlated across all sites (r = 0.29, p > 0.05) suggesting different sources of these compounds within or between sites. Here, $CHCl_3$ is strongly correlated to heterotrophic cell numbers, but $CHBr_3$ is not, which tentatively suggests that $CHCl_3$ is produced biologically. At sites *established mat* and *tundra*, $CHCl_3$ and $CHBr_3$ were not significantly correlated suggesting multiple sources or a possible unknown consumption process. There is no evidence prior to this study that terrestrial or freshwater cyanobacteria are involved in halocarbon production. However, marine cyanobacteria have been implicated in the production of $CHBr_3$ and CH_2Br_2 and the bromoperoxidase enzyme has been identified in some marine species (Johnson et al., 2011; Karlsson et al., 2008). The highest emissions of CH_2Br_2 at site *tundra*, could be due to a different microbial community make-up or a plant-mediated process. We suggest

that a possible mixture of abiogenic and biogenic production mechanisms are responsible for $CHCl_3$ and $CHBr_3$ emissions, whereas CH_2Br_2 emissions seem more likely to be driven biologically.

4.6.4 Glacial forefields as a source and sink of halocarbons?

Determining the local or regional importance of the proglacial halocarbon fluxes would require further study into diurnal, seasonal and spatial variations. However, estimations of the yearly regional source or sink of each gas is still worthwhile, particularly for $CHBr_3$ and CH_2Br_2 for which no prior fluxes have been measured from terrestrial Arctic environments. We calculate an Arctic tundra source of 0.11 Gg yr^{-1} of $CHBr_3$ and 0.10 Gg yr^{-1} of CH_2Br_2 from the Arctic tundra by assuming no fluxes occur outside of the growing season when the land would be snow-covered (Section 4.4.6.2). The sources are minor compared to the estimated global oceanic sources of 180-530 Gg $CHBr_3$ yr^{-1} and 62-113 Gg CH_2Br_2 yr^{-1} (Hossaini et al., 2013, and references within; see Figure 4.8 for summary of regional fluxes). However, although Arctic macroalgae are a source of both gases (Laturnus, 1996), polar oceans as a whole have been suggested to be a sink (e.g. Chuck et al., 2005; Ziska et al., 2013). Therefore, a terrestrial Arctic source could be regionally important. We estimate that the tundra source of $CHBr_3$ and CH_2Br_2 is equivalent, respectively, to 0.04 and 0.05 ppt in the Arctic troposphere (Section 4.4.6.2).

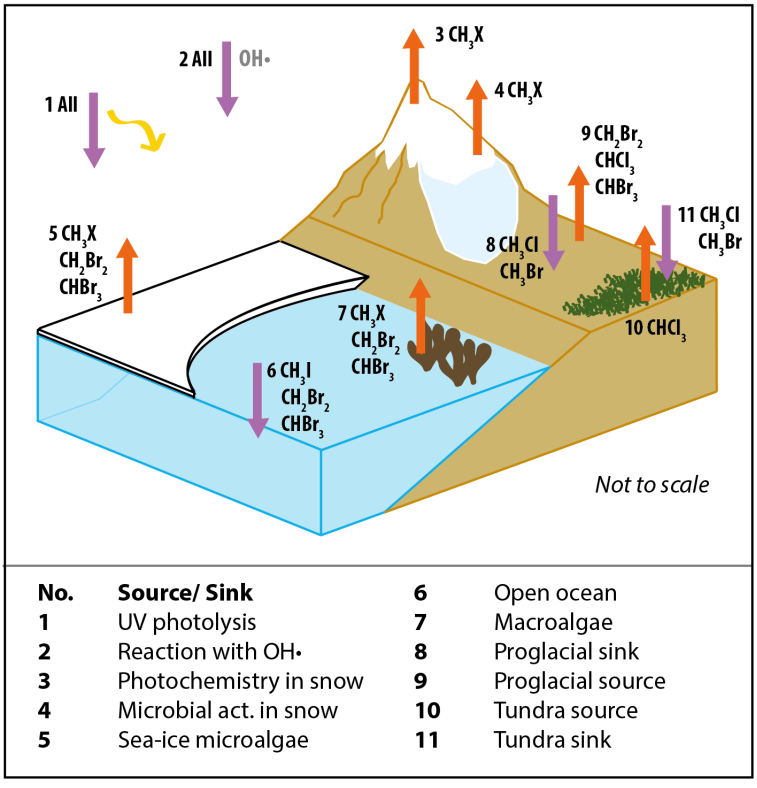

No.	Source/ Sink	No.	Source/ Sink
1	UV photolysis	6	Open ocean
2	Reaction with OH•	7	Macroalgae
3	Photochemistry in snow	8	Proglacial sink
4	Microbial act. in snow	9	Proglacial source
5	Sea-ice microalgae	10	Tundra source
		11	Tundra sink

Figure 4.8 Schematic diagram summarising natural sources and sinks for the 6 halocarbons of interest in polar regions. (CH_3X = CH_3Cl, CH_3Br, CH_3I; act. = activity). References for presence of each flux is as follows: 1, 2 (see Montzka et al., 2011 for review), 3 (Swanson et al., 2007), 4 (Redeker et al., 2017), 5 (Laturnus et al., 1998; Sturges et al., 1993), 6 (Stemmler et al., 2014; Ziska et al., 2013), 7 (Laturnus, 1996; 2001), 8 (Rhew et al., 2008b; Albers et al., 2017), 9 (Rhew et al., 2007).

This represents 2 and 5 % of Arctic tropospheric $CHBr_3$ and CH_2Br_2 (based on a 2010-2017 mean ambient Arctic tropospheric concentration of 2.0 and 1.1 ppt, respectively). However, as the magnitude of the Arctic coastal macroalgal source is unknown, this source could still be regionally important.

For the other halocarbons analysed across the glacial forefield, we calculated a potential proglacial regional flux from an estimated Arctic proglacial land area (Section 4.4.6.1). Small net sinks of 8 tonnes of CH_3Cl, 0.2 tonnes of CH_3Br, 0.01 tonnes of CH_3I, and small net sources of 0.02 Gg of $CHCl_3$, 0.2 tonnes of CH_2Br_2 and 0.3 tonnes of $CHBr_3$ were calculated. All of these are minor compared to global fluxes, due to the relatively small area of land covered by proglacial surfaces. Fluxes from the Alaskan tundra, which were similar to our fluxes for *established mat* and *tundra*, were found to be regionally important, where they represent the equivalent of approximately 20-25 % and 10-15 % of the seasonal variation in the Arctic troposphere of CH_3Cl and CH_3Br, respectively (Rhew et al., 2007). However, our estimated proglacial land surface area is 2 orders of magnitude smaller than the estimated area of Arctic tundra (7.3×10^{12} m^2) meaning even within the Arctic troposphere the proglacial sink of CH_3Cl and CH_3Br is insignificant.

Although our daily fluxes are likely an underestimate (due to calculation from concentration change over 1 hour, after the rate of change had slowed; Section 4.4.3), the magnitude of this underestimate will not be large enough to alter the significance of the total gas fluxes regionally. Despite all halocarbons studied here appearing to represent only minor fluxes globally and regionally, this study has shown the potential for younger surfaces to be involved in halocarbon flux processes which may become more important due to expansion of these surfaces under future warming.

4.7 Conclusions

We present the first measurements of halocarbon fluxes from proglacial land surfaces, showing an overall net sink of CH_3Cl, CH_3Br and CH_3I and net source of $CHCl_3$, $CHBr_3$ and CH_2Br_2. Relatively young, under-developed soils exposed by glacial retreat can have larger than expected fluxes of halocarbons due to the formation of cyanobacterial mats, particularly as sinks of CH_3Cl, CH_3Br, CH_3I and sources of $CHCl_3$ and $CHBr_3$. The latter two gases also show appreciable fluxes even from bare sediment adjacent to

cyanobacterial mats. This is the first research known to us conducted on terrestrial cyanobacteria, and additionally we have provided comparatively rare terrestrial flux measurements of $CHBr_3$ and CH_2Br_2. Future work should: identify if cyanobacteria themselves or other microbes are responsible for the high fluxes over the mats; improve the spatial and temporal distribution of these measurements; conduct gas analyses at < 1 hour intervals to reduce the suspected underestimation of the flux calculations; and identify if other terrestrial environments emit $CHBr_3$ and CH_2Br_2, particularly in areas where the fluxes might be higher (i.e. in move developed and more active soils) and therefore more regionally important. The significance of proglacial fluxes may become more important in the future with continuing change in the Arctic and the resultant retreat of glacial systems and exposure of proglacial land.

5 Influence of local sources and sinks on ambient tropospheric halocarbon observations in the High Arctic

This chapter quantifies long-term and seasonal trends of the halocarbons measured in Chapter 4 (CH_3Cl, CH_3Br, CH_3I, CH_2Br_2, $CHCl_3$ and $CHBr_3$) in the High Arctic. It determines whether the fluxes measured on the proglacial forefield influence wider atmospheric concentrations of these gases.

The analysis was conducted using a 5 year time series of atmospheric measurements taken at the Zeppelin observatory, located ~ 4 km west of the Chapter 4 field site (Midtre Lovenbreen). CH_2Br_2, CH_3I and $CHBr_3$ data sets were calibrated on preliminary scales, and thus data for these gases from this section of the thesis *should not be reproduced elsewhere* without permission from Chris Lunder at the Norsk Institutt for Luftforskning (NILU; Norwegian Institute for Air Research). Permission to use the CH_2Br_2, CH_3I and $CHBr_3$ data collected at Zeppelin Observatory for this thesis was kindly given by Chris Lunder.

The purpose of this chapter is to provide a local atmospheric context to the analysis conducted in Chapter 4. This chapter discusses how different emission and consumption processes occurring in the local area (i.e. in and around the fjord, and neighbouring fjords) may impact the local atmospheric composition.

5.1 Abstract

Halocarbons are important carriers of halogens to the atmosphere where they are involved in the destruction of tropospheric and stratospheric ozone. Most anthropogenic and natural halocarbons have their largest sources in the low-mid latitudes, either in the industrialised mid-latitudes of Europe, Russia, the U.S. and East Asia, or in the natural terrestrial and marine environments of the tropics, sub-tropics and temperate zones. Despite being lower contributors to global budgets, Arctic sources and sinks are important for regional budgets due to proximity to the major ozone destroying location of the Arctic atmosphere and due to their distance from the lower latitudes. The Arctic is changing more rapidly than the rest of the planet and, therefore, it is important to understand how local sources and sinks of halocarbons influence atmospheric chemistry in this region. We analyse frequent ambient air measurements made at the Zeppelin Observatory in north-west Svalbard between 2013 and 2017. We focus on six halocarbons with recorded natural sources and sinks in Arctic environments: methyl chloride (CH_3Cl), methyl bromide (CH_3Br), methyl iodide (CH_3I), dibromomethane (CH_2Br_2), chloroform ($CHCl_3$) and bromoform ($CHBr_3$). CH_2Br_2, $CHBr_3$ and CH_3I have not been widely studied in the ambient air at high latitudes. All three gases show large variability, particularly in the summer (June-September). We suggest a marine source for these compounds, with macroalgae a likely source of the brominated compounds. The soil sink of CH_3Cl and CH_3Br that has been measured locally was not distinguishable from the atmospheric sink (OH radicals) in the ambient observations. This study shows that the influence of local fluxes is observable in the Arctic's ambient atmospheric record for CH_2Br_2, $CHBr_3$, $CHCl_3$ and CH_3I in particular.

5.2 Introduction

Halocarbons are a group of halogenated hydrocarbons which play an important role in stratospheric and tropospheric ozone destruction (e.g. Butler, 2000; Mellouki et al., 1992). Halocarbons include solely anthropogenic compounds, such as CFCs (chlorofluorocarbons) and HFCs (hydrofluorocarbons), as well as a wide variety of naturally produced compounds, including the methyl halides (CH_3X, X = Cl, Br, I), dihalomethanes (e.g. CH_2Br_2) and the haloforms (e.g. $CHBr_3$ and $CHCl_3$; Carpenter et

al., 2014; Montzka et al., 2011). Anthropogenic sources of these compounds are dominated by the industrialised mid-latitudes of the northern hemisphere, i.e. Europe, Russia, the U.S. and east Asia (Table 5.1). The natural sources which contribute the most to the global budgets of these halocarbons are also predominantly located in the tropics, sub-tropics or temperate regions (Table 5.1).

Despite lower latitudes being the dominant location of anthropogenic and natural sources for many halocarbons, these gases are still prevalent in the Arctic. Anthropogenic pollutants, including nitrous oxides, aerosols, hydrocarbons and halocarbons, are transported to the Arctic in episodic pulses from the industrialised mid-latitudes (e.g. Beine et al., 1996; Solberg et al., 1996). Natural compounds that are long-lived (e.g. CH_3Cl and CH_3Br) and have major source regions in the lower latitudes can also be transported into the Arctic atmosphere (Stohl, 2006). The low surface temperatures experienced in the Arctic winter result in stable thermal stratification of the atmosphere. Combined with the 'desert' conditions of the Arctic this causes low deposition of

Table 5.1 Details of each compound analysed here, with length of total atmospheric lifetime in years (yr) or days (d), indication of whether the 'source type' of the compound is anthropogenic (A) and/or natural (N), and an indication of the major sources of each compound, including their global location. Where multiple sources are described (up to 3), these are provided in order of the magnitude of the source, from highest to lowest. Information from the following and references therein: [1] Carpenter et al. (2014); [2] Montzka et al. (2011).

Compound	Atmos. lifetime	Source type(s)	Largest sources (top 3, in descending order).
CH_3Cl	0.9 yr [1]	N	Tropical and sub-tropical plants, the ocean (low-mid latitudes), biomass burning (including anthropogenically influenced) [1]
CH_3Br	0.8 yr [1]	A/N	Ocean (low-mid latitudes), biomass burning (including anthropogenically influenced); fumigant (industrialised nations) [1]
CH_3I	7 d [2]	N/A	Oceans: photochemical and phytoplankton (tropical, sub-tropical, temperate), rice production (S Asia) [2]
CH_2Br_2	123 d [2]	N	Oceans (tropical and sub-tropical in particular), coastal macroalgae (tropical, sub-tropical) [2]
$CHCl_3$	149 d [2]	A/N	Production of HCFC-22 and fluoropolymers (industrialised nations), biomass burning (tropical-temperate), soils (temperate)[2]
$CHBr_3$	24 d [2]	N	Oceans (tropical and sub-tropical in particular), coastal macroalgae (tropical, sub-tropical) [2]

atmospheric compounds in the winter (Barrie and Platt, 1997). Additionally, the periods of complete darkness during the Arctic winter inhibit photochemically driven degradation reactions of halogenated compounds and other species (e.g. Edwards et al., 2011; Yokouchi et al., 2008). The result is a build-up of pollutants and natural compounds throughout the winter, many of which rapidly decrease in atmospheric concentration with the onset of polar sunrise and photochemical degradation processes (Gautrois et al., 2003). Sunlight driven halocarbon destruction is caused by direct UV photolysis and, more importantly for the compounds of interest here, by photolytic generation of hydroxyl radicals (OH•) which degrade halocarbons (e.g. Equation 5.1; Edwards et al., 2011; Montzka et al., 2011).

Equation 5.1

$$\mathbf{OH\bullet + CH_3X \rightarrow H_2O + CH_2X\bullet \quad (X = Cl, Br \text{ or } I).}$$

The Arctic seasonal cycle of some compounds, including CH_3Cl, CH_3Br and CH_3I, is well established (Gautrois et al., 2003; Wingenter et al., 1998; Yokouchi et al., 2002, 2012). However, the seasonality and variability of some species, including CH_2Br_2 and $CHBr_3$, has not been previously described from frequent, multi-year measurements.

Although the natural sources for most halocarbons are at lower latitudes, Arctic sources have been identified. For example, several species of Arctic macroalgae have been shown to emit CH_3I, CH_2Br_2, $CHBr_3$ and other multi-halide species (Laturnus, 1996; Schall et al., 1994). Production of CH_3Cl and CH_3Br has been recorded in several species of macroalgae in Antarctica, and plausibly would be produced by Arctic macroalgae as well (Laturnus et al., 1998). Arctic microalgae, particularly sea-ice microalgae, are also known to emit CH_2Br_2, CH_3I and, at the highest rates, $CHBr_3$ (Atkinson et al., 2014; Sturges et al., 1992; Tokarczyk and Moore, 1994). Terrestrial sources are less well recognised in the Arctic. However, $CHCl_3$ emissions have been measured from Arctic tundra soils contributing an estimated 1-2 % of the global atmospheric $CHCl_3$ source (Albers et al., 2017; Rhew et al., 2008b). Additionally, Arctic tundra soil has been identified as a regionally, but not globally, important sink of CH_3Br and CH_3Cl (Rhew et al., 2007). Similar rates of CH_3Br and CH_3Cl soil consumption and of $CHCl_3$ soil emission have also been identified in comparatively under-developed proglacial soils exposed by retreating Arctic glaciers (Chapter 4). These relatively recently exposed soils and more established

Arctic tundra soils have also been found to emit CH_2Br_2 and $CHBr_3$ and variably emit and consume CH_3I (Chapter 4).

Routine measurements (every 3 hours) of the aforementioned halocarbons have been made for several years at the Zeppelin Observatory in Svalbard as part of the Advanced Global Atmospheric Gases Experiment (AGAGE) which monitors ozone-depleting compounds around the world. CH_3Cl, CH_3Br and $CHCl_3$ have been measured for over a decade. CH_3I, CH_2Br_2 and $CHBr_3$ have more recently begun to be monitored and have yet to be analysed for long term or seasonal trends in the Arctic. It has not been determined if the influence of local sources and sinks on the long-term Zeppelin dataset is visible. This study analysed trends of these six halocarbons over a 5-year period from 2013 to 2017. We investigated whether *in situ* terrestrial or marine sources and sinks could be influencing the measured concentrations of these gases, particularly in the summer month of August in 2016 and 2017.

5.3 Methods

5.3.1 Description of site

The Zeppelin atmospheric observatory (78° 54' 29" N, 11° 52' 53" E) is located on Zeppelinfjellet mountain (475 m a.s.l), 2 km south of Ny-Ålesund (Figure 5.1). The observatory provides a long-term, high-frequency record of halocarbon concentrations in the troposphere as part of the AGAGE network of monitoring stations. The observatory is owned by the Norwegian Polar Institute (Norsk Polarinstitutt, NPI) and the instruments of relevance to this study are run by the Norwegian Institute for Air Research (Norsk Institutt for Luftforskning, NILU). The remote nature of the site allows the study of the Arctic atmosphere and the long-range transport of pollutants. The altitude of the observatory means that it is often above the local inversion layer and thus pollution from Ny-Ålesund does not commonly contaminate the measurements (Beine et al., 1996, 2001). It is unclear if the inversion layer would prevent halocarbons fluxes from the fjord, such as those measured at Midtre Lovenbreen (Chapter 4), from influencing ambient concentrations at Zeppelin. However, it is likely that Zeppelin would record natural fluxes from the wider Kongsfjorden area or from neighbouring fjords. We assume that halocarbon flux processes recorded at Midtre Lovenbreen (Chapter 4) are similar to those occurring on proglacial land surfaces around Kongsfjorden, in neighbouring fjords, and more broadly, across Svalbard. CH_3Cl, CH_3Br and $CHCl_3$ fluxes measured at Midtre Lovenbreen were within the ranges of fluxes measured from Alaskan tundra, supporting this assumption (Rhew et al., 2007, 2008; Chapter 4).

5.3.2 Measurement of halogenated gases

Measurement of the halogenated gases of interest here (CH_3Cl, CH_3Br, CH_3I, CH_2Br_2, $CHCl_3$ and $CHBr_3$) and of the two anthropogenic compounds used as pollution event markers (HFC-125 and HFC-134a) was conducted by the 'Medusa' system. The system is described in detail elsewhere (Miller et al., 2008). Briefly, the Medusa pre-concentrated approximately 2 L of air onto a micro-trap (-165 ^oC; 200 mg of 100/120 mesh HayeSep D) with refocussing of very volatile compounds on to a second microtrap (-165 ^oC; 5.5 mg of HayeSep D). The compounds were then separated by a gas chromatograph (GC; 6890N Agilent with a CP-PoraBOND Q fused silica PLOT column, 25m x 0.32 mm i.d.) and quantified by quadrupole mass spectrometry (MS; 5975 Agilent).

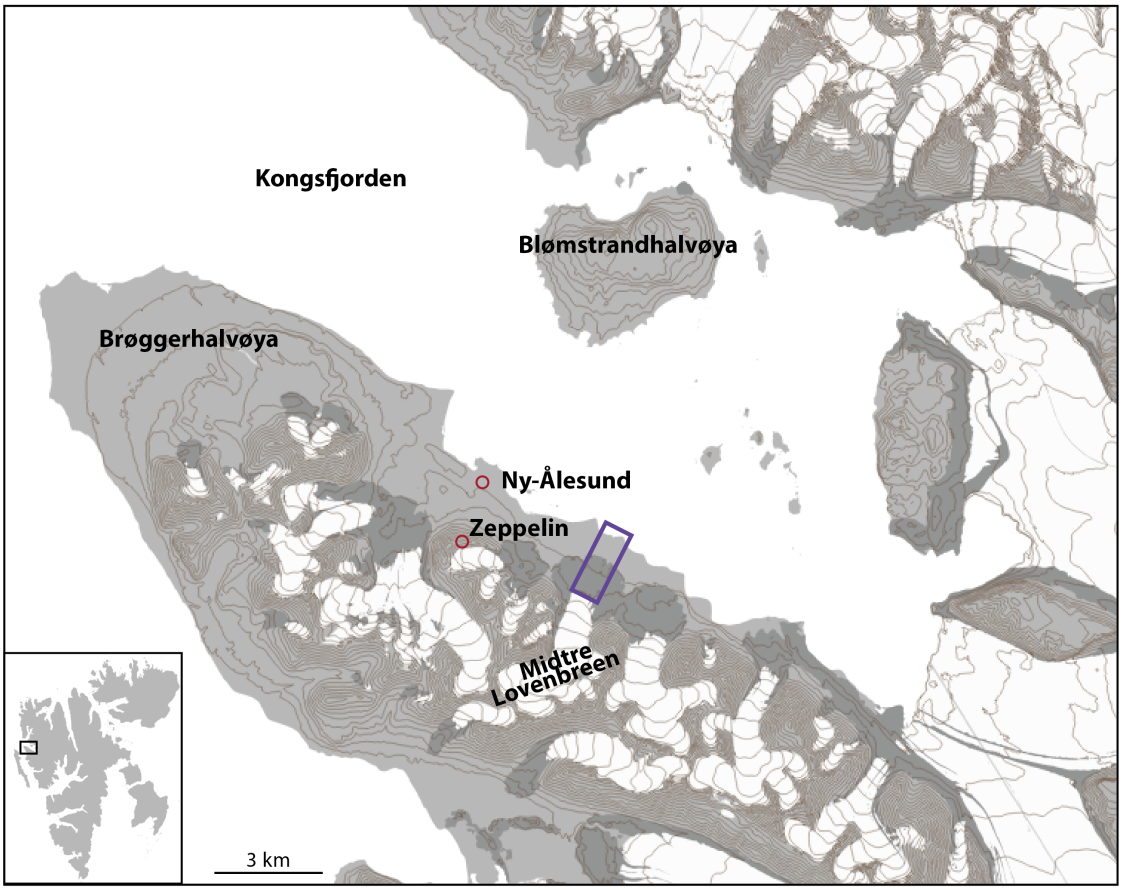

Figure 5.1 The study area in northwest Svalbard showing the fjord (Kongsfjorden) and the peninsula (Broggerhalvøya) where the Zeppelin observatory is located, just south of the research town Ny-Ålesund. Also shown is the island where macroalgal biomass measurements were made on the west side (Blomstrandhalvøya; Section 5.3.6) and the glacier in front of which soil halocarbon fluxes were measured (Midtre Lovenbreen; Section 5.3.7). The purple box shows the section of fjord where the relative areas of macroalgae and soil were calculated. Dark grey areas depict moraine fields, light grey depicts other land surfaces and white areas with contours depict glacial ice. Data used to create the base map was from: Norwegian Polar Institute (2014).

The Medusa sampled 2 L of ambient air via a tower inlet at the Zeppelin observatory approximately every 3 hours. Samples were run alternately with a working standard which was calibrated using a tertiary standard linked to the primary standards prepared at Scripps Institution of Oceanography (SIO). The specific SIO calibration scales used for HFC-134a, HFC-125, CH_3Cl, CH_3Br and $CHCl_3$ are shown in Table 5.2 with precisions for all halocarbons. CH_3I, $CHBr_3$ and CH_2Br_2 were calibrated via AGAGE tank comparisons to NOAA calibration scales at La Jolla (CH3I, NOAA-2009; $CHBr_3$, NOAA-2003) and at Mace Head (CH_2Br_2, NOAA-2004) using NOAA cylinders SX-3526, SX-3537 (La Jolla) & SX-3570 (Mace Head). Because only single tank comparisons were analysed to transfer these calibration scales at both locations, data

presented is preliminary until further comparisons are undertaken to improve the link or AGAGE prepares their own primary calibrations.

Sample analyses were manually inspected by Chris Lunder (from NILU) using GCWerks software (developed by AGAGE) and submitted to the 'EBAS' database (ebas.nilu.no). 2013-2017 data for HFC-125, HFC-134a, CH_3Cl, CH_3Br, $CHCl_3$ and CH_2Br_2 were downloaded for this study from the EBAS database. $CHBr_3$ and CH_3I were not publicly published on the database due to being calibrated on the preliminary scale. Data for these two gases in 2016-2017 was downloaded directly from the Medusa at the Zeppelin observatory by remotely accessing the gas records with GCWerks (with permission from Chris Lunder for use in this thesis only).

Baseline data of CH_3Cl, CH_3Br, CH_3I, CH_2Br_2, $CHCl_3$ and $CHBr_3$ for 2013-2017 were also obtained from AGAGE. The baseline data was used to analyse long-term changes in concentration by calculating mean annual concentrations and was used to calculate the amplitude of seasonal cycles by comparing mean monthly concentrations at the annual maxima and minima. The baseline data was produced by AGAGE by statistical means described in detail elsewhere (e.g. O'Doherty et al., 2001). Briefly, for a selected day, a second-order polynomial was fit to the daily minima of a 121 day period (60 days before the selected day and 60 days after). The polynomial values were subtracted from the data points and the median of the resultant values found. A root-mean-square deviation was calculated using values less than this median and any data point more than 3 times this

Table 5.2 The precisions and the calibration scales used for the 6 halocarbons of interest plus the two HFC compounds analysed here. The precision for each gas is the typical precision reported by AGAGE (Prinn et al., 2018). (*) denotes calibration scales that have only been preliminarily transferred to the Medusa system.

Common name	Formula	Precision (%)	Calibration Scale
HFC-134a	CH_2FCF_3	0.7	SIO-05
HFC-125	CHF_2CF_3	0.5	SIO-14
Methyl chloride	CH_3Cl	0.2	SIO-05
Methyl bromide	CH_3Br	0.6	SIO-05
Methyl iodide	CH_3I	2	*NOAA-2009
Dibromomethane	CH_2Br_2	1.5	*NOAA-2003
Chloroform	$CHCl_3$	0.4	SIO-98
Bromoform	$CHBr_3$	0.6	*NOAA-2004

deviation was flagged as polluted. The process was repeated for each day. The whole process was repeated again as the median calculated initially was likely biased due to the presence of the high pollution events. Data points between 2-3 deviations above the median on the second pass were determined to be polluted if immediately adjacent to polluted data points (> 3 deviations). Mean annual or monthly concentrations are presented with ± 1 standard deviation.

5.3.3 Measurement of non-halogenated gases and meteorological variables

Carbon monoxide (CO) and methane (CH_4) were measured every hour at the Zeppelin observatory by spectroscopy using a Picarro G2401. Both gases were calibrated on the following World Meteorological Organisation calibration scales: WMO-CO-X2014A for CO and WMO-CH4-X2004 for CH_4.

Meteorological data was continuously logged and presented as a 1 hour mean value. Temperature (^oC) was measured by a platinum resistance thermometer, wind direction (^{o}) was measured by a wind vane and wind speed (m s^{-1}) was measured by a cup anemometer at the observatory. All meteorological data and data for CO and CH_4 were obtained for 2016-2017 from the EBAS database.

5.3.4 Data processing

2016 and 2017 were used as two 'focus years' for more detailed analysis of the influence of local fluxes. 2017 was chosen due to it being the year where flux measurements of the gases were made from soils in the fjord (Chapter 4) and 2016 was used as a comparison. The baseline halocarbon data was not used for this analysis because the statistical method used to obtain baseline measurements does not discriminate between anthropogenic and natural peaks in concentration. Therefore the complete data set was used. Preliminary processing of the halogenated gas data was required due to it being available at slightly irregular time intervals at approximately 3-hour intervals. In contrast, meteorological data and the non-halogenated gas data were presented as a mean of every hour, on the hour. To allow all data to be analysed together, a new time stamp was created for the halocarbon data with the time rounded to the nearest hour so they could be analysed together. For all data (halocarbons, non-halogenated gases and meteorological variables), entries that were flagged in the dataset as either incomplete or erroneous were removed.

An in-depth analysis of changes in gas concentration in the month of August was conducted for 2016 and 2017. August was chosen as a focus month because there was a complete dataset of halocarbon measurements that month, it is within the growing season and it has 24-hour daylight for most of the month. The 24 hour daylight means biological production and consumption processes should be occurring and diurnal variation should be minimised. The sun does set from the 27th August for ~ 2 hours (increasing to 4.5 hours by the 31st of August), but the month of July, which has continuous 24-hour daylight, was missing over two weeks of data due to machine maintenance in both 2016 and 2017. The processing and analysis conducted on the gas measurements made in the month of August are described in the following sections.

5.3.4.1 Removal of pollution events

Large-scale pollution events were removed from the data to maximise the likelihood of detecting the influence of anthropogenic processes on ambient concentrations. Pollution events were identified by significant extrusions from the baseline in the anthropogenic gases HFC-125 and HFC-134a (Figure 5.2). Significant extrusions were defined as more than 1 standard deviation above the monthly mean. Measurements made during these excursions were removed for all gases. Large peaks in the CO dataset were also treated as pollution events and removed, as elevated CO indicates the airmass has been carried from a region of biomass burning (Stohl et al., 2007). Because the CO data did not have a horizontal baseline, 'significant extrusions' were defined by the following method described using the example of removing the CO extrusion around the 22nd August 2017 (Figure 5.2). A regression line was estimated using a linear model in R for the period where the baseline was not horizontal (17th – 31st August 2017). CO residuals from the model that were more than one standard deviation greater than their predicted value were classed as pollution events. Measurements made within the identified CO pollution event were removed for all gases.

5.3.4.2 Analysis of the influence of wind direction and speed

To identify if the relationship between gas concentration and wind direction could indicate the influence of local fluxes, 'pollution roses' were created in R (Version 3.5.0) using package 'openair' (Carslaw and Ropkins, 2012). The pollution roses were created using data for the month of August following the removal of identified pollution events. Pollution roses were created for each gas at all wind speeds and for measurements made

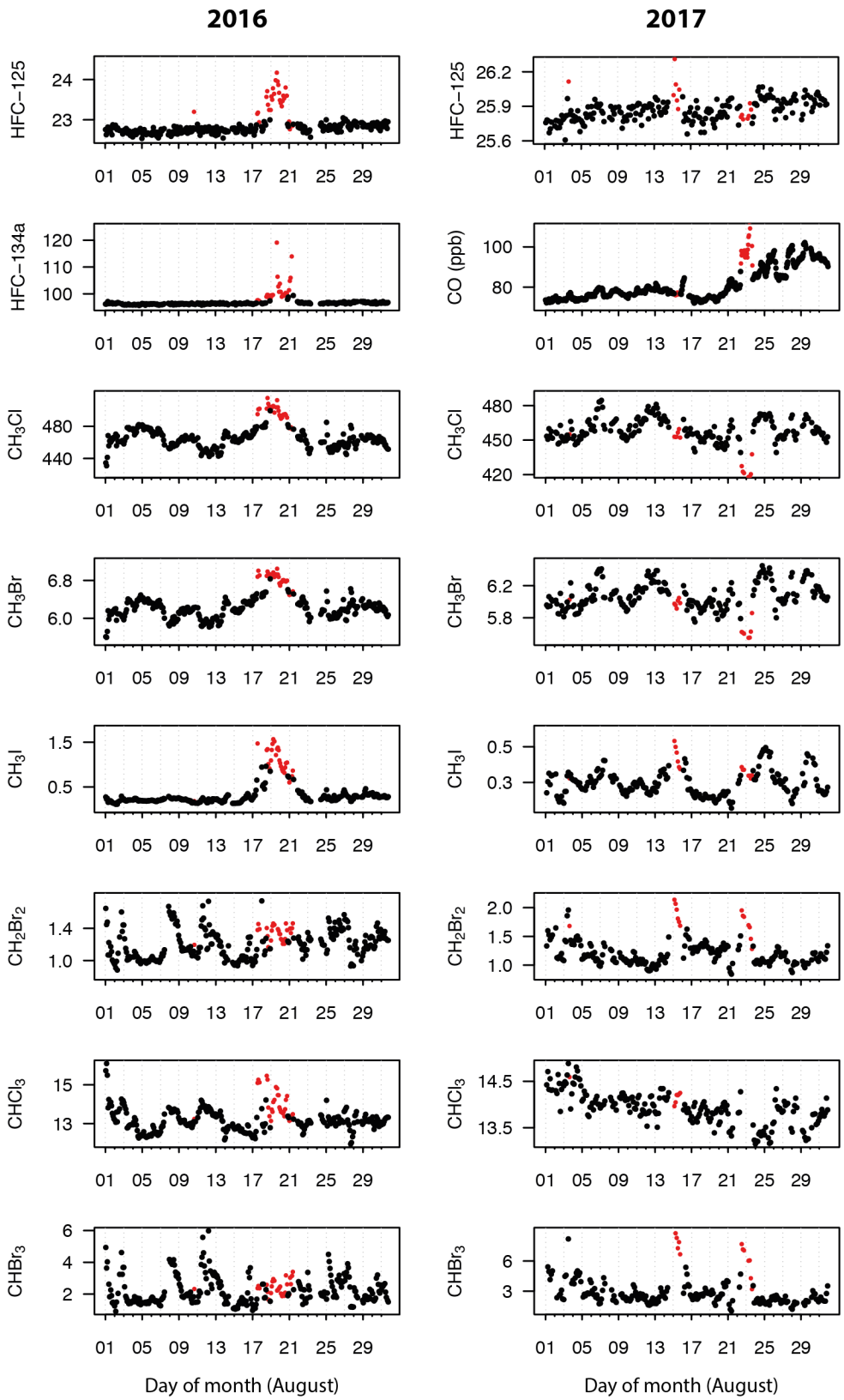

Figure 5.2 Halocarbon observations (all in ppt) for August 2016 and 2017. The red points were values identified as occurring during a pollution event which were determined statistically using HFC-125, HFC-134a or CO observations (Section 5.3.4.1). These data points were subsequently removed from all gas data for the August analyses.

during low wind speeds only. Low wind speed periods were defined as gas measurements taken when the wind speed was less than 4 m s^{-1}, and was less than this speed for 6 hours prior to the measurement (after Simmonds et al. (2004)). The removal of periods of time with higher wind speeds broadly corresponded with the removal of large pollution events identified previously. The gas concentration distribution is indicated by differentiating between the lower, second, third and upper quartiles of measurements in the month of August. This was determined for the 'all wind' speed data with the same quartile breaks used for the low wind speed roses to determine if low winds influenced the proportion of gas concentrations present in each quartile.

5.3.5 Comparison of ground-level to Zeppelin measurements

Spot ground-level (< 50 m a.s.l.) measurements of the ambient air were compared to ambient measurements made at Zeppelin (495 m a.s.l.) on the same days, to determine if a ground-level source was influencing the ambient concentration nearer to the potential source. Spot ground-level measurements of the 6 halocarbons were made in late July 2017 on the forefield of Midtre Lovenbreen glacier ~ 3.5 km east of the Zeppelin observatory (Chapter 4, Figure 5.1). The ground-level spot measurements were made with sample bags and then analysed, rather than sampled directly from the air as at Zeppelin. The instrument at Zeppelin and the instrument used to analyse the ground-level measurements were calibrated on the same calibration scales (Chapter 4). Ground level concentrations were compared with the average zeppelin measurement made within +/- 12 hours of the ground spot measurement. Measurements at Zeppelin made within 12 hours of the spot measurement were available on 6 days in July 2017. For 2 of those days, measurements at Zeppelin were only available in the 12 hours after the spot-measurement due to ongoing maintenance when the field measurements were undertaken.

5.3.6 Calculation of macroalgal halocarbon fluxes

CH_2Br_2 and $CHBr_3$ have both marine (i.e. macroalgae) and terrestrial (i.e. soil) sources in the Arctic. To determine if macroalgal or soil sources were more likely to be influencing ambient measurements of CH_2Br_2 and $CHBr_3$, published rates of macroalgal emission were scaled to a flux rate (nmol m^{-2} d^{-1}) using rates and distributions of macroalgae made in Kongsfjorden. This rate was directly comparable to rates measured from soils in the fjord (Chapter 4). Wiencke et al. (2004) detailed the four most common macroalgae species by biomass in the upper sublittoral (0 to 3 metres depth) and mid

sublittoral (3 to 15 m) zones on the west side of Blomstrandhalvøya island (Figure 5.1). Estimates of total biomass per metre squared in these zones were 4.5 and 6.5 kg m^{-2}, for the upper and mid sublittoral respectively. The proportion of each species present was not given, and so each of the four most common species were assumed to be responsible for 25 % of the biomass of each zone. Emission rates of $CHBr_3$, CH_2Br_2 and CH_3I had been detailed for two of the four most common species: *Laminaria saccharina* (mid sublittoral zone) and *Fucus distichus* (upper to mid sublittoral zone). In the mid sublittoral zone the two species were assumed to account for 25 % of biomass each (50 % in total) and 100 % of the emissions from macroalgae, in the absence of emission rates from other macroalgal species. In the upper sublittoral *F*. *distichus* was assumed to account for 25 % of biomass and 100 % of emissions. Emission by *L. Saccharina* was measured as 72 to 150 ng $CHBr_3$ [g wet algal mass]$^{-1}d^{-1}$; 8 to 150 ng CH_2Br_2 [g wet algal mass]$^{-1}d^{-1}$; and 0.2 ng CH_3I [g wet algal mass]$^{-1}d^{-1}$ (Laturnus, 1996; Schall et al., 1994). Emissions from *F. distichus* were measured as 17.4, 8.1 and 0.8 ng [g wet algal mass]$^{-1}d^{-1}$ for $CHBr_3$, CH_2Br_2 and CH_3I respectively (Schall et al., 1994). These emission rates were converted to nanomoles (nmol [g wet algae]$^{-1}$) and were multiplied with 25 % of the biomass present in the respective zone (g m^{-2}) to obtain a flux comparable to terrestrial measurements (nmol m^{-2} d^{-1}). The fluxes were combined to obtain a total upper to mid sublittoral flux. Emission from macroalgae in the lower sublittoral was assumed to be negligible because this zone has low biomass (0.9 km m^{-2}; Schall et al., 1994) and was dominated by red macroalgae which have been found to have very low or negligible emission rates of $CHBr_3$ and CH_2Br_2 (Laturnus, 1996).

5.3.7 Estimated areal coverage of known marine and soil fluxes

An areal estimate of soil and macroalgae was calculated for a section of the fjord to determine whether differences in the sources' areal coverage were large enough to impact the difference in their emission rates per metre squared (Section 5.3.6). The section chosen was between the snout of Midtre Lovenbreen glacier and the fjord where soil emission rates had been measured (Chapter 4; Figure 5.1). The section was defined as a rectangle roughly perpendicular to the coastline and the glacier's terminus, which contained the sites where soil fluxes had been measured. If the rest of the fjord was subdivided into similar sections, some would have different proportions of ice-free land area versus macroalgal bed area. However, we assume that these differences were small enough to still use these proportions as an order of magnitude estimate.

Macroalgae biomass has not been measured at the chosen section of coastline. Macroalgal biomass estimates may be lower at this section than at Blomstrandhalvøya due to being less sheltered form abrasion by drifting ice bergs (Wiencke et al., 2004). However, for the purposes of this comparison we assumed that the macroalgae were present at this section of coastline in similar proportion and abundance as measured at Blomstrandhalvøya (Wiencke et al., 2004). The macroalgal fluxes described in Section 5.3.5 were recorded from species found in abundance between 0 and 15 metres water depth (Wiencke et al., 2004). The corresponding area of water where macroalgae are present on the sea-bed was estimated using the length of coastline of the section and the distance between the shoreline and where the water is 15 metres of water depth. The distance between the shore and the 15 metre depth line was determined as the midway between the 10 and 20 metre isobars marked on a bathymetric chart of the fjord (from toposvalbard.npolar.no, Norsk Polar Institutt).

Terrestrial emissions of $CHBr_3$ and CH_2Br_2 were observed from vegetated tundra near to the shoreline and cyanobacterial mats and sediment behind the terminal moraine (Chapter 4). The areal extent of tundra and cyanobacterial mats cannot be accurately determined from the areal images available without more detailed field observations of the extent of the land surfaces. However, the macroalgal emission rates per metre squared (Section 5.3.6) were 2-3 orders of magnitude larger than those measured from the soil (Chapter 4). Therefore, we compared the total terrestrial land surface area in the section to determine if this extreme upper limit of soil coverage was large enough to impact the difference in flux measurements. The total land surface area in this section was an overestimate of the area emitting at the measured rates due to the presence of unvegetated rocky moraines and shifting streams which presumably have negligible emissions of $CHBr_3$ and CH_2Br_2. The upper terrestrial area was 9 times larger, but the same order of magnitude as the area of sea-water under which halocarbon emitting macroalgae were present.

5.4 Results

5.4.1 Five year trends

Five year trends were determined for CH_3Cl, CH_3Br, $CHCl_3$, CH_2Br_2, CH_3I and $CHBr_3$ for the period 2013-2017 using baseline measurements (Figure 5.3). Over the five year period, $CHCl_3$ increased in concentration at an average of 5.1 ± 4.0 % yr^{-1}, resulting in a 22 % difference between 2013 and 2017. CH_3Br decreased by 6.6 % over the same period at an average of -1.7 ± 1.0 % yr^{-1}. Both $CHCl_3$ and CH_3Br have anthropogenic sources. CH_3Cl, CH_2Br_2, $CHBr_3$ and CH_3I have primarily natural sources and had inconsistent year on year changes (both positive and negative changes) with means of -0.1 ± 1.0 yr^{-1} % for CH_3Cl, -0.8 ± 1.4 % yr^{-1} for CH_2Br_2, -2.6 ± 8.5 % yr^{-1} for $CHBr_3$ and -8.7 ± 17 % yr^{-1} for CH_3I. The inconsistency in the year on year changes for these four gases means that they did not demonstrate a clear 5-year trend.

5.4.2 Seasonal variation

There were seasonal variations in the concentration of all six gases (Figure 5.3). CH_3Cl and CH_3Br showed broadly similar trends with the highest mean monthly concentrations in April for CH_3Cl, and in April or May for CH_3Br. Minimum mean concentrations occurred in August or September for both gases. In the spring, CH_3Br transitioned from increasing to decreasing in concentration more sharply than CH_3Cl. The mean magnitude of the seasonal variation was 104 ± 10 ppt against a 5-year mean concentration of 517 ppt for CH_3Cl and 1 ± 0.2 ppt against a 5-year mean concentration of 6.7 ppt for CH_3Br. Baseline maxima for the other halocarbons occurred earlier than for CH_3Cl and CH_3Br, with maxima in February or March for CH_2Br_2 and in December or January for $CHCl_3$ and CH_3I. Baseline minima for these three gases also occurred earlier, usually in June or July for $CHCl_3$ and CH_2Br_2, and in April or May for CH_3I. CH_3I, $CHBr_3$ and CH_2Br_2 showed more variability and larger peaks in concentration in the summer than in the winter.

5.4.3 Variability in August

To investigate if it is possible to detect the impact that local halocarbon fluxes could be having on ambient atmospheric concentrations, a series of analyses were conducted for the month of August. Variability in gas concentrations in August was seen for the 6 halocarbons, but with no evidence of a regular cycle (e.g. diurnal; Figure 5.2). As discussed above, several gases share similar seasonal patterns (Figure 5.3). Some gases

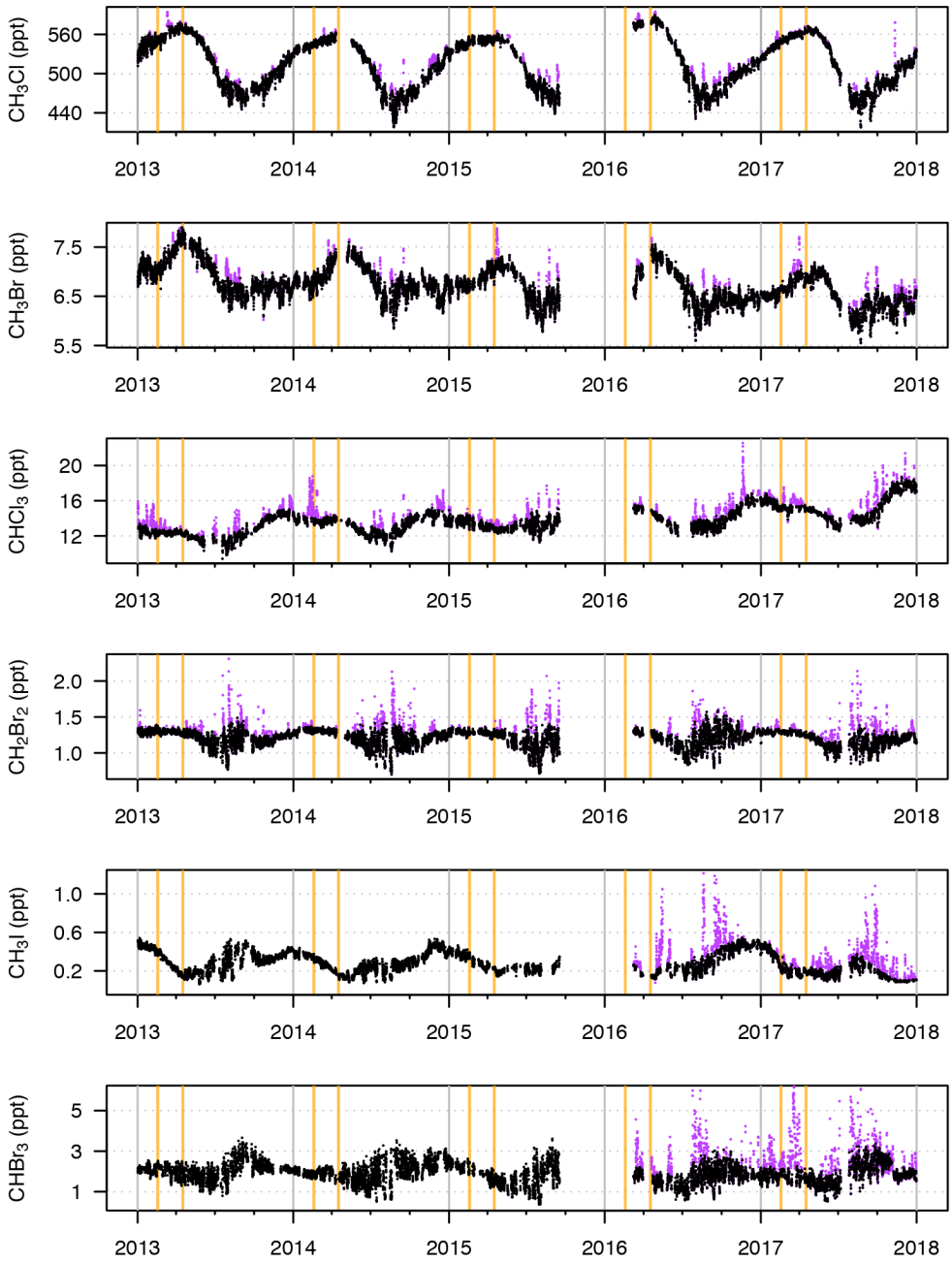

Figure 5.3 Measurements of CH_3Cl, CH_3Br, CH_3I, CH_2Br_2, $CHCl_3$ and $CHBr_3$ made at the Zeppelin observatory between 2013-2017. The black points are AGAGE determined baseline measurements, the purple points are all other measurements, which were only available for 2016-2017 for CH_3I and $CHBr_3$. The gaps in the dataset represent periods when the instrument was down for maintenance or repair. The two orange lines represent polar sunrise (17-18th of February) and the first day of 24hr daylight (17th April).

also share sub-seasonal patterns of variation (Figure 5.2). For example, CH_3Cl and CH_3Br were well correlated over the whole of 2016 and 2017 (r = 0.90 and 0.85, p-values < 0.001) and were slightly better correlated in August of both years (r = 0.92 and 0.93, respectively, p-values < 0.001; Figure 5.4a, b). However, other gases had different

relationships in August compared to across the whole year. For example, CH_2Br_2 and $CHBr_3$ were well correlated across the whole of 2016 (r = 0.74, p-values < 0.001) and moderately correlated across 2017 (r = 0.59, p-values < 0.001). However, they were strongly correlated in August 2016 and 2017 (r = 0.91 and 0.89, respectively, p-values < 0.001; Figure 5.4c, d). Similarly, $CHCl_3$ was not correlated with any gas across either year (-0.1 < r < 0.4), but was negatively correlated with CH_3Cl and CH_3Br in August 2016 (r = 0-.65 and -0.70, respectively, p-values < 0.001) and was positively correlated with CH_2Br_2 and $CHBr_3$ in the same month (r = 0.65 for both , p-values < 0.001; Figure 5.4e, f). Interestingly these relationships were weaker in August 2017 (r = -0.41, -0.58, 0.51 and 0.60, respectively for CH_3Cl, CH_3Br, CH_2Br_2 and $CHBr_3$, p-values < 0.001). CH_3I was not well correlated with any gas over the whole year or in August 2016 and 2017 (-0.22 < r < 0.43). No relationships were seen with meteorological variables (e.g. temperature, wind speed or wind direction), CO or CH_4 in August.

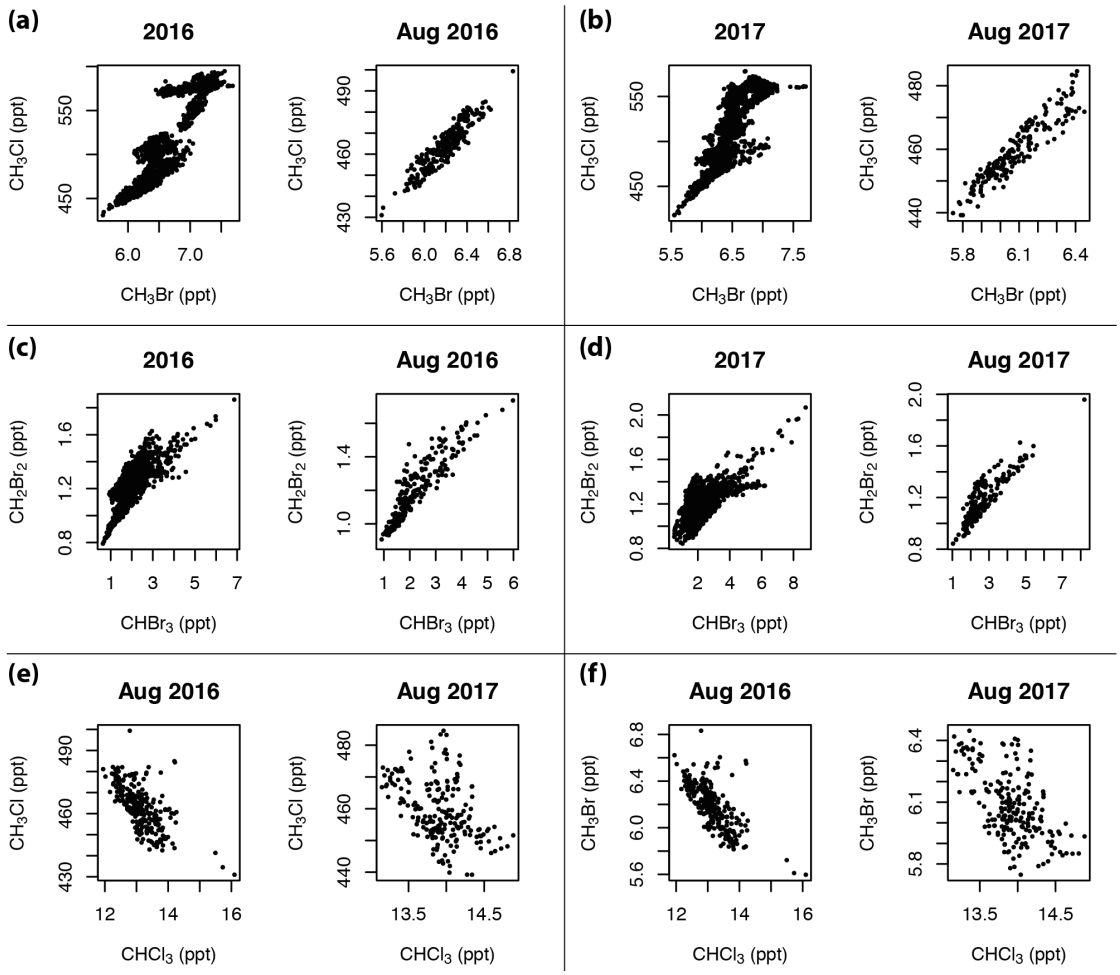

Figure 5.4 Comparison of the relationship between halocarbon measurements across the whole year and across the month of August for CH_3Cl and CH_3Br in 2016 (a) and 2017 (b), CH_2Br_2 and $CHBr_3$ in 2016 (c) and 2017 (d) and for CH_3Cl and $CHCl_3$ in 2016 (e) and 2017 (f).

5.4.3.1 Gas variability and the relationship with wind speed and direction

Local fluxes were more likely to influence ambient gas concentrations when air masses were relatively static and, thus, measurements made at low wind speeds were identified (Section 5.3.4.2). There was little difference in the relationships between the gases and meteorological data described above when analysing low wind data alone. Wind directions measured at Zeppelin in August of both years were dominated by southerly and south-easterly winds, with less common north-westerlies. Winds from the northeast

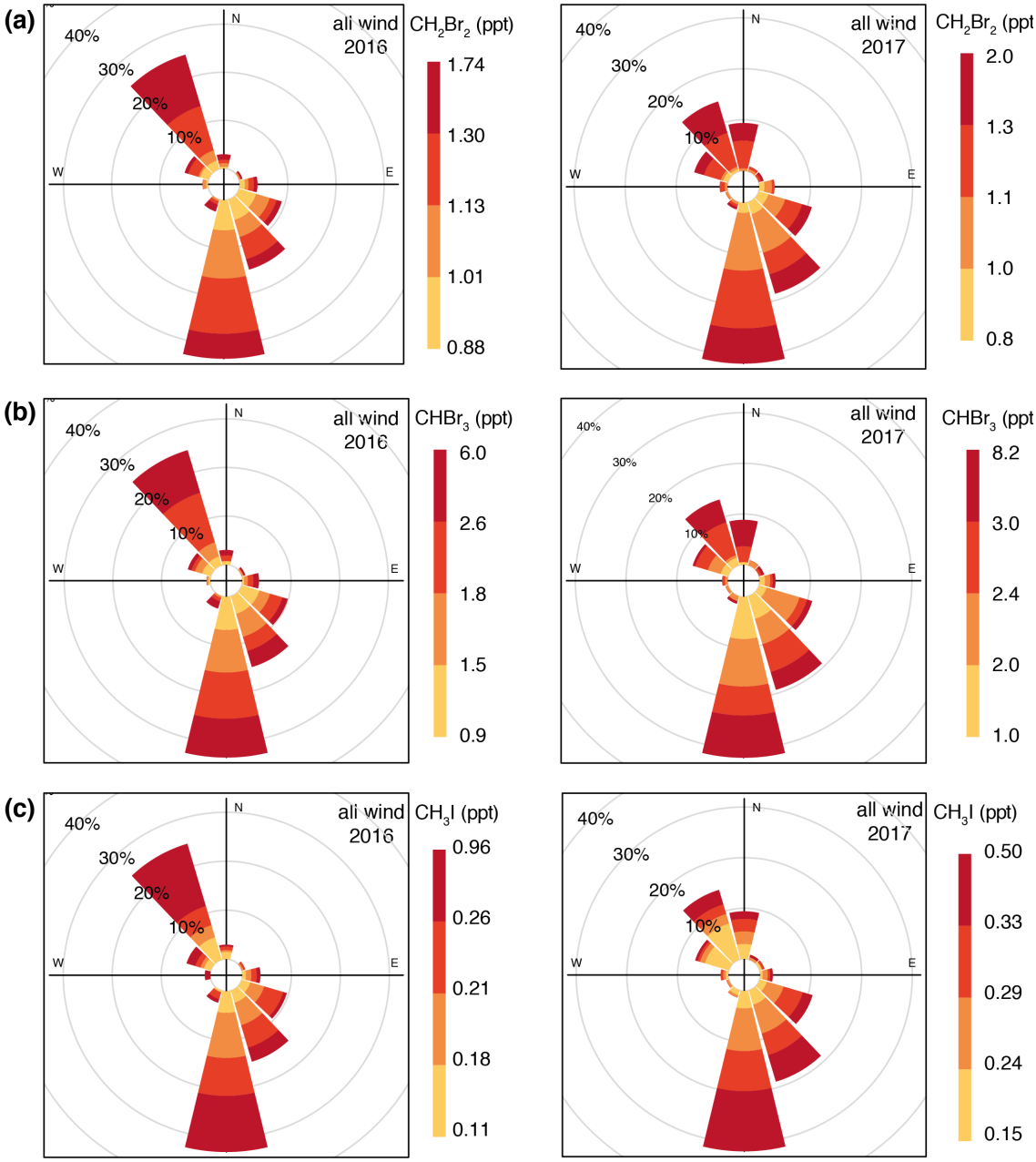

Figure 5.5 Pollution roses of CH_2Br_2 (a), $CHBr_3$ (b) and CH_3I (c) for all wind speeds in 2016 and 2017. Concentrations are categorised into lower, second (lower to median), third (median to upper) and upper quartiles of measurements.

and southwest were uncommon. For CH_3I, CH_2Br_2, $CHBr_3$ and $CHCl_3$, it is noteworthy that measurements with concentrations in their respective upper quartiles were observed from both north-westerly and south/south-easterly directions (Figure 5.5, 5.6). This was in contrast to CH_3Cl and CH_3Br which have upper quartile measurements dominated by south/south-easterly directions, particularly in 2016 (Figure 5.7). For CH_3Cl and CH_3Br, the difference between all and low wind data was not consistent when comparing 2016 and 2017. For example, in 2016, the proportion of lowest quartile CH_3Cl concentrations increased from 24 to 40 % when low wind data was analysed alone, whereas in 2017 the proportion of lowest quartile measurements remained at 23 % for all and low winds. Similarly, for CH_2Br_2 there was an increase in the proportion of measurements in the upper quartile in the low wind data from 24 to 35 % in 2016, whereas in 2017 the proportion of upper quartile concentrations was similar at 26 and 23 % for all and low wind respectively. However, some pattern changes were consistent in both years. For example, in both years, the proportion of upper quartile $CHCl_3$ measurements was higher in the low wind data, at 40 and 42 % for 2016 and 2017 respectively, than in the all wind data, at 27 and 29 % for 2016 and 2017 respectively (Figure 5.6).

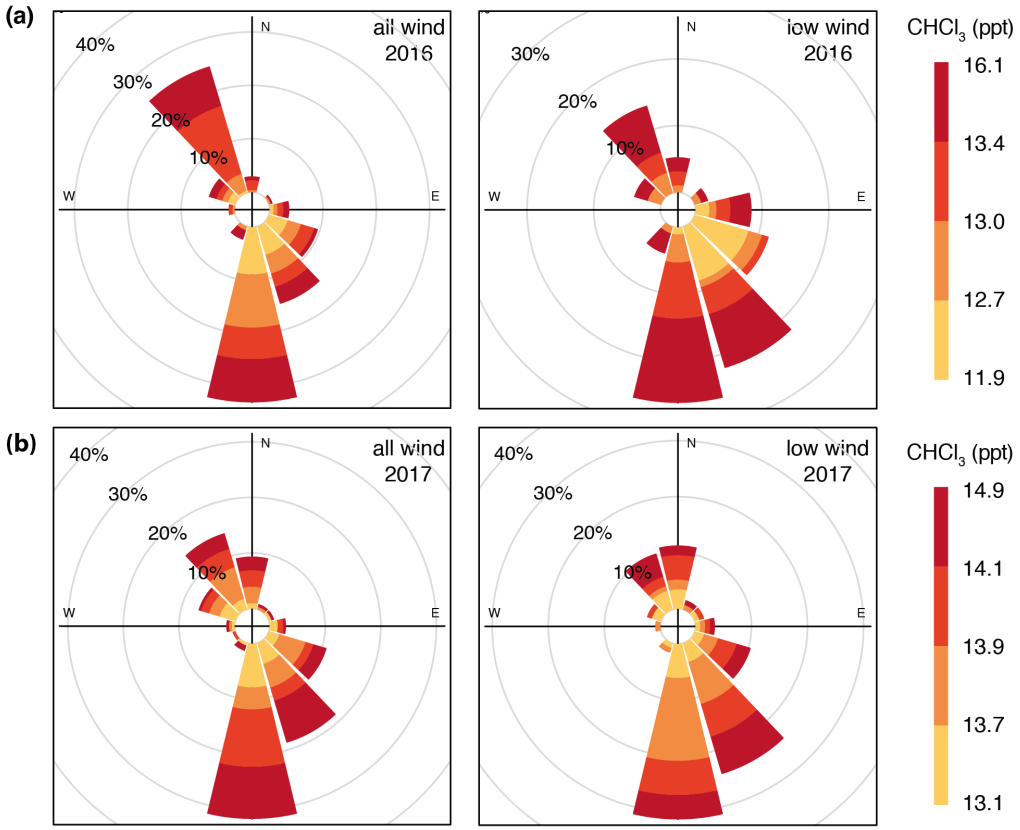

Figure 5.6 Pollution roses of $CHCl_3$ comparing all wind speeds to low wind speeds in 2016 (a) and 2017 (b). Concentrations are categorised into lower, second (lower to median), third (median to upper) and upper quartiles of measurements as measured during all wind speeds.

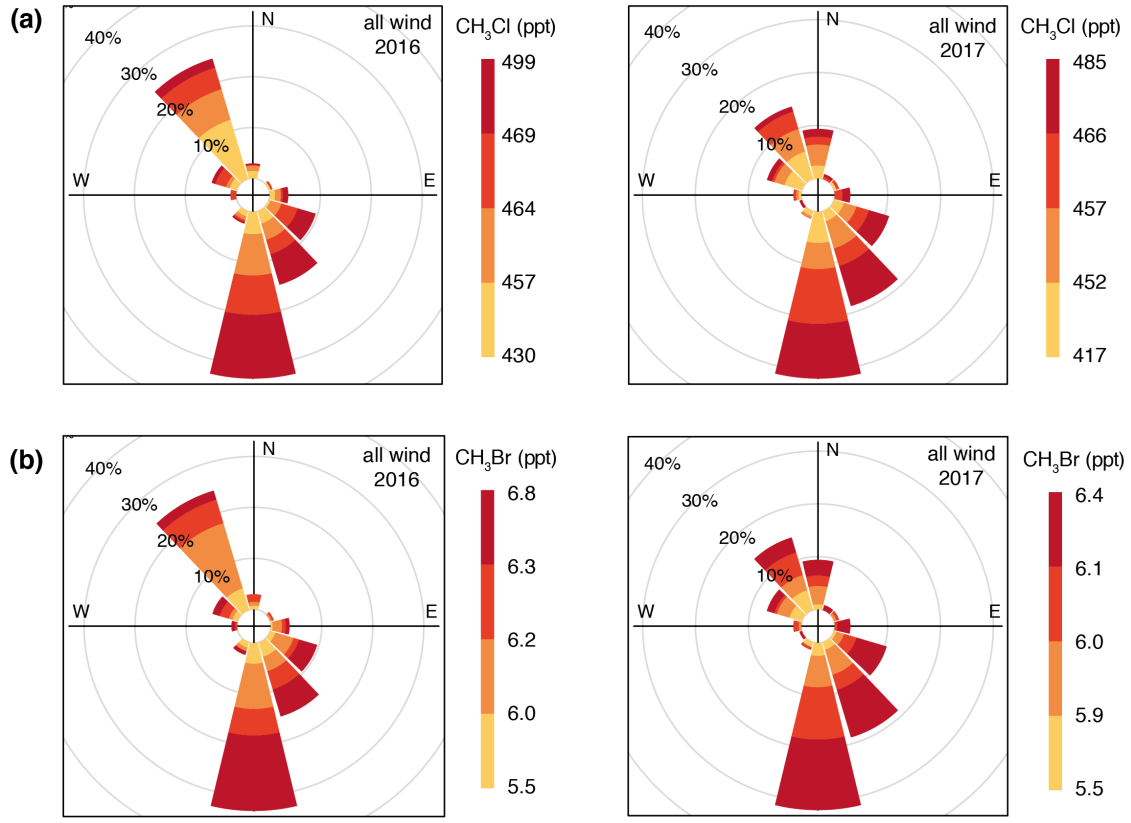

Figure 5.7 Pollution roses of CH_3Cl (a) and CH_3Br (b) for all wind speeds in 2016 and 2017. Concentrations are categorised into lower, second (lower to median), third (median to upper) and upper quartiles of measurements.

5.4.3.2 Comparison between Zeppelin measurements and ground-level measurements

Spot measurements made in 2017 near sea-level found that two halocarbons were consistently elevated at ground-level compared to measurements made within 12 hours at the Zeppelin observatory (Section 5.3.5). Most strikingly, $CHCl_3$ was a mean of 1.5 ± 0.2 times higher at ground-level (where the mean concentration was 20. 1 ± 2.6 ppt) than at Zeppelin (where the mean concentration was 14.2 ± 0.1 ppt). CH_3I was also always higher at ground-level than at Zeppelin but by a more variable amount (1.8 - 4.7 times; 0.3-0.7 ppt) than for $CHCl_3$. The variability in the difference between the two locations was driven by a variable ground-level concentration (mean 0.85 ± 0.15 ppt) compared to a more stable concentration at Zeppelin (mean of 0.29 ± 0.07 ppt). $CHBr_3$ showed a similar pattern to CH_3I, where the ground-level concentration (mean of 4.18 ± 1.25 ppt) was higher by a variable amount (1.1-3.0 times; 0.4-1.7 ppt) than at Zeppelin (mean of 2.57 ± 0.91 ppt).

CH_3Cl, CH_3Br and CH_2Br_2 did not show consistently elevated concentrations at one site compared to the other. Of these three gases, CH_2Br_2 was the most consistent, with concentrations elevated by up to 0.77 ppt at ground level (mean 1.47 ± 0.27 ppt) compared to Zeppelin (1.21 ± 0.15 ppt) on 5 out of 6 days. The ground-level concentration was 0.06 ppt lower than Zeppelin on 1 day. For CH_3Cl, the concentration at ground-level was between 11 ppt lower and 78 ppt higher than at Zeppelin (against an ambient Zeppelin concentration of ~ 470 ppt), with ground-level concentrations lower than Zeppelin on 2 out of 6 days. CH_3Br shows the reverse relationship, with concentrations higher at ground level (by up to 0.2 ppt) than at Zeppelin on 2 out of 6 days, and lower at ground level on 4 out of 6 days (by up to -0.6 ppt). For all the gases, there was no evidence that the ambient concentrations measured were elevated/depleted at locations where the soil had been found to consume/produce the gas (Chapter 4). For example, CH_3Cl was found elevated relative to Zeppelin measurements even at sites, such as on the tundra, that had showed consistent and strong draw-down by the soil in previous studies (Chapter 4).

5.5 Discussion

5.5.1 Long-term and seasonal variation

Halocarbon measurements have been made at Zeppelin observatory since 2001 as part of the AGAGE monitoring network. Attention has primarily been paid to species that are anthropogenic pollutants (e.g. HFC-134a, HFC-125) and thus can be used to understand transport to the 'pristine' High Arctic (e.g. O'Doherty et al., 2009; Prinn et al., 2018). Longer-lived halocarbons with solely or partly natural origins can also be transported. Anthropogenic emissions of CH_3Br have been restricted by the Montreal Protocol for several years which was reflected in the gradually decreasing annual concentration of this gas between 2013 and 2017 (Figure 5.3). Sources of $CHCl_3$ are estimated to be up to 25 % anthropogenic, but the compound is not regulated by the Montreal Protocol due to its low (< 0.5 months) atmospheric lifetime which minimises its impact on stratospheric ozone (Montzka et al., 2011). The unregulated anthropogenic emissions may be contributing to the gradual increase in concentration seen over the 5 year period. CH_3Cl, CH_2Br_2, $CHBr_3$ and CH_3I are primarily natural in origin which was reflected in their relatively stable concentrations over the 5 years.

Transport of longer-lived natural compounds, such as CH_3Cl and CH_3Br, from lower latitudes also occurs. This raises their concentrations in winter until polar sunrise and the onset of the photochemical reactions (e.g. photolytic production of OH radicals) that cause halocarbon degradation (Gautrois et al., 2003; Wingenter et al., 1998; Yokouchi et al., 2002). The seasonal trend measured here reflected this pattern, with the spring decrease in both gases occurring after polar sunrise and around the beginning of 24 hour daylight (Figure 5.3). The seasonality of $CHCl_3$ shows broadly similar seasonal cycles for the same reason (e.g. O'Doherty et al., 2001). CH_2Br_2, $CHBr_3$ and CH_3I have seasonal cycles that are also partially caused by the onset of photochemical and OH-radical destruction in spring. However, the seasonal cycle of these compounds appears to be further influenced by summertime emissions causing the large peaks in concentration and greater variability than in the winter (Figure 5.3).

5.5.2 Do the Zeppelin observations show the influence of local fluxes?

Terrestrial soil consumption of CH_3Cl and CH_3Br and production of $CHCl_3$, $CHBr_3$ and CH_2Br_2 has been measured in soils via this PhD about 4 km east of Zeppelin (Chapter 4). Additionally, production of CH_3I, CH_2Br_2 and $CHBr_3$ have been measured from samples

of macroalgae taken in the fjord (Laturnus, 1996; Schall et al., 1994). The impact of local fluxes on the ambient measurements of CH_3Cl, CH_3Br, CH_3I, CH_2Br_2, $CHCl_3$ and $CHBr_3$ taken at Zeppelin have not been investigated. We assumed that the soil fluxes and macroalgal emissions were representative of fluxes throughout the fjord and in neighbouring fjords. Because the Zeppelin observatory is located on the Broggerhalvøya peninsula, air masses were likely to have travelled over a mixture of marine and terrestrial environments (Figure 5.1; Beine et al., 2001). The local wind field is complex due to funnelling by the fjord, katabatic winds from Konsvegen glacier at the head of the fjord (~ 120 °), and orographic effects which, in particular, twist winds from the south-east to the south at Zeppelin (Beine et al., 2001). As a result, even air masses appearing to have travelled directly over the peninsula (from the southeast) were assumed to have travelled over a mixture of marine and terrestrial environments. Therefore, it was not possible to use wind direction to distinguish between marine and terrestrial influences. Airmasses form the north and northwest were considered the most pristine due to the lack of anthropogenic activities in that direction and, therefore, could be used to broadly infer the influence of natural Arctic fluxes. The following two sections discuss the evidence for local terrestrial and marine fluxes influencing the Zeppelin record.

5.5.2.1 Limited evidence for a soil sink of CH_3Cl and CH_3Br

'Pollution roses' show that the upper quartile of CH_3Cl and CH_3Br measurements were dominated by southerly/ south-easterly wind directions (Figure 5.7). The lack of upper quartile CH_3Cl and CH_3Br measurements from the north-northwest suggests that there was not a strong net source of these compounds in the Arctic. Although it is possible that the lower concentrations measured in winds to the north indicates an Arctic sink of these compounds, it is not possible to distinguish the soil sink from the atmospheric sink (OH radicals). This is also true of the overall seasonal cycle which sees minimum concentrations in the summer when both the atmospheric and soil sinks were assumed to be at their maximum due to 24 hour daylight. The soil sink has not been measured in Svalbard outside of the growing season, but seems likely to be inhibited at least partially during periods of snow-cover or sub-freezing temperatures in the soil, as has been found for CO_2 emission rates (e.g. Welker et al., 2000). If this is the case, the onset of photochemically-driven destruction (approximately late February) of CH_3Cl and CH_3Br is earlier than the presumed onset of the local soil sink after the snow melts (which is locally late June). From late June to August, it is possible that the seasonally low CH_3Cl

and CH_3Br concentrations were being driven by a combination of atmospheric and soil sinks.

5.5.2.2 Evidence of a local source of CH_3I, CH_2Br_2, $CHCl_3$ and $CHBr_3$

In contrast to CH_3Cl and CH_3Br, upper quartile measurements were observed for CH_3I, $CHCl_3$, CH_2Br_2 and $CHBr_3$ during northerlies and north-westerlies, as well as southerlies and south-easterlies (Figures 5.5). This suggests an Arctic source of CH_3I, $CHCl_3$, CH_2Br_2 and $CHBr_3$. It is also less likely these compounds would be transported over long-distances due to their shorter atmospheric lifetimes (Table 5.1). Therefore, they require an Arctic source to explain the higher concentrations observed in the summer. This was particularly true for CH_2Br_2 and $CHBr_3$ which were both observed to repeatedly spike in concentration, particularly between July and October (Figure 5.3). $CHBr_3$ showed more variability than CH_2Br_2 outside of the summer and particularly during early spring. The peaks in the spring of $CHBr_3$ possibly indicate rapid release by sea-ice microalgae which have been measured emitting $CHBr_3$ shortly after polar sunrise (Granfors et al., 2013; Sturges et al., 1992). The variability of the two gases was strongly correlated in the summer (r = 0.91 and 0.89 in August 2016 and 2017, p-value < 0.001), indicating a shared source. The correlations were weaker across the whole year (r = 0.74 and 0.59 in 2016 and 2017, p-value < 0.001), possibly due to a combination of the 100 day difference in their atmospheric lifetimes (Table 5.1) and the aforementioned emission of $CHBr_3$ by sea ice microalgae in spring (Granfors et al., 2013; Sturges et al., 1992). The difference in the atmospheric lifetimes of CH_2Br_2 and $CHBr_3$ (Table 5.1) mean it is unlikely that the high collinearity of the two gases in the August dataset was due to a shared atmospheric sink process. Positive fluxes of CH_2Br_2 and $CHBr_3$ have been measured from terrestrial surfaces in the fjord in July but showed much less collinearity (r = 0.54 across the soil transect; Chapter 4) than were seen at Zeppelin in August (r > 0.89, p-value < 0.001). The different relationships suggest soil emissions were unlikely to be driving the trend between CH_2Br_2 and $CHBr_3$ seen at Zeppelin. Further, emission rates from macroalgae were calculated here to be considerably more significant at 475 – 877 nmol $CHBr_3$ m^{-2} d^{-1} and 130 - 1193 nmol CH_2Br_2 m^{-2} d^{-1} (Section 5.3.6), than terrestrial fluxes at 0.3 – 0.7 nmol $CHBr_3$ m^{-2} d^{-1} and 0.2 – 0.8 nmol CH_2Br_2 m^{-2} d^{-1} (Chapter 4). The larger (up to 9 times) area of soil compared to macroalgal bed coverage was not large enough to offset the 2-3 orders of magnitude higher emission rate by the macroalgae (Section 5.3.7). Even if the macroalgal species with known emission rates were present at a 100th of the

estimated biomass, the emission rate would still be 1 order of magnitude higher than measured terrestrially. Therefore, macroalgae were likely a more significant source of CH_2Br_2 and $CHBr_3$ to the atmosphere than the soil in the fjord. At other locations in the Arctic, where there is more ice-free and vegetated land at the coast (e.g. Canadian and Siberian tundra), the terrestrial sources may be more significant.

It is interesting that CH_3I did not correlate with any other halocarbon ($r < 0.4$ for August and whole year analyses of 2016 and 2017), despite it being a predominantly marine origin gas like CH_2Br_2 and $CHBr_3$ (Stemmler et al., 2014; Yokouchi et al., 2008). However, CH_3I can be produced abiotically by photochemical reactions in seawater (Moore and Zafiriou, 1994), perhaps contributing to the less colinear relationship with CH_2Br_2 and $CHBr_3$ which we suggest has a predominantly macroalgal source in August.

The 13-14 % rise in the proportion of upper quartile concentrations of $CHCl_3$ measured at low wind speeds (Figure 5.6) and the consistently elevated emissions at ground level compared to Zeppelin suggest a local source of this gas. Some macroalgae species have been found to emit $CHCl_3$, including *Laminaria digitate* as measured in Scotland (Nightingale et al., 1995). This species was also found in the mid sublittoral zone of the fjord here (Wiencke et al., 2004). However, further studies would be required to determine the significance of macroalgal emission of $CHCl_3$ in the fjord. The relatively weak relationship with CH_2Br_2 and $CHBr_3$ (r = 0.51-0.65, p-value < 0.001) and the elevated concentrations in spot-measurements over land suggests the local source of $CHCl_3$ could be the soil. If $CHCl_3$ emission rates were the same order of magnitude as $CHBr_3$ rates from *Laminaria saccharina*, then $CHCl_3$ would be emitted at a similar rate from macroalgae as from soils in the fjord (73 – 104 nmol m^{-2} d^{-1}; Chapter 4). Therefore, the larger areal coverage of soil compared to macroalgae means that the net source of $CHCl_3$ per day could be similar or higher for the soils.

5.6 Conclusion

This study presents multi-year ambient atmospheric observations for 6 halocarbon species with natural sources and sinks in the High Arctic. We suggest that a terrestrial source of $CHCl_3$ was influencing ambient measurements due to elevated concentrations at ground-level and increased proportions of high concentration measurements made during low wind periods. The ambient observations indicate the influence of a local marine source of $CHBr_3$, CH_2Br_2 and CH_3I, due to their high and variable concentrations in the summer and elevated concentrations measured in air masses from the 'pristine' north. We suggest a macroalgae source of $CHBr_3$ and CH_2Br_2 was responsible for much of their summer variation, but was not responsible for the CH_3I variation due to poor collinearity with the brominated compounds. Future work should focus on the following: constraining the onset of the CH_3Cl and CH_3Br soil sink with the retreat of snow cover in the spring; determining if macroalgae in the fjord release $CHCl_3$ at significant rates; determining if halocarbons are released into the atmosphere at the same rate that they are emitted from the macroalgae into sea water; characterising the proportion that each macroalgae species contributes to biomass in the fjord. This study has suggested that the Zeppelin ambient measurements may be influenced by local fluxes, particularly of the shorter-lived natural halocarbons likely from marine environments.

6 Conclusions

The primary aims of this thesis were to identify trace gas fluxes in sub- and pro- glacial environments and to better understand the interaction between abiotic and biotic processes which involve trace gases in these marginal environments. Chapter 3 focussed on abiotic trace gas production in the subglacial environment and the impact upon *in situ* biotic and abiotic processes. Chapter 4 investigated both biotic and abiotic fluxes of halogenated trace gases from proglacial land surfaces, with a focus on understanding how length of soil exposure may influence trace gas production. Chapter 5 explored whether local halogenated trace gas fluxes influenced ambient atmospheric concentrations. This final chapter summarises the main findings of this thesis and discusses the limitations of this work. These limitations, in combination with the results of this thesis, shape the discussion around future work.

6.1 Summary of main findings

6.1.1 The liberation of trace gases by glacial erosion into the subglacial environment

The aim of Chapter 3 was to determine the potential of glacial erosion to release trace gases from the bedrock and sediment, with a specific focus on gases that could be influential for subglacial microbes and *in situ* chemical weathering. To address this, gas production was measured during a series of laboratory grinding experiments. These experiments used rock samples from a variety of glaciated catchments as an analogue to glacial erosion. Suspended sediment export from glacial catchments was used as a proxy for long-term glacial erosion rates to 'scale-up' the release of gas to the potential production beneath the glacier. The key findings of this chapter were as follows:

- Grinding of all rock samples produced quantifiable hydrogen and methane. Ethane, ethylene and carbon dioxide were detected during grinding of all samples, but not always at quantifiable amounts. Some rock samples produced carbon monoxide, acetylene and propane. Production of hydrocarbons was orders of magnitudes higher from rocks that were sedimentary in origin.

- Scaling up the experimental results to catchment-scaled rates of trace gas generation showed that rates of hydrogen, carbon dioxide and methane production from the mechanical erosion of rocks was significant enough to influence subglacial microbial and weathering processes.

This chapter showed for the first time that mechanical glacial erosion of rocks and minerals releases several trace gases into the subglacial environment, some of which are important for understanding how subglacial microbes can survive in isolation. Importantly, grinding-generated carbon dioxide was shown to have the potential impacts on presumed atmospheric drawdown, thus influencing the interpreted impact of glacial weathering upon the carbon cycle.

6.1.2 Halogenated trace gas fluxes from proglacial land surfaces

Chapter 4 aimed to examine halocarbon trace gas fluxes (CH_3Cl, CH_3Br, CH_3I, $CHCl_3$, $CHBr_3$ and CH_2Br_2) from proglacial land surfaces in the High Arctic. Most terrestrial gas fluxes are thought to be driven by soil bacteria, fungi, plants or reactions with organic matter. Therefore, particular attention was paid to how halocarbon fluxes may be influenced by increasing soil development and colonisation with greater distance from the retreating glacier's terminus. Halocarbon fluxes were measured using flux chambers deployed across the proglacial forefield of a retreating glacier. Flux rates were compared to biological, chemical and physical variations in the soil. The main findings of this chapter were as follows.

- Halocarbon fluxes were smallest where the sediment had been most recently exposed. However, halocarbon fluxes were not always largest at the oldest sites: halocarbon fluxes on younger soils with cyanobacterial mats were similar in rate to fluxes from much older sites with established tundra-type flora.
- Proglacial soils were found to be sinks of CH_3Cl and CH_3Br and sources of $CHCl_3$, $CHBr_3$ and CH_2Br_2. Fluxes of $CHBr_3$ and CH_2Br_2 were small relative to marine fluxes of both compounds. Proglacial soils do not cover large enough areas to constitute globally or regionally important fluxes of these gases at the present day.

The halocarbon fluxes measured across the proglacial land surfaces showed for the first time that terrestrial mat-forming cyanobacteria were as significant at consuming CH_3Cl

and CH_3Br and producing $CHBr_3$, $CHCl_3$ and CH_2Br_2 as tundra-type soils. This was the case even on relatively under-developed and recently exposed soils. This chapter also provided some of the first quantified terrestrial emissions of $CHBr_3$ and CH_2Br_2 in any environment.

6.1.3 The influence of proglacial halocarbon fluxes on atmospheric concentrations

The aim of Chapter 5 was to determine if the proglacial halocarbon fluxes measured in Chapter 4 had an influence on the local ambient atmospheric measurements made at a nearby atmospheric observatory (Zeppelin). To achieve this, a multi-year data set of the halocarbons (CH_3Cl, CH_3Br, CH_3I, $CHCl_3$, $CHBr_3$ and CH_2Br_2) was analysed for annual and seasonal variation. Particular focus was placed upon ambient measurements made during the summer when soil fluxes were presumed to be highest. The primary findings were as follows.

- The proglacial soil sink of CH_3Cl and CH_3Br was not visible in the ambient atmospheric record, primarily because it is indistinguishable from the major atmospheric sink of destruction by OH radicals.
- The proglacial soil source of $CHCl_3$ was possibly influencing the ambient atmospheric records due to the appearance of higher concentrations during low wind periods. A local source of $CHBr_3$ and CH_2Br_2 did appear to influence the ambient atmospheric record. However, a macroalgal source is more likely than a proglacial soil source, due to the orders of magnitude higher emission rates from macroalgae.

This chapter provided the first analysis of multi-year records of CH_2Br_2, $CHBr_3$ and CH_3I in the Arctic showing high variability and high concentrations in the summer. This indicated a local source, which is presumed to be marine due to the lower emission rate from local soils compared to macroalgae. The proglacial soil fluxes were not immediately distinguishable in the Zeppelin record.

6.2 Limitations of this work and future research

The research chapters of this thesis described the specific limitations relevant to them. Here, these limitations are summarised and discussed in the context of future research.

6.2.1 Limitations and future work surrounding trace gas production by glacial erosion

Chapter 3 used rock and sediment samples from five catchments in the Northern hemisphere, with rock types from each of the sedimentary, metamorphic and igneous categories. However, there is a wide variety of other rock types within each category that underlie other glacial catchments and they may release different quantities or species of trace gases. Future work should investigate a wider variety of rock types with samples from Antarctica and the Himalayas in particular. Additionally, conducting grinding-experiments in water, rather than dry as was done here, could give a more realistic indication of conditions beneath the ice.

Microbial activity rates in the subglacial environment (i.e. rates of microbial CH_4 production) were only available at two of the study glaciers. As a result, the significance of grinding-generated gas production to subglacial microbes is only known at two glaciers but could be very different at others. Further, there is little knowledge of the depth of sediment beneath glaciers, making it difficult to determine the overall catchment rate of microbial CH_4 production beneath a glacier. Work to constrain such sediment depths would also help to determine glacial abrasion rates. In this study, suspended sediment fluxes were used as a proxy for subglacial abrasion rates. We assumed that longer-term (i.e. decadal and longer) rates of glacial abrasion would be approximately equal to suspended sediment fluxes. However, several catchments have suspended sediment fluxes published only for a few years, or in some cases, only 1 year, meaning that the sediment flux of the measured year may not be in equilibrium with erosion rates. This would be particularly true in catchments underlain by relatively thick subglacial sediment deposits. Better characterisation of glacial erosion rates from suspended sediment fluxes would aid this study, as well as many other studies which investigate subglacial biogeochemical processes and their wider impacts.

6.2.2 Limitations and future work relating to proglacial trace gas fluxes

The major limitation in Chapter 4 was lack of spatially and temporally variable measurements of halocarbon gas fluxes. Fluxes were measured at one glacier with only 4 sites, which may mean the results are not representative of other glacial forefields or of the forefield as a whole. In particular, the smaller sample size meant comparing flux rates to chemical, physical and biological soil variability was potentially prone to error, with the differences between site location potentially masking the importance of these soil characteristics. Site locations were restricted to areas with relatively soft soil or sediment as the chamber collars were made of Perspex. It would be interesting to establish the magnitude of fluxes from rockier ground that still had cyanobacterial crusts present. Future studies could utilise an aluminium collar or other material that is strong enough to be hammered in to hard or rocky soil to overcome this limitation. One of the most interesting areas for future work would involve determining if terrestrial emission of $CHBr_3$ and CH_2Br_2 occur at greater magnitudes in warmer climates, as both gases have an unbalanced atmospheric budget.

Because all fluxes were measured during the summer, there may be a seasonal variation in these fluxes. The soil processes would presumably be influenced by frozen ground and snow cover, and also potentially by the much wetter ground conditions during the snow melt period. As such, the measurements used in this thesis may be unrepresentative of year-round variation in fluxes. Understanding these processes would help to more accurately determine the magnitude of the annual fluxes from these soils.

Lastly, the higher than expected fluxes measured from cyanobacterial mats could be caused by the cyanobacteria themselves or by other microbes common to both the mats and the sites with tundra-type fauna (e.g. grasses and plants). Laboratory incubation experiments of cultured species, or of whole samples with inhibitors, could identify which groups or species are responsible for the fluxes and give an indication of where else similar fluxes may be found.

6.2.3 Limitations and future work relating to the influence of soil fluxes on ambient records

There were two main limitations involved in determining if local fluxes influenced the ambient record. Both involve the difficulties in distinguishing between marine and terrestrial fluxes which prevents the impact of proglacial soil fluxes on ambient

concentrations from being definitively identified. Firstly, the site's location on a peninsula means that observations made during certain wind directions cannot be attributed solely to a marine or terrestrial origin. Secondly, interpreting the relative contribution from known marine or terrestrial sources is complicated by lack of spatial measurements of both sources. For example, macroalgal biomass studies have been conducted at one site. Similarly, soil flux measurements have not been widely conducted, nor have measurements of the extent of soil surface types, particularly the extent of cyanobacterial mats. Importantly, there have been many measurements of macroalgal halocarbon fluxes from small samples of macroalgal species, but there have been no analyses in the fjord of the actual sea-air flux. This should be determined to understand the magnitude of the macroalgal influence on ambient concentrations.

6.3 Concluding remarks

The biogeochemical impacts of glaciers have been studied more intensely in recent decades, particularly for understanding export of nutrients. However, the importance of trace gases in glaciated environments has been less well studied. This thesis has shown the importance of trace gases to a range of microbial, weathering and atmospheric processes in the rapidly changing glaciated environments. Extreme life in the isolated subglacial environment could be supported by abiogenic trace gases produced by glacial erosion. The same trace gas production can contribute protons to chemical weathering thus influencing how we interpret the drawdown of atmospheric carbon dioxide during glaciations. Soils recently exposed by retreating glaciers contribute sources and sinks of halogenated trace gases, despite the soils' underdevelopment. Local sources of halogenated trace gases appear to influence ambient atmospheric concentrations. Therefore, this thesis has highlighted the importance of trace gas production and consumption to biotic and abiotic processes in the glaciated environment, helping us to understand these dynamic environments as they undergo rapid change in the warming world.

7 Reference List

ACIA (2005). *Arctic climate impacts assessment*. Cambridge, UK: Cambridge University Press.

Albers, C. N., Jacobsen, O. S., Flores, E. M. M., and Johnsen, A. R. (2017). Arctic and subarctic natural soils emit chloroform and brominated analogues by alkaline hydrolysis of trihaloacetyl compounds. *Environ. Sci. Technol.* 51, 6131–6138. doi:10.1021/acs.est.7b00144.

Amachi, S., Kamagata, Y., Kanagawa, T., and Muramatsu, Y. (2001). Bacteria mediate methylation of iodine in marine and terrestrial environments. *Appl. Environ. Microbiol.* 67, 2718–2722. doi:10.1128/AEM.67.6.2718.

Anderson, S. P., Drever, J. I., and Humphrey, N. F. (1997). Chemical weathering in glacial environments. *Geology* 25, 399–402. doi:10.1130/0091-7613(1997)025<0399:CWIGE>2.3.CO.

Atashgahi, S., Häggblom, M. M., and Smidt, H. (2017). Organohalide respiration in pristine environments: implications for the natural halogen cycle. *Environ. Microbiol.* 20, 934–948. doi:10.1111/1462-2920.14016.

Atkinson, H. M., Huang, R. J., Chance, R., Roscoe, H. K., Hughes, C., Davison, B., et al. (2012). Iodine emissions from the sea ice of the Weddell Sea. *Atmos. Chem. Phys.* 12, 11229–11244. doi:10.5194/acp-12-11229-2012.

Atkinson, H. M., Hughes, C., Shaw, M. J., Roscoe, H. K., Carpenter, L. J., and Liss, P. S. (2014). Halocarbons associated with Arctic sea ice. *Deep. Res. Part I* 92, 162–175. doi:10.1016/j.dsr.2014.05.012.

Bakermans, C., and Skidmore, M. (2011). Microbial respiration in ice at subzero temperatures (−4°C to −33°C). *Environ. Microbiol. Rep.* 3, 774–782. doi:10.1111/j.1758-2229.2011.00298.x.

Barrie, L. A., Bottenheim, J. W., Schnell, R. C., Crutzen, P. J., and Rasmussen, R. A. (1988). Ozone destruction and photochemical reactions at polar sunrise in the lower Arctic atmosphere. *Nature* 334, 138–141.

Barrie, L., and Platt, U. (1997). Arctic tropospheric chemistry: An overview. *Tellus, Ser. B Chem. Phys. Meteorol.*, 450–454. doi:10.1034/j.1600-0889.49.issue5.2.x.

Beine, H. J., Argentini, S., Maurizi, A., Mastrantonio, G., and Viola, A. (2001). The local wind field at Ny-Ålesund and the Zeppelin mountain at svalbard. *Meteorol. Atmos. Phys.* 78, 107–113. doi:10.1007/s007030170009.

Beine, H. J., Engardt, M., Jaffe, D. A., Hov, Ø., Holmén, K., and Stordal, F. (1996). Measurements of NOx and aerosol particles at the Ny-Ålesund Zeppelin mountain station on Svalbard: Influence of regional and local pollution sources. *Atmos. Environ.* 30, 1067–1079. doi:10.1016/1352-2310(95)00410-6.

Bekku, Y. S., Nakatsubo, T., Kume, A., Adachi, M., and Koizumi, H. (2003). Effect of warming on the temperature dependence of soil respiration rate in arctic, temperate and tropical soils. *Appl. Soil Ecol.* 22, 205–210. doi:10.1016/S0929-1393(02)00158-0.

Bhatia, M. P., Das, S. B., Longnecker, K., Charette, M. A., and Kujawinski, E. B. (2010). Molecular characterization of dissolved organic matter associated with the Greenland ice sheet. *Geochim. Cosmochim. Acta* 74, 3768–3784. doi:10.1016/j.gca.2010.03.035.

Blunden, J., Arndt, D. S., Hartfield, G., and Eds. (2018). State of the Climate in 2017. *Bull. Am. Meteorol. Soc.* 99, 1–332. doi:doi:10.1175/2018BAMSStateoftheClimate.1.

Bogen, J. (1996). Erosion rates and sediment yields of glaciers. *Ann. Glaciol.* 22, 48–52.

Bone, N. (2014). The Daily Grind: a novel source of hydrogen generated during subglacial bedrock crushing. Msc thesis, University of Bristol, 47 pp.

Boyd, E. S., Hamilton, T. L., Havig, J. R., Skidmore, M. L., and Shock, E. L. (2014). Chemolithotrophic primary production in a subglacial ecosystem. *Appl. Environ. Microbiol.* 80, 6146–6153. doi:10.1128/AEM.01956-14.

Boyd, E. S., Skidmore, M., Mitchell, A. C., Bakermans, C., and Peters, J. W. (2010). Methanogenesis in subglacial sediments. *Environ. Microbiol. Rep.* 2, 685–692.

doi:10.1111/j.1758-2229.2010.00162.x.

Bradley, J. A., Arndt, S., Šabacká, M., Benning, L. G., Barker, G. L., Blacker, J. J., et al. (2016). Microbial dynamics in a High Arctic glacier forefield: A combined field, laboratory, and modelling approach. *Biogeosciences* 13, 5677–5696. doi:10.5194/bg-13-5677-2016.

Bradley, J. A., Singarayer, J. S., and Anesio, A. M. (2014). Microbial community dynamics in the forefield of glaciers. *Proc. R. Soc. B* 281, 1–9. doi:http://dx.doi.org/10.1098/rspb.2014.0882.

Burke, E. A. J. (2001). Raman microspectrometry of fluid inclusions. *Lithos* 55, 139–158. doi:10.1016/S0024-4937(00)00043-8.

Butler, J. H. (2000). Better budgets for methyl halides? *Nature* 403, 260. doi:10.1038/35002232.

Carpenter, L. J., Malin, G., Liss, P. S., and Küpper, F. C. (2000). Novel biogenic iodine-containing trihalomethanes and other short-lived halocarbons in the coastal East Atlantic. *Global Biogeochem. Cycles* 14, 1191–1204. doi:10.1029/2000GB001257.

Carpenter, L. J., Reimann, S., Burkholder, J. B., Clerbaux, C., Hall, B. D., Hossaini, R., et al. (2014). "Ozone-Depleting Substances (ODSs) and Other Gases of Interest to the Montreal Protocol," in *Scientific Assessment of Ozone Depletion: 2014, Global Ozone Research and Monitoring Project-Report No. 55* (Geneva, Switzerland: World Meteorological Organization).

Carpenter, L. J., Wevill, D. J., Palmer, C. J., and Michels, J. (2007). Depth profiles of volatile iodine and bromine-containing halocarbons in coastal Antarctic waters. *Mar. Chem.* 103, 227–236. doi:10.1016/j.marchem.2006.08.003.

Carslaw, D. C., and Ropkins, K. (2012). Openair: an R package for air quality data analysis. *Environ. Model. Softw.* 27–28, 52–61. doi:10.1016/j.envsoft.2011.09.008.

Challinor, A. (1967). The Structure of Broggerhalvoya, Spitsbergen. *Geol. Mag.* 104, 322–336. doi:10.1017/S0016756800048913.

Chandler, D. M., Wadham, J. L., Lis, G. P., Cowton, T., Sole, A., Bartholomew, I., et al.

(2013). Evolution of the subglacial drainage system beneath the Greenland Ice Sheet revealed by tracers. *Nat. Geosci.* 6, 195–198. doi:10.1038/ngeo1737.

Chiri, E., Nauer, P. A., Henneberger, R., Zeyer, J., and Schroth, M. H. (2015). Soil–methane sink increases with soil age in forefields of Alpine glaciers. *Soil Biol. Biochem.* 84, 83–95. doi:https://doi.org/10.1016/j.soilbio.2015.02.003.

Christner, B. C., Montross, G. G., and Priscu, J. C. (2012). Dissolved gases in frozen basal water from the NGRIP borehole: Implications for biogeochemical processes beneath the Greenland Ice Sheet. *Polar Biol.* 35, 1735–1741. doi:10.1007/s00300-012-1198-z.

Christner, B. C., Priscu, J. C., Achberger, A. M., Barbante, C., Carter, S. P., Christianson, K., et al. (2014). A microbial ecosystem beneath the West Antarctic ice sheet. *Nature* 512, 310–313. doi:10.1038/nature13667.

Chuck, A. L., Turner, S. M., and Liss, P. S. (2005). Oceanic distributions and air-sea fluxes of biogenic halocarbons in the open ocean. *J. Geophys. Res. C Ocean.* 110, 1–12. doi:10.1029/2004JC002741.

Conrad, R. (1996). Soil Microorganisms as Controllers of Atmospheric Trace Gases (H_2, CO, CH_4, OCS, N_2O, and NO). *Microbiol. Rev.* 60, 609–640.

Cowton, T., Nienow, P., Bartholomew, I., Sole, A., and Mair, D. (2012). Rapid erosion beneath the Greenland ice sheet. *Geology* 40, 343–346. doi:10.1130/G32687.1.

Deeds, D. A., Kulongoski, J. T., Mühle, J., and Weiss, R. F. (2015). Tectonic activity as a significant source of crustal tetrafluoromethane emissions to the atmosphere: Observations in groundwaters along the San Andreas Fault. *Earth Planet. Sci. Lett.* 412, 163–172. doi:10.1016/j.epsl.2014.12.016.

Derendorp, L., Wishkerman, A., Keppler, F., McRoberts, C., Holzinger, R., and Röckmann, T. (2012). Methyl chloride emissions from halophyte leaf litter: Dependence on temperature and chloride content. *Chemosphere* 87, 483–489. doi:10.1016/j.chemosphere.2011.12.035.

Diamond, L. W. (2001). Review of the systematics of CO_2-H_2O fluid inclusions. *Lithos*

55, 69–99. doi:10.1016/S0024-4937(00)00039-6.

Dieser, M., Broemsen, E. L. J. E., Cameron, K. A., King, G. M., Achberger, A., Choquette, K., et al. (2014). Molecular and biogeochemical evidence for methane cycling beneath the western margin of the Greenland Ice Sheet. *ISME J.* 8, 2305–2316. doi:10.1038/ismej.2014.59.

Dimmer, C. H., Simmonds, P. G., Nickless, G., and Bassford, M. R. (2001). Biogenic fluxes of halomethanes from Irish peatland ecosystems. *Atmos. Environ.* 35, 321–330. doi:10.1016/S1352-2310(00)00151-5.

Doronina, N. V, Sokolov, A. P., and Trotsenko, Y. A. (1996). Isolation and initial characterization of aerobic chloromethane-utilizing bacteria. *FEMS Microbiol. Lett.* 142, 179–183. doi:10.1016/0378-1097(96)00262-5.

Dow, C. F., Hubbard, A., Booth, A. D., Doyle, S. H., Gusmeroli, A., and Kulessa, B. (2013). Seismic evidence of mechanically weak sediments underlying Russell Glacier, West Greenland. *Ann. Glaciol.* 54, 135–141. doi:10.3189/2013AoG64A032.

Doxsey-Whitfield (2012). Magnitude and controls of microbial nitrate production in the streams and till of a glaciated alpine catchment, Canadian Rocky Mountains, Alberta. MSc thesis, Queen's University, 191 pp.

Edwards, P., Evans, M. J., Commane, R., Ingham, T., Stone, D., Mahajan, A. S., et al. (2011). Hydrogen oxide photochemistry in the northern Canadian spring time boundary layer. *J. Geophys. Res. Atmos.* 116. doi:10.1029/2011JD016390.

Ekström, G., Nettles, M., and Abers, G. A. (2003). Glacial Earthquakes. *Science (80-.).* 302, 622–624. doi:10.1126/science.1088057.

Engelhardt, M., Schuler, T. V., and Andreassen, L. M. (2015). Sensitivities of glacier mass balance and runoff to climate perturbations in Norway. *Ann. Glaciol.* 56, 79–88. doi:10.3189/2015AoG70A004.

Fahey, D. W., and Hegglin, M. I. (2011). “Twenty Questions and Answers About the Ozone Layer: 2010 Update,” in *Scientific Assessment of Ozone Depletion: 2010,*

Global Ozone Research and Monitoring Project— Report No. 52, 516 pp. (Geneva, Switzerland), 72.

Farhan Ul Haque, M., Besaury, L., Nadalig, T., Bringel, F., Mutterer, J., Schaller, H., et al. (2017). Correlated production and consumption of chloromethane in the *Arabidopsis thaliana* phyllosphere. *Sci. Rep.* 7, 17589. doi:10.1038/s41598-017-17421-y.

Forczek, S. T., Laturnus, F., Doležalová, J., Holík, J., and Wimmer, Z. (2015). Emission of climate relevant volatile organochlorines by plants occurring in temperate forests. *Plant, Soil Environ.* 61, 103–108. doi:10.17221/900/2014-PSE.

Fujimori, T., Yoneyama, Y., Taniai, G., Kurihara, M., Tamegai, H., and Hashimoto, S. (2012). Methyl halide production by cultures of marine proteobacteria erythrobacter and pseudomonas and isolated bacteria from brackish water. *Limnol. Oceanogr.* 57, 154–162. doi:10.4319/lo.2012.57.1.0154.

Gautrois, M., Brauers, T., Koppmann, R., Rohrer, F., Stein, O., and Rudolph, J. (2003). Seasonal variability and trends of volatile organic compounds in the lower polar troposphere. *J. Geophys. Res. Atmos.* 108. doi:10.1029/2002JD002765.

Gjelten, H. M. (2018). Duration of snow cover on land; MOSJ - environmental monitoring of Svalbard and Jan Mayen. *Nor. Meteorol. Inst.* Available at: http://www.mosj.no/en/climate/land/duration-snow-cover.html [Accessed June 20, 2018].

Granfors, A., Andersson, M., Chierici, M., Fransson, A., Gårdfeldt, K., Torstensson, A., et al. (2013). Biogenic halocarbons in young Arctic sea ice and frost flowers. *Mar. Chem.* 155, 124–134. doi:10.1016/j.marchem.2013.06.002.

Graversen, R. G., Mauritsen, T., Tjernström, M., Källén, E., and Svensson, G. (2008). Vertical structure of recent Arctic warming. *Nature* 451, 53. doi:10.1038/ Nature06502.

Gray, N. D., McCann, C. M., Christgen, B., Ahammad, S. Z., Roberts, J. A., and Graham, D. W. (2014). Soil geochemistry confines microbial abundances across an arctic landscape; implications for net carbon exchange with the atmosphere.

Biogeochemistry 120, 307–317. doi:10.1007/s10533-014-9997-7.

Hallet, B., Hunter, L., and Bogen, J. (1996). Sediment evacuation and glacial erosion rates at a small alpine glacier. *Glob. Planet. Change* 12, 213–235. doi:10.1016/0921-8181(95)00021-6.

Harnisch, J., and Eisenhauer, A. (1998). Natural CF_4 and SF_6 on Earth. *Geophys. Res. Lett.* 25, 2401–2404. doi:10.1029/98GL01779.

Harper, J. T., Humphrey, N. F., Meierbachtol, T. W., Graly, J. A., and Fischer, U. H. (2017). Borehole measurements indicate hard bed conditions, Kangerlussuaq sector, western Greenland Ice Sheet. *J. Geophys. Res. Earth Surf.* 122, 1605–1618. doi:10.1002/2017JF004201.

Hasholt, B., and Mernild, S. H. (2006). Glacial erosion and sediment transport in the Mittivakkat Glacier catchment, Ammassalik Island, southeast Greenland, 2005. *Sediment Dyn. hydromorphology Fluv. Syst. (Proceedings a Symp. held Dundee, UK, July 2006).* 306, 45–55.

Hawkings, J. R., Wadham, J. L., Benning, L. G., Hendry, K. R., Tranter, M., Tedstone, A., et al. (2017). Ice sheets as a missing source of silica to the polar oceans. *Nat. Commun.* 8, 14198. doi:10.1038/ncomms14198.

Hawkings, J. R., Wadham, J. L., Tranter, M., Lawson, E., Sole, A., Cowton, T., et al. (2015). The effect of warming climate on nutrient and solute export from the Greenland Ice Sheet. *Geochemical Perspect. Lett.* 1, 94–104. doi:10.7185/geochemlet.1510.

Hawkings, J., Wadham, J., Tranter, M., Telling, J., Bagshaw, E., Beaton, A., et al. (2016). The Greenland Ice Sheet as a hot spot of phosphorus weathering and export in the Arctic. *Global Biogeochem. Cycles* 30, 191–210. doi:10.1002/2015GB005237.

Hirose, T., Kawagucci, S., and Suzuki, K. (2011). Mechanoradical H_2 generation during simulated faulting: Implications for an earthquake-driven subsurface biosphere. *Geophys. Res. Lett.* 38, 1–5. doi:10.1029/2011GL048850.

Hodkinson, I. D., Coulson, S. J., and Webb, N. R. (2003). Community assembly along

proglacial chronosequences in the high Arctic: Vegetation and soil development in north-west Svalbard. *J. Ecol.* 91, 651–663. doi:10.1046/j.1365-2745.2003.00786.x.

Hodson, A., Gurnell, A., Tranter, M., Bogen, J., Hagen, J. O., and Clark, M. (1998). Suspended sediment yield and transfer processes in a small High-Arctic glacier basin, Svalbard. *Hydrol. Process.* 12, 73–86. doi:10.1002/(SICI)1099-1085(199801)12:1<73::AID-HYP564>3.3.CO;2-J.

Hodson, A. J., Mumford, P. N., Kohler, J., and Wynn, P. M. (2005). The High Arctic glacial ecosystem: New insights from nutrient budgets. *Biogeochemistry* 72, 233–256. doi:10.1007/s10533-004-0362-0.

Hodson, A., Mumford, P., and Lister, D. (2004). Suspended sediment and phosphorous in proglacial rivers: Bioavailability and potential impacts upon the P status of ice-marginal receiving waters. *Hydrol. Process.* 18, 2409–2422. doi:10.1002/hyp.1471.

Hodson, A., Tranter, M., and Vatne, G. (2000). Contemporary rates of chemical denudation and atmospheric CO_2 sequestration in glacier basins: An arctic perspective. *Earth Surf. Process. Landforms* 25, 1447–1471. doi:10.1002/1096-9837(200012)25:13<1447::AID-ESP156>3.0.CO;2-9.

Hossaini, R., Mantle, H., Chipperfield, M. P., Montzka, S. A., Hamer, P., Ziska, F., et al. (2013). Evaluating global emission inventories of biogenic bromocarbons. *Atmos. Chem. Phys.* 13, 11819–11838. doi:10.5194/acp-13-11819-2013.

Hu, L., Yvon-Lewis, S. A., Butler, J. H., Lobert, J. M., and King, D. B. (2013). An improved oceanic budget for methyl chloride. *J. Geophys. Res. Ocean.* 118, 715–725. doi:10.1029/2012JC008196.

Hu, L., Yvon-Lewis, S., Liu, Y., and Bianchi, T. S. (2012). The ocean in near equilibrium with atmospheric methyl bromide. *Global Biogeochem. Cycles* 26. doi:10.1029/2011GB004272.

Huber, S. G., Kotte, K., Scholer, H. F., and Williams, J. (2009). Natural abiotic formation of trihalomethanes in soil: results from laboratory studies and field samples. *Environ. Sci. Technol.* 43, 4934–4939. doi:10.1021/Es8032605.

Ichikawa, K., Kurihara, M., Tamegai, H., and Hashimoto, S. (2015). Decomposition of brominated organic halogens by cultures of marine proteobacteria: Phaeobacter, Roseobacter, and Rhodobacter. *Mar. Chem.* 176, 133–141. doi:10.1016/j.marchem.2015.09.003.

Irvine-Fynn, T. D. L., and Hodson, A. J. (2010). Biogeochemistry and dissolved oxygen dynamics at a subglacial upwelling, Midtre Lovenbreen, Svalbard. 51, 41–46. doi:10.3189/172756411795931903.

Ito, T., Nagamine, K., Yamamoto, K., and Adachi, M. (1999). Preseismic hydrogen gas anomalies caused by stress-corrosion process preceding earthquakes. *Geophys. Res. Lett.* 26, 2009–2012.

Jaeger, N., Besaury, L., Röhling, A. N., Koch, F., Delort, A.-M., Gasc, C., et al. (2018). Chloromethane formation and degradation in the fern phyllosphere. *Sci. Total Environ.* 634, 1278–1287. doi:https://doi.org/10.1016/j.scitotenv.2018.03.316.

Johnson, T. L., Palenik, B., and Brahamsha, B. (2011). Characterization of a functional vanadium-dependent bromoperoxidase in the marine cyanobacterium synechococcus SP. CC9311. *J. Phycol.* 47, 792–801. doi:10.1111/j.1529-8817.2011.01007.x.

Jones, C. E., and Carpenter, L. J. (2005). Solar Photolysis of CH_2I_2, CH_2ICl, and CH_2IBr in Water, Saltwater, and Seawater. *Environ. Sci. Technol.* 39, 6130–6137. doi:10.1021/es050563g.

Kameda, J., Saruwatari, K., and Tanaka, H. (2003). H2 generation in wet grinding of granite and single-crystal powders and implications for H_2 concentration on active faults. *Geophys. Res. Lett.* 30, 3–7. doi:Artn 2063\rDoi 10.1029/2003gl018252.

Kameda, J., Saruwatari, K., Tanaka, H., and Tsunomori, F. (2004). Mechanisms of hydrogen generation during the mechanochemical treatment of biotite within D_2O media. *Earth, Planets Sp.* 56, 1241–1245. doi:10.1186/BF03353346.

Karl, D. M., Bird, D. F., Björkman, K., Houlihan, T., Shackelford, R., and Tupas, L. (1999). Microorganisms in the Accreted Ice of Lake Vostok, Antarctica. *Science (80-.).* 286, 2144 LP – 2147. doi:10.1126/science.286.5447.2144.

Karlsson, A., Auer, N., Schulz-Bull, D., and Abrahamsson, K. (2008). Cyanobacterial blooms in the Baltic - A source of halocarbons. *Mar. Chem.* 110, 129–139. doi:10.1016/j.marchem.2008.04.010.

Kastovská, K., Elster, J., Stibal, M., and Santrůcková, H. (2005). Microbial assemblages in soil microbial succession after glacial retreat in Svalbard (high arctic). *Microb. Ecol.* 50, 396–407. doi:10.1007/s00248-005-0246-4.

Kateřina, J., Klára, Ř., Jiří, D., Miloslav, Š., Zuzana, C., Miroslav, D., et al. (2013). Community structure of soil phototrophs along environmental gradients in arid Himalaya. *Environ. Microbiol.* 15, 2505–2516. doi:10.1111/1462-2920.12132.

Keng, F. S. L., Phang, S. M., Rahman, N. A., Leedham, E. C., Hughes, C., Robinson, A. D., et al. (2013). Volatile halocarbon emissions by three tropical brown seaweeds under different irradiances. *J. Appl. Phycol.* 25, 1377–1386. doi:10.1007/s10811-013-9990-x.

Keppler, F., Eiden, R., Niedan, V., Pracht, J., and Scholer, H. F. (2000). Halocarbons produced by natural oxidation processes during degradation of organic matter. *Nature* 403, 298–301.

Khan, M. A. H., Whelan, M. E., and Rhew, R. C. (2012). Effects of temperature and soil moisture on methyl halide and chloroform fluxes from drained peatland pasture soils. *J. Environ. Monit.* 14, 241–249. doi:10.1039/C1EM10639B.

Khomenko, V. M., and Langer, K. (1999). Aliphatic hydrocarbons in structural channels of cordierite: A first evidence from polarized single-crystal IR-absorption spectroscopy. *Am. Mineral.* 84, 1181–1185.

Kohler, J., James, T. D., Murray, T., Nuth, C., Brandt, O., Barrand, N. E., et al. (2007). Acceleration in thinning rate on western Svalbard glaciers. *Geophys. Res. Lett.* 34, 1–5. doi:10.1029/2007GL030681.

Kolusu, S. R., Schlünzen, K. H., Grawe, D., and Seifert, R. (2018). Determination of chloromethane and dichloromethane in a tropical terrestrial mangrove forest in Brazil by measurements and modelling. *Atmos. Environ.* 173, 185–197. doi:https://doi.org/10.1016/j.atmosenv.2017.10.057.

Konnerup-Madsen, J. (2001). A review of the composition and evolution of hydrocarbon gases during solidification of the Ilímaussaq alkaline complex, South Greenland. *Geol. Greenl. Surv. Bull.* 190, 159–166.

Konnerup-Madsen, J., and Rose-Hansen, J. (1982). Volatiles associated with alkaline igneous rift activity: Fluid inclusions in the Ilimaussaq intrusion and the Gardar granitic complexes (south Greenland). *Chem. Geol.* 37, 79–93. doi:10.1016/0009-2541(82)90068-7.

Kristof, V. A., Juhasz, A., and Vassanyi, I. (1993). The effect of mechanical treatment on the crystal structure and thermal behavior of kaolinite. *Clays Clay Miner.* 41, 608–612. doi:10.1346/CCMN.1993.0410511.

Kulessa, B., Hubbard, A. L., Booth, A. D., Bougamont, M., Dow, C. F., Doyle, S. H., et al. (2017). Seismic evidence for complex sedimentary control of Greenland Ice Sheet flow. *Sci. Adv.* 3. doi:10.1126/sciadv.1603071.

Lamarche-Gagnon, G., Wadham, J., Sherwood Lollar, B., Arndt, S., Fietzek, P., Beaton, A., et al. (2019). Greenland melt drives continuous export of methane from the ice-sheet bed. *Nature* 565, 73–77. doi:10.1038/s41586-018-0800-0.

Laturnus, F. (1996). Volatile halocarbons released from Arctic macroalgae. *Mar. Chem.* 55, 359–366. doi:10.1016/S0304-4203(97)89401-7.

Laturnus, F. (2001). Marine macroalgae in polar regions as natural sources for volatile organohalogens. *Environ. Sci. Pollut. Res.* 8, 103–108. doi:10.1007/BF02987302.

Laturnus, F., Adams, F. C., and Wiencke, C. (1998). Methyl halides from Antarctic macroalgae. *Geophys. Res. Lett.* 25, 773–776. doi:10.1029/98GL00490.

Law, K., Sturges, W. T., Blake, D. R., Bake, N. J., Burkholder, J. B., Butler, J. H., et al. (2006). "Halogenated Very Short-Lived Substances," in *Scientific Assessment of Ozone Depletion: 2006, Global Ozone Research and Monitoring Project-Report No. 50* (Geneva, Switzerland: World Meteorological Organization), 57.

Lawson, E. C., Wadham, J. L., Tranter, M., Stibal, M., Lis, G. P., Butler, C. E. H., et al. (2014). Greenland ice sheet exports labile organic carbon to the arctic oceans.

Biogeosciences 11, 4015–4028. doi:10.5194/bg-11-4015-2014.

Lee-Taylor, J., and Redeker, K. R. (2005). Reevaluation of global emissions from rice paddies of methyl iodide and other species. *Geophys. Res. Lett.* 32, 5–9. doi:10.1029/2005GL022918.

Lee, A. G. G., and Rutter, E. H. (2004). Experimental rock-on-rock frictional wear: Application to subglacial abrasion. *J. Geophys. Res. B Solid Earth* 109, 1–11. doi:10.1029/2004JB003059.

Leedham, E. C., Hughes, C., Keng, F. S. L., Phang, S. M., Malin, G., and Sturges, W. T. (2013). Emission of atmospherically significant halocarbons by naturally occurring and farmed tropical macroalgae. *Biogeosciences* 10, 3615–3633. doi:10.5194/bg-10-3615-2013.

Lelieveld, J., Gromov, S., Pozzer, A., and Taraborrelli, D. (2016). Global tropospheric hydroxyl distribution, budget and reactivity. *Atmos. Chem. Phys.* 16, 12477–12493. doi:10.5194/acp-16-12477-2016.

Lin, L. H., Hall, J., Lippmann-Pipke, J., Ward, J. A., Lollar, B. S., DeFlaun, M., et al. (2005). Radiolytic H_2 in continental crust: Nuclear power for deep subsurface microbial communities. *Geochemistry, Geophys. Geosystems* 6, 1–13. doi:10.1029/2004GC000907.

Lovley, D. R., and Goodwin, S. (1990). Hydrogen concentrations as an indicator of the predominant terminal electron accepting reaction sin aquatic sediments. *Geochim. Cosmochim. Acta* 52, 2993–3003.

Manley, S. L. (2002). Phytogenesis of halomethanes: A product of selection or a metabolic accident? *Biogeochemistry* 60, 163–180. doi:10.1023/A:1019859922489.

Manley, S. L., and Barbero, P. E. (2001). Physiological constraints on bromoform ($CHBr_3$) production by Ulva lactuca (Chlorophyta). *Limnol. Oceanogr.* 46, 1392–1399. doi:10.4319/lo.2001.46.6.1392.

Manley, S. L., Wang, N.-Y., Walser, M. L., and Cicerone, R. J. (2007). Methyl halide emissions from greenhouse-grown mangroves. *Geophys. Res. Lett.* 34.

doi:10.1029/2006GL027777.

Martinelli, G., and Plescia, P. (2005). Carbon dioxide and methane emissions from calcareous-marly rock under stress: experimental tests results. *Ann. Geophys.* 48, 167–173. doi:10.4401/ag-3191.

Matthews, E. (1983). Global Vegetation and Land Use: New High-Resolution Data Bases for Climate Studies. *J. Clim. Appl. Meteorol.* 22, 474–487. doi:10.1175/1520-0450(1983)022<0474:GVALUN>2.0.CO;2.

McCann, C. M., Wade, M. J., Gray, N. D., Roberts, J. A., Hubert, C. R. J., and Graham, D. W. (2016). Microbial communities in a high arctic polar desert landscape. *Front. Microbiol.* 7, 1–10. doi:10.3389/fmicb.2016.00419.

McDonald, I. R., Warner, K. L., McAnulla, C., Woodall, C. A., Oremland, R. S., and Murrell, J. C. (2002). A review of bacterial methyl halide degradation: biochemistry, genetics and molecular ecology. *Environ. Microbiol.* 4, 193–203. doi:10.1046/j.1462-2920.2002.00290.x.

Mellouki, A., Talukdar, R. K., Schmoltner, Anne-Marie, M., Gierczak, T., Mills, M. J., Solomon, S., et al. (1992). Atmospheric lifetimes and ozone depletion potentials of methyl bromide (CH_3Br) and dibromomethane (CH_2Br_2). *Geophys. Res. Lett.* 19, 2059–2062. doi:10.1029/92GL01612.

Méndez-Díaz, J. D., Shimabuku, K. K., Ma, J., Enumah, Z. O., Pignatello, J. J., Mitch, W. A., et al. (2014). Sunlight-driven photochemical halogenation of dissolved organic matter in seawater: a natural abiotic source of organobromine and organoiodine. *Environ. Sci. Technol.* 48, 7418–7427. doi:10.1021/es5016668.

Michaud, A. B., Dore, J. E., Achberger, A. M., Christner, B. C., Mitchell, A. C., Skidmore, M. L., et al. (2017). Microbial oxidation as a methane sink beneath the West Antarctic Ice Sheet. *Nat. Geosci.* 10, 582–586. doi:10.1038/NGEO2992.

Miller, B. R., Weiss, R. F., Salameh, P. K., Tanhua, T., Greally, B. R., Mühle, J., et al. (2008). Medusa: A sample preconcentration and GC/MS detector system for in situ measurements of atmospheric trace halocarbons, hydrocarbons, and sulfur compounds. *Anal. Chem.* 80, 1536–1545. doi:10.1021/ac702084k.

Mitchell, A. C., Lafrenière, M. J., Skidmore, M. L., and Boyd, E. S. (2013). Influence of bedrock mineral composition on microbial diversity in a subglacial environment. *Geology* 41, 855–858. doi:10.1130/G34194.1.

Mithoo-Singh, P. K., Keng, F. S.-L., Phang, S.-M., Leedham Elvidge, E. C., Sturges, W. T., Malin, G., et al. (2017). Halocarbon emissions by selected tropical seaweeds: species-specific and compound-specific responses under changing pH. *PeerJ* 5, e2918. doi:10.7717/peerj.2918.

Montross, S. N., Skidmore, M., Tranter, M., Kivimäki, A. L., and Parkes, R. J. (2013). A microbial driver of chemical weathering in glaciated systems. *Geology* 41, 215–218. doi:10.1130/G33572.1.

Montzka, S. a., Reimann, S., Engel, A., Kruger, K., O'Doherty, S., Sturges, W., et al. (2011). "Ozone depleting substances (ODSs) and related chemicals," in *Scientific Assessment of Ozone Depletion: 2010, Global Ozone Research and Monitoring Project-Report No. 52* (Geneva, Switzerland: World Meteorological Association), 516.

Moore, R. M., and Zafiriou, O. C. (1994). Photochemical production of methyl iodide in seawater. *J. Geophys. Res.* 99, 16415–16420. doi:10.1029/94JD00786.

Moreau, M., Mercier, D., Laffly, D., and Roussel, E. (2008). Impacts of recent paraglacial dynamics on plant colonization: A case study on Midtre Lovénbreen foreland, Spitsbergen (79°N). *Geomorphology* 95, 48–60. doi:10.1016/j.geomorph.2006.07.031.

Muraoka, H., Noda, H., Uchida, M., Ohtsuka, T., Koizumi, H., and Nakatsubo, T. (2008). Photosynthetic characteristics and biomass distribution of the dominant vascular plant species in a high Arctic tundra ecosystem, Ny-Ålesund, Svalbard: implications for their role in ecosystem carbon gain. *J. Plant Res.* 121, 137. doi:10.1007/s10265-007-0134-8.

Nadalig, T., Greule, M., Bringel, F., Keppler, F., and Vuilleumier, S. (2014). Probing the diversity of chloromethane-degrading bacteria by comparative genomics and isotopic fractionation. *Front. Microbiol.* 5, 1–11. doi:10.3389/fmicb.2014.00523.

Nandi, R., and Sengupta, S. (1998). Microbial Production of Hydrogen: An Overview. *Crit. Rev. Microbiol.* 24, 61–84. doi:10.1080/10408419891294181.

Ni, X., and Hager, L. P. (1999). Expression of Batis maritima methyl chloride transferase in Escherichia coli. *Proc. Natl. Acad. Sci.* 96, 3611–3615. doi:10.1073/pnas.96.7.3611.

Nightingale, P. D., Malin, G., and Liss, P. S. (1995). Production of chloroform and other low molecular-weight halocarbons by some species of macroalgae. *Limnol. Oceanogr.* 40, 680–689. doi:10.4319/lo.1995.40.4.0680.

NIST (2014). NIST Chemistry WebBook, SRD 69. *Natl. Inst. Stand. Technol. U.S. Dep. Commer.* Available at: https://webbook.nist.gov/chemistry/form-ser/ [Accessed December 1, 2014].

Norway MET (2017). Weather and climate data. *eKlima; Nor. Meteorol. Inst.* Available at: http://eklima.met.no [Accessed April 19, 2018].

Norwegian Polar Institute, N. (2014). Kartdata Svalbard 1:100 000 (S100 Kardata)/ Map data. *Nor. Polar Inst.* Available at: https://doi.org/10.21334/npolar.2014.645336c7 [Accessed February 8, 2017].

O'Doherty, S., Miller, B. R., Miihle, J., McCulloch, A., Simmonds, R. G., Manning, A. J., et al. (2009). Global and regional emissions of HFC-125 (CHF_2CF_3) from in situ and air archive atmospheric observations at AGAGE and SOGE observatories. *J. Geophys. Res. Atmos.* 114. doi:10.1029/2009JD012184.

O'Doherty, S., Simmonds, P. G., Cunnold, D. M., Wang, H. J., Sturrock, G. A., Fraser, P. J., et al. (2001). In situ chloroform measurements at Advanced Global Atmospheric Gases Experiment atmospheric research stations from 1994 to 1998. *J. Geophys. Res. Atmos.* 106, 20429–20444. doi:10.1029/2000JD900792.

Oelgeschläger, E., and Rother, M. (2008). Carbon monoxide-dependent energy metabolism in anaerobic bacteria and archaea. *Arch. Microbiol.* 190, 257–269. doi:10.1007/s00203-008-0382-6.

Osborn, S. G., and McIntosh, J. C. (2010). Chemical and isotopic tracers of the

contribution of microbial gas in Devonian organic-rich shales and reservoir sandstones, northern Appalachian Basin. *Appl. Geochemistry* 25, 456–471. doi:10.1016/j.apgeochem.2010.01.001.

Paul, C., and Pohnert, G. (2011). Production and role of volatile halogenated compounds from marine algae. *Nat. Prod. Rep.* 28, 186–195. doi:10.1039/C0NP00043D.

Peretti, A., Dubessy, J., Mullis, J., Frost, B. R., and Trommsdorff, V. (1992). Highly reducing conditions during Alpine metamorphism of the Malenco peridotite (Sondrio, northern Italy) indicated by mineral paragenesis and H_2 in fluid inclusions. *Contrib. to Mineral. Petrol.* 112, 329–340. doi:10.1007/BF00310464.

Potter, J., and Konnerup-Madsen, J. (2003). A review of the occurrence and origin of abiogenic hydrocarbons in igneous rocks. *Geol. Soc. London, Spec. Publ.* 214, 151–173. doi:10.1144/GSL.SP.2003.214.01.10.

Prinn, R. G., Weiss, R. F., Arduini, J., Arnold, T., Langley Dewitt, H., Fraser, P. J., et al. (2018). History of chemically and radiatively important atmospheric gases from the Advanced Global Atmospheric Gases Experiment (AGAGE). *Earth Syst. Sci. Data* 10, 985–1018. doi:10.5194/essd-10-985-2018.

Priscu, J. C., Christner, B. C., Foreman, C. M., and Royston-Bishop, G. (2007). Biological material in ice cores. *Encycl. Quat. Sci.*, 1156–1166.

R Development Core Team (2018). R: A language and environment for statistical computing. Available at: http://www.r-project.org.

Rasche, M. E., Hyman, M. R., and Arp, D. J. (1990). Biodegradation of Halogenated Hydrocarbon Fumigants by Nitrifying Bacteria. *Appl. Environ. Microbiol.* 56, 2568–2571.

Raymo, M. E., and Ruddiman, W. F. (1992). Tectonic forcing of late Cenozoic climate. *Nature* 359, 117. doi:10.0.4.14/359117a0.

Redeker, K. R., Chong, J. P. J., Aguion, A., Hodson, A., and Pearce, D. A. (2017). Microbial metabolism directly affects trace gases in (sub) polar snowpacks. *J. R. Soc. Interface* 14, 20170729. doi:10.1098/rsif.2017.0729.

Redeker, K. R., and Cicerone, R. J. (2004). Environmental controls over methyl halide emissions from rice paddies. *Global Biogeochem. Cycles* 18. doi:10.1029/2003GB002042.

Redeker, K. R., and Kalin, R. M. (2012). Methyl chloride isotopic signatures from Irish forest soils and a comparison between abiotic and biogenic methyl halide soil fluxes. *Glob. Chang. Biol.* 18, 1453–1467. doi:10.1111/j.1365-2486.2011.02600.x.

Redeker, K. R., Meinardi, S., Blake, D., and Sass, R. (2003). Gaseous emissions from flooded rice paddy agriculture. *J. Geophys. Res.* 108, 4386. doi:10.1029/2002JD002814.

Redeker, K. R., Treseder, K. K., and Allen, M. F. (2004). Ectomycorrhizal fungi: A new source of atmospheric methyl halides? *Glob. Chang. Biol.* 10, 1009–1016. doi:10.1111/j.1529-8817.2003.00782.x.

Rhew, R. C., Chen, C., Teh, Y. A., and Baldocchi, D. (2010). Gross fluxes of methyl chloride and methyl bromide in a California oak-savanna woodland. *Atmos. Environ.* 44, 2054–2061. doi:10.1016/j.atmosenv.2009.12.014.

Rhew, R. C., Miller, B. R., Vollmer, M. K., and Weiss, R. F. (2001). Shrubland fluxes of methyl bromide and methyl chloride. *J. Geophys. Res. Atmos.* 106, 20875–20882. doi:10.1029/2001JD000413.

Rhew, R. C., Miller, B. R., and Weiss, R. F. (2008a). Chloroform, carbon tetrachloride and methyl chloroform fluxes in southern California ecosystems. *Atmos. Environ.* 42, 7135–7140. doi:10.1016/j.atmosenv.2008.05.038.

Rhew, R. C., Teh, Y. A., and Abel, T. (2007). Methyl halide and methane fluxes in the northern Alaskan coastal tundra. *J. Geophys. Res. Biogeosciences* 112, 1–11. doi:10.1029/2006JG000314.

Rhew, R. C., Teh, Y. A., Abel, T., Atwood, A., and Mazéas, O. (2008b). Chloroform emissions from the Alaskan Arctic tundra. *Geophys. Res. Lett.* 35. doi:10.1029/2008GL035762.

Rhew, R. C., Whelan, M. E., and Min, D. H. (2014). Large methyl halide emissions from

south Texas salt marshes. *Biogeosciences* 11, 6427–6434. doi:10.5194/bg-11-6427-2014.

Roedder, E. (1990). Fluid inclusion analysis-Prologue and epilogue. *Geochim. Cosmochim. Acta* 54, 495–507. doi:10.1016/0016-7037(90)90347-N.

Roy, R., Pratihary, A., Narvenkar, G., Mochemadkar, S., Gauns, M., and Naqvi, S. W. A. (2011). The relationship between volatile halocarbons and phytoplankton pigments during a Trichodesmium bloom in the coastal eastern Arabian Sea. *Estuar. Coast. Shelf Sci.* 95, 110–118. doi:10.1016/j.ecss.2011.08.025.

Saalmann, K., and Thiedig, F. (2002). Thrust tectonics on Brøggerhalvøya and their relationship to the Tertiary West Spitsbergen fold-and-thrust belt. *Geol. Mag.* 139, 47–72. doi:10.1017/S0016756801006069.

Scanlon, R. (2017). Modeling mass balance at Robertson Glacier, Alberta, Canada 1912-2012. MSc thesis, Montana State University, 108 pp.

Scarratt, M. G., and Moore, R. M. (1996). Production of methyl chloride and methyl bromide in laboratory cultures of marine phytoplankton. *Mar. Chem.* 54, 263–272. doi:10.1016/0304-4203(96)00036-9.

Scarratt, M. G., and Moore, R. M. (1999). Production of chlorinated hydrocarbons and methyl iodide by the red microalga Porphyridium purpureum. *Limnol. Oceanogr.* 44, 703–707. doi:10.4319/lo.1999.44.3.0703.

Schall, C., Laturnus, F., and Heumann, K. G. (1994). Biogenic volatile organoiodine and oragnobromine compounds released from polar macroalgae. *Chemosphere* 28, 1315–1324.

Sharp, M., Parkes, J., Fairchild, I. J., Lamb, H., and Tranter, M. (1999). Widespread bacterial populations at glaciers beds and their relationship to rock weathering and carbon cycling. *Geology* 27, 107–110. doi:10.1130/0091-7613(1999)027<0107:WBPAGB>2.3.CO.

Shorter, J. H., Kolb, C. E., Crill, P. M., Kerwin, R. A., Talbot, R. W., Hines, M. E., et al. (1995). Rapid degradation of atmospheric methyl bromide in soils. *Nature* 377, 717.

doi:10.0.4.14/377717a0.

Simmonds, P. G., Derwent, R. G., Manning, A. J., Fraser, P. J., Krummel, P. B., O'Doherty, S., et al. (2004). AGAGE observations of methyl bromide and methyl chloride at Mace Head, Ireland, and Cape Grim, Tasmania, 1998-2001. *J. Atmos. Chem.* 47, 243–269. doi:10.1023/B:JOCH.0000021136.52340.9c.

Simmonds, P. G., Derwent, R. G., Manning, A. J., O'Doherty, S., and Spain, G. (2010). Natural chloroform emissions from the blanket peat bogs in the vicinity of Mace Head, Ireland over a 14-year period. *Atmos. Environ.* 44, 1284–1291. doi:10.1016/j.atmosenv.2009.12.027.

Simmonds, P. G., O'Doherty, S., Nickless, G., Sturrock, G. A., Swaby, R., Knight, P., et al. (1995). Automated Gas Chromatograph/Mass Spectrometer for Routine Atmospheric Field Measurements of the CFC Replacement Compounds, the Hydrofluorocarbons and Hydrochlorofluorocarbons. *Anal. Chem.* 67, 717–723. doi:10.1021/ac00100a005.

Skidmore, M. (2011). "Microbial communities in Antarctic subglacial aquatic environments," in *Antarctic Subglacial Aquatic Environments*, eds. Siegert, Bindschadler, and Kennicutt (Washington D.C.: AGU Press), 61–81. doi:10.1029/2010GM000995.

Skidmore, M., Anderson, S. P., Sharp, M., Foght, J., and Lanoil, B. D. (2005). Comparison of microbial community compositions of two subglacial environments reveals a possible role for microbes in chemical weathering processes. *Appl. Environ. Microbiol.* 71, 6986–6997. doi:10.1128/AEM.71.11.6986-6997.2005.

Skidmore, M. L., Foght, J. M., and Sharp, M. J. (2000). Microbial life beneath a high Arctic glacier. *Appl. Environ. Microbiol.* 66, 3214–3220. doi:10.1128/AEM.66.8.3214-3220.2000.Updated.

Sleep, N. H., and Zoback, M. D. (2007). Did earthquakes keep the early crust habitable? *Astrobiology* 7, 1023–32. doi:10.1089/ast.2006.0091.

Solberg, S., Dye, C., Schmidbauer, N., Herzog, A., and Gehrig, R. (1996). Carbonyls and nonmethane hydrocarbons at rural European sites from the mediterranean to the

arctic. *J. Atmos. Chem.* 25, 33–66. doi:10.1007/BF00053285.

Staehelin, J., Harris, N. R. P., Appenzeller, C., and Eberhard, J. (2001). Ozone trends: A review. *Rev. Geophys.* 39, 231–290. doi:10.1029/1999RG000059.

Stemmler, I., Hense, I., Quack, B., and Maier-Reimer, E. (2014). Methyl iodide production in the open ocean. *Biogeosciences* 11, 4459–4476. doi:10.5194/bg-11-4459-2014.

Stibal, M., Hasan, F., Wadham, J. L., Sharp, M. J., and Anesio, A. M. (2012a). Prokaryotic diversity in sediments beneath two polar glaciers with contrasting organic carbon substrates. *Extremophiles* 16, 255–265. doi:10.1007/s00792-011-0426-8.

Stibal, M., Wadham, J. L., Lis, G. P., Telling, J., Pancost, R. D., Dubnick, A., et al. (2012b). Methanogenic potential of Arctic and Antarctic subglacial environments with contrasting organic carbon sources. *Glob. Chang. Biol.* 18, 3332–3345. doi:10.1111/j.1365-2486.2012.02763.x.

Stohl, A. (2006). Characteristics of atmospheric transport into the Arctic troposphere. *J. Geophys. Res. Atmos.* 111. doi:10.1029/2005JD006888.

Stohl, A., Berg, T., Burkhart, J. F., Fjæraa, A. M., Forster, C., Herber, A., et al. (2007). Arctic smoke - Record high air pollution levels in the European Arctic due to agricultural fires in Eastern Europe in spring 2006. *Atmos. Chem. Phys.* 7, 511–534. doi:10.5194/acp-7-511-2007.

Stone, D., Whalley, L. K., and Heard, D. E. (2012). Tropospheric OH and HO2 radicals: field measurements and model comparisons. *Chem. Soc. Rev.* 41, 6348–6404. doi:10.1039/c2cs35140d.

Sturges, W. T., Cota, G. F., and Buckley, P. T. (1992). Bromoform emission from Arctic ice algae. *Nature* 358, 660–662. doi:10.1038/355242a0.

Sturges, W. T., Sullivan, C. W., Schnell, R. C., Heidt, L. E., and Pollock, W. H. (1993). Bromoalkane production by Antarctic ice algae. *Tellus B* 45, 120–126. doi:10.1034/j.1600-0889.1993.t01-1-00004.x.

Sugisaki, R., Ido, M., Takeda, H., Isobe, Y., Hayashi, Y., Nakamura, N., et al. (1983). Origin of hydrogen and carbon dioxide in fault gases and its relation to fault activity. *J. Geol.* 91, 239–258. doi:10.1086/628769.

Suzuki, N., Saito, H., and Hoshino, T. (2017). Hydrogen gas of organic origin in shales and metapelites. *Int. J. Coal Geol.* 173, 227–236. doi:https://doi.org/10.1016/j.coal.2017.02.014.

Swanson, A. L., Blake, N. J., Blake, D. R., Sherwood Rowland, F., Dibb, J. E., Lefer, B. L., et al. (2007). Are methyl halides produced on all ice surfaces? Observations from snow-laden field sites. *Atmos. Environ.* 41, 5162–5177. doi:10.1016/j.atmosenv.2006.11.064.

Takahashi, H. (1959). Effects of dry grinding on kaolin minerals, i. Kaolinite. *Bull. Chem. Soc. Jpn.* 32, 235–245. doi:10.1246/bcsj.32.374.

Teh, Y. A., Mazéas, O., Atwood, A. R., Abel, T., and Rhew, R. C. (2009). Hydrologic regulation of gross methyl chloride and methyl bromide uptake from Alaskan Arctic tundra. *Glob. Chang. Biol.* 15, 330–345. doi:10.1111/j.1365-2486.2008.01749.x.

Telling, J., Boyd, E. S., Bone, N., Jones, E. L., Tranter, M., Macfarlane, J. W., et al. (2015). Rock comminution as a source of hydrogen for subglacial ecosystems. *Nat. Geosci.* 8, 851–855. doi:10.1038/ngeo2533.

Tokarczyk, R., and Moore, R. M. (1994). Production of volatile organo halogens by phytoplankton cultures. *Geophys. Res. Lett.* 21, 285–288. doi:10.1029/94GL00009.

Tranter, M., Brown, G. H., Hodson, A., and Gurnell, A. M. (1996). Hydrochemistry as an indicator of subglacial drainage system structure: a comparison of alpine and sub-polar environments. *Hydrol. Process.* 10, 541–556. doi:10.1002/(SICI)1099-1085(199604)10:4<541::AID-HYP391>3.3.CO;2-0.

Tranter, M., Sharp, M. J., Lamb, H. R., Brown, G. H., Hubbard, B. P., and Willis, I. C. (2002). Geochemical weathering at the bed of Haut glacier d'Arolla, Switzerland - A new model. *Hydrol. Process.* 16, 959–993. doi:10.1002/hyp.309.

Tranter, M., Skidmore, M., and Wadham, J. (2005). Hydrological controls on microbial

communities in subglacial environments. *Hydrol. Process.* 19, 995–998. doi:10.1002/hyp.5854.

Vetaas, O. R. (1994). Primary succession of plant assemblages on a glacier foreland - Bodalsbreen, Southern Norway. *J. Biogeogr.* 21, 297–308. doi:10.2307/2845531.

Wadham, J. L., Arndt, S., Tulaczyk, S., Stibal, M., Tranter, M., Telling, J., et al. (2012). Potential methane reservoirs beneath Antarctica. *Nature* 488, 633–637. doi:10.1038/nature11374.

Wadham, J. L., Bottrell, S., Tranter, M., and Raiswell, R. (2004). Stable isotope evidence for microbial sulphate reduction at the bed of a polythermal high Arctic glacier. *Earth Planet. Sci. Lett.* 219, 341–355. doi:10.1016/S0012-821X(03)00683-6.

Wadham, J. L., De'Ath, R., Monteiro, F. M., Tranter, M., Ridgwell, A., Raiswell, R., et al. (2013). The potential role of the Antarctic Ice Sheet in global biogeochemical cycles. *Earth Environ. Sci. Trans. R. Soc. Edinburgh* 104, 55–67. doi:10.1017/S1755691013000108.

Wadham, J. L., Hodson, A. J., Tranter, M., and Dowdeswell, J. A. (1998). The hydrochemistry of meltwaters draining a polythermal-based, high Arctic glacier, south Svalbard: I. The ablation season. *Hydrol. Process.* 12, 1825–1849. doi:10.1002/(SICI)1099-1085(19981015)12:12<1825::AID-HYP669>3.0.CO;2-R.

Wadham, J. L., Tranter, M., Hodson, A. J., Hodgkins, R., Bottrell, S., Cooper, R., et al. (2010a). Hydro-biogeochemical coupling beneath a large polythermal Arctic glacier: Implications for subice sheet biogeochemistry. *J. Geophys. Res. Earth Surf.* 115, 1–16. doi:10.1029/2009JF001602.

Wadham, J. L., Tranter, M., Skidmore, M., Hodson, A. J., Priscu, J., Lyons, W. B., et al. (2010b). Biogeochemical weathering under ice: Size matters. *Global Biogeochem. Cycles* 24. doi:10.1029/2009GB003688.

Wadham, J. L., Tranter, M., Tulaczyk, S., and Sharp, M. (2008). Subglacial methanogenesis: A potential climatic amplifier? *Global Biogeochem. Cycles* 22, 1–16. doi:10.1029/2007GB002951.

Wang, J. J., Jiao, Y., Rhew, R. C., and Chow, A. T. (2016). Haloform formation in coastal wetlands along a salinity gradient at South Carolina, United States. *Environ. Chem.* 13, 745–756. doi:10.1071/EN15145.

Wang, Q., Shen, C., Chen, Q., Zhang, L., and Lu, H. (2015). Pore characteristics and gas released by crush methods of Wufeng-Longmaxi Shale in the northwest of Hubei Province, China. *Acta Geol. Sin. - English Ed.* 89, 93–96. doi:10.1111/1755-6724.12302_40.

Wei, T., and Simko, V. (2017). R package "corrplot": Visualization of a Correlation Matrix (Version 0.84). Available from https://github.com/taiyun/corrplot.

Weinberg, I., Bahlmann, E., Eckhardt, T., Michaelis, W., and Seifert, R. (2015). A halocarbon survey from a seagrass dominated subtropical lagoon, Ria Formosa (Portugal): Flux pattern and isotopic composition. *Biogeosciences* 12, 1697–1711. doi:10.5194/bg-12-1697-2015.

Weinberg, I., Bahlmann, E., Michaelis, W., and Seifert, R. (2013). Determination of fluxes and isotopic composition of halocarbons from seagrass meadows using a dynamic flux chamber. *Atmos. Environ.* 73, 34–40. doi:10.1016/j.atmosenv.2013.03.006.

Welker, J. M., Fahnestock, J. T., and Jones, M. H. (2000). Annual CO2 flux in dry and moist Arctic tundra: field responses to increases in summer temperatures and winter snow depth. *Clim. Change* 44, 139–150. doi:10.1023/A:1005555012742.

Wever, R., and van der Horst, M. A. (2013). The role of vanadium haloperoxidases in the formation of volatile brominated compounds and their impact on the environment. *Dalt. Trans.* 42, 11778. doi:10.1039/c3dt50525a.

WGMS (2012). World Glacier Inventory, Version 1. *Boulder, Color. USA.* Available at: https://doi.org/10.7265/N5/NSIDC-WGI-2012-02 [Accessed August 1, 2016].

Wiencke, C., Vögele, B., Kovaltchouk, N. A., and Hop, H. (2004). "Species composition and zonation of marine benthic macroalgae at Hansneset in Kongsfjorden, Svalbard," in *The coastal ecosystem of Kongsfjorden, Svalbard. Synopsis of biological research performed at the Koldewey Station in the years 1991 - 2003.*,

ed. C. Wiencke (Ber. Polarforsch. Meeresforsch), 55–62.

Wingenter, O. W., Sive, B. C., Blake, D. R., Rowland, F. S., and Ridley, B. A. (2003). Unexplained enhancements of CH_3Br in the Arctic and sub-Arctic lower troposphere during TOPSE spring 2000. *Geophys. Res. Lett.* 30, 1–4. doi:10.1029/2003GL018159.

Wingenter, O. W., Wang, C. J. L., Blake, D. R., and Rowland, F. S. (1998). Seasonal variation of tropospheric methyl bromide concentrations: Constraints on anthropogenic input. *Geophys. Res. Lett.* 25, 2797–2800. doi:10.1029/98GL02179.

Wishkerman, A., Gebhardt, S., Mcroberts, C. W., Hamilton, J. T. G., Williams, J., and Keppler, F. (2008). Abiotic methyl bromide formation from vegetation, and its strong dependence on temperature. *Environ. Sci. Technol.* 42, 6837–6842. doi:10.1021/es800411j.

Wuosmaa, A. M., and Hager, L. P. (1990). Methyl chloride transferase: a carbocation route for biosynthesis of halometabolites. *Science (80-.).* 249, 160 LP – 162.

Wynn, P. M., Hodson, A., and Heaton, T. (2006). Chemical and isotopic switching within the subglacial environment of a High Arctic glacier. *Biogeochemistry* 78, 173–193. doi:10.1007/s10533-005-3832-0.

Yang, X., Pyle, J. A., Cox, R. A., Theys, N., and Van Roozendael, M. (2010). Snow-sourced bromine and its implications for polar tropospheric ozone. *Atmos. Chem. Phys.* 10, 7763–7773. doi:10.5194/acp-10-7763-2010.

Yokouchi, Y., Noijiri, Y., Barrie, L. A., Toom-Sauntry, D., Machlda, T., Inuzuka, Y., et al. (2000). A strong source of methyl chloride to the atmosphere from tropical coastal land. *Nature* 403, 295–298. doi:10.1038/35002049.

Yokouchi, Y., Nojiri, Y., Toom-Sauntry, D., Fraser, P., Inuzuka, Y., Tanimoto, H., et al. (2012). Long-term variation of atmospheric methyl iodide and its link to global environmental change. *Geophys. Res. Lett.* 39, 1–5. doi:10.1029/2012GL053695.

Yokouchi, Y., Osada, K., Wada, M., Hasebe, F., Agama, M., Murakami, R., et al. (2008). Global distribution and seasonal concentration change of methyl iodide in the

atmosphere. *J. Geophys. Res. Atmos.* 113, 1–9. doi:10.1029/2008JD009861.

Yokouchi, Y., Toom-Sauntry, D., Yazawa, K., Inagaki, T., and Tamaru, T. (2002). Recent decline of methyl bromide in the troposphere. *Atmos. Environ.* 36, 4985–4989. doi:https://doi.org/10.1016/S1352-2310(02)00650-7.

Zhang, T., Yang, R., Milliken, K. L., Ruppel, S. C., Pottorf, R. J., and Sun, X. (2014). Chemical and isotopic composition of gases released by crush methods from organic rich mudrocks. *Org. Geochem.* 73, 16–28. doi:10.1016/j.orggeochem.2014.05.003.

Ziska, F., Quack, B., Abrahamsson, K., Archer, S. D., Atlas, E., Bell, T., et al. (2013). Global sea-to-air flux climatology for bromoform, dibromomethane and methyl iodide. *Atmos. Chem. Phys.* 13, 8915–8934. doi:10.5194/acp-13-8915-2013.

Zoet, L. K., Alley, R. B., Anandakrishnan, S., and Christianson, K. (2013). Accelerated subglacial erosion in response to stick-slip motion. *Geology* 41, 159–162. doi:10.1130/G33624.1.